## Effect of AMPK mediated RUNX phosphorylation on progression of cancer and diabetic bone health

Thesis submitted for the degree of

#### **DOCTOR OF PHILOSOPHY**

To

# THE DEPARTMENT OF ANIMAL BIOLOGY SCHOOL OF LIFE SCIENCES UNIVERSITY OF HYDERABAD HYDERABAD – 500 046 INDIA



By B. Meher Gayatri

Under the supervision of

Dr. A. Bindu Madhava Reddy

University of Hyderabad

Dept of Animal Biology School of Life Sciences University of Hyderabad Hyderabad- 500 034

Nov 2022

Enrolment No: 16LAPH09



# University of Hyderabad School of Life Sciences Department of Animal Biology Hyderabad-500 046, India

#### **CERTIFICATE**

This is to certify that this thesis entitled "Effect of AMPK mediated RUNX phosphorylation on progression of cancer and diabetic bone health." submitted by Mrs. B. Meher Gayatri bearing registration number 16LAPH09 for the degree of Doctor of Philosophy to the University of Hyderabad is a Bonafede record of research work carried out by her Department of Animal Biology, University of Hyderabad, Hyderabad under my supervision. The contents of this thesis, in full or parts have not been submitted to any other University or Institution for the award of any degree or diploma. I hereby, recommend her thesis for submission, for the award of the degree of Doctor of Philosophy from the University.

Dr. A. Bindu Madhava Reddy

Supervisor

Dr. A. Bindu Madhava Reddy
Assistant Professor
Dept. of Animal Biology
School of Life Sciences
University of Hyderabad
Hyderabad-500 046.

K. Sami Leson

Head,
Department of
Animal Biology
अध्यक्ष / HEAD
जंत् जैविकी विभाग

Department of Animal Biology

Mc 3/11/22

School of Life

DEAN
School of Life Sciences
University of Hyderabad
Hyderabad-500 046.



#### University of Hyderabad Hyderabad-500 046, India

#### **CERTIFICATE**

This is to certify that this thesis entitled "Effect of AMPK mediated RUNX phosphorylation on progression of cancer and diabetic bone health." submitted by Mrs. B. Meher Gayatri bearing registration number 16LAPH09 in partial fulfillment of the requirements for the award of Doctor of Philosophy in the Department of Animal Biology, School of Life Sciences, is a Bonafede work carried out by her under my supervision and guidance. This thesis is free from plagiarism and has not been submitted previously in full or parts, have not been submitted to any other University or Institution for the award of any degree or diploma.

Parts of this thesis have been:

#### A. Published Publications:

- Gayatri MB, Gajula NN, Chava S, Reddy ABM. (2022) High glutamine suppresses osteogenesis through mTORC1-mediated inhibition of the mTORC2/AKT-473/RUNX2 axis. Cell Death Discov. 8, 277. <a href="https://doi.org/10.1038/s41420-022-01077-3">https://doi.org/10.1038/s41420-022-01077-3</a>
- 2. Arolla RG, Malladi S, Bhaduri U, <u>Gayatri MB</u>, Pattamshetty P, Mohan V, Katika MR, Reddy ABM, Rao MRS, Vudem DR, Kancha RK. (2020) Analysis of cellular models of clonal evolution reveals co-evolution of imatinib and HSP90 inhibitor resistances. *Biochemical and Biophysical Research Communications*, 1;534:461-467. https://doi.org/10.1016/j.bbrc.2020.11.059
- 3. Vadlakonda, L., Indracanti, M., Kalangi, S.K. <u>Gavatri BM</u>, Naidu NG, Reddy ABM. (2020) The Role of Pi, Glutamine and the Essential Amino Acids in Modulating the Metabolism in Diabetes and Cancer. *J Diabetes Metab Disord* 1731–1775. <a href="https://doi.org/10.1007/s40200-020-00566-5">https://doi.org/10.1007/s40200-020-00566-5</a>. <a href="https://doi.org/10.1007/s40200-020-00566-5">https://doi.org/10.1007/s40200-020-00566-5</a>. <a href="https://doi.org/10.1007/s40200-020-00566-5">https://doi.org/10.1007/s40200-020-00566-5</a>.
- 4. Chava S, Chennakesavulu S, <u>Gayatri MB</u>, Reddy ABM. (2018) Novel phosphorylation by AMP-activated kinase regulates RUNX2 from ubiquitination in osteogenesis over adipogenesis. *Cell Death Dis*, 9;9(7):754. https://doi.org/10.1038/s41419-018-0791-7 Book Chapter:
- 5. Suresh C, <u>Gayatri BM</u>, Reddy ABM.Chapter-3 "EMT contributes to chemoresistance in pancreatic cancer". Breaking tolerance to pancreatic cancer unresponsiveness to chemotherapy. Volume -5 (2019) Elsevier. (ISBN: 9780128176610).

#### B. Presented in the following conferences

1. Presented in "The international congress for cell biology (ICCB-2018) Conference on the dynamic cell: Molecules and Networks to form and function" at CCMB, Hyderabad, 2018 (International).

Further, the student has passed the following courses towards fulfillment of coursework requirements for Ph.D.

Name	Credits	Pass/Fail
AS 801-Seminar 1	1	Pass
AS 802- Research Ethics &	2	Pass
Management		
AS 803- Biostatistics	2	Pass
AS 804- Analytical Techniques	3	Pass
AS 805- Lab Works	4	Pass

Dr. A. Bindu Madhava Reddy

Supervisor

Dr. A. Bindu Madhava Reddy
Assistant Professor
Dept. of Animal Biology
School of Life Sciences
University of Hyderabad
Hyderabad-500 046.

K. Sommas on

Head, Department of Animal Biology

अध्यक्ष / HEAD जंतु जैविकी विभाग Department of Animal Biology ۳ ع ۱۹۱۱ Dean,

School of Life Sciences

School of Life Sciences University of Hyderabad Hyderabad-500 046.



### University of Hyderabad

#### School of Life Sciences

Department of Animal Biology

Hyderabad-500 046, India

#### DECLARATION

I, Mrs. B. Meher Gayatri hereby declare that this thesis entitled "Effect of AMPK mediated RUNX phosphorylation on progression of cancer and diabetic bone health." submitted by me under the guidance and supervision of Dr. A. Bindu Madhava Reddy, is an original and independent research work. I also declare that it has not been submitted to any other University or Institution for the award of any degree or diploma.

Date: 04-11-2022

B. Meher Gayatri

16LAPH09

#### **Acknowledgments**

- ➤ I would like to express my deepest sense of gratitude to my supervisor **Dr. A. Bindu Madhava Reddy**, for giving me an opportunity to work under his guidance, constant cooperation, and encouragement throughout my work and for allowing me to pursue my questions in science.
- ➤ I would like to thank Dr. Ramakrishna K for providing with K562 drug resistant cell lines.
- ➤ I would also like to thank Dr. Sadasivudu, Dr. Dorababu and Nagaraj from NIMS for providing with CML patient blood samples.
- ➤ I would like to thank Prof. Ganesh form Sri Ramachandra Medical college and Prof. Suresh from IIM for providing me with breast cancer patient tissue samples.
- > I would like to thank **Prof. Lakshmipathi** V for his timely guidance and motivation.
- ➤ I thank Head, Dept. of Animal Biology, Prof. K. Sreenivasulu and previous HOD's Prof. Anita Jagota, Prof. Jagan Pongubala, Prof. Senthilkumaran, and Prof. Manjula Sritharan for allowing me to use the departmental facilities.
- ➤ I thank the Dean, School of Life Sciences, Prof. S. Dayanada and former Dean Prof. K.V.A. Ramaiah, Prof.M. N. V. Prasad, Prof. P. Reddanna, Prof. A.S. Raghavendra, Prof. Aparna Dutta Gupta, Prof. R.P. Sharma and Prof. M. Ramanadham for providing the central facilities at the School of Life Sciences.
- I thank the doctoral committee experts who were involved in the validation survey for this research work Prof. G. Ravi Kumar and Prof. K. Sreenivasulu for constructive criticism and valuable guidance, without their passionate participation and inputs, the validation survey could not have been successfully conducted.
- ➤ I thank all my present and past lab mates Dr. Suresh Chava, Dr. Chenna keshavulu, Preeti vyakaranam, Naga Chaitanya, Navya Naidu, Charita, Venkat, Elina for their help and support during my stay in lab.
- ➤ I thank Nandu singh, Bangaraiah, Kumar, Chandram and Prashanth Kumar Yadav for their assistance in the laboratory.
- ➤ I thank all the office staff of Dept. of Animal biology for their help in office work during my course of study.

- ➤ The financial support from DST-SERB, DBT-RGYI, DBT-RNAi, DAE-BRNS, UPE-Phase II, DST, CSIR, ICMR, UGC, DST-PURSE and DBT-CREBB is highly acknowledged.
- ➤ Financial support through UGC-JRF and SRF is highly acknowledged.
- ➤ I am extremely grateful to my parents (B. Meher Baba, B. Meher Madhavi) and my family who have been my real strength throughout my life.
- ➤ I would like to extend my thanks to my friends Amruta, Dhanya, Prabhu and Akash for their presence in my life.
- ➤ Above the all, I owe my thanks to GOD.

## Dedication

I dedicate this thesis to the awakener of the age

"AVATAR MEHER BABA"

#### **INDEX**

S.No.	Page. No.
ABBREVATIONS	1
BACKGROUND	9
HYPOTHESIS	15
OBJECTIVES	17
<b>OBJECTIVE 1: Understanding the role of AMPK and RUNX</b>	18
interactions on progression of cancer.	
<b>OBJECTIVE 1.1 : Is RUNX1 a physiological substrate of AMPK?</b>	19
1.1.1. LITERATURE REVIEW	19
1.1.2. MATREIALS and METHODS	20
1.1.2.1. Cell culture	20
1.1.2.2. Chemicals	20
1.1.2.3. Sub cloning	20
1.1.2.4. Bacterial protein expression and purification	22
1.1.2.5. AMPK kinase assay Invitro	22
1.1.2.6. Nuclear and cytosolic extraction	22
1.1.2.7. Electrophoretic mobility shift assay (EMSA)	22
1.1.2.8. Plasmid transfection	23
1.1.2.9. Immunoblotting	23
1.1.2.10. Immunoprecipitation (IP)	24
1.1.2.11. RNA isolation and real time PCR (RT-PCR)	25
1.1.2.12. Confocal microscopy	25

1.1.2.13. Statistical analysis	26
1.1.2.13. Suitsucat anatysis	20
1.1.3. RESULTS	26
1.1.3.1. RUNX1 is a physiological substrate of AMPK	27
1.1.3.2. RUNX1 Ser 94 phosphorylation inhibits nuclear	27
localization of RUNX1	
1.1.3.3. AMPK inhibits STAT3 activation through RUNX1 Ser 94 phosphorylation	29
1.1.4. DISSCUSSION	30
<b>OBJECTIVE 1.2:</b> Analyzing the role of AMPK substrates in	36
improving drug sensitivity of CML subjects.	
1.2.1. LITERATURE REVIEW	37
1.2.2. MATERIALS and METHODS	39
1.2.2.1. Cell culture	40
1.2.2.2. Chemicals	40
1.2.2.3. Isolation of PBMCs from CML patients	40
1.2.2.4. shRNA transduction and permanent line generation	40
1.2.2.5. Nuclear and cytosolic extraction	41
1.2.2.6. Plasmid transfection	41
1.2.2.7. Cell viability assay	41
1.2.2.8. Immunoblotting	41
1.2.2.9. Immunoprecipitation (IP)	42
1.2.2.10. RNA isolation and real time PCR (RT-PCR)	42
1.1.2.11. Confocal microscopy	42

1.2.2.12. Statistical analysis	42
1.2.3. RESULTS	44
1.2.3.1. RUNX1 serves as an AMPK substrate in imatinib resistance cells	45
1.2.3.2. RUNX1 Ser 94 phosphorylation inhibits STAT3 activation in imatinib resistant cells	45
1.2.3.3. Metformin improves imatinib sensitivity in imatinib resistant subjects through AMPK/RUNX1 S 94 axis	51
1.2.3.4. Metformin inhibits expression of HSP70 and p-STAT3 in imatinib-geldanamycin double resistant lines	51
1.2.3.5. Metformin inhibits HSF1 protein stability through AMPK-mediated proteasomal degradation	53
1.2.3.6. Metformin inhibits STAT3 phosphorylation through AMPK/RUNX1/SOCS3 axis in imatinib-geldanamycin double resistant lines	55
1.2.3.7. Metformin improves sensitivity of K562 cells towards geldanamycin and imatinib through inhibition of HSP-70 and MDR1	57
1.2.3.8. Metformin improves geldanamycin sensitivity of CML subjects through AMPK/HSF1/ HSP70 axis	59
1.2.4. DISSCUSSION	61
OBJECTIVE 1.3: Analyzing the effect of RUNX1 and AMPK interactions in improving MDS	65
1.3.1. LITERATURE REVIEW	66
1.3.2. MATREIALS and METHODS	66
1.3.2.1. Cell culture	68

1.3.2.2. Chemicals	68
1.3.2.3. Isolation of PBMCs from CML patients	68
1.3.2.4. Cell viability assay	68
1.3.2.5. Nuclear and cytosolic extraction	68
1.3.2.6. Electrophoretic mobility shift assay (EMSA)	68
1.3.2.7. Plasmid transfection	69
1.3.2.8. Immunoblotting	69
1.3.2.9. Immunoprecipitation (IP)	69
1.3.2.10. Confocal microscopy	69
1.3.2.11. RNA isolation and real time PCR (RT-PCR)	69
1.3.2.12. Statistical analysis	69
1.3.3. RESULTS	71
1.3.3.1. Metformin inhibits expression of HIF1-\alpha and MDR1 in pre-leukemic and leukemic lines	72
1.3.3.2. Metformin promotes HIF1-a ubiquitination through PHD2 mediated HIF1-a hydroxylation	72
1.3.3.3. AMPK induced RUNX1 Ser 94 phosphorylation alters PHD2 substrate affinity	74
1.3.3.4. Metformin inhibits STAT3 mediated transcription of HIF1- $\alpha$	77
1.3.3.5. Metformin promotes HIF1-a hydroxylation and MDR1 suppression in PBMCs of CML subjects	79
1.3.4. DISSCUSSION	80

OBJECTIVE 1.4: Analyzing the effect of RUNX2 and AMPK interactions in bone metastasis of breast cancer	83
1.4.1. LITERATURE REVIEW	84
1.4.2. MATREIALS and METHODS	85
1.4.2.1. Cell culture	86
1.4.2.2. Chemicals	86
1.4.2.3. Sub-cloning	86
1.4.2.4. Nuclear and cytosolic extraction	86
1.4.2.5. Electrophoretic mobility shift assay (EMSA)	86
1.4.2.6. Plasmid transfection	87
1.4.2.7. siRNA transfection	87
1.4.2.8. Immunoblotting	87
1.4.2.9. Immunoprecipitation (IP)	87
1.4.2.10. Confocal microscopy	88
1.4.2.11. RNA isolation and real time PCR (RT-PCR)	88
1.4.2.12. Trans-well migration assay	89
1.4.2.13. Breast tumor samples	89
1.4.2.14. Statistical analysis	89
1.4.3. RESULTS	90
1.4.3.1. RUNX2 is a substrate of AMPK in breast cancer cells	91
1.4.3.2. AMPK mediated phosphorylation of RUNX2 results in increased nuclear localization and transcriptional activity of RUNX2	91

1.4.3.3. mTORC2 is crucial for AMPK/RUNX2 axis	95
1.4.3.4. Metformin promotes EMT and induces osteoblast like phenotype to breast cancer cells thorough p-	98
AMPK/RUNX2/mTORC2 axis	
1.4.3.5. Metformin promotes chemotaxis/ metastasis of transformed breast cancer cells	99
1.4.3.6. AMPK induced RUNX2 Ser 118 phosphorylation is highly expressed in breast tumor tissues	103
1.4.4. DISSCUSSION	104
OBJECTIVE 2: Understanding the effect of AMPK activation on glucose and glutamine metabolism in cancer and diabetes.	108
<b>OBJECTIVE 2.1 : Analyzing the effect of metformin in altering</b>	109
glucose metabolism in CML	
2.1.1. LITERATURE REVIEW	109
2.1.2. MATREIALS and METHODS	110
2.1.2.1. Cell culture	111
2.1.2.2. Chemicals	111
2.1.2.3. Isolation of PBMCs from CML patients	111
2.1.2.4. Cell viability assay	111
2.1.2.5. Lactate assay	111
2.1.2.6. Glucose uptake assay	111
2.1.2.7. ATP assay	112
2.1.2.8. RNA isolation and real time PCR (RT-PCR)	112
2.1.2.9. Western blotting	112

2.1.2.10. Plasmid transfection	113
2.1.2.11. siRNA transfection	113
2.1.2.12. Statistical analysis	113
2.1.3. RESULTS	114
2.1.3.1. Metformin treatment inhibits lactate export in K562 (WT and resistant) cell lines	115
2.1.3.2. Metformin exerts anti-leukemic effect by inhibiting the expression of MCT1 & MCT4 through p-AMPK	115
2.1.3.3. Metformin attenuates glucose uptake in WT and resistant cells by inhibition of GLUT1	118
2.1.3.4. Activated AMPK results in suppression of HIF1- $\alpha$	120
2.1.3.5. Metformin inhibits lactate export through mTORC1 in WT and imatinib-resistant cells	120
2.1.3.6. GLUT1 overexpression renders metformin resistance to K562 WT and imatinib-resistant cells	122
2.1.3.7. Metformin attenuates glucose uptake and lactate export in PBMCs derived from CML subjects	124
2.1.4. DISSCUSSION	127
<b>OBJECTIVE 2.2:</b> Analyzing the effect of metformin on expression	133
of GLUT1 and GLUT4 in breast cancer.	
2.2.1. LITERATURE REVIEW	134
2.2.2. MATREIALS and METHODS	135
2.2.2.1. Cell culture	136
2.2.2.2. Chemicals	136

2.2.2.3. siRNA transfection	136
2.2.2.4. Cell viability assay	136
2.2.2.5. Glucose uptake assay	136
2.2.2.6. Immunoblotting	136
2.2.2.7. Statistical analysis	137
2.2.3. RESULTS	138
2.2.3.1. Insulin and nutrients induce expression of GLUT1, but not GLUT4 in breast cancer	139
2.2.3.2. GLUT1 expression was dependent on mTORC1, whereas GLUT4 was dependent on mTORC2	139
2.2.3.3. Metformin treatment inhibits GLUT1 expression, but promotes GLUT4 induction	142
2.2.4. DISSCUSSION	143
OBJECTIVE 2.3 : Analyzing the effect of metformin treatment on diabetes induced bone adipogenicity.	147
2.3.1. LITERATURE REVIEW	148
2.3.2. MATREIALS and METHODS	150
2.3.2.1. Cell culture	151
2.3.2.2. Chemicals	151
2.3.2.3. Ethics statement	151
2.3.2.4. Streptozotocin-induced diabetic model	151
2.3.2.5. Differentiation and transdifferentiation protocols	152
2.3.2.6. Oil- red-o staining	152
2.3.2.7. Alizarin-red-s staining	152

2.3.2.8. siRNA transfection	153
2.3.2.9. RNA isolation and real-time PCR (RT-PCR)	153
2.3.2.10. Western blotting	153
2.3.2.11. Immunoprecipitation (IP)	154
2.3.2.12. Confocal microscopy	154
2.3.2.13. Statistical analysis	154
2.3.3. RESULTS	155
2.3.3.1. mTORC1, but not mTORC2, is indispensable for adipogenesis and vice versa	156
2.3.3.2. mTORC1 promotes the adipogenic lineage through inhibition of the mTORC2/AKT-473/RUNX2 axis	156
2.3.3.3. mTORC2 stabilizes RUNX2 through the AKT-473/GSK3\beta axis	160
2.3.3.4. Diabetes-induced RUNX2 loss is mediated through the mTORC1/p-70S6K/GSK3β axis	162
2.3.3.5. High glucose induced glutamine sparring triggers RUNX2 loss under diabetic conditions	162
2.3.3.6. Metformin rescues the mTORC2/RUNX2 axis by inhibition of the mTORC1/p-70S6K pathway	166
2.3.4. DISSCUSSION	169
CONCLUSIONS	174
SIGNIFICANCE	176
FUTURE ASPECTS	179
PUBLICATIONS	181

REFERRENCES	183
SUPPLEMENTARY FIGURES	207
ANTI-PLAGARISM CERTIFICATE	232

#### **ABBREVATIONS**

2DG	2-deoxy glucose
2DG6P	2-deoxy glucose-6-phosphate
4EBP1	Eukaryotic translation initiation factor 4E-binding protein 1
17-AAG	17-N-allylamino-17-demethoxygeldanamycin
A	Alanine
Adipo Q	Adiponectin C1Q
AICAR	5-aminoimidiazole-4-carboxamide ribonucleotide
AKT/Akt	Protein kinase B
AM	Adipogenic medium
AMP	Adenosine monophosphate
AMPK	AMP- activated protein kinase
ANOVA	Analysis of variance
ATCC	American Type Culture Collection
ATF 4	Activating transcription factor 4
ATP	Adenosine triphosphate
BAX	Bcl-2-associated X protein
BC	Blast crisis
BCL2	B-cell lymphoma 2
BCR-ABL	Breakpoint cluster region-Abelson oncogene locus
BM-MSCs	Bone marrow derived mesenchymal stem cells
ВМР	Bone morphogenic protein
bp	Base pair
BRGs	Bone related genes

BSA	Bovine serum albumin
C2C12	Murine myoblast cell line
C3H10T1/2	Murine mesenchymal stem cell line
cAMP	Cyclic adenosine monophosphate
СВГВ	Core binding factor β
CD	Cluster differentiation
CDH11	Cadherin 11
cDNA	Complimentary DNA
CE	Cytoplasmic extracts
CML	Chronic myelogenous leukemia
CO <sub>2</sub>	Carbon dioxide
COL1A1	Type 1 collagen
Comp C	Compound C/ Dorsomorphin
Cont	Control
CPCSEA	Control and Supervision of Experiments on Animals
CTSK	Cathepsin K
D	Aspartic acid
DAPI	4,6-diamidino-2-phenylindole
del	Deletions
DMEM	Dulbecco's modified essential Medium
DMSO	Dimethyl sulfoxide
DNA	Deoxyribose nucleic acid
dI.dC	Deoxyinosinic deoxycytidylic
DTT	DL-Dithiothreitol
ECL	Enhanced chemiluminescence

ECM	Extracellular matrix								
EDTA	Ethylene diamine tetra acetic acid								
EGTA	Ethylene glycol tetra acetic acid								
eIFs	Eukaryotic initiation factors								
EMSA	Electrophoretic mobility shift assays								
EMT	Epithelial mesenchymal transition								
ERK1/2	Extracellular signal-regulated kinase 1/2								
ЕТО	Eight-Twenty-One oncoprotein								
ETV6	ETS Variant Transcription Factor 6								
EV	Empty vector								
EVI1	Ecotropic viral integration site-1								
F	Phenylalanine								
FACS	Fluorescence-activated cell sorting								
FBS	Fetal bovine serum								
FCS	Fetal calf serum								
FP	Forward primer								
GCN2	General control nonderepressible 2								
Gel	Geldanamycin								
GLUT	Glucose transporter								
GPCRs	G-protein coupled receptors								
GR	Geldanamycin resistant								
GSK3β	Glycogen synthase kinase 3 beta								
GST	Glutathione S-transferase								
НЕК-293 Т	Human Embryonic Kidney cells								
HEPES	2-hydroxyethyl-1-piperazineethanesulfonic acid								

HG	High glucose								
HGlut	High glutamine								
HK-II	Hexose kinase II								
HIF1	Hypoxia inducible factor 1								
HRP	Horse radish peroxidase								
HSCs	Hematopoietic stem cells								
HSF1	Heat shock inducible factor 1								
HSPs	Heat shock proteins								
IAEC	Institutional Animal Ethics Committee								
IB	Immunoblotting								
IBMX	3-isobutyl-1-methylxanthine								
IC50	Half-maximal inhibitory concentration								
ID	Inhibitory domain								
IgG	Immunoglobulin G								
IGR	Imatinib geldanamycin dual resistance								
IL-3	Interleukin- 3								
IMDM	Iscove's Modified Dulbecco's Medium								
Ima	Imatinib								
IP	Immunoprecipitation								
IPTG	Isopropyl β-D-1-thiogalactopyranoside								
IR	Imatinib resistant								
IS	Imatinib sensitive								
JAK	Janus kinases								
JNK	c-Jun N-terminal kinases								
Kb	Kilo base pairs								
KD	Knock down								

KDa	Kilo Dalton							
L	Lysine							
L-15	Leibovitz-15							
LG	Low glucose							
LiCl	Lithium chloride							
M	Molar							
M + I	Metformin plus imatinib							
MAPK	Mitogen-activated protein kinase							
MATE	Multi drug and toxic extrusion proteins							
MCF-7	Michigan Cancer Foundation-7, breast cancer cell lines							
MCL1	Myeloid cell leukemia 1							
MCT	Monocarboxylate transporter							
MDA-MB-231	Triple negative breast cancer cell line							
MDR1	Multidrug resistance protein 1							
MDS	Myelodysplastic syndrome							
Met	Metformin							
MgCl <sub>2</sub>	Magnesium chloride							
μg	Micro grams							
miRNA	Micro RNA							
mL	Milli liter							
μL	Micro liter							
mLST8	Mammalian lethal with SEC13 protein 8							
mM	Milli molar							
μΜ	Micro molar							
MMPs	Matrix metalloproteases							
mRNA	Messenger RNA							

MSCs	Mesenchymal stem cells
mSIN1/MAPKAP1	Mitogen-activated protein kinase-associated protein 1
mTORC1/2	Mammalian target of rapamycin complex 1/2
N	Asparagine
NaCl	Sodium chloride
NaF	Sodium fluoride
NE	Nuclear extract
ng	Nano grams
NLS	Nuclear localization signal
nM	Nano meters
nM	Nano molar
NMTS	Nuclear matrix targeting sequence
Na <sub>3</sub> VO <sub>4</sub>	Sodium ortho vanadate
NP-40	Nonidet p-40 or octyl phenoxy poly ethoxy ethanol
NS	Not significant
OCT	Organic cation transporters
OCN	Osteocalcin
OD	Optical density
ОН	Hydroxyl group
OPTI-MEM	Optimum minimum essential medium
OSE2	Osteoblast Specific cis acting Element 2
OXD PHOSP	Oxidative phosphorylation
P	Proline
PBMCs	Peripheral blood mononuclear cells
PBS	phosphate-buffered saline
PCR	Polymerase chain reaction

PDAC	pancreatic ductal adenocarcinoma								
Ph + ve	Philadelphia chromosome positive  Prolyl hydroxylases								
PHDs	Prolyl hydroxylases								
PI3K	Phosphatidylinositol-4,5-bisphosphate 3-kinase								
PKA	Protein kinase A Protein kinase C								
PKC	Protein kinase C								
PMSF	Phenyl methyl sulfonyl fluoride								
POSTN	Periostin								
PPAR	Peroxisome proliferator-activated receptor								
PY	Proline tyrosine motif								
R	Arginine								
RAP	Raptor								
Rap	Rapamycin								
Res	Resistant								
RFP	Red fluorescent protein								
RIC	Rictor								
RIPA	Radio immunoprecipitation assay								
RNA	Ribonucleic acid								
RP	Reverse primer								
rpm	Rotations per minute								
RPMI-1640	Roswell Park Memorial Institute-1640								
RTKs	Receptor tyrosine kinases								
RT-PCR	Real Time Polymerase chain reaction								
RUNX	Runt related transcription factors								
S/ Ser	Serine								
S6K	Ribosomal protein S6 kinase								
Scr	Scrambled								
SD	Standard deviation								
SDS-PAGE	Sodium dodecyl sulfate polyacrylamide gel electrophoresis								
SEM	Standard error of the mean								

Sens	Sensitive
Ser	Serum
SGLTs	Sodium dependent glucose transporters
shRNA	Short hairpin RNA
siRNA	Small interfering RNA
SOCS3	Suppressor Of Cytokine Signaling 3
STAT	Signal transducer and activator of transcription
T/ Thr	Threonine
T4PNK	T4 ploy nucleotide kinase
TBE	Tris Borate EDTA
TBST	Tris buffer saline with tween-20 or triton-X-100
TCA	Tri-carboxylic acid
TKI	Tyrosine kinase inhibitors
TLE	Groucho/transducing like enhancer protein
Tris HCL	Tris hydrochloride
U2OS	Human Bone Osteosarcoma Epithelial Cells
Ub	Ubiquitin
Unsp	Unspecified
UT	Untreated
V	Valine
VEGF	Vascular endothelial growth factor
vHL	Von Hippel-Lindau
WT	Wild type
°C	Degree Celsius
%	Percent

### **BACKGROUND**

#### **BACKGROUND**

Cancer and diabetes are the major leading metabolic disorders worldwide (1, 2). Runt related transcription factors (RUNX) family of proteins are one of the major drivers of cancer (3, 4). Apart from cancer progression RUNX2 is also involved in diabetes induced bone adiposity (5). Metformin, is the most widely used anti-glycemic biguanide for treatment of type 2 diabetes. Apart from regulation of glucose metabolism, metformin was known to have anti-proliferative (6) as well as osteo-protective functions, however the molecular pathways underlying were undeciphered. The current work is an effort to shed light on the molecular players involved in metformin induced anti-cancerous effects. The hallmark of both cancer and diabetes is altered metabolism, which aids in the progression of these disorders. The major nutrient sensors present in the cell that can alter metabolism are mTORC1, mTORC2 and AMPK.

#### mTORC1 and mTORC2

Mammalian target of rapamycin (mTOR) is a serine/threonine kinase which is present in two distinct complexes mTORC1 and mTORC2, defined by their interacting partners. mTORC1 mainly consists of mTOR, which is the kinase domain, raptor (regulatory-associated protein of mTOR), DEPTOR (DEP domain-containing mTOR-interacting protein) GβL/mLST8, Tti1/Tel2, and PRAS40 (proline-rich Akt substrate 40 kDa) (7). PRAS40 is a negative regulator of mTORC1 activation (8) and raptor is the essential scaffold of the complex mTORC1 which determines the substrate phosphorylations (9). The downstream targets for mTORC1 pathway include activation of global cap-dependent protein translation through phosphorylation of p70S6K1/2 and 4E-BP1/2; inhibition of autophagy through phosphorylation of unc-51 like kinase (ULK) (10, 11); promotes fatty acid and sterol biosynthesis through activation of sterol regulatory element binding proteins (SREBPs) (12); promotes mitochondrial biosynthesis (13). Activation of mTORC1 is biphasic, dependent on both growth factor signaling like insulin-like growth factor (IGF), EGF and on availability of nutrients like amino acids. Growth factor signaling acts through activation Akt (Protein kinase B), which inhibits tuberous sclerosis (TSC) complex resulting in hyper activation of mTORC1 (14, 15), whereas amino acids like glutamine, leucine activate mTORC1 through increase in active GTP- bound Ras homolog enriched in brain (Rheb) (16). Amino acid stimulation increases the docking of mTORC1 at lysosomes through Rag GTPases (17) and p62 (18). Amino acids can hyperactivate mTORC1, independent of growth factor signaling (19, 20).

mTORC2 mainly consists of mTOR, rictor (Rapamycin-insensitive companion of mammalian target of rapamycin) (21), mSIN1 (22), DEPTOR (23), Protor (24), PRR5L (25) and mLST8 (GβL). The stability of the mTORC2 complex is mainly defined by rictor and SIN1, where loss of either one results in disassembly of mTORC2. The well-established downstream targets of mTORC2 include AGC (Protein kinases A, G and C) family kinases (26). Of which the well-studied targets are Akt (27, 28), SGKs (Serum gluco-corticoids) (29) and PKCs (Protein kinase C) (30, 31). These substrates target pathways that are involved in actin filament formation (32), cytoskeleton reorganization (33) and cell migration which has a great impact in promoting metastasis of cancer cells (32), at the same time these pathways are implicated in regulation of nutrient uptake through regulation of exo and endocytosis by the cell which has implication in diabetes. In contrast to mTORC1, not much is known with regards to activation of mTORC2. However, activation of mTORC2 by PI3Ks is a well-established concept in the recent times (34, 35). Recent findings shed possibility that nutrient depletion especially amino acid starvation can activate mTORC2, albeit the mechanisms are undeciphered. The current work is an effort to unravel the possible mechanism involved in activation of mTORC2 in response to varying glucose and glutamine levels in cancer and diabetes.

#### **AMPK and Metformin**

The other energy sensor of the cell is AMPK, a serine/ threonine kinase which gets activated under starved conditions through AMP. AMPK consists three subunits alpha, beta and gamma. Gamma subunit is responsible for the kinase activity. The downstream targets include ACC (Acetyl-coA Carboxylase) which results in stimulation of fatty acid beta oxidation, TBC1D1 and D4 (TBC1 domain family member 1 and 4) which regulate GLUT4 vesicle trafficking, TSC2 and raptor which leads to inhibition of cap-dependent protein translation, PGC1-α (Peroxisome proliferator-activated receptor-gamma co-activator 1-alpha) which is a key transcriptional co-activator for mitochondrial biogenesis. The kinase activity of AMPK depends on the phosphorylation status of AMPK and the two major kinases involved include LKB1 (Liver Kinase B1) and CAMKK (Calcium/ Calmodulin dependent Kinase Kinases) (36). Metformin activates AMPK through LKB1 mediated phosphorylation at thr 172

residue. The dynamics between mTORC1, C2 and AMPK dictate the energy homeostasis of the cell. The current study is an aim to unravel the dynamics between these in context of cancer and diabetes.

#### **RUNX family of proteins**

RUNX family consists of three members namely RUNX1, RUNX2 and RUNX3. All the members of the family share the common DNA binding runt homology domain present at the N terminus which recognizes TGt/cGGT motif present on target genes. Apart from runt domain, VWRPY and PY motifs are highly conserved. The valine-tryptophan-arginineproline-tyrosine (VWRPY) motif is involved in interaction with co-repressors like Groucho/transducing like enhancer protein (TLE), while the proline-tyrosine motif is needed for interaction with WW domain that is present in several modular proteins involved in various signal transduction. Adjacent to the runt domain all members have nuclear localization sequence (NLS) and nuclear matrix target sequence (NMT) (Fig 1) which is responsible for their nuclear translocation and transactivation (3, 37). Both NLS and NMT are also highly conserved across the RUNX family. Hitherto, only RUNX2 consists of a small amino acid stretch of poly glutamine and alanine residues just before runt domain (Fig 1), whose exact function is yet to be determined, but it is speculated to play a role in protein aggregate formation. The RUNX proteins form heterodimers with CBFβ, which increases their DNA binding affinity. Along with runt domain the transactivation domain present at the c-terminus is involved in interaction with CBFβ. RUNX proteins vary greatly in their regulatory regions which bestows specificity towards diverse targets.

RUNX proteins also share a similar genomic architecture, where RUNX1 is located on chromosome 21q22.12 spanning over 1,216,867 bases with 9 exons and 12 isoforms. RUNX2 is located on chromosome 6p21.1 spanning over 336,193 bases with 8 exons and 12 possible isoforms. RUNX3 is located on chromosome 1 spanning over 65,648 bases with 6 exons and 2 possible isoforms. All the RUNX genes have two promoters proximal (P1) and distal (P2). The presence two distinct promoters form an additional level of regulation for RUNX protein expression. Though all the RUNX proteins share same DNA binding element, their expression is tissue specific, with RUNX1 playing a major role in differentiation of erythroid and lymphoid lineages and in maintenance haemopoietic stem cell population, one of the reasons for haemopoietic specific lineage expression of RUNX1 is due to the binding of tissue specific

enhancers (regulatory element1 and 2) which facilitate binding of erythroid and lymphoid specific proteins. RUNX2 transcription is regulated by covalent histone modifications and is expressed mainly during mesenchymal differentiation towards osteogenic and myoblastic lineages. RUNX3 is mainly involved in development of gastric epithelium. It is of worth to note that both RUNX1 and RUNX3 P2 promoters have interspersed CpG islands.

Apart from regulating differentiation, RUNX proteins also play an important role in cancer. Though debatable, in most scenarios RUNX proteins act as oncogenes with few exceptions where RUNX haploinsufficiency predisposes cells to leukemia or gastric cancers. Aberrant expression of RUNX proteins is noted in various cancers like RUNX2 in breast, prostrate, lung and osteosarcoma; RUNX3 in pancreatic ductal adenocarcinoma (PDAC), gastric cancer, esophageal cancer; RUNX1 is mainly involved but not limited to leukemia. RUNX proteins have an emerging role in invasion and metastasis of solid tumors. RUNX point mutations and translocations are also frequently reported in cancers, especially RUNX1 fusion proteins like RUNX1-ETO, RUNX1-EVI1, TEL-RUNX1, ETV6-RUNX1 play a key role in progression of leukemia. Taken together it seems that RUNX proteins can act either as tumor suppressors or as oncogenes depending on cues and this double-edged ability of RUNX proteins is mainly due to their vast repertoire of targets and interacting partners.

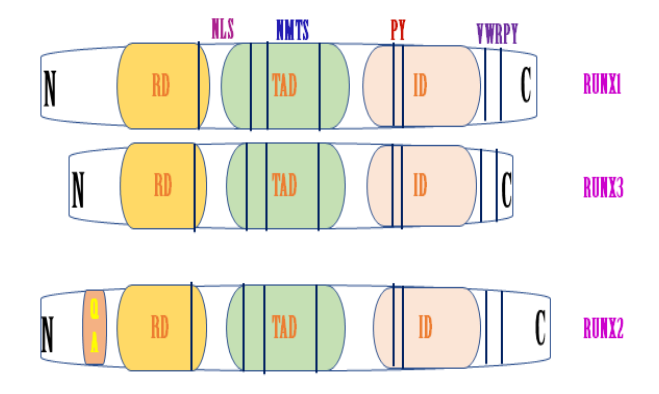


**FIGURE 1: RUNX family protein structure.** The above figure summarizes the known motifs present in all RUNX family members, along with the highly conserved motifs.

RD: runt homology domain, TAD: trans-activation domain, ID: inhibitory domain, QA: poly alanine glutamine motif, NLS: nuclear localization domain, NMTS: nuclear matrix targeting signal, PY: proline-tyrosine motif, VWRPY: valine-tryptophan-arginine-proline-tyrosine motif.

The other major disorder in which RUNX proteins play a critical role is diabetes induced secondary disorders like bone adipogenesis, proliferative diabetic retinopathy and cardiovascular diseases. Expression of RUNX proteins in response to high glucose conditions is context dependent; where it was seen that RUNX2 expression is decreased in bone leading

to loss of bone mineralization and increased adipogenesis in response to high glucose, it was also observed that in smooth muscle cells RUNX2 expression was increased under diabetic conditions leading to arterial calcification (38). Hitherto, RUNX1 and 3 expression was increased in retinal vascular endothelial cells and in endothelial progenitor cells exposed to high glucose (39, 40). These possible variations in RUNX protein levels towards same cue could be due to differences in expression pattern of regulators like kinases or E3 ligases or miRNAs (40) involved in RUNX protein regulation. In the current study we have investigated the role of one such regulator AMP activated protein kinase (AMPK) involved in RUNX protein stability with respect to varying physiological scenarios like diabetes, breast cancer and leukemia.

#### **HYPOTHESIS**

Initial invitro analysis of RUNX proteins using phospho motif finder 3.0 and NET phos tools have revealed the presence of AMPK binding sites on RUNX proteins in the runt homology domain. In our earlier work it was seen that RUNX2 was a novel substrate of AMPK in MSCs. Thus, we have hypothesized that RUNX1 could also be a possible AMPK substrate, since all the RUNX proteins had conservation of AMPK binding motif (Fig 2). Also, metformin, an activator of AMPK could be involved in regulation of RUNX proteins. Since metformin was reported to induce cell cycle arrest in cancers, and RUNX deregulation is involved in progression of cancer and secondary diabetic complications, we have hypothesized that RUNX induced malignancy or metformin mediated cell cycle arrest could be due to modulation of RUNX protein functional activity due to phosphorylation by AMPK.

As, AMPK substrate domain resides in the DNA binding runt domain, AMPK mediated RUNX phosphorylation may affect DNA binding ability as well as protein-protein interactions of RUNX proteins. Owing to the vast target repertoire of RUNX proteins, AMPK induced RUNX phosphorylation can affect various cellular pathways like cell cycle progression, cell death, drug uptake, transport of cellular metabolites like lactate, glucose uptake etc., Keeping in the view of these various processes which could be affected by RUNX phosphorylations we have designed the following objectives.

A)													
	Position	Motif VRTDSPNFL			Sco	re	Signific	Significance			Kinase		
RUNX1	94				0.928 0.928		YES		Unsp				
RUNX2	118	VRTDSPNFL VRTDSPNFL		YES			YES		Unsp				
RUNX3	85			FL	0.928		YES		Unsp				
В)													
Protein name	Position of S	- <mark>5</mark>	-4	-3	-2	-1	•	+1	+2	+3	+4		
RUNX1 a	67		V	R	Т	D	S	Р	N	F			
RUNX1 b	67	L	V	R R	Т	D	S	Р	N	F	L		
RUNX1 c	94	L	V	R	Т	D	S	Р	N	F	L		
RUNX1T1	67		V	R	T	D	S	Р	N	F			
RUNX1-MECOM	94		V	R	T	D	S	P	N	F			
RUNX3 p46	85	Ē	V	R	T	D	S	Р	N	F			
RUNX3 p44	71		V	R R	T	D	S	Р	N	F			
RUNX2	118	<u> </u>	V	K	Т	D	S	Р	N	F	_		
C)													
Species	Position	<b>-5</b>	-4	-3	-2	-1		+1	+2	+3	+4		
Homo sapiens	94	L	V	R	Т	D	S	Р	N	F			
Mus musculus	81	L	V	R	Т	D	S	Р	N	F			
Rattus norvegicus	82	L	V	R	Т	D	S	Р	N	F			
Pan troglodytes	81	L	V	R	Т	D	S	Р	N	F			
Macaca mulatta	94		V	R	Т	D	S	Р	N	F	Ŀ		
Bos taurus	94		V	R	Т	D	S	Р	N	F	ı		

FIGURE 2: Insilico analysis showing AMPK binding motif prediction on RUNX1. A) List of putative AMPK binding motif present on RUNX proteins along with the scores, predicted using phospho motif finder.

B) Conservation of putative AMPK binding motif across RUNX family splice variants and fusion proteins. C) Conservation of putative AMPK binding motif present on RUNX1 across species.

#### **OBJECTIVES**

# 1. Understanding the role of AMPK and RUNX interactions on progression of cancer.

- 1. Is RUNX1 a physiological substrate of AMPK?
- 2. Analyzing the role of AMPK substrates on drug sensitivity of CML subjects.
- 3. Analyzing the effect of RUNX1 and AMPK interactions in MDS.
- 4. Analyzing the effect of RUNX2 and AMPK interactions in bone metastasis of breast cancer.

# 2. Understanding the effect of AMPK activation on glucose and glutamine metabolism in cancer and diabetes.

- 1. Analyzing the effect of metformin on glucose metabolism in CML.
- 2. Analyzing the effect of metformin on expression of GLUT1 and GLUT 4 in breast cancer.
- 3. Analyzing the effect of metformin treatment in diabetes induced bone adipogenesis.

## OBJECTIVE -1

Understanding the role of AMPK and RUNX interactions on progression of cancer.

### **OBJECTIVE 1.1**

### Is RUNX1 a physiological substrate of AMPK?

### 1.1.1. LITERATURE REVIEW

RUNX1 is the major transcription factor involved in HSC maintenance and lineage commitment (41). RUNX1 and RUNX1 somatic mutations are involved in progression of CML (42), it is a hotspot for chromosomal translocations resulting in generation of fusion proteins like RUNX1-ETO, RUNX1-EVII etc., Initial school of thought on function of these fusion proteins was that they would act as negative regulators for wild type RUNX1, resulting in loss of function, which enables in progression of CML to blast crisis (BC) phase by generation of drug resistance (43-46). However, recent studies have shown that even in absence of fusion proteins RUNX1 acts as an oncogene by co-operating with BCR-ABL to induce BC phase like phenotype in CML cases. There is growing evidence suggesting oncogenic role of wild type RUNX1 in case of CML, nevertheless the underlying molecular mechanisms remain elusive (47, 48). One of such mechanisms is suppression of expression of SOCS3 (49, 50), which is a negative regulator of JAK/STAT pathway (51). JAK/STAT is one of the major pathways that drives CML along with RUNX1 (52). Consistent activation of BCR-ABL results in activation of JAK/STAT pathway through phosphorylation which in turn activates cascade of genes that are involved in proliferation and anti-apoptotic signaling resulting in generation of IR (53, 54). Thus, there is a need for development of new drugs capable of targeting RUNX1 and JAK/STAT pathway inorder to treat CML. Metformin is an anti-glycemic drug which, recently emerged as an anti-leukemic drug owing to its ability in inhibiting mTORC1 through AMPK activation (54, 55). However, role of metformin in inhibiting JAK/STAT pathway and in overcoming CML is unexplored.

# **MATERIALS and METHODS**

### 1.1.2. MATERIALS and METHODS

### 1.1.2.1. Cell culture

K562 wild type (WT) cells were cultured in RPMI-1640 (Gibco, USA) medium supplemented with 10% FBS, 1% pen-strep. HEK-293 T cells were cultured in DMEM (Gibco, USA) medium supplemented with 10% FBS (Gibco, USA), 1% pen-strep (Gibco, USA). All cell lines were maintained in 5% CO<sub>2</sub> incubator at 37°C. Sub culturing for adherent cells was done using 0.5% trypsin-EDTA (HiMedia, India).

### **1.1.2.2.** *Chemicals*

Metformin, Isopropyl  $\beta$ -D-1-thiogalactopyranoside (IPTG) and dorsomorphin (compound C) were purchased from Sigma (USA).

### **1.1.2.3.** *Sub cloning*

RUNX1 cDNA (NM\_001754.4) was purchased from DNASU (USA) (HS CD00630733). RUNX1 site directed mutants RUNX1 S94 A, D along with WT were subcloned into pDsRed1-N1 (Clonetech, USA) containing red fluorescent protein for mammalian expression. For bacterial protein expression RUNX1 WT, R 91 A and S 94 A constructs were sub-cloned into GST-tagged vector pGEX-4T1. The list of primers used for sub-cloning were:

Target	Forward primer (5'-3')	Reverse primer (5'-3')
RUNX1 WT	GGAAGATCTATGGCTTCAG	GAAGTTGGGGTCGTCGGTGCG
(pGEX-4T1)	ACACAGCATA	
RUNX1 WT	CCGCTCGAGATGGCTTCAG	GGAATTCATTCAGTAGGGCCT
(pDsRed1-N1)	AC	CCA
RUNX1 S94 D	CGCACCGACGACCCCAACT	GAAGTTGGGGTCGTCGGTGCG
	TC	
RUNX1/3 S94 A	CGCACCGACGCCCCAACT	GAAGTTGGGGGCGTCGGTGC
	TC	G
RUNX1/3 R91 A	GAGCTGGTGGCCACCGACA	GCTGTCGGTGGCCACCAGCTC
	GC	
RUNX3 WT	CGCGGATCCATGGCATCGA	CCGCTCGAGTCAGTAGGGCCA
(pGEX-4T1)	ACAGCATC	CAC

### 1.1.2.4. Bacterial protein expression and purification

GST-tagged fusion proteins RUNX1-WT, R 91 A and S 94 A were transformed in to rosetta strain and induced for protein expression by 1mM IPTG at 18°C and cells were pelleted by centrifuging at 8,000 rpm for 15 minutes at 4°C, the pellet was resuspended in lysis buffer and sonicated for 1 minute at 20% power, until a clear solution was obtained. The solution was then centrifuged at 8,000 rpm for 15 minutes at 4°C. The supernatant was then purified using GST beads (GE health care, USA).

### 1.1.2.5. AMPK kinase assay Invitro

For kinase assay, reaction mixture was prepared containing 5  $\mu$ g of RUNX1-WT or RUNX1- R 91 A or RUNX1- S 94 A along with kinase buffer (20 mM HEPES (pH 7.4), 100  $\mu$ M ATP and 5  $\mu$ M AMPK, 1 mM dithiothreitol, 10 mM magnesium acetate) and 100 ng of AMPK purified enzyme (Cat #14-840 – EMD Millipore, USA) which was incubated for 30 minutes at 37°C. After incubation the complex was subjected to SDS-PAGE analysis.

### 1.1.2.6. Nuclear and cytosolic extraction

Cells were treated with indicated drugs for 6 hours and cells were collected in 1X PBS. Following which they were resuspended in buffer A (20 mM Tris-HCl, pH-7.4, 10 mM NaCl, 3 mM MgCl<sub>2</sub>) (Sigma, USA) for 15 minutes on ice and 10% NP-40 was added with vortexing at high speed, then subjected to centrifugation for 10 minutes at 8,000 rpm at 4°C. The supernatant represents cytosolic fraction. To the pellet buffer B (10mM Tris- HCl, pH-7.4, 2 mM Na3VO4, 0.5 mM DTT, 100 mM NaCl, 1% Triton- X-100, 1mM EDTA, 5% glycerol, 0.1% SDS, 1 mM NaF, 1 mM EGTA, 0.5% deoxycholate) (Sigma, USA) was added and incubated on ice for 30 minutes with vortexing at 5 minutes interval, then subjected to centrifugation at 14,000 rpm for 20 minutes. The supernatant represents nuclear fraction.

### 1.1.2.7. Electrophoretic mobility shift assay (EMSA)

Cells were treated with indicated drugs and nuclear extracts were prepared as mentioned above. The RUNX1 or RUNX2 or STAT3 binding consensus on target promoters was taken as wild type probe and mutant probe was designed with mutations in critical sites. Both wild type and mutant probes were labelled with  $\gamma$ -<sup>32</sup>P using T4PNK (NEB, USA) enzyme following manufacturer's instructions. The labelled probe was then purified using G50 Spin

columns (Sigma, USA) following manufacturer's manual and estimated. The binding reaction was prepared as mentioned below:

Labelled probe: 10 ng,

Nuclear extract: 3-5 μg,

Poly (dI. dC): 2 μg,

Purified BSA: 1 µg,

Antibody: 1 µg,

2X gel shift buffer:  $2~\mu L$ , the reaction was set up for  $20~\mu L$  and remaining volume was made up using milliq water and the mixture was incubated at  $37^{\circ}C$  for 45 minutes. Then it was incubated on ice for 10 minutes. To the mixture 4X purple loading dye was added and the samples were loaded on to non-denaturing 6% TBE- native gel. Post to pre-run at 200V for 30 minutes. After running, the gels were vacuum dried at  $70^{\circ}C$  for 30-60 minutes. Later, the gels were exposed to X- ray films.

Promoter	Wild type probe (5'-3')	Mutant probe (5'-3')	Position
SOCS3	TAGAGACGAGGTTTCAC	TAGAGACCAAAATTCACC	-2.07Kb
	С		

### 1.1.2.8. Plasmid transfection

For transfection cells were seeded in six well plate and were grown to a confluency of 50 %. 2  $\mu g$  of purified plasmid (RUNX1 WT or S 94 A or S 94 D) was diluted in 500 $\mu$ L of OPTI-MEM medium and incubated for 5 minutes. Concomitantly 1.5  $\mu$ L of Lipofectamine-3000 (Thermo Fischer, USA) was diluted in 500 $\mu$ L of OPTI-MEM medium and incubated for 5 minutes. The diluted plasmid mixture was added to lipofectamine and incubated for 20 minutes and then added to cells. The cells were grown in OPTI-MEM for six hours, post to which the medium was replaced with complete medium and grown for 48 hours.

### 1.1.2.9. Immunoblotting

Suspension cells were collected by centrifuging at 3,000 rpm for 5 minutes and washed twice with ice cold 1X PBS following addition of 1X RIPA (with protease and phosphatase inhibitor cocktails (Sigma, USA)) and adherent cells were scrapped in 1X RIPA and subjected to vortexing for 60 minutes with interval of 10 minutes. Protein isolation was carried out by centrifugation at 14,000 rpm for 30 minutes at 4°C. Equal amounts of protein (60µg) were taken using Bradford's assay and subjected to SDS-PAGE. Post to transfer, blocking was done using

5% milk solution. Primary antibodies were incubated either over night at 4°C or for 2 hours at room temperature. RUNX1/AML1, GST, SOCS3, Cyclin D1, AMPK, β-actin antibodies were procured from Santa Cruz Biotechnology Inc., USA. p-STAT3(Y705), STAT3, Lamin B1 were purchased from Abcam, USA. Paxillin, p-AMPK, p-AMPK substrate motif specific antibodies were procured from Cell Signaling Technologies, USA. Corresponding HRP (horseradish peroxidase enzyme) linked secondary antibodies were procured from GeNeI labs, India and incubated for 1 hour at room temperature. The signal was detected by Clarity Western ECL blotting substrates (Bio-Rad, USA) and images were processed using Bio-Rad Chemidoc MP system.

### 1.1.2.10. Immunoprecipitation (IP)

In case of suspension cultures, cells were collected by centrifuging at 3,000 rpm for 5 minutes and washed twice with ice cold 1X PBS then resuspended in IP lysis buffer (buffer 1: 25mM Tris (pH-7.4), 150mM NaCl, 1% NP-40, 1mM EDTA, 5% Glycerol, 1mM PMSF and leupeptin along with phosphatase inhibitor cocktail (Sigma, USA) for RUNX and AMPK interactions or buffer 2: 25mM Tris (pH-7.4), 100mM NaCl, 1% NP-40, 1mM EGTA, 0.5mM EDTA, 10% Glycerol, 1mM PMSF and leupeptin along with phosphatase inhibitor cocktail for RUNX and STAT3) and for adherent cultures cells were directly scrapped in IP lysis buffer of choice and subjected to protein isolation by centrifuging at 14,000 rpm for 30 minutes. For pull down 750µg (incase of cell lines) of protein was taken along with 1 µg of antibody (p-AMPK, STAT3 or RUNX1) and left at 4°C overnight for binding. Protein agarose-A-G plus beads (Santa Cruz Biotechnology Inc., USA) were used for pulling down antigen antibody complex. Prior to subjecting for binding beads were equilibrated using 1X TBST (Triton-X-100, 1M Tris-base pH-7.4, 1M NaCl), by centrifuging at 5,000 rpm for 5 minutes at 4°C and was repeated for 3 times. Beads were kept for binding for 3 hours at 4°C. Post to pull down the lysates were suspended in 1X SDS loading dye and subjected to SDS-PAGE followed by immunoblotting. However, the secondary antibodies used were TrueBlot antibodies conjugated to HRP (Rockland Immunochemicals, USA).

### 1.1.2.11. RNA isolation and real time PCR (RT-PCR)

Suspension cells were centrifuged at 3,000 rpm for 5 minutes and were washed twice with ice cold 1X PBS. TRIzol (Thermo Fisher Scientific, USA) was then added to the pellet, whereas for adherent cultures cells were directly lysed in TRIzol. The cells were incubated in TRIzol for 10 minutes on ice, followed by addition of chloroform (Sigma, USA) (0.2 ml for 1

ml of TRIzol) and inverted 3-4 times and incubated on ice for 5 minutes, prior to centrifugation at 14,000 rpm for 15 minutes at 4°C. The upper aqueous phase is collected into a new tube and isopropanol (Finar, India) (0.5 ml for 1 ml of TRIzol) is added and incubated for 15 minutes on ice prior to centrifugation at 14,000 rpm for 30 minutes at 4°C. Discard the supernatant and wash the pellet with 75% ethanol (Sigma, USA) by centrifuging at 10,000 rpm for 5 minutes at 4°C. The pellet was then air dried and dissolved in 30 μL of nuclease free water. Equal amounts of RNA (1μg) were taken and cDNA synthesis was carried out by iSCRIPT Bio-Rad c-DNA synthesis kit (Bio-Rad, USA). Real-time PCR was carried out by Bio-Rad SYBR Green QRT- PCR Master mix (Bio-Rad, USA). The quantification of real time data was done using 2-Δ ΔCT method. The sequences of primers used were:

Target	Forward primer (5'-3')	Reverse primer (5'-3')
Cyclin D1	AGGTCTGCGAGGGAACAGAAGTG	TGCAGGCGGCTCTTTTTC
Cyclin D3	CTGGCCATGAACTACCTGGA	CCAGGAAATCATGTGCAATC
BCL2	ATGTGTGGAGAGCGTCAACC	TGAGCAGAGTCTTCAGAGACAGCC
SOCS3	GGAGACTTCGATTCGGGACC	GAAACTTGCTGTGGGTGACC
Actin	GAGAGGGAAATCGTGCGTGAC	CATCTGCTGGAAGGTGGACA

### 1.1.2.12. Confocal microscopy

Suspension cells were grown on cover slips coated with poly-lysine (Sigma, USA) followed by treatment with drugs, for indicated timepoints and were washed with PBS before fixing in 4% formalin for 10 min at room temperature. Cells were washed twice in 1X PBS. Prior to blocking cells were permeabilized in 0.2% TRITON-X-100 (Sigma, USA) for 15 minutes followed by washes with 1X PBS. Bocking was done in 5% bovine serum (Hi-media, India) for 1 hour at room temperature. Cells were stained with primary antibodies AMPK, RUNX1/AML1 or STAT3 for 2 hours at room temperature, followed by respective fluorescence secondary antibody staining (Alexa Flour 488 and 546, Invitrogen, USA)). Cells were counterstained with 4',6-diamino-2-phenylindole (DAPI) (Thermo Scientific, USA) for nuclei and images were captured using laser scanning confocal microscope (LSM 780, Carl Zesis, Germany).

### 1.1.2.13. Statistical analysis

All data points are represented as mean  $\pm$  SEM. Statistical analysis was done using one-way ANOVA. P < 0.05 was considered to be statistically significant. All data points were done

in duplicates and a minimum of set of three independent experiments were carried out for all in-vitro studies and patient data.

# **RESULTS**

### **1.1.3. RESULTS**

### 1.1.3.1. RUNX1 is a physiological substrate of AMPK

In order to validate the AMPK binding motif, present on RUNX1, invitro AMPK kinase assay was carried out in a cell free system. Indeed, RUNX1 serves as a substrate of AMPK and this phosphorylation occurs on Ser residue present at 94<sup>th</sup> position, as confirmed by site directed mutagenesis of RUNX1 (Fig 3A). The prerequisite for phosphorylation of RUNX1 by AMPK is physical interaction between them. We have used K562 cells to confirm the phosphorylation of RUNX1 by AMPK. Upon metformin treatment of K562 cells, enrichment of p-AMPK in RUNX1 immunoprecipitates was observed, which was not seen when cells were treated with compound C (an inhibitor of p-AMPK) (Fig 3B). The phosphorylation of RUNX1 by p-AMPK was confirmed by immunoblotting with AMPK substrate-specific antibody on RUNX1 immunoprecipitated lysates (as p-RUNX antibody was commercially unavailable). AMPK substrate-specific antibody signal was enriched in metformin-treated lanes post to immunoprecipitation by RUNX1 (Fig 3B), suggesting RUNX1 as a physiological substrate of AMPK. The interaction between RUNX1 and p-AMPK was further validated by immunoprecipitation of p-AMPK, following treatment with either metformin or compound C. Enrichment of RUNX1 in metformin-treated lysates indicating RUNX1 as a substrate of AMPK (Fig 3C) was observed. This interaction was further confirmed by immunofluorescence analysis of K562 (wild type) cells post to treatments with either metformin or compound C (Fig 3D &E).

### 1.1.3.2. RUNX1 Ser 94 phosphorylation inhibits nuclear localization of RUNX1

We, next analyzed the effect of RUNX1 Ser 94 phosphorylation on nuclear localization and transactivation function of RUNX1. K562 (wild type) cells were treated with either metformin or with compound C and subjected to subcellular fractionation. Upon metformin treatment, nuclear localization of RUNX1 was reduced along with increased cytoplasmic retention (Fig 3F &SF 1B), which was not seen in compound C treated cells. Similar trend was observed in STAT3 localization (Fig 3F &SF 1C). We then analyzed the levels of phosphorylated RUNX1 present in nuclear compartments, for this K562 WT cells were treated with metformin and subjected to immunoprecipitation by RUNX1 in nuclear fraction. Phosphorylated RUNX1 was greatly reduced in metformin treated lanes (Fig 3G). As AMPK induced phosphorylation was observed on the DNA binding domain of RUNX1, we next analyzed the DNA binding ability of phosphorylated RUNX1. Since RUNX1 was known to

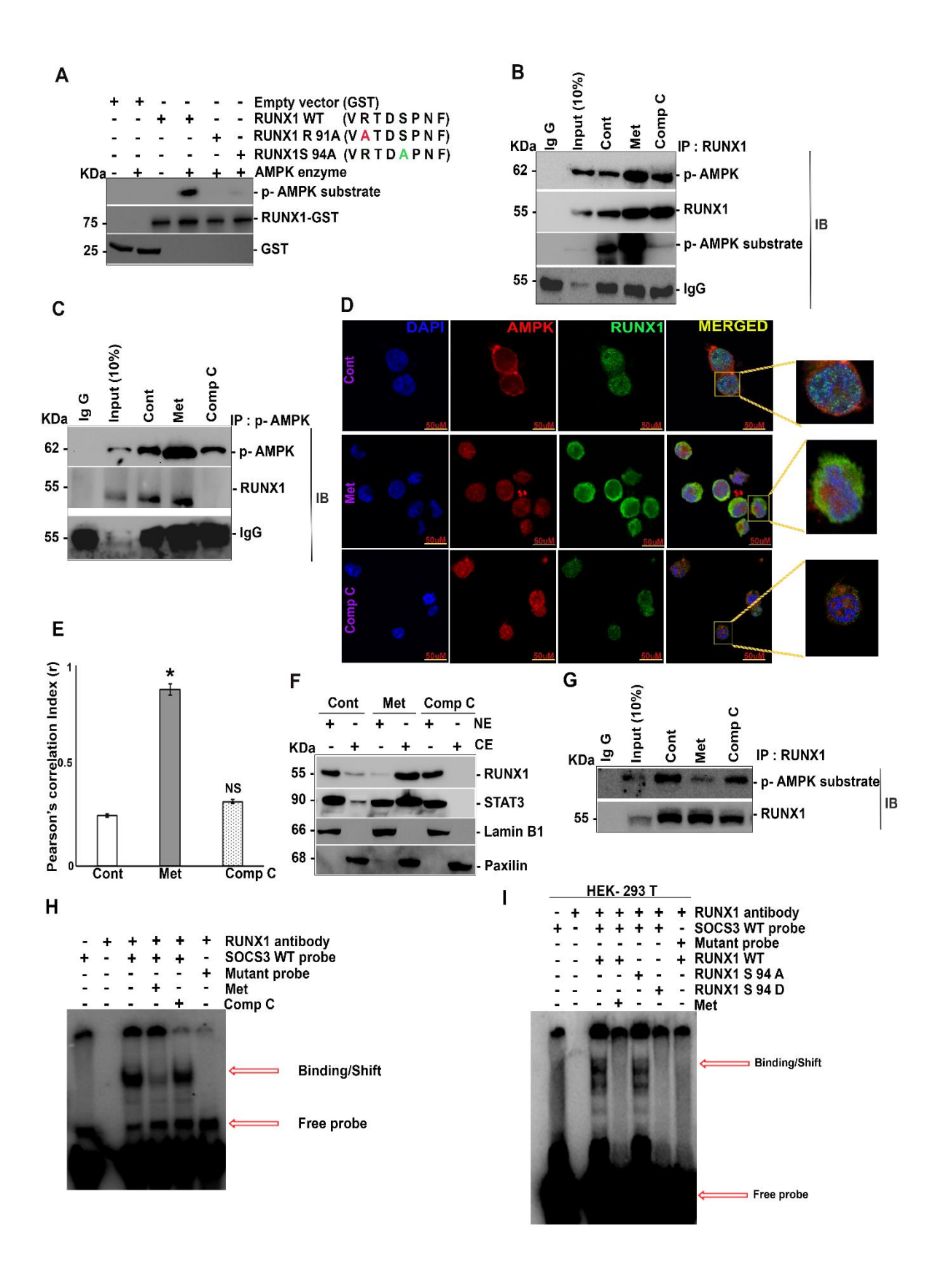


FIGURE 3: AMPK phosphorylates RUNX1 at Ser 94 position. A) Invitro phosphorylation of RUNX1 by AMPK at Ser 94 position detected by p-AMPK substrate specific antibody. B &C) Immunoprecipitation analysis of endogenous RUNX1 with AMPK in K562 WT cells post to treatment with either metformin (10mM) or treatment with compound C (5μM) for 12 hours, showing increased physical interaction in metformin treated lane. D) Co-localization analysis showing increased physical interaction between endogenous RUNX1 (Alexa 488) and AMPK (Alexa 546) in the presence of metformin treatment, following same treatment regime as mentioned earlier. E) Quantification of Immunofluorescence data using Image J software on three independent fields and experiments. F) Sub- cellular fractionation of K562 WT cells showing decreased nuclear localization of RUNX1 and STAT3 in metformin treated conditions (following same treatment regime as above). G) K562 WT cells were subjected to immunoprecipitation analysis of endogenous RUNX1 with p-AMPK substratespecific antibody post to nuclear fraction isolation, showing decreased phospho-RUNX1 in metformin treated lanes. H) K562 WT nuclear extracts were isolated post to treatment with either metformin (10mM) alone or with compound C (5µM) alone or none for 6 hours and subjected to EMSA with SOCS3 probe, showing decreased binding in metformin treated lanes. I) HEK-293 T cells were transfected with RUNX1 WT, S 94 A and S 94 D, with or without metformin (10mM) treatment post to transfection (after 48 hours) for 6 hours and nuclear extracts were subjected to EMSA, showcasing decreased binding in phospho mimic mutant. N=3, Mean ± S.E.M. \*p<0.05 versus control or as indicated, NSp>0.05 versus control or as indicated.

Cont: control, Met: metformin, comp C: compound C, CE: cytoplasmic extract, NE: nuclear extract, WT: wild type, IP: immunoprecipitation, IB: immunoblotting.

promote STAT3 activation through suppression of SOCS3, we have assessed the effect of RUNX1 Ser 94 phosphorylation on SOCS3 expression. Analysis of SOCS3 promoter revealed the presence of RUNX1 binding consensus at -355 bp upstream. Thus, we have analyzed RUNX1 binding on SOCS3 promoter in response to metformin treatment. Upon metformin treatment, RUNX1 binding on SOCS3 promoter was lost (Fig 3H). The role of RUNX1 Ser 94 phosphorylation was further confirmed by transfecting HEK-293 T (which were known to have either low or no endogenous RUNX1 levels) cells with RUNX1 wild type, RUNX1 S 94 A (phospho-null mutant) and RUNX1 S 94 D (phosphor-mimetic mutant) variants and nuclear extracts were subjected to EMSA. It could be seen that RUNX1 WT and phospho-null mutant had a potent binding to SOCS3 promoter compared to RUNX1 WT treated with metformin or phospho-mimetic mutant (Fig 3I).

### 1.1.3.3. AMPK inhibits STAT3 activation through RUNX1 Ser 94 phosphorylation

In our earlier section it was observed that metformin treatment resulted in increased cytoplasmic retention of both RUNX1 and STAT3. Thus, we analyzed the interaction between RUNX1 and STAT3 through immunoprecipitation, since one of the reasons behind increased

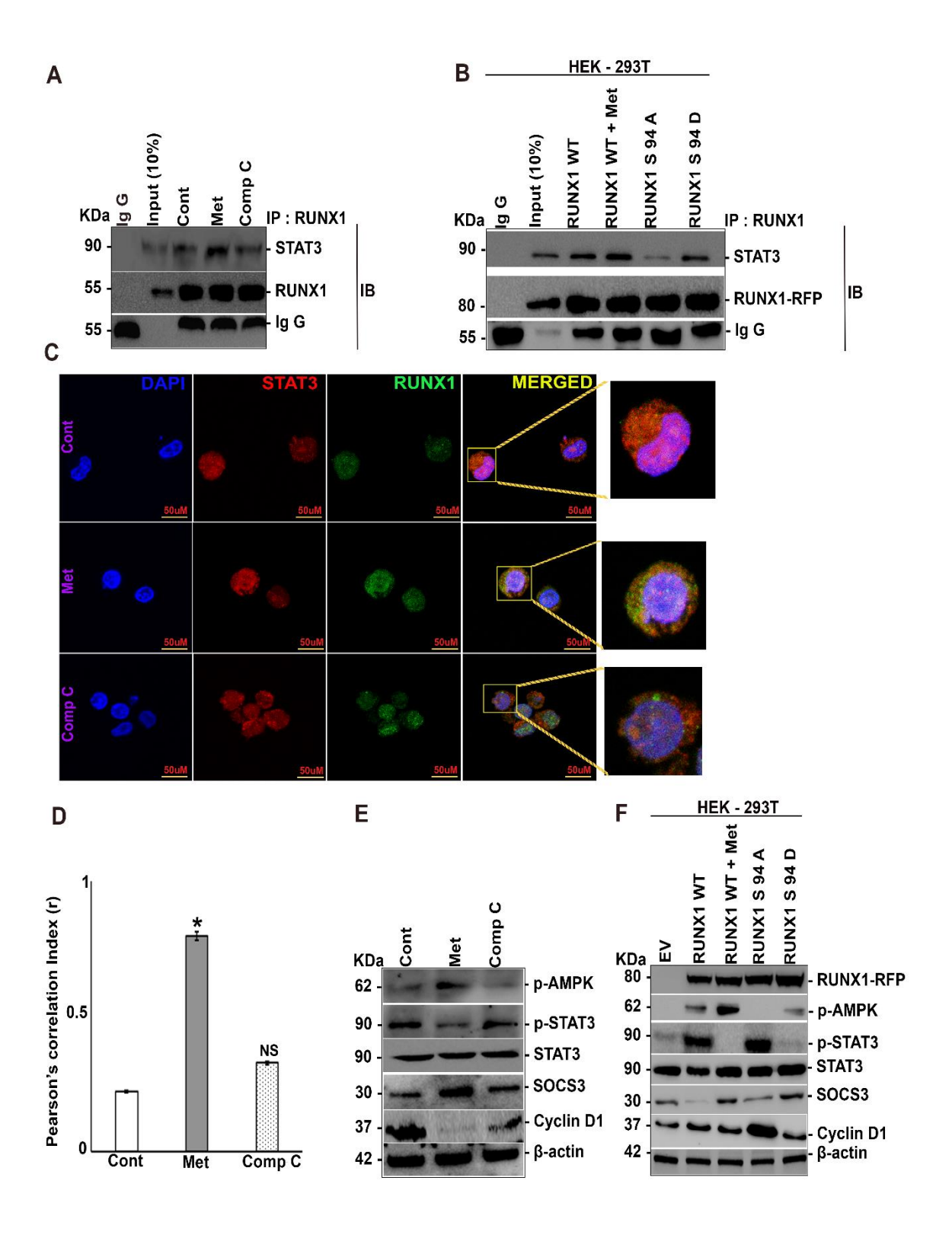


FIGURE 4: Phospho- RUNX1 inhibits STAT3 phosphorylation in K562 WT cells. A) Immunoprecipitation analysis of endogenous RUNX1 with STAT3 in K562 WT cells showing increased physical interaction post to treatment with metformin (treatment regime is same as above). B) Immunoprecipitation analysis of ectopically expressed RUNX1 site directed mutants with endogenous STAT3 in HEK-293 T cells in the presence of metformin (10mM, for 12 hours, given 48 hours after transfection) showing increased physical interaction in metformin treated lane and phospho mimic mutant lane. C) Co-localization analysis showing increased physical interaction between endogenous RUNX1 (Alexa 488) and STAT3 (Alexa 594) in the presence of metformin. D) Quantification of Immunofluorescence data using Image J software on three independent fields and experiments. E) Immunoblot analysis of K562 WT showing levels of p-STAT3, STAT3, SOCS3 and Cyclin D1 in response to metformin treatment alone for 12 hours or a with treatment of compound C (5μM). F) Immunoblot analysis of HEK-293T cells transfected with either RUNX1 WT or RUNX1 S 94 A or RUNX1 S 94 D with or without metformin (10mM) treatment post to transfection (after 48 hours) for 12 hours showing levels of p-STAT3, STAT3, SOCS3 and Cyclin D1. N=3, Mean ± S.E.M. \*p<0.1 versus control or as indicated. The immunofluorescence and quantification experiments were carried out on three independent fields.

Cont: control, Met: metformin, comp C: compound C, CE: cytoplasmic extract, NE: nuclear extract, WT: wild type, IP: immunoprecipitation, IB: immunoblotting.

cytoplasmic retention could be physical sequestration of RUNX1 and STAT3. Enrichment of STAT3 in immunoprecipitated lysates of RUNX1 was observed in metformin-treated cells but not in compound C treated cells (Fig 4A). The effect of RUNX1 Ser 94 phosphorylation on interaction between RUNX1 and STAT3 was further established by transfecting HEK 293T cells with RUNX1 wild type, phospho-null and phosphomimic variants followed by IP with RUNX1; Enrichment of STAT3 was seen in RUNX1 wild type treated with metformin and in phosphomimic mutant which was lost in case of phospho-null mutant (Fig 4B). The interaction between RUNX1 and STAT3 was further established in K562 (wild type) cells by immunofluorescence (Fig 4C &D). Metformin treatment resulted in reduced nuclear localization of both RUNX1 and STAT3, resulting in reduced expression of their target genes like Cyclin D1, D3 and BCL2 at both m-RNA (SF 1A) and protein level (Fig 4E; SF 1D &E). The role of RUNX1 Ser 94 phosphorylation in mediating the inhibitory effects of AMPK was confirmed by transfecting HEK 293T cells with RUNX1 wild type, phospho-null and phosphomimic variants, followed by immunoblotting for STAT3 targets. It was observed that activation of STAT3 signaling (measured through p-STAT3) and expression of STAT3 targets, was lost in RUNX1 wild type treated with metformin and in phosphomimic mutant whereas it was increased in phospho-null mutant. Correlating with the phosphorylation status of STAT3,

SOCS3 levels were increased in RUNX1 wild type treated with metformin and in phosphomimic mutant but were decreased in phospho-null mutant (Fig 4F &SF 1F).

# **DISCUSSION**

### 1.1.4. DISCUSSION

RUNX1 is a novel substrate of AMPK and AMPK phosphorylates RUNX1 at Ser 94 position, resulting in decreased nuclear localization of RUNX1. The increased cytoplasmic retention of RUNX1 decreases the transactivation of RUNX1 and at the same time increases its binding with STAT3. RUNX1 negatively regulates SOCS3 (49, 50), which is a repressor of STAT3 signaling (51) and this repression was lost owing to cytosolic retention of RUNX1 due to metformin treatment which was reversed when treated with compound C. Metformin treatment resulted in cytoplasmic retention of both RUNX1 and STAT3, resulting in downregulation of their target genes. The downstream targets of RUNX1 and STAT3 include players critical for cell proliferation like Cyclin D's (56, 57) and anti-apoptotic regulation like BCL2, MCL1 etc., (58, 59). The RUNX1 phospho-mimic and phosho-null mutants have further established the effect of RUNX1 Ser 94 phosphorylation on inducing RUNX1 interaction with STAT3, where the phospho-null and WT clones had minimal interaction with STAT3, whilst phospho mutant and WT treated with metformin had increased interaction with STAT3. Metformin through AMPK/ RUNX1 Ser 94 phosphorylation upregulated SOCS3, which results in dephosphorylation of STAT3, that is key to activation of STAT3 pathway (60). Metformin treatment along with RUNX1 WT clone resulted in absence of RUNX1 binding to SOCS3 promoter similar to phosphor-mimic mutant whilst RUNX1 WT and phosphor-null mutant had binding to SOCS3 promoter. These findings reflected in suppression of STAT3 targets when ectopically expressed in HEK-293 T cells. Summarizing the results, it sheds light on inhibitory effect of metformin on STAT3 activation by upregulation of SOCS3 expression and phospho-RUNX1 mediated physical sequestration in K562 cells (Fig 5).

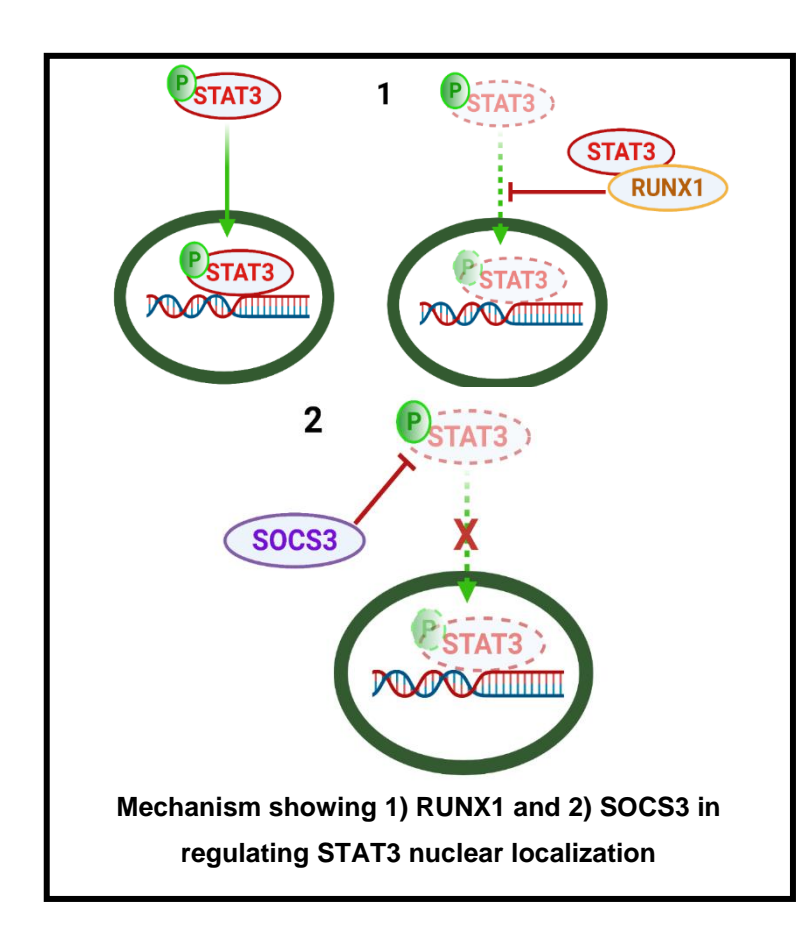


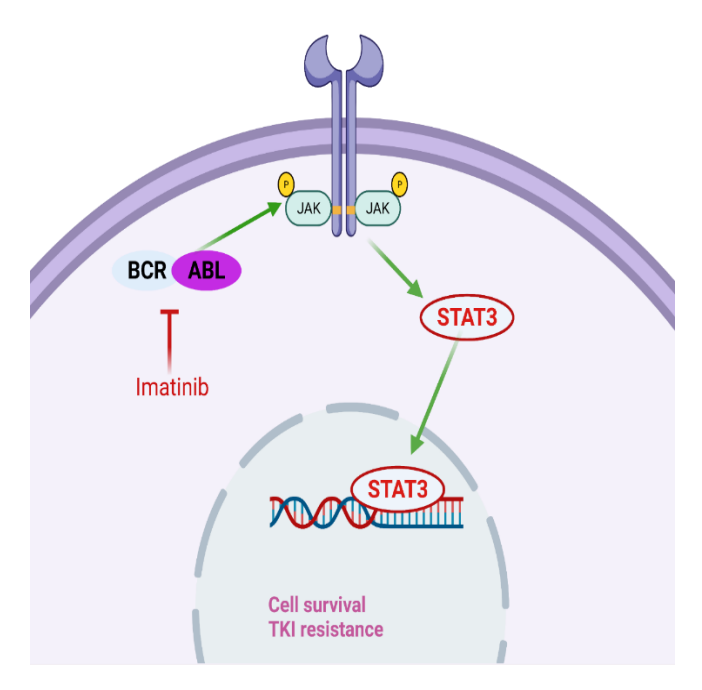
**FIGURE** 5: Metformin inhibits STAT3 activation and nuclear localization. Under STAT3 normal conditions signaling is activated through tyrosine phosphorylation of STAT3 resulting in nuclear localization and transcriptional activation of STAT3. Metformin inhibits STAT3 phosphorylation by 1) cytoplasmic retention of STAT3 through RUNX1 Ser 94 phosphorylation mediated physical sequestration and through 2) upregulation of SOCS3 expression.

### **OBJECTIVE 1.2**

Analyzing the role of AMPK substrates on drug sensitivity of CML subjects.

### 1.2.1. LITERATURE REVIEW

Imatinib is the golden standard of CML treatment, where imatinib blocks the ATP binding domain of BCR-ABL, which is needed for carrying out kinase activity of BCR-ABL (61, 62). However, imatinib treatment is not free of generation of drug resistance in CML subjects (63-66). BCR-ABL aids in progression of CML by phosphorylating several down streams signaling molecules like JAK1/2 (Fig 6), ERK1/2 that are involved in cell cycle progression and anti-apoptotic signaling (67, 68). ABL consists of catalytic kinase domain which is involved in phosphorylation of downstream targets. For sustained CML growth constitutively active BCR-ABL is a prerequisite (69). Thus, there is a need to explore other alternative drug targets for CML treatment, which can be used in combination with imatinib for treatment.



resistance. Under normal conditions STAT3 signaling is activated through tyrosine phosphorylation of STAT3 by growth factor activated phosphorylated JAK, resulting in nuclear localization and transcriptional activation of STAT3. However, in context of CML, BCR-ABL is involved in phosphorylation of JAK resulting in aberrant activation of STAT3, which in turn activates genes involved in generation of TKI resistance and cell survival.

One such targets is HSP-90, being a chimeric fusion protein BCR-ABL requires HSP-90 for its stabilization. Thus, HSP-90 inhibitors like geldanamycin (or 17-AAG) have a potential in CML treatment (70-72). Hitherto, HSP-90 clinical trials have displayed mixed results (73, 74), owing to activation of heat shock response and multi drug response in cancer cells (75). HSP-90 inhibits activation of heat shock response by physical sequestration of HSF-1 (76). Thus, upon HSP-90 inhibition by geldanamycin, HSF-1 is indirectly activated which then results in activation of HSP-70, 27 etc., (75, 77) which can aid in progression of CML.

So, targeting of heat shock response through HSF-1 can be a promising target for overcoming geldanamycin resistance.

In order to understand the effect of metformin in improving drug sensitivity of CML subjects we have developed imatinib and geldanamycin resistant K562 lines. Our earlier work has shown that there is a co-evolution of imatinib resistance in K562 cells along with geldanamycin resistance. Where in K562-GR1 cells which were never exposed to imatinib throughout their screening for geldanamycin resistance have developed imatinib resistance also (78). Recent works and our earlier data, have shed light on anti-leukemic activity of metformin (79, 80). So, we have analyzed the role of metformin in overcoming imatinib-geldanamycin dual resistance.



### 1.2.2. MATERIALS and METHODS

### 1.2.2.1. Cell culture

K562 wild type (WT), imatinib resistant (IR1, IR2, GR1, IR2-GR1 (IGR1) and IR2-GR2 (IGR2)) cells were cultured in RPMI-1640 (Gibco, USA) medium supplemented with 10% FBS, 1% pen-strep. Additionally, for IR1 & IR2 0.25 μM imatinib was added to growth medium, while GR1, IGR1 and IGR2 were cultured in the presence of 0.25 μM geldanamycin. HEK-293 T cells were cultured in DMEM (Gibco, USA) medium supplemented with 10% FBS (Gibco, USA), 1% pen-strep (Gibco, USA). All cell lines were maintained in 5% CO<sub>2</sub> incubator at 37°C.

#### **1.2.2.2.** *Chemicals*

Metformin, imatinib, 5-aminoimidiazole-4-carboxamide ribonucleotide (AICAR), MG-132 and dorsomorphin (compound C) were purchased from Sigma (USA). Geldanamycin (17-AAG) was procured from TCI chemicals (Japan). Imatinib, MG-132 and geldanamycin were dissolved in DMSO (Finar, India).

### 1.2.2.3. Isolation of PBMCs from CML patients

Samples from human subjects were collected with prior approval from institutional ethics committee and informed patient consent by adhering to approved protocols (EC/NIMS/2350/2019). Whole blood (~10ml) from each CML patient and age matched normal individuals as controls were collected in heparinized vacutainers (BD, USA) along with duly signed consent forms. Peripheral blood mononuclear cells (PBMCs) were isolated using histopaque (Sigma, USA). 10 mL of histopaque was added to a 50 ml tube an hour before the initiation of isolation by slowly adding equal volumes of blood without disturbing the histopaque layer and centrifuged at 400 x g for 30 minutes with zero break in a swing bucket rotor centrifuge. After centrifugation, upper layer was discarded, interphase was collected separately and washed twice with 1X PBS. The pellet was resuspended to make a single cell suspension and grown in RPMI-1640 medium supplemented with 10% FBS, 2mM L-glutamine (HiMedia, India), 1% non-essential amino acids (Gibco, USA) 1% sodium pyruvate (Gibco, USA) and 1% pen-strep.

### 1.2.2.4. shRNA transduction and permanent line generation

shRNA's for RUNX1 were shRNA 1 (TRCN0000338427), shRNA 2 (TRCN0000338492) (Sigma, USA) along with Scr shRNA were transfected into HEK-293T

cells using Lipofectamine 3000 (Thermo Fischer, USA) as described above. 48 hours post to transfection the medium containing lenti viral particles was collected and stored in -80°C. K562 cells were plated in a 96 well plate and treated with puromycin to determine final concentration of puromycin to be used for selection. Lenti viral particles were thawed on ice and added to K562 cells and were centrifuged at 800Xg for 30 minutes at room temperature in medium containing polybrene (8µg/mL) (Sigma, USA). The pellet was resuspended in fresh medium without polybrene and seeded in a six well plate. 72 hours post transduction medium was replaced with medium containing puromycin and maintained until death was observed in control cells.

### 1.2.2.5. Nuclear and cytosolic extraction

Was performed as mentioned in the earlier section (1.1.2.6).

### 1.2.2.6. Plasmid transfection

For ectopic expression of RUNX and its mutants, RUNX1 knock-down cells were transfected with 2µg of purified plasmid (RUNX1 WT or S 94 A or S 94 D) using Lipofectamine-3000 (Thermo Fischer, USA) as described in 1.1.2.8 methods section.

### 1.2.2.7. Cell viability assay

4,000 cells per well in a 96 well plate was seeded either with or without indicated drugs to RPMI-1640 medium of 250μL final volume and were grown for 3 days. AlamarBlue (Invitrogen, USA) was then added and incubated for 4 hours. Following incubation, fluorescence was measured (excitation at 560nM and emission at 590nM).

### 12.2.8. *Immunoblotting*

Protein isolation and SDS-PAGE was done as described in 1.1.2.9 methods section. The blots were probed for antibodies HSF1, BCR-ABL, MDR-1, HSP-70, Ubiquitin, RUNX1/AML1, GST, CDH11, SOCS3, Cyclin D1, AMPK, β-actin (Santa Cruz Biotechnology Inc., USA.) p-STAT3(Y705), STAT3, BCL2, Lamin B1 (Abcam, USA.) p-AMPK, p-AMPK substrate motif specific antibodies (Cell Signaling Technologies, USA.)

### 1.2.2.9. Immunoprecipitation (IP)

Cells were collected as described earlier. For pull down 750µg (incase of cell lines) or 500 µg (incase of PBMCs or tissues) of protein was taken along with 1 µg of antibody (p-AMPK, STAT3, RUNX1 or HSF1) and left at 4°C overnight for binding. Protein agarose-A-G

plus beads (Santa Cruz Biotechnology Inc., USA) were used for pulling down antigen antibody complex.

### 1.2.2.10. RNA isolation and real time PCR (RT-PCR)

RNA isolation and quantification was carried out as described in earlier section (1.1.2.11). The sequences of primers used were:

Target	Forward primer (5'-3')	Reverse primer (5'-3')
HSF1	GGAAAGTGGTCCACATCGAG	TTCACTCTCCCGCAGGATGG
HSP70	AGCTAAAGGCCCGTCTATCG	AACACCCCACACAGGAGTA
Actin	GAGAGGGAAATCGTGCGTGAC	CATCTGCTGGAAGGTGGACA

### 1.2.2.11. Confocal microscopy

Cells were stained with primary antibodies AMPK, RUNX1/AML1, STAT3 or HSF1 for 2 hours at room temperature, followed by respective fluorescence secondary antibody staining (Alexa Flour 488 and 546, Invitrogen, USA)). Cells were counterstained with 4',6-diamino-2-phenylindole (DAPI) (Thermo Scientific, USA) for nuclei and images were captured using laser scanning confocal microscope (LSM 780, Carl Zesis, Germany).

### 1.2.2.12. Statistical analysis

All data points are represented as mean  $\pm$  SEM. Statistical analysis was done using one-way ANOVA. P < 0.05 was considered to be statistically significant. All data points were done in duplicates and a minimum of set of three independent experiments were carried out for all in-vitro studies and patient data.

# **RESULTS**

### **1.2.3. RESULTS**

### 1.2.3.1. RUNX1 serves as an AMPK substrate in imatinib resistance cells

RUNX1 is one of the key drivers involved in imatinib resistance. So, we analyzed if RUNX1 and AMPK interactions hold true even in imatinib resistant cell lines. For this we have used imatinib resistant K562 cells, namely K562-IR1 and K562- IR2 (here after referred as IR1 and IR2) both having a differential sensitivity towards imatinib (IC50:  $1.2 \pm 0.2 \mu M$  and  $2.2 \pm 0.2 \mu M$ 0.1 µM respectively). Both IR1 and IR2 were treated with either metformin or compound C and subjected to IP by RUNX1. Both in IR1 and IR2 there was an enrichment of p-AMPK in metformin treated lysates and which was lost in compound C treatment (Fig 7A). Immunoblotting with p-AMPK substrate specific antibody revealed that indeed RUNX1 was a substrate of AMPK in both IR1 and IR2 (Fig 7A). This interaction was further confirmed by immunofluorescence in both IR1 (SF 2A &B) and IR2 (Fig 7B &C) cells. We then analyzed if RUNX1 Ser 94 phosphorylation is inhibiting the nuclear localization of RUNX1 and STAT3 in imatinib resistant cells. Upon treatment with metformin alone or in combination with imatinib, there was a decrease in nuclear localization of both RUNX1 and STAT3 in IR1 (Fig. 7D; SF 2C &D) and IR2 (Fig 7E; SF 2E &F). However, when treated with imatinib alone, nuclear localization of RUNX1 and STAT3 was high compared to untreated in IR1 (Fig 7D; SF 2C &D) and IR2 (Fig 7E; SF 2E &F). Both RUNX1 and STAT3 regulate cell proliferation thus, we next analyzed the effect of metformin treatment on viability of K562 WT, IR1 and IR2 cells. K562 cells were treated with imatinib alone or in combination with metformin (IC50:  $0.25 \pm 0.05$  mM) and cell viability was assessed. It was observed that compared to wild type both IR1 and IR2 were resistant to imatinib alone treatment whereas in presence of metformin the sensitivity of both IR1 and IR2 towards imatinib has increased, since the IC50 for IR1 came down to  $0.75 \pm 0.1 \,\mu\text{M}$  from  $1.2 \pm 0.2 \,\mu\text{M}$  (Fig 7F) and for IR2 it changed to  $0.7 \pm 0.2 \,\mu\text{M}$ from  $2.2 \pm 0.2 \,\mu\text{M}$  (Fig 7G).

### 1.2.3.2. RUNX1 Ser 94 phosphorylation inhibits STAT3 activation in imatinib resistant cells

IR1 and IR2 cells were treated with either metformin or imatinib, either alone or in combination, and subjected to immunoprecipitation by RUNX1. STAT3 enrichment was observed in lysates treated with either metformin alone or in combination with imatinib compared to untreated and imatinib alone (Fig 8A). This was further validated by immunofluorescence in both IR1 (SF 3A &B) and IR2 (Fig 8B &C) cells. IR1 and IR2 cells treated with either metformin or imatinib alone or in combination were subjected to

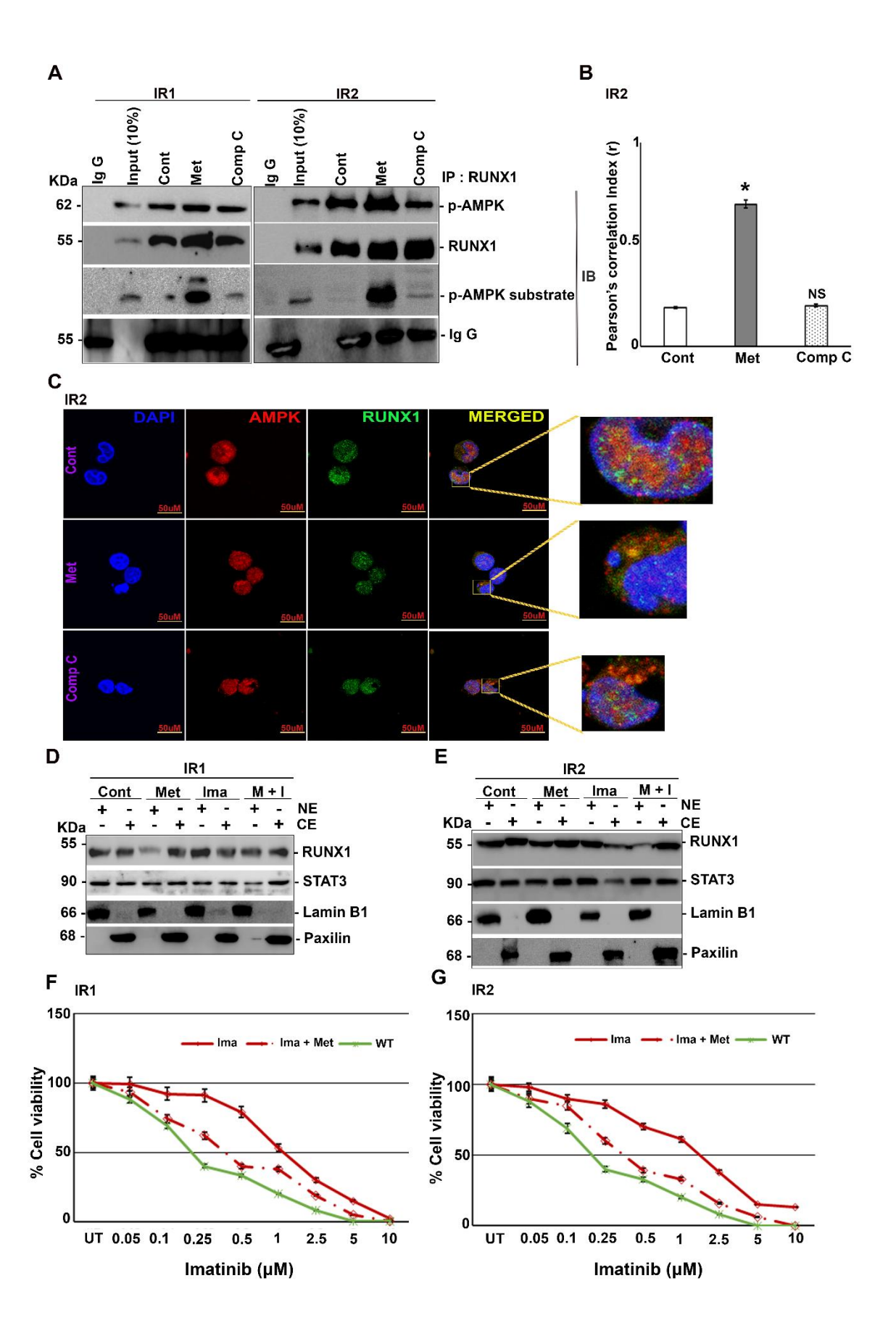


FIGURE 7: Metformin improves imatinib sensitivity of resistant lines (IR1 and IR2) through p-AMPK/ RUNX1 axis. A) Immunoprecipitation analysis of endogenous RUNX1 with p-AMPK in K562 IR1 and IR2 cells post to treatment with either metformin (10 mM) alone or with compound C (5 µM) for 12 hours, showing increased physical interaction in metformin treated lane. B) Quantification of Immunofluorescence data using Image J software on three independent fields and experiments. C) Co-localization analysis showing increased physical interaction between endogenous RUNX1 (Alexa 488) and AMPK (Alexa 594) in the presence of metformin in K562 IR2 cells (treatment regime is same as above). D) Sub- cellular fractionation of K562 IR1 cells showing with metformin (10mM) alone or with imatinib (1μM) or none or both (imatinib 1μM; metformin 10mM) for 6 hours, showcasing decreased nuclear localization of RUNX1 and STAT3 in metformin treated conditions. E) Sub- cellular fractionation of K562 IR2 cells following similar treatment conditions, showing decreased nuclear localization of RUNX1 and STAT3 in metformin treated conditions. F) Cell viability analysis of K562 IR1 cells in response to imatinib treatment alone or along with metformin (0.25 mM) for 72 hours with K562 WT as control, showing decreased cell viability in presence of metformin. G) Cell viability analysis of K562 IR2 cells in response to imatinib treatment alone or along with metformin (0.25 mM) for 72 hours with K562 WT as control, showing decreased cell viability in presence of metformin. N=3, Mean ± S.E.M. \*p<0.05 versus control or as indicated. The immunofluorescence and quantification experiments were carried out on three independent fields.

Cont: control, Met: metformin, comp C: compound C, Ima: imatinib, CE: cytoplasmic extract, NE: nuclear extract, WT: wild type, IP: immunoprecipitation, IB: immunoblotting.

immunoblotting. Following metformin treatment, either alone or in combination with imatinib, the activation of STAT3 (Fig 8D &SF 3G) and its downstream targets like Cyclin D1 and BCL2 were reduced compared to untreated and imatinib alone (Fig 8D; SF 3C-F). However, SOCS3 levels were increased in metformin treatment alone or in combination with imatinib (Fig 8D & SF 3C-F). We next analyzed the role of RUNX1 in mediating the anti-proliferative effects of metformin. RUNX1 knockdown was carried out in both IR1 and IR2 cells using shRNA's mediated RUNX1 knockdown stable cell lines. Out of shRNA 1 and shRNA 2, the efficiency of knockdown by shRNA 2 was significant, thus we have used shRNA 2 stable lines for all further experiments (SF 4A &B). Upon RUNX1 knockdown, the anti-proliferative effects of metformin were lost (Fig 8E &SF 4G). IC50 for imatinib has increased to  $1 \pm 0.2$  $\mu$ M for IR1 from 0.3  $\pm$  0.1  $\mu$ M (calculated for imatinib treatment along with metformin) post RUNX1 knockdown, which is similar to imatinib alone treated scenario (SF 4G). Similar results were observed in IR2 where IC50 has increased to  $1.25 \pm 0.2~\mu M$  from  $0.75 \pm 0.1~\mu M$ (Fig 8E). In both IR1 and IR2 RUNX1 knockdown has resulted in marginal reduction of cell viability, as RUNX1 WT is known to promote cell proliferation in leukemia (81). To decipher the role of RUNX1 Ser 94 phosphorylation in mediating metformin effects, RUNX1 WT,

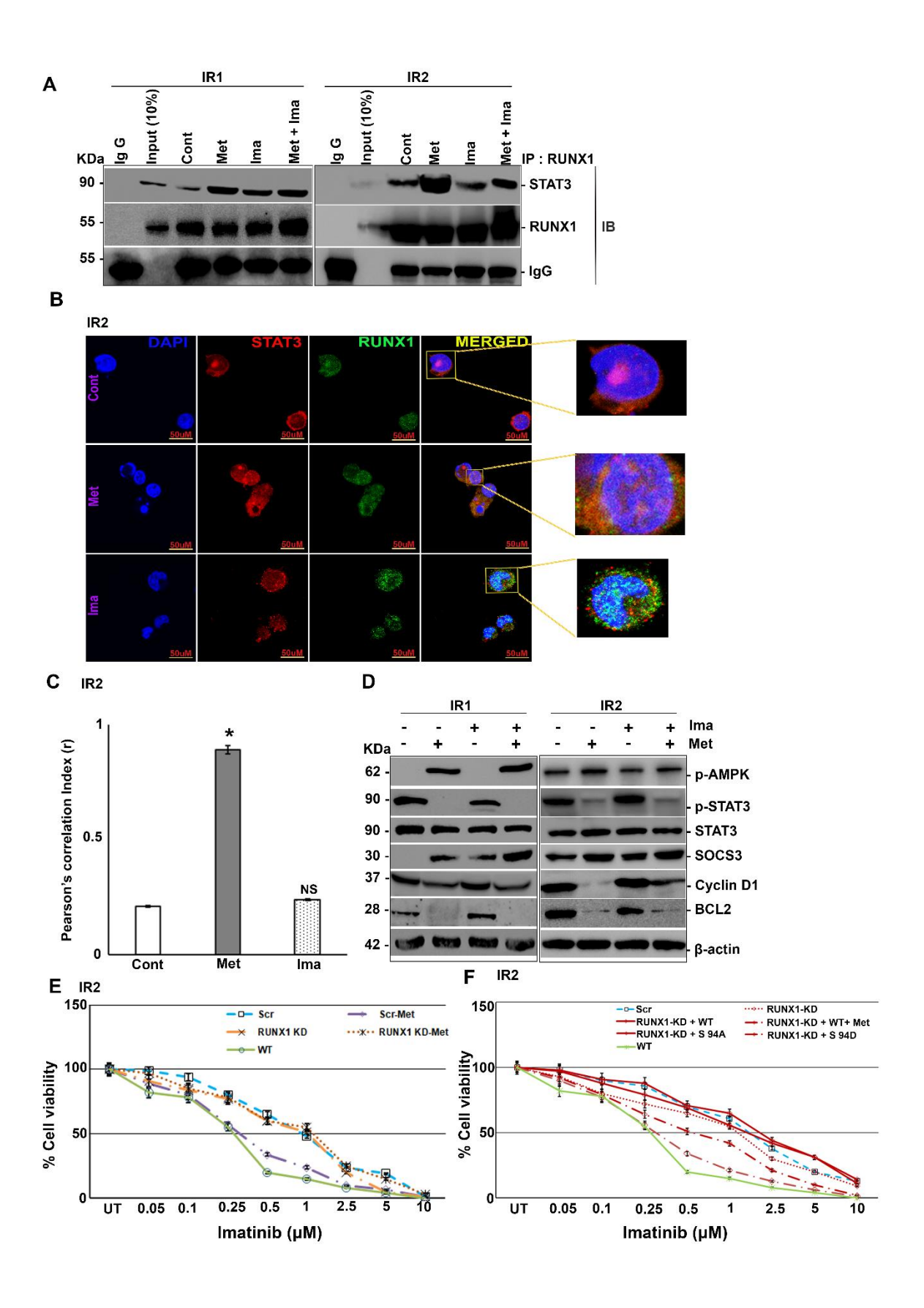
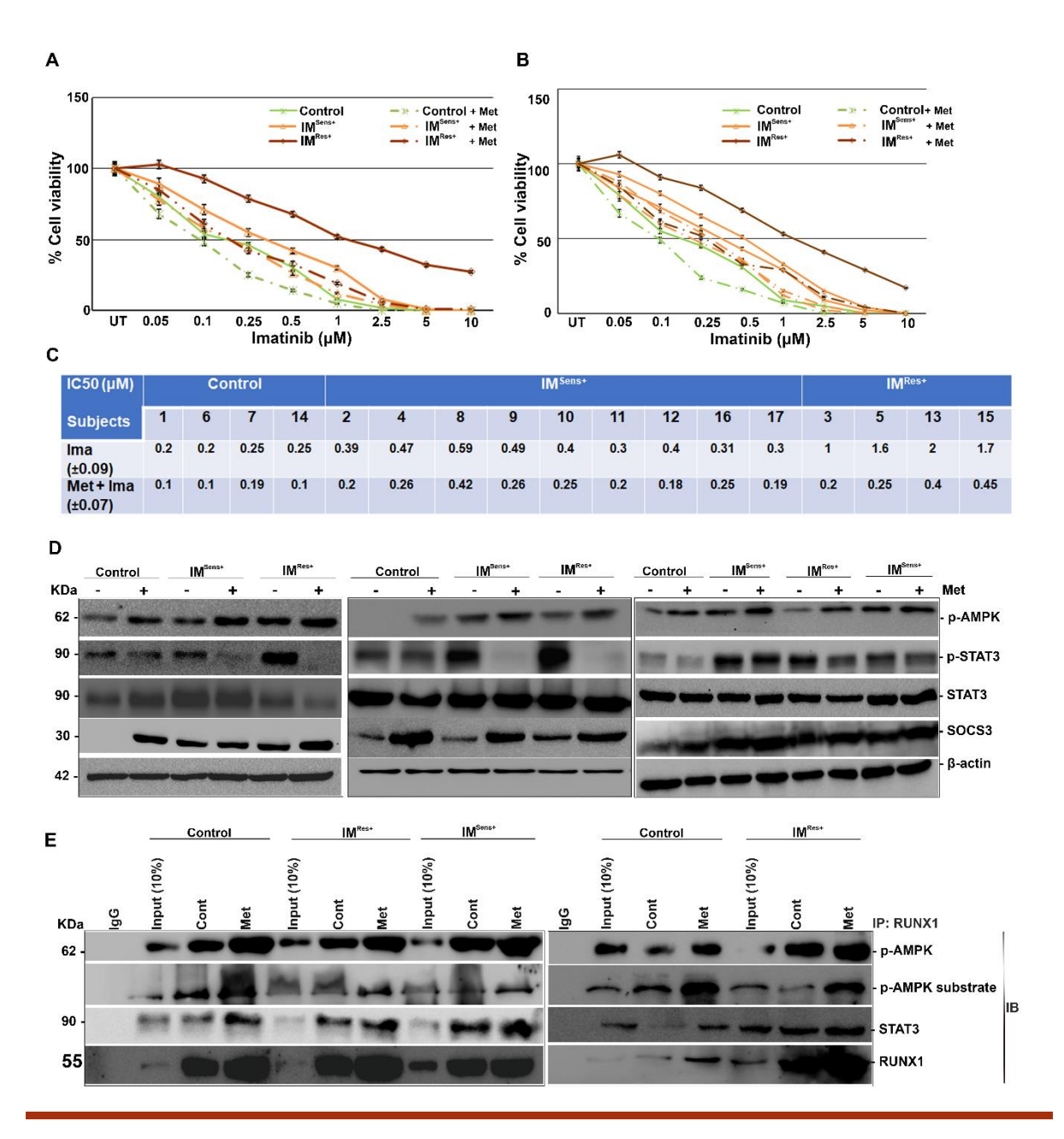


FIGURE 8: Metformin inhibits STAT3 phosphorylation through RUNX1 Ser 94 phosphorylation. A) Immunoprecipitation analysis of endogenous RUNX1 with STAT3 in K562 IR1 and IR2 cells post to treatment with either metformin (10 mM) alone or imatinib (1 µM) alone or none or both for 12 hours, showing increased physical interaction in metformin treated lane. B) Co-localization analysis in K562 IR2 cells with similar treatment conditions as above for metformin and imatinib, showing increased physical interaction between endogenous RUNX1 (Alexa 488) and STAT3 (Alexa 594) in the presence of metformin. C) Quantification of Immunofluorescence data using Image J software on three independent fields and experiments. D) Immunoblot analysis of K562 IR1 and IR2 cells showing levels of p-STAT3, STAT3, SOCS3, Cyclin D1 and BCL2 in response to metformin (10 mM) treatment alone or along with imatinib (1 μM) or none for 12 hours. E) Cell viability analysis of K562 IR2-RUNX1 KD cells in response to imatinib treatment alone or along with metformin (0.25 mM) for 72 hours with K562 WT as control, showing decreased cell viability in presence of metformin which was reversed upon RUNX1 KD. F) Cell viability analysis of K562 IR2-RUNX1 KD, RUNX1 WT, RUNX1 S 94 A and RUNX1 S 94 D transduced cells in response to imatinib treatment alone or along with metformin (0.25 mM) for 72 hours with K562 WT as control, showing decreased cell viability in presence of metformin and in RUNX1 S 94 D cells which was reversed upon RUNX1 KD and in RUNX1 WT and RUNX1 S 94 A. N=3, Mean ± S.E.M. NSp>0.05 versus control, \*p<0.05 versus control or as indicated. The immunofluorescence and quantification experiments were carried out on three independent fields.

Cont: control, met: metformin, Ima: imatinib, WT: wild type, Scr: scrambled, KD: knock down, IP: immunoprecipitation, IB: immunoblotting, NS: non-significant.

RUNX1 S 94 A and RUNX1 S 94 D were expressed in RUNX1 knockdown IR1 and IR2 cells (SF 4C-F), followed by treatment with imatinib alone or in combination with metformin. RUNX1 KD resulted in reduction of imatinib IC50 by a factor of 0.25, which was reverted to original when RUNX1 WT expression was restored in both IR1 (SF 4H) and IR2 (Fig 8F). However, when treated with metformin along with imatinib in RUNX1 WT overexpressed cells, imatinib sensitivity has improved as IC50 values changed to 0.3 ± 0.1 μM and 0.75 ± 0.18 μM for IR1 and IR2 respectively. But when cells were transfected with phospho-null variant, there was a decrease in imatinib sensitivity as IC50 values were near to that of control (scrambled) in both IR1 and IR2 cells. The effect was reversed when IR1 and IR2 were transfected with phosphomimic variant, which followed the trend similar to K562 WT (SF 4H & Fig 8F). In line with reduced cell proliferation, STAT3 phosphorylation was reduced in both IR1, and IR2 transfected with RUNX1 shRNA 2 and RUNX1 S 94 D, with contaminant increase in SOCS3 expression (SF 4C-F).



**FIGURE 9:** Metformin reduces the viability of PBMCs from CML subjects through AMPK/ RUNX1 Ser 94/ STAT3 axis. A, &B) Cell viability of PBMCs derived from CML subjects in response to treatment with imatinib alone or along with 0.25 mM metformin for 72 hours, showing decreased viability in presence of metformin. C) Tabulated IC50 values of PBMCs for imatinib treatment with and without presence of metformin. D) Immunoblot analysis of PBMCs showing levels of p-STAT3, STAT3 and SOCS3 in response to metformin (10 mM) treatment for 12 hours. E) Immunoprecipitation analysis of endogenous RUNX1 with p-AMPK and STAT3 in PBMCs post to treatment with metformin (10 mM) showing increased physical interaction in metformin treated lanes. N=3, Mean ± S.E.M.

Cont: control, Met: metformin, Subj: subject, IP: immunoprecipitation, IB: immunoblotting, Control: healthy subjects, IM <sup>Sens+</sup>: imatinib sensitive subjects, IM <sup>Res+</sup>: imatinib resistant subjects.

# 1.2.3.3. Metformin improves imatinib sensitivity in imatinib resistant subjects through AMPK/RUNX1 S 94 axis

From the above observations, it was clear that metformin could increase imatinib sensitivity through the p-AMPK/RUNX1 axis by inhibiting activation of the STAT3 pathway. Thus, here we intend to validate the same observation using peripheral blood monocytes (PBMCs) derived from CML subjects and age-matched healthy subjects of sample size n=17, where healthy subjects (controls) (n=4: Subj 1, 6, 7 &14), imatinib-sensitive subjects (IM Sen+) (n=9: Subj 2, 4, 8-12, 16, 17) and imatinib-resistant subjects (IM Res+) (n=4: subj 3, 5, 13 & 15) were treated with either imatinib alone or in combination with metformin and cell viability was assessed. Metformin treatment resulted in increased imatinib sensitivity of both imatinib subjects as well as imatinib resistant subjects as well as in control subjects (Fig 9A-C; SF 5A &B). However, the fold by which imatinib sensitivity was increased is high in imatinib resistant (IM Res+) subjects where the IC50 was decreased by 4-6-fold upon metformin treatment. IC50 for imatinib in control and imatinib sensitive subjects (IM Sen+) was decreased by 1.25-2 folds in both groups, which is low compared to imatinib resistant subjects (Fig 9C). Since, metformin improved imatinib sensitivity we then analyzed the activation of STAT3 pathway. There was a decrease in STAT3 activation in PBMCs derived from both imatinib sensitive and imatinibresistant subjects post to metformin (10mM for 12 hours) treatment (Fig 9D; SF 5C, 9A-D). Simultaneously, there was an increase in SOCS3 expression (Fig 9D; SF 4E&F). Next, RUNX1/AMPK and STAT3 interactions were analyzed. Upon treatment with metformin, it was seen that there was an enrichment of p-AMPK and RUNX1 phosphorylation as assessed by p-AMPK substrate-specific antibody in RUNX1-antibody pull-down lysates and along with STAT3 enrichment (Fig 9E).

# 1.2.3.4. Metformin inhibits expression of HSP70 and p-STAT3 in imatinib-geldanamycin double resistant lines

Since metformin treatment could improve imatinib sensitivity of imatinib resistant lines, we next went on to confirm the effect of metformin on imatinib-geldanamycin double resistance, as there was a co-evolution of imatinib-geldanamycin double resistance. For thus we have used K562-GR1, IGR1 and IGR2 cell lines which were previously shown to exhibit varying degrees of double resistance (78). HSP70 and STAT3 are the major pathways involved in generation of imatinib-geldanamycin double resistance (75, 77). Thus, we have first analyzed the levels of HSP70 and p-STAT3 in imatinib-geldanamycin double resistance lines compared to K562-WT. It could be seen that compared to WT all the three resistant lines GR1,

IGR1 and IGR2 had higher levels of both HSP70 and p-STAT3 (Fig 10A). Next, we have treated K562 WT and double resistant lines with metformin or with compound C and the expression of HSP-70 and p-STAT3 were analyzed. It was seen that post to metformin treatment in both K562 WT (SF 6A &B) and double resistant lines (Fig 10B &C) expression of HSP-70 was decreased at both protein as well as mRNA levels. In line with HSP-70 expression, phosphorylation of STAT3 was also reduced post to metformin treatment (Fig 10B). Phosphorylation of STAT3 is a prerequisite for transcriptional activity of STAT3; thus, we next analyzed the expression of STAT3 targets CYCLIN D1 and BCL2. It was observed that expression of CYCLIN D1 and BCL2 was reduced post to metformin treatment at both

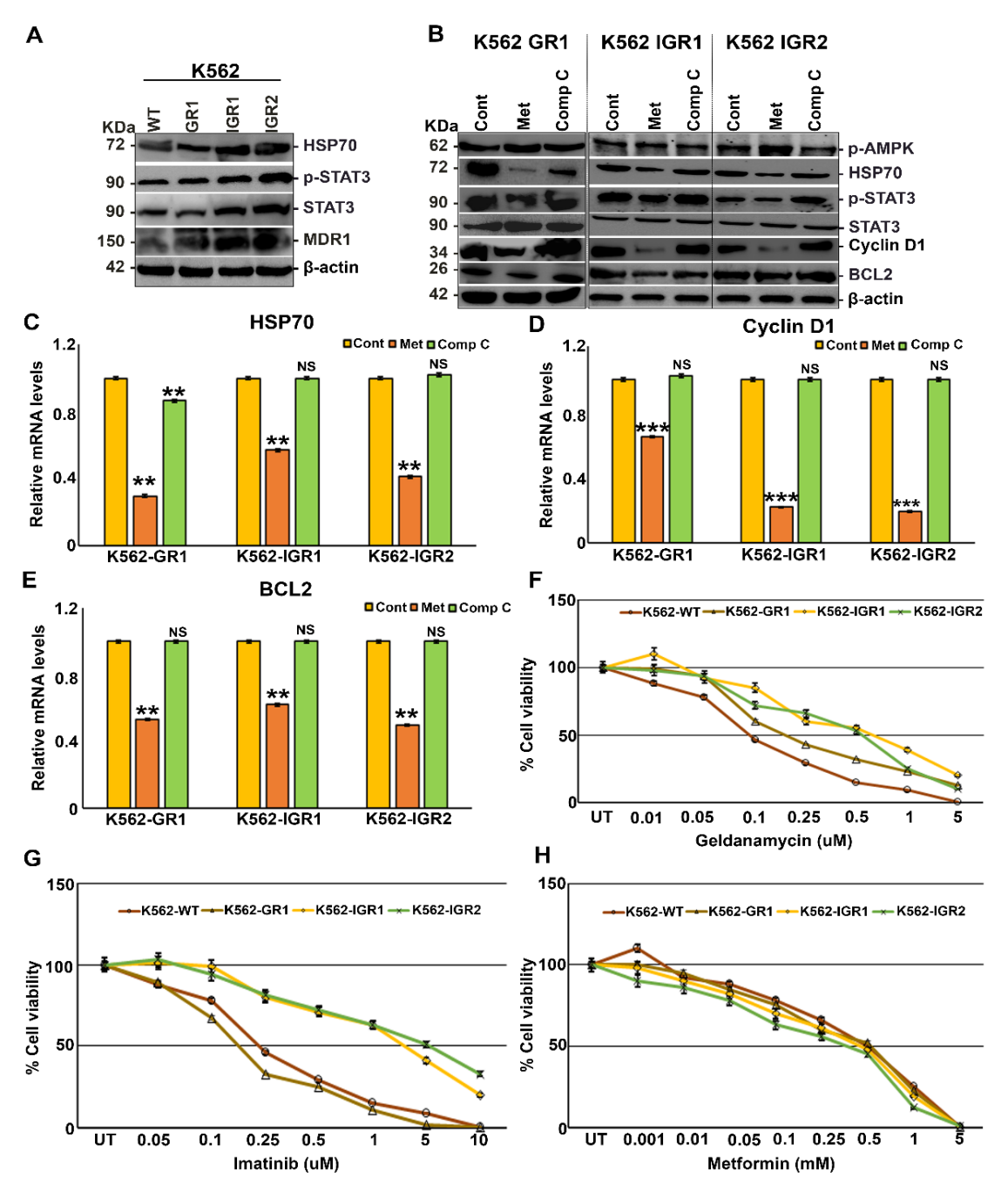


**FIGURE 10:** Metformin inhibits expression of HSP70 and p-STAT3 in imatinib-geldanamycin double resistant lines. **A)** K562-WT and double resistant cell lines were subjected to immunoblot analysis to assess HSP70, p-STAT3 and MDR1 levels. **B)** K562- GR1, IGR1 & IGR2 cells were subjected to metformin (10 mM for 12 hours) or compound C (5 μM for 12 hours) or none and immunoblot analysis was carried out to assess levels of STAT3 activation and its targets. K562- GR1, K562- IGR1 and IGR2 cells were treated with either metformin (10 mM) or with compound C (5 μM) or none for 6 hours and subjected to RT- PCR analysis to analyze levels of **C)** HSP70, **D)** CYCLIN D1 and **E)** BCL2. K562- GR1, K562- IGR1 and IGR2 cells were treated with either **F)** geldanamycin or **G)** imatinib or **H)** metformin at indicated concentrations for 72 hours and cell viability was assessed by alamar blue. Mean  $\pm$  S.E.M.; N=3, \*\*p<0.005 versus control, \*\*\*p<0.0005 versus control, NS p>0.05 versus control.

Cont: control, Met: metformin, Comp C: compound C, UT: untreated, NS: non-significant.

protein and mRNA levels all double resistant lines (Fig 10B, D &E). All the above observed results were reversed when treated with compound C, indicating the specificity of HSP70 and p-STAT3 repression to activation of AMPK (SF 6A &B; Fig 10B-E). As, metformin treatment resulted in reduction of CYCLIN D1 and BCL2 levels we, further assessed the viability of K562 WT and double resistant cells post to treatment with geldanamycin (Fig 10F) or imatinib (Fig 10G) or metformin (Fig 10H). It was seen that only when treated with metformin the viability of double resistant lines followed a trend similar to that of K562 WT.

# 1.2.3.5. Metformin inhibits HSF1 protein stability through AMPK-mediated proteasomal degradation

It was seen that HSP70 mRNA levels were also reduced following metformin treatment (Fig 10C), indicating a transcriptional repression of HSP70. So, we assessed the levels of HSF1, which is a transcription factor of HSP70 (82). K562 WT and double resistant lines were treated with metformin or with compound C. Post to metformin treatment HSF1 mRNA levels were unaffected in both K562 WT (SF 6B) and double resistant lines (Fig 11A). However, HSF1 protein expression was decreased following metformin treatment and the scenario was reverted when treated with compound C in both K562 WT (SF 6A) and double resistant lines (Fig 11B). Since, there was a decrease in protein levels without altering mRNA levels, proteasomal degradation could be one of the possible mechanisms involved thus, we have treated K562 WT and double resistant lines with either metformin alone or with MG-132 (inhibitor of proteasomal degradation) alone or in combination. It was seen that post to combination treatment with MG-132 the protein levels of HSF1 were restored in both K562 WT (SF 6F) and double resistant lines (Fig 11C). Dai *et al* has shown that HSF1 serves as a

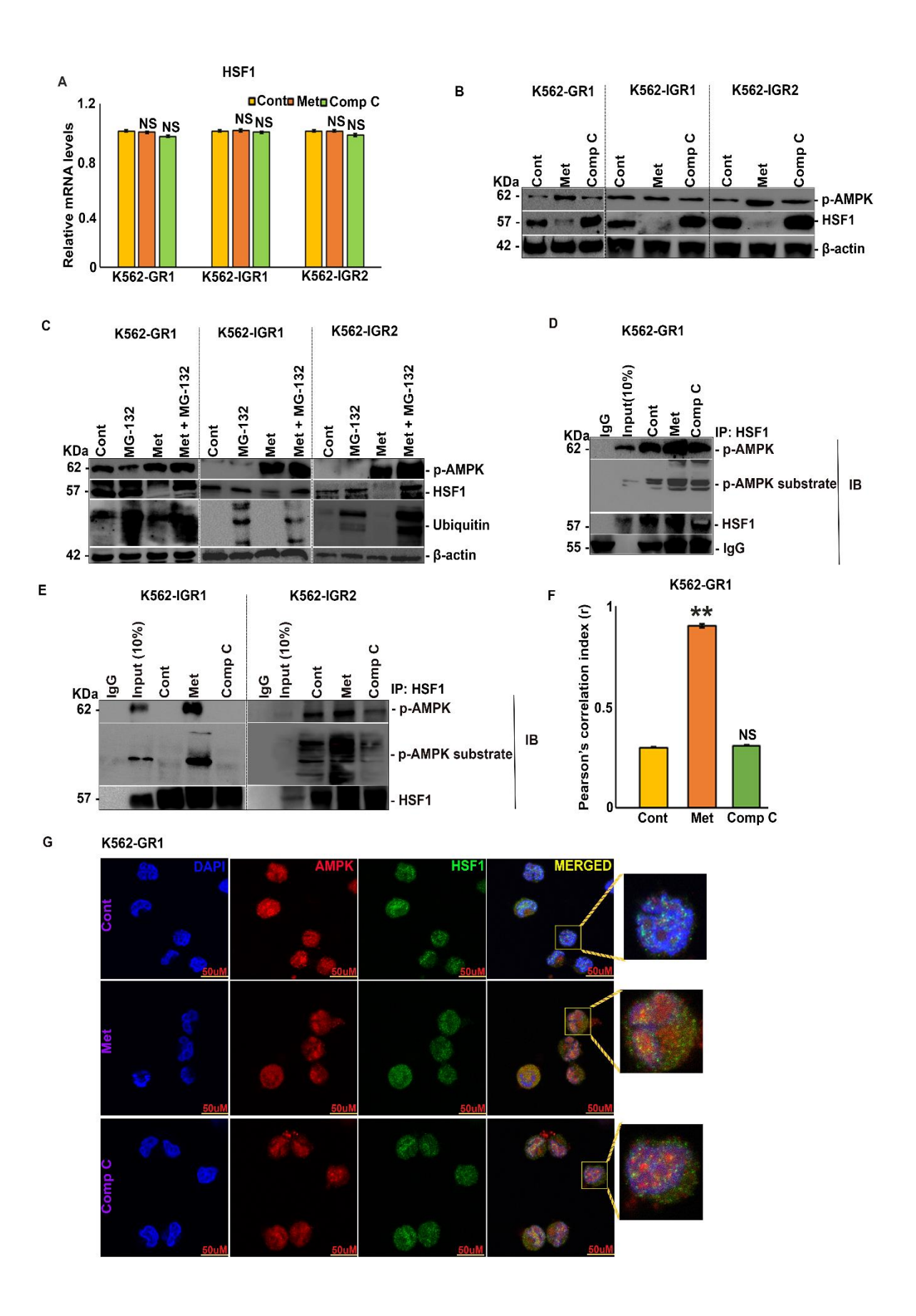


FIGURE 11: Metformin inhibits HSF1 protein stability through AMPK-mediated proteasomal degradation. A) HSF1 mRNA levels were analyzed in K562- GR1, K562- IGR1 and IGR2 cells post to treatment with either metformin (10 mM for 6 hours) or compound C (5 μM) or none. B) K562- GR1, IGR1 and IGR2 cells were subjected to metformin (10 mM for 12 hours) or compound C (5 μM for 12 hours) treatment or none and subjected to immunoblot analysis to assess HSF1 levels. C) K562- GR1, IGR1 and IGR2 cells were subjected to metformin (10 mM for 12 hours) or MG-132 (3 mM for 12 hours) or both treatments or none and immunoblot analysis was carried out to assess HSF1 levels. D) K562- GR1 and E) K562- IGR1 and IGR2 cells were subjected to immunoprecipitation by HSF1 to assess HSF1 interaction with p-AMPK post metformin (10 mM for 12 hours) or compound C (5 μM for 12 hours) treatment or none. F) Quantification of immunofluorescence data using ImageJ. G) K562- GR1 cells were treated with either metformin (10 mM) or with compound C (5 μM) or none for 12 hours and subjected to immunofluorescence by anti-HSF1 (Alexa 488) and anti-AMPK (Alexa 594) antibodies counter stained with DAPI. Mean  $\pm$  S.E.M.; N=3, \*\*p<0.005 versus control, NSp>0.05 versus control. The immunofluorescence and quantification experiments were carried out on three independent fields and experiments.

Cont: control, Met: metformin, comp C: compound C, IP: immunoprecipitation, IB: immunoblotting, NS: non-significant.

direct substrate of activated AMPK and this phosphorylation primes HSF1 for ubiquitination under proteotoxic stress response scenario (83). Taking from here, we have analyzed if this mechanism holds true in context of CML. For this, both K562 WT and double resistant lines were treated with metformin or with compound C and subjected to IP by HSF1 pull down. It was observed that after metformin treatment interaction between HSF1 and p-AMPK was enhanced and this enrichment was lost under compound C treatments in both K562 WT (SF 6C) and double resistant lines (Fig 11D &E), immunoblotting with p-AMPK substrate specific antibody supported the idea of HSF1 being a substrate of AMPK. The physical interaction between AMPK and HSF1 was further confirmed by immunofluorescence analysis of both K562 WT (SF 6D &E) and double resistant lines (Fig 11F &G; SF 7A-D).

# 1.2.3.6. Metformin inhibits STAT3 phosphorylation through AMPK/RUNX1/SOCS3 axis in imatinib-geldanamycin double resistant lines

As observed earlier along with upregulation of HSP70 there was also increase in STAT3 phosphorylation in all double-resistant cell lines (Fig 10A) which was reduced post to metformin treatment (Fig 10B). Our earlier work we have shown that metformin through AMPK induced RUNX1 Ser 94 phosphorylation, has resulted in down regulation of STAT3 phosphorylation in imatinib resistant CML subjects (Fig 9C &D). Thus, we have analyzed if the same holds true even in the context of double resistant cell lines. For this, K562 double

resistant cells were treated with AICAR, metformin and compound C and SOCS3 levels were analyzed. It was noted that upon treatment with AMPK activators SOCS3 expression was increased at both protein and mRNA level and this induction was lost when treated with compound C (Fig 12A &B). As reported earlier, SOCS3 upregulation requires AMPK induced RUNX1 phosphorylation in context of K562-WT and imatinib resistant lines, so we next

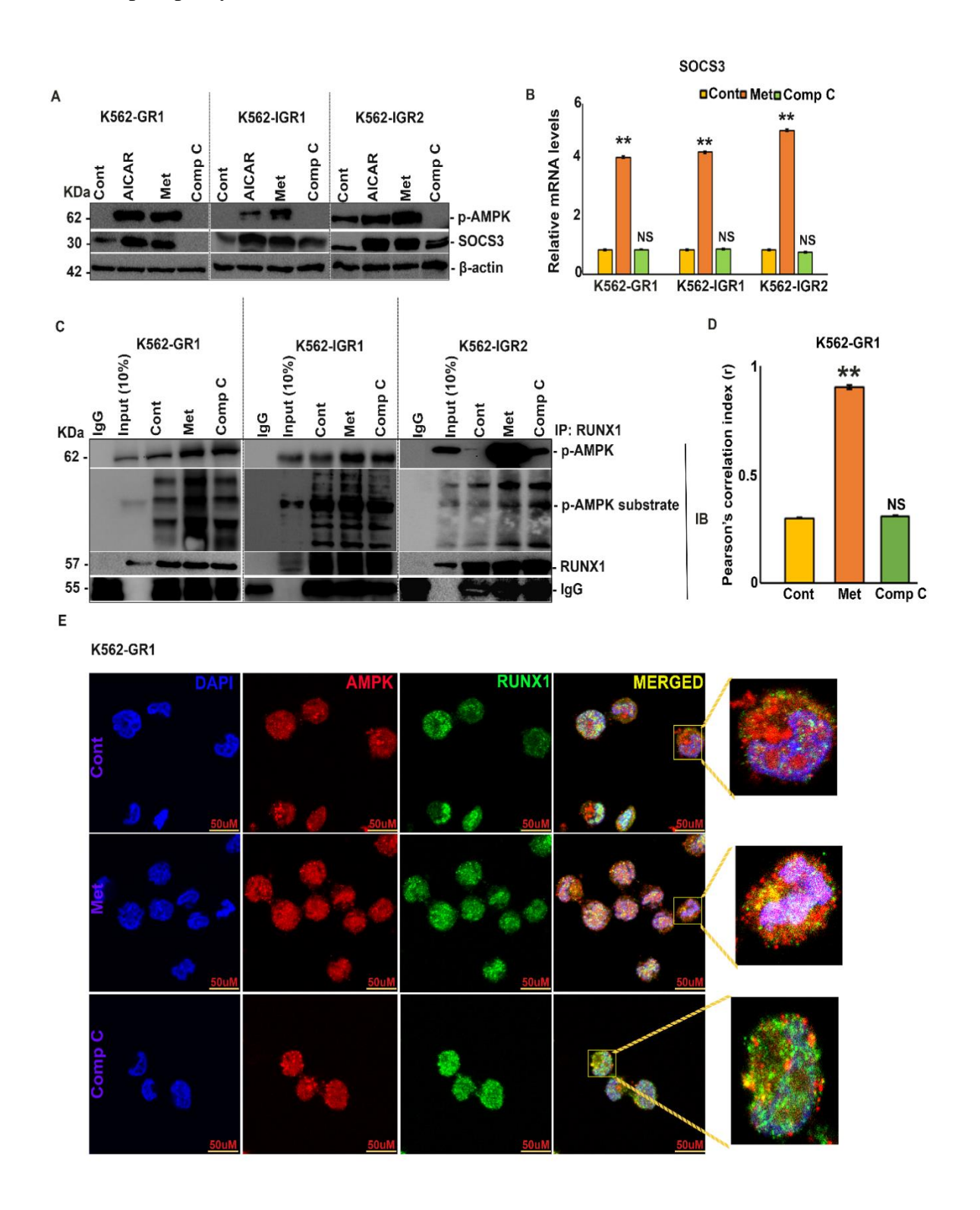


FIGURE 12: Metformin inhibits STAT3 phosphorylation through AMPK/RUNX1/SOCS3 axis. A) SOCS3 levels were assessed in K562- GR1, IGR1 and IGR2 cells post to treatment with either AICAR (0.5 mM) or metformin (10 mM) or compound C (5  $\mu$ M) or none for 12 hours and subjected to immunoblot analysis. B) SOCS3 mRNA levels were assessed in K562- GR1, K562- IGR1 and IGR2 cells post metformin (10 mM) or compound C (5  $\mu$ M) treatment or none for 6 hours and subjected to RT- PCR analysis. C) K562- GR1, IGR1 and IGR2 cells were treated with either metformin (10 mM) or with compound C (5  $\mu$ M) or none for 12 hours and subjected to immunoprecipitation by RUNX1 to assess RUNX1 interaction with p-AMPK. D) Quantification of immunofluorescence data using ImageJ. E) K562- GR1 cells were treated with either metformin (10 mM) or with compound C (5  $\mu$ M) or none for 12 hours and subjected to immunofluorescence by anti-RUNX1 (Alexa 488) and anti-AMPK (Alexa 594) antibodies counter stained with DAPI. Mean  $\pm$  S.E.M.; N=3, \*\*p<0.005 versus control, <sup>NS</sup>p>0.05 versus control. The immunofluorescence and quantification experiments were carried out on three independent fields.

Cont: control, Met: metformin, comp C: compound C, IP: immunoprecipitation, IB: immunoblotting, NS: non-significant.

analyzed if RUNX1served as a substrate for AMPK in K562 double resistant cells. K562 double resistant cells were subjected to IP by RUNX1 pull down, by treating cells with metformin or with compound C for 12 hours. It was observed that after metformin treatment interaction between RUNX1 and p-AMPK was enhanced and this enrichment was lost under compound C treatment in all double resistant lines (Fig 12C), immunoblotting with p-AMPK substrate specific antibody indicated RUNX1 was a substrate of AMPK. The physical interaction between AMPK and RUNX1 was further confirmed by immunofluorescence analysis in all double resistant lines (Fig 12D &E; SF 8A-D).

# 1.2.3.7. Metformin improves sensitivity of K562 cells towards geldanamycin and imatinib through inhibition of HSP70 and MDR1

From above data it was evident that metformin when given alone could inhibit both HSF1 as well as STAT3 phosphorylation. So, we next sort to find out if metformin can be used in combination with geldanamycin or imatinib and still be capable of eliciting anti-proliferative effects. For this, the cell viability of K562 double resistant cells was assessed under geldanamycin or imatinib alone treatment or in combination with metformin along with K562-WT as a reference. In line with above observations metformin treatment reduced the IC50 of both geldanamycin as well as imatinib for all K562 double resistant cells (Fig 13A-F). Next, we assessed the molecular players involved in improving the drug sensitivity of K562 double resistant cells, post to metformin treatment. K562 double resistant cells were treated with either

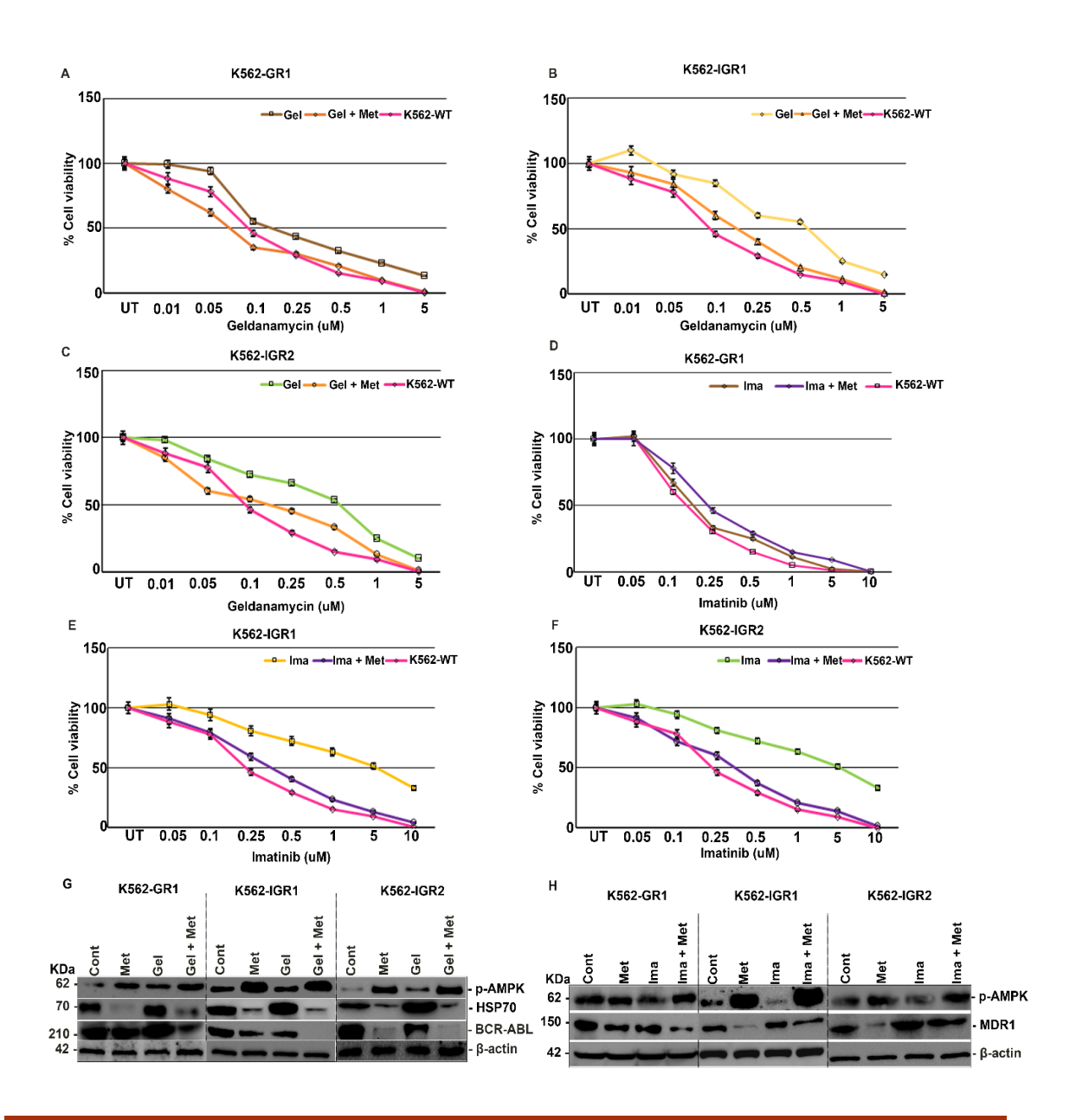


FIGURE 13: Metformin improves sensitivity of K562 cells towards geldanamycin and imatinib through inhibition of HSP70 and MDR1. A) K562- GR1, B) K562- IGR1 and C) K562- IGR2 cells were treated with metformin (0.25 mM) and indicated levels of geldanamycin for 72 hours and cell viability was assessed by alamar blue. D) K562- GR1, E) K562- IGR1 and F) K562- IGR2 cells were treated with metformin (5 mM) and indicated levels of imatinib for 72 hours and cell viability was assessed by alamar blue. G) K562- GR1, IGR1 and IGR2 cells were treated with either geldanamycin (0.5  $\mu$ M) or metformin (10 mM) or both or none for 12 hours and subjected to immunoblot analysis to assess levels of HSP70 and BCR- ABL. H) K562- GR1, IGR1 and IGR2 cells were treated with either metformin (10 mM) alone or with imatinib alone (1  $\mu$ M), or both (metformin- 10 mM; imatinib- 1  $\mu$ M) or none for 12 hours and subjected to immunoblot analysis to assess levels of MDR1. Mean  $\pm$  S.E.M.; N=3.

Cont: control, Met: metformin, Gel: geldanamycin, Ima: imatinib.

geldanamycin alone or metformin alone or in combination or none for 12 hours. It was observed that geldanamycin alone treatment upregulated expression of HSP70 in all double resistant cells (Fig 13G), whereas in K562-WT their expression was inhibited (SF 9A), but when treated with metformin alone or in combination with metformin the upregulation observed in double resistant cells was lost (Fig 13G). The direct downstream effector of HSP90 is BCR-ABL, where in inhibition of HSP90 results in destabilization and ubiquitination of BCR-ABL (84, 85). Since, we could see that metformin could improve geldanamycin sensitivity of resistant K562 cells, we have checked if this was also translated to stability of BCR-ABL. It could be seen that metformin to certain extent could reduce BCR-ABL levels but when used in combination the stability of BCR-ABL was reduced to a greater extent (Fig 13G & SF 9A). As seen earlier metformin could improve even imatinib sensitivity of K562 cells, thus we have looked into the possible molecular players involved. Review of literature has shown MDR1 as one of the major transporters in generation of imatinib resistance (86) and in our earlier sections we have observed that indeed there is an increased expression of MDR1 in K562 double resistant cells (Fig 10A). Thus, we have checked the effect of metformin treatment in combination with imatinib by treating K562 cells (WT and double resistant cells) with either imatinib alone or with metformin alone or in combination for 12 hours. It was observed that compared to imatinib alone treatment, imatinib along with metformin in K562 double resistant cells had more potent inhibition of MDR1 levels (Fig 13H). Whereas imatinib alone or with metformin showed significant inhibition of MDR1 compared with K562 WT (SF 9B).

# 1.2.3.8. Metformin improves geldanamycin sensitivity of CML subjects through AMPK/HSF1/ HSP70 axis

From above results it was evident that metformin could improve geldanamycin sensitivity of K562 double resistant cells through downregulation of HSF1 by AMPK induced phosphorylation, thus inhibiting activation of heat shock response, which otherwise could help in CML progression. To further validate our results, we have isolated PBMCs from CML subjects (n=13, h=4) and assessed their viability in response to geldanamycin treatment alone or in combination with metformin. It was observed that metformin treatment resulted in reduction of IC50 values for geldanamycin in all CML subjects (Fig 14A &B; SF 10E &F) irrespective of their degree of response to geldanamycin treatment alone. Further, PBMCs were subjected to immunoblot analysis post to metformin treatment to examine levels of HSF1 and HSP70. It was observed that metformin treatment resulted in reduction of HSF1 levels, due to which HSP70 mRNA levels (SF 10A-D) as well as protein levels (Fig 14C &SF 10G) were

reduced in all CML subjects. Since, HSF1 levels were downregulated in response to metformin treatment, we then analyzed if HSF1 served as a physiological substrate of AMPK in CML subjects. Upon, IP with HSF1, there is an enrichment of p-AMPK in metformin treated lanes in CML subjects. Immunoblotting with p-AMPK substrate specific antibody established HSF1 being a substrate of AMPK in CML subjects (Fig. 14D &SF 10H).

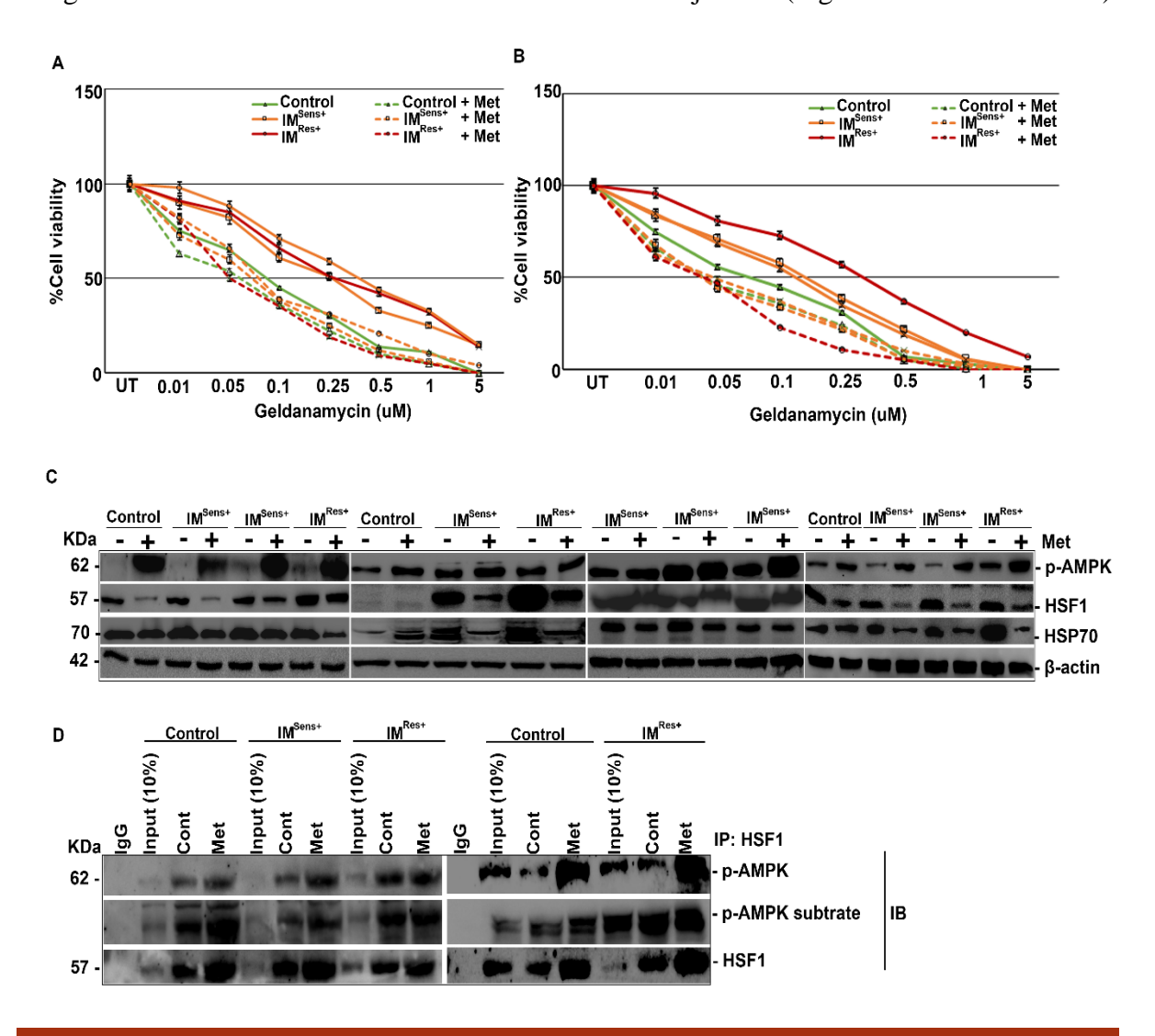


**FIGURE 14:** Metformin improves geldanamycin sensitivity of CML subjects through AMPK/HSF1/HSP70 axis. A-C) Cell viability of PBMCs isolated from CML subjects was assessed by alamar blue, post to treatment with geldanamycin alone or along with metformin (0.25 mM) at indicated concentrations for 72 hours. **D-G**) PBMCs isolated from CML subjects were treated with either metformin (10 mM) or none for 12 hours and subjected to immunoblot analysis to assess HSF1 and HSP70 levels. **H & I**) PBMCs isolated from CML subjects were treated with either metformin (10 mM) or none for 12 hours and subjected to immunoprecipitation by HSF1 to validate HSF1 interaction with p-AMPK. Mean  $\pm$  S.E.M.; N=3.

Cont: control, Met: metformin, Subj: subject, IP: immunoprecipitation, IB: immunoblotting, Control: healthy subjects, IM <sup>Sens+</sup>: imatinib sensitive subjects, IM <sup>Res+</sup>: imatinib resistant subjects.

# **DISCUSSION**

### 1.2.4. DISCUSSION

The current work highlights the possibility of metformin to be used as a therapeutic alternative for treatment of CML. Though, metformin was shown to inhibit the growth of CML cells by inhibition of mTORC1 (79), the role of metformin in overcoming drug resistance in CML was unknown. Above work sheds light on possible mechanisms involved in generation of double resistance in CML as well as the potential of metformin in bypassing them. From our earlier works and in the current study it could be seen that there is co-evolution of resistance towards imatinib and geldanamycin (78). The major pathways involved in generation of imatinib resistance are JAK/STAT pathway and increased expression of MDR1(86). Whereas upregulation of HSF1owing to inhibition of HSP90 could be the possible mechanism responsible for generation of geldanamycin resistance. Active HSF1 upregulates genes involved in heat shock response like HSP70, HSP27, HSP40, HSP20 etc., which are involved in over riding replicative senescence (87), increasing cell proliferation, inhibition of apoptosis (88), bypassing DNA damage check points and finally in immunosuppression (89) to aid in tumor growth (90). We, have shown that both RUNX1 and HSF1 are direct substrates of AMPK in context of CML and these phosphorylation primed HSF1 for ubiquitination and induced cytoplasmic retention and interaction with STAT3 for RUNX1. Similar results were reported by Dai et al that under proteotoxic stress response HSF1served as a substrate for AMPK (83). Owing to down regulation of HSF1 by AMPK, HSP70 levels were also reduced. Finally, metformin showed to inhibit geldanamycin induced HSF1 and HSP70 activation and reduced the IC50 values of geldanamycin (as seen by cell viability plots) in CML subjects. Metformin could be used in combination with geldanamycin, where geldanamycin treatment would destabilize BCR-ABL expression (as shown by us (Fig 13G; SF 9A) and several others (84, 91)) and metformin could suppress activation of heat shock response arm, which otherwise would be activated due to inhibition of HSP90.

Both our cell line data (78) and data from PBMCs have brought forth the concept of co-evolution of resistance towards geldanamycin and imatinib. It could be seen that CML subjects that were resistant to imatinib treatment also had higher IC50 values for geldanamycin treatment, despite never being exposed to geldanamycin. One, of the possible reasons behind dual resistance to imatinib and geldanamycin could be attributed to higher expression of MDR1 in double resistant cells (Fig 10A) (P-glycoprotein), which acts as an efflux pump for both imatinib and geldanamycin (92). The drug bio-availability inside cell depends on influx to efflux ratio. Imatinib is mainly routed in to cells through OCT1 (93) and MATE1 (94).

However, MATE1 also acts as an efflux pump for metformin and it was seen that in imatinib non-responders MATE1 levels were very low, but OCT1 levels were unaltered or with little decrease (94). Metformin entry is mainly facilitated by OCT's including OCT1, 2 & 3 (95-97), but its efflux is routed through MATE1 and MATE2- K (98). Reduced MATE1 levels with little to no change in OCT levels (94) could increase the intracellular concentration of metformin, thus increasing metformin's effectiveness and aid in treatment of dual resistant CML subjects. However, further studies are warranted to understand the generation of multi drug resistance seen during progression to blast crisis (BC)-phase of CML.

Additionally, STAT3 activation which played a major role in generation of imatinib resistance (99-101) was inhibited by metformin treatment through AMPK/ RUNX1/ SOCS3 axis. Where in AMPK mediated RUNX1 Ser 94 phosphorylation resulted in relieving of SOCS3 from RUNX1 mediated transcriptional repression. It also resulted in cytoplasmic retention of both RUNX1 and STAT3 resulting suppression of their target genes which otherwise would aid in cell proliferation. In conclusion, the current study established the potential mechanisms involved in generation of dual resistance towards geldanamycin and imatinib and the role of metformin in overcoming this dual resistance (Fig 15).

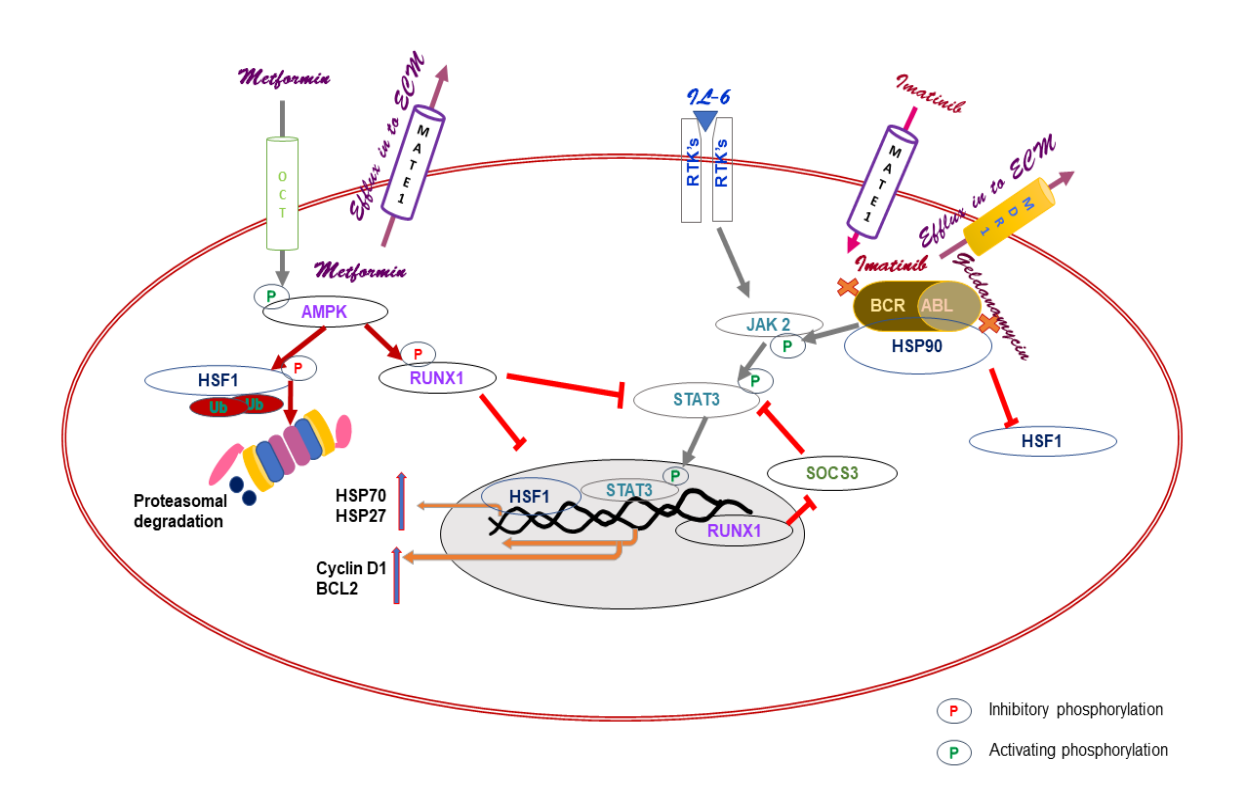


FIGURE 15: Schematic representation of metformin as a therapeutic alternative for treatment of imatinib resistant CML cases. The current figure summarizes the findings from the presented paper along with already known facts inregards with evolution of resistance towards imatinib and geldanamycin. The entry of imatinib is facilitated through OCT1 and MATE1 and efflux of imatinib and geldanamycin is carried out by MDR1. Once, inside imatinib inhibits BCR-ABL kinase activity and geldanamycin disrupts HSP90 interaction with BCR-ABL. Active BCR-ABL aids in STAT3 activation by JAK2 phosphorylation. phosphorylated STAT3 enters in to nucleus, upregulation expression of CYCLIN D1 and BCL2 and other targets involved in cell proliferation and antiapoptosis. Active HSP90 inhibits HSF1 expression, which otherwise would translocate to nucleus activating heat shock response (upregulation of HSP70, HSP27 etc.,). Geldanamycin treatment results in activation of HSF1. Metformin enters into cell through OCT's and effluxes through MATE1. Metformin activates AMPK inside the cell through phosphorylation. RUNX1 and HSF1 are substrates of AMPK. AMPK mediated RUNX1 phosphorylation inhibits RUNX1 nuclear localization and HSF1 phosphorylation by AMPK primes HSF1 for ubiquitination. Active RUNX1 suppresses SOCS3 transcription. SOCS3 is a STAT3 dephosphorylase which inhibits STAT3 activation.

# **OBJECTIVE 1.3**

Analyzing the effect of RUNX1 and AMPK interactions in MDS

### 1.3.1. LITERATURE REVIEW

Myelodysplastic syndrome (MDS or pre-leukemic stage) is a heterogenous group of hematological disorders characterized by dysplastic bone marrow resulting in ineffective hematopoiesis (102, 103). The symptoms depend on the type of cell lineage effected, which include but not limited to fatigue, anemia etc., (103). Incidences of MDS are rare and usually occur in elderly people, however in India it is mostly reported in younger population (104). About one- third of MDS cases progress to acute leukemia (105). Cytogenetics of MDS include several chromosomal translocations like deletions of chromosomes 5, 7 and or del 20q (106, 107) or presence of Philadelphia chromosome (generated due to translocation between chromosomes 9 and 22 resulting in generation of fusion protein BCR-ABL), of which the latter is highly associated with poor prognosis of MDS (108-111). Though rare, about 2% of MDS cases are reported to be positive for Philadelphia chromosome and these cases are usually resistant to conventional chemotherapy employing Tyrosine Kinase Inhibitors (TKIs) like imatinib (112), possibility due to expression of multi drug resistant gene 1 (MDR1) (113). The mechanisms present behind manifestation of MDS and its progression to leukemia are unknown. As, of now the treatment options for MDS include blood transfusions and bone marrow transplant which can only help to manage the syndrome but not cure (114). Thus, there is an immediate requirement to develop alternative strategies to treat MDS.

Recent studies by Hayashi *et al* have shown that normoxic stabilization of HIF1- $\alpha$  to be a driving factor present behind generation of MDS and knockdown of HIF1- $\alpha$  could reverse MDS phenotype (115). But the mechanisms involved in such aberrant stabilization of HIF1- $\alpha$  are unexplored. Studies on hematopoietic stem cells (HSCs) isolated from MDS subjects revealed overexpression of STAT3 and correlated with cytogenic abnormalities culminating in poor prognosis (116). Earlier we have observed the potential of metformin to inhibit STAT3 activation through upregulation of SOCS3 expression. Thus, we have tested the possibility of metformin to treat MDS.

# **MATERIALS and METHODS**

### 1.3.2. MATERIALS and METHODS

### 1.3.2.1. *Cell culture*

MDS-L cell lines were a kind gift from Dr. Kaoru Tohymama. MDS-L cell were grown in RPMI-1640 medium supplemented with 40% FCS (Gibco, USA), 25ng of IL-3 (Bio legend, USA) and 1% pen-strep. K562 wild type (WT), IR2 and HEK-293 T cells were cultured as described earlier. All cell lines were maintained in 5% CO<sub>2</sub> incubator at 37°C. Sub culturing for adherent cells was done using 0.5% trypsin-EDTA (HiMedia, India).

### **1.3.2.2.** *Chemicals*

Metformin, MG-132, 5-aminoimidiazole-4-carboxamide ribonucleotide (AICAR), imatinib, and dorsomorphin (compound C) were purchased from Sigma (USA). IL-3 was procured from Bio-legend (USA).

## 1.3.2.3. Isolation of PBMCs from CML patients

Was performed as mentioned in the earlier section (1.2.2.3).

### 1.3.2.4. Cell viability assay

3,000 cells per well in a 96 well plate was seeded either with or without indicated drugs to RPMI-1640 medium of  $250\mu L$  final volume and were grown for 3 days. assay was performed as described in earlier section (1.2.2.7)

### 1.3.2.5. Nuclear and cytosolic extraction

Was performed as mentioned in the earlier section (1.1.2.6).

### 1.3.2.6. Electrophoretic mobility shift assay (EMSA)

Cells were treated with indicated drugs and nuclear extracts were prepared as mentioned in earlier section. The STAT3 binding consensus present on HIF1- $\alpha$  promoter at -355 upstream was taken as wild type probe and mutant probe was designed with mutations in critical sites. Both wild type and mutant probes were labelled with  $\gamma$ -<sup>32</sup>P using T4PNK (NEB, USA) enzyme following manufacturer's instructions. The labelled probe is then purified using G50 Spin columns (Sigma, USA) following manufacturer's manual and estimated. The binding reaction is set up as mentioned earlier.

Promoter	Wild type probe (5'-3')	Mutant probe (5'-3')	Position	

HIF1a	ACCGCCTTCCTTCGGAG	ACCACGAGTATTCGGAGA	-355 bp
	A		

## 1.3.2.7. Plasmid transfection

HEK-293 T cells were seeded in six well plate and were grown to a confluency of 50 %. 3μg of purified plasmid (RUNX1 WT or S 94 A or S 94 D) was transfected using Lipofectamine-3000 (Thermo Fischer, USA) as described in earlier section (1.1.2.8).

### 1.3.2.8. *Immunoblotting*

Suspension cells and adherent cells were collected as mentioned earlier. Equal amounts of protein (60  $\mu$ g) were subjected to SDS-PAGE. Blots were probed for HIF-PHD2 (Santa Cruz Biotechnology Inc., USA.), HIF1- $\alpha$  and HIF1- $\alpha$ -OH (Cell Signaling Technologies, USA.) antibodies as described in earlier section (1.1.2.9).

### 1.3.2.9. Immunoprecipitation (IP)

Cells were collected as described earlier. For pull down 750μg (incase of cell lines) or 500 μg (incase of PBMCs or tissues) of protein was taken along with 1 μg of antibody (PHD2 or HIF1-α or RUNX1) and left at 4°C overnight for binding. Protein agarose-A-G plus beads (Santa Cruz Biotechnology Inc., USA) were used for pulling down antigen antibody complex.

### 1.3.2.10. Confocal microscopy

Was performed as mentioned earlier section (1.1.2.12).

## 1.3.2.11. RNA isolation and real time PCR (RT-PCR)

RNA isolation and quantification was carried out as described in earlier section (1.1.2.11). The sequences of HIF1- $\alpha$  primers used were FP: 5' GAAAGCGCAAGTCTTCAAAG 3', RP: 5' TGGGTAGGAGATGGAGATG 3'.

### 1.3.2.12. Statistical analysis

All data points are represented as mean  $\pm$  SEM. Statistical analysis was done using one-way ANOVA. P < 0.05 was considered to be statistically significant. All data points were done in triplicates.

# **RESULTS**

### **1.3.3. RESULTS**

# 1.3.3.1. Metformin inhibits expression of HIF1- $\alpha$ and MDR1 in pre-leukemic and leukemic lines

Expression of HIF1-α and MDR1 was assessed in MDS-L (pre-leukemic), K562-WT and IR2 (leukemic wild type and imatinib resistant respectively) cell lines. It was observed that expression of both HIF1-α and MDR1 was high in MDS-L and K562-IR2 cells compared to K562-WT, whereas HIF1α-OH and p-AMPK levels were high only in K562- WT (Fig 16A). Since, activation status of AMPK and expression pattern of HIF1-α and MDR1 seems to follow a reciprocal relation, we then examined the effect of AMPK activation on expression of HIF1a. MDS-L, K562-WT and IR2 cells were treated with AMPK activators and inhibitor and subjected to immunoblot analysis. It could be seen that AMPK activation resulted in loss of HIF1-α expression, mostly due to increased HIF1-α hydroxylation and the scenario was reversed upon inhibition of AMPK by compound C (Fig 16B-D). In addition to suppression of HIF1-α at protein level, HIF1-α mRNA levels were also reduced post to activation of AMPK (Fig 16E-G). In line with HIF1-α expression, MDR1 levels were also suppressed post to metformin treatment (Fig 16H &I). As both HIF1-α and MDR1 are involved in improving cell viability despite imatinib treatment; we next assessed the viability of MDS-L, K562-WT and IR2 cells in response to treatment with metformin and imatinib at given concentrations. It was observed that post to metformin treatment viability of all the three lines was reduced and MDS-L and K562-IR2 followed trend similar to K562-WT (Fig 16J). However, post to imatinib treatment MDS-L and K562-IR2 cell viability was higher than compared to K562-WT (Fig. 16K).

# 1.3.3.2. Metformin promotes HIF1-a ubiquitination through PHD2 mediated HIF1-a hydroxylation

Since metformin treatment resulted in loss of HIF1- $\alpha$  expression, we then examined if this loss is mediated by proteasomal degradation. For this MDS-L, K562-WT and IR2 cells were treated with either metformin alone or with MG-132 alone or in combination or none for 12 hours. It was observed that metformin induced loss of HIF1- $\alpha$  expression was rescued when treated in cells were treated with MG-132, indicating ubiquitination to be one of the plausible reasons (Fig 17A-C). Prerequisite for HIF1- $\alpha$  ubiquitination is hydroxylation of HIF1- $\alpha$  at proline residues by prolyl hydroxylases (PHD's). Thus, we next checked if metformin treatment alters interaction between HIF1- $\alpha$  and PHD2. MDS-L, K562-WT and IR2 cells were

treated with either metformin or with compound C or none and subjected to IP by HIF1- $\alpha$ . It was noted that PHD2 interaction with HIF1- $\alpha$  was enhanced post to metformin treatment and

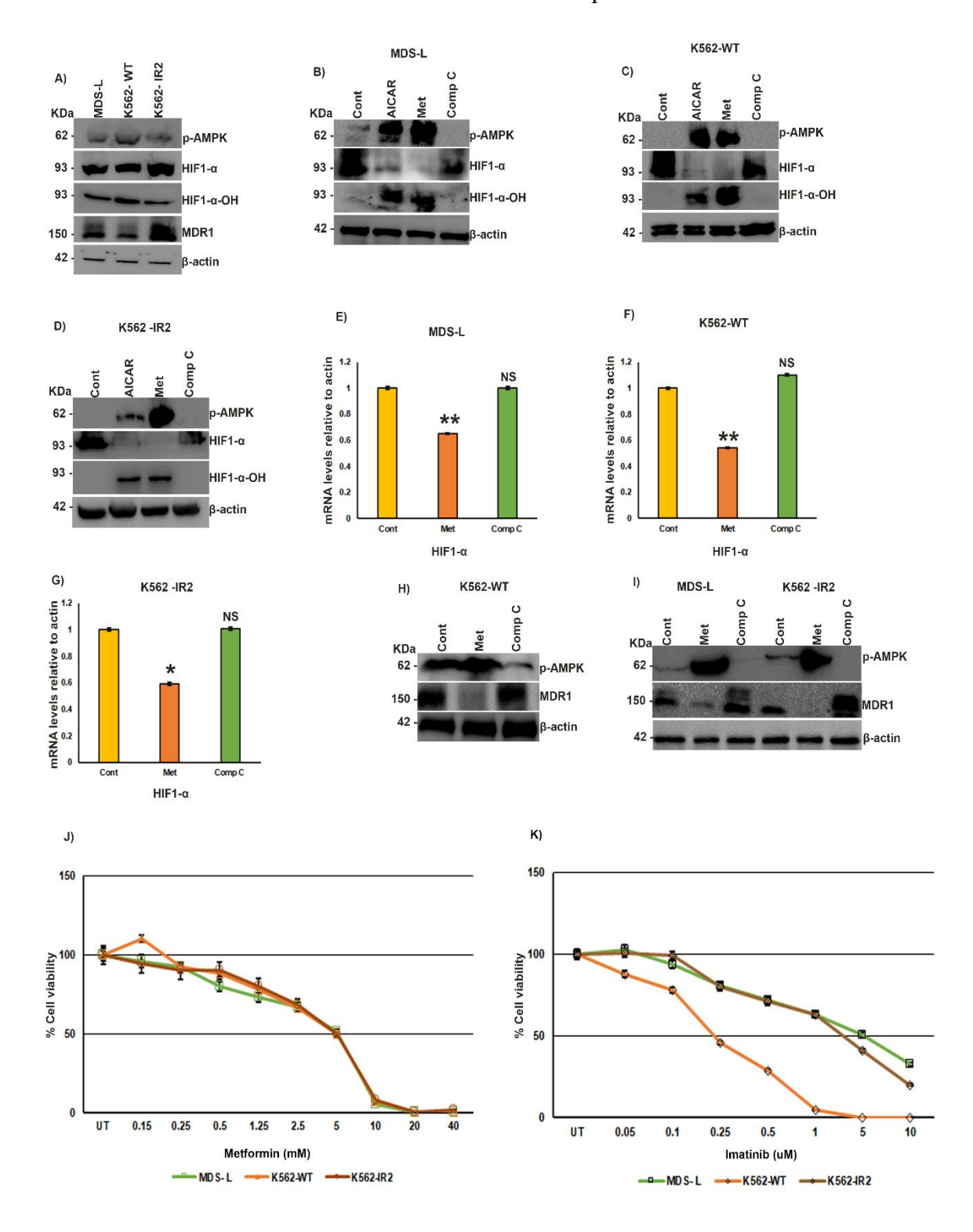


FIGURE 16: Metformin inhibits expression of HIF-1α and MDR-1 in pre-leukemic and leukemic lines. A) MDS-L, K562- WT and K562-IR2 cells were subjected to immunoblot analysis and levels of p-AMPK, HIF1-α, MDR1 and HIF1-α-OH were analyzed. B) MDS-L, C) K562- WT and D) K562-IR2 cells were treated with metformin (10 mM for 12 hours) or AICAR (0.5 mM for 12 hours) or compound C (5 μM for 12 hours) or none and subjected to immunoblot analysis and levels of p-AMPK, HIF1-α and HIF1-α-OH were analyzed. E) MDS-L, F) K562-WT and G) K562-IR2 cells were subjected to metformin (10 mM) or compound C (5 μM) treatment or none for 6 hours and RT-PCR analysis was carried out to assess HIF1-α mRNA levels. H) K562- WT cells were treated with metformin (10 mM) or compound C (5 μM) or none for 6 hours and subjected to immunoblot analysis and levels of p-AMPK and MDR1 were analyzed. I) p-AMPK, and MDR1 were analyzed in MDS-L and K562-IR2 cells post metformin (10 mM for 12 hours) or compound C (5 μM for 12 hours) treatment or none and subjected to immunoblot analysis. J) MDS-L, K562- WT and K562- IR2 cells were treated with metformin at indicated concentrations for 72 hours and cell viability was assessed. K) MDS-L, K562- WT and K562- IR2 cells were treated with imatinib at indicated concentrations for 72 hours and cell viability was assessed. Mean  $\pm$  S.E.M.; N=3, \*\*p<0.005 versus control, NSp>0.05 versus control.

Cont: control, Met: metformin, Comp C: compound C, NS: non-significant.

the reverse was observed when treated with compound C. Also, HIF1- $\alpha$  hydroxylation was high in metformin treated panel, validating increased PHD2 interaction with HIF1- $\alpha$  (Fig 17D-F).

### 1.3.3.3. AMPK induced RUNX1 Ser 94 phosphorylation alters PHD2 substrate affinity

As noted in earlier section metformin treatment increased PHD2 interaction with HIF1-α and the mechanism involved seems to be related to AMPK activation. Thus, we have set out to identify the possible AMPK substrates that can bind to PHD2. Literature review revealed involvement of RUNX3 in altering PHD2 substrate affinity towards HIF1-α in context of gastric cancer. It was reported that runt-homology domain of RUNX3 plays a key role in HIF1α-PHD2 interaction (117). As, runt homology domain is conserved across the RUNX family and RUNX1 was also an AMPK substrate, we analyzed if RUNX1 can interact with PHD2 and alter affinity towards HIF1-α. MDS-L, K562-WT and IR2 cells were treated with either metformin or with compound C or none and subjected to IP by RUNX1. It was noted that PHD2 interaction with RUNX1 was enhanced upon metformin treatment and the reverse was observed when treated with compound C. Also, the RUNX1 interacting with PHD2 served as a substrate of AMPK (verified by immunoblotting with p-AMPK substrate specific increased interaction between PHD2 and HIF1-α (Fig 18A-C). The interaction between PHD2,

antibody) and phosphorylated RUNX1 has enhanced interaction with PHD2, this in turn

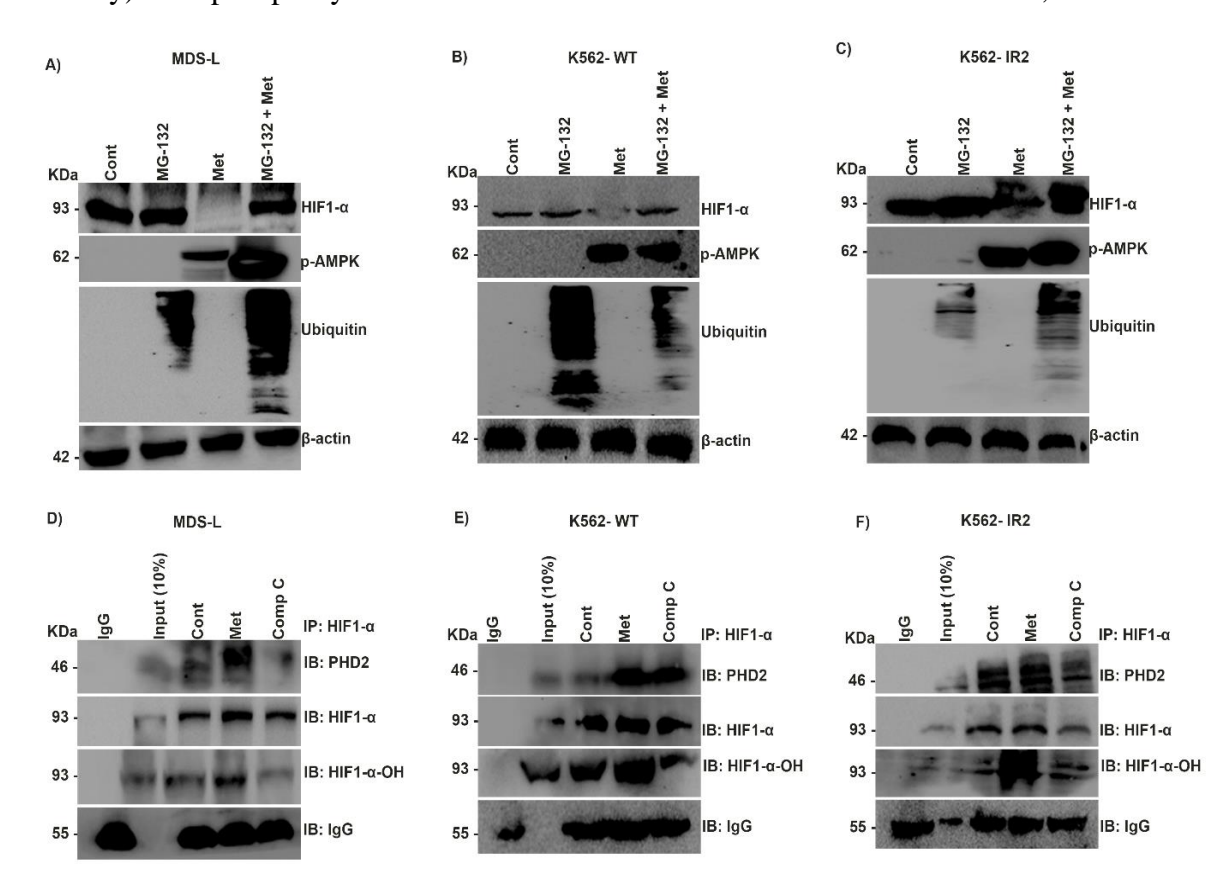


FIGURE 17: Metformin promotes HIF1- $\alpha$  ubiquitination through PHD2 mediated HIF1- $\alpha$  hydroxylation. A) MDS-L, B) K562-WT and C) K562-IR2 cells were subjected to metformin (10 mM) or MG-132 (3 mM) or both treatments or none for 12 hours and subjected to immunoblot analysis. IP analysis by HIF1- $\alpha$  pull down was carried out in D) MDS-L, E) K562-WT and F) K562-IR2 cells post metformin (10 mM) or compound C (5 μM) treatment or none for 12 hours and levels of PHD2, HIF1- $\alpha$  and HIF1- $\alpha$ -OH were assessed. Mean  $\pm$  S.E.M.; N=3.

Cont: control, Met: metformin, Comp C: compound C, IP: immunoprecipitation, IB: immunoblotting.

RUNX1 and HIF1- $\alpha$  was further established by subjecting MDS-L, K562-WT and IR2 cells to IP by PHD2 post to metformin or compound C or none. Enrichment of RUNX1 and HIF1- $\alpha$  with PHD2 was observed in metformin treated lanes compared to control and compound C lanes (Fig 18D-F). The role of RUNX1 Ser 94 phosphorylation was further established by transfecting HEK-293 T cells with RUNX1 WT, S 94 A and S 94 D clones. It was observed that upon transfection with RUNX1 WT or RUNX1 S 94 A HIF1- $\alpha$  expression was high and HIF1- $\alpha$  hydroxylation was low compared to control or metformin treated lanes. On the other hand, metformin treatment or transfection with RUNX1 S 94 D resulted in loss of HIF1- $\alpha$  expression and increased HIF1- $\alpha$  hydroxylation (Fig 18G). Next, influence of RUNX1 Ser 94

# phosphorylation on regulation of HIF1-α ubiquitination was analyzed. As, transfection with

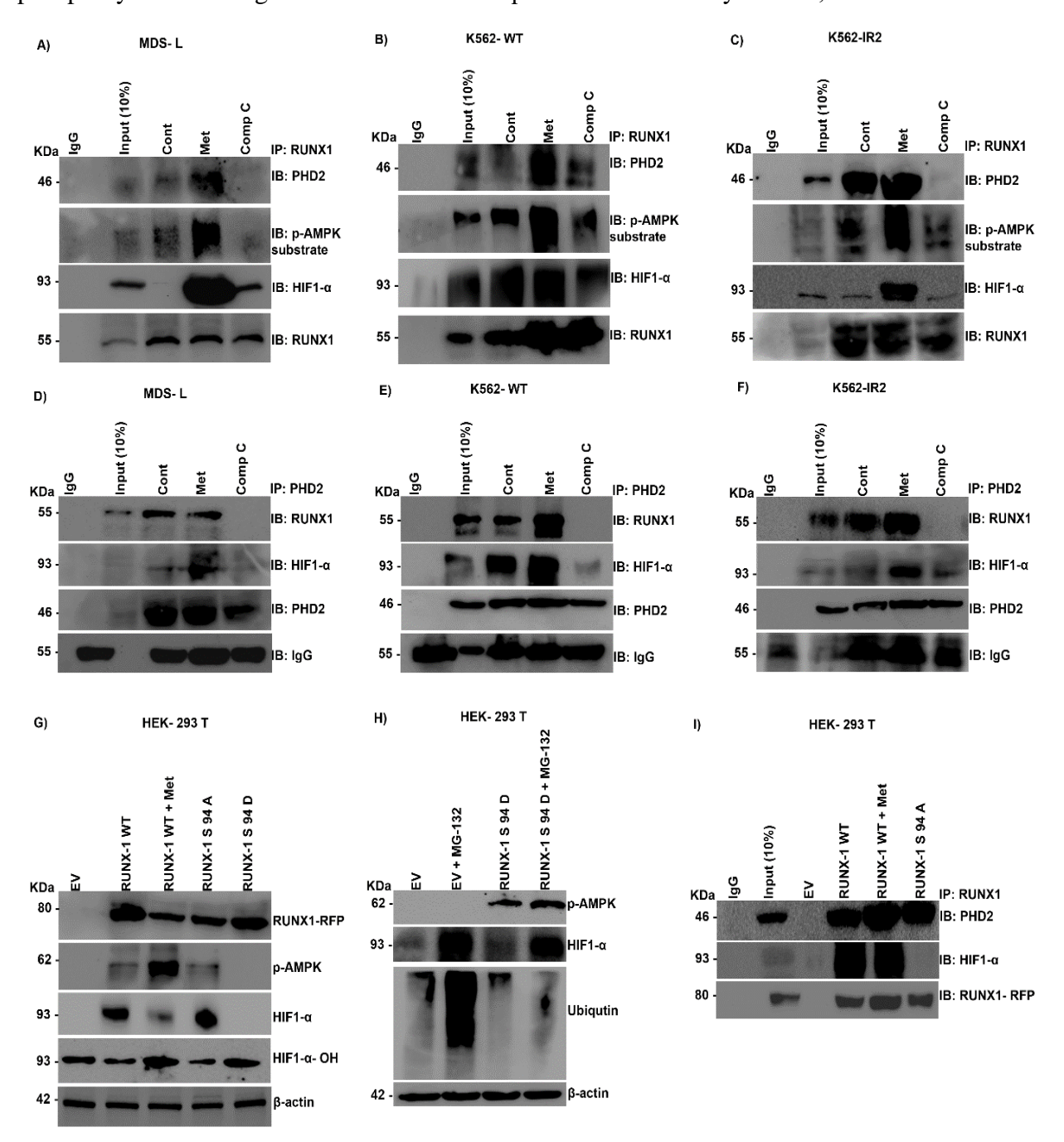


FIGURE 18: AMPK induced RUNX1 Ser 94 phosphorylation alters PHD2 substrate affinity. A) MDS-L, B) K562-WT and C) K562-IR2 cells were subjected to metformin (10 mM) or compound C (5  $\mu$ M) treatments or none for 12 hours and subjected to IP analysis by RUNX1 pull down and levels of PHD2, RUNX1, p-AMPK substrate and HIF1- $\alpha$  were analyzed. D) MDS-L, E) K562-WT and F) K562-IR2 cells were subjected to metformin (10 mM) or compound C (5  $\mu$ M) treatments or none for 12 hours and subjected to IP analysis by PHD2 pull down and levels of PHD2, RUNX1 and HIF1- $\alpha$  were analyzed. G) HEK-293 T cells were transfected with either RUNX1 WT or RUNX1 S 94 A or RUNX1 S 94 D, with or without metformin (10 mM) treatment for 12 hours post to 48 hours of transfection and subjected to immunoblot analysis and levels of p-AMPK, HIF1- $\alpha$ , RUNX1-RFP and HIF1- $\alpha$ -OH were analyzed. H) HEK-293 T cells were transfected with RUNX1 S 94 D or none, along with or without MG-132 (3 mM) treatment for 12 hours post to 48 hours of transfection and subjected to immunoblot analysis and levels of p-AMPK and HIF1- $\alpha$  were analyzed. I) HEK-293 T cells were transfected with either RUNX1 WT or RUNX1 S 94 A, along with or without metformin (10 mM) treatment for 12 hours post to 48 hours of transfection and subjected to IP analysis by RUNX1 pull down and levels of HIF1- $\alpha$ , RUNX1-RFP and PHD2 were analyzed. Mean  $\pm$  S.E.M.; N=3. Cont: control, Met: metformin, Comp C: compound C, IP: immunoprecipitation, IB: immunoblotting, EV: empty vector.

RUNX1 S 94 D resulted in loss of HIF1- $\alpha$  expression, we treated HEK-293 T cells with MG-132 post to transfection with RUNX1 S 94 D. It was seen that MG-132 treatment rescued HIF1- $\alpha$  expression (Fig 18H), confirming role of phospho RUNX1 in promoting HIF1- $\alpha$  ubiquitination. The role of phospho RUNX1 in altering PHD2 affinity towards HIF1- $\alpha$  was analyzed by subjecting HEK-293 T cells to IP by RUNX1, post to transfection with RUNX1 WT, S 94 A clones along with or without metformin treatment. It was observed that upon transfection with RUNX1 WT accompanied by metformin treatment there was an enrichment of PHD2 interaction with HIF1- $\alpha$  which was lost when transfected with RUNX1 WT alone or RUNX1 S 94 A (Fig 18I).

## 1.3.3.4. Metformin inhibits STAT3 mediated transcription of HIF1- a

As seen in our earlier panel, metformin treatment resulted in reduction of HIF1-α mRNA indicating apart from post translation regulation of HIF1-α, metformin regulates HIF1-α at transcript level also. Literature review revealed presence of STAT3 binding elements on HIF1-α promoter(118). So, we first analyzed the effect of metformin treatment on STAT3 activation in MDS-L cells. MDS-L cells were treated with metformin or compound C or none and subjected to immunoblot analysis. Post to metformin treatment STAT3 phosphorylation was repressed and so were the levels of STAT3 targets CYCLIN D1 and BCL2. Repression of STAT3 phosphorylation can be due to increase in SOCS3 expression (Fig 19A). STAT3 nuclear localization requires activation of STAT3 through tyrosine phosphorylation and as seen

metformin repressed STAT3 phosphorylation, subsequently STAT3 nuclear localization was also reduced upon metformin treatment and this were reversed upon compound C treatment

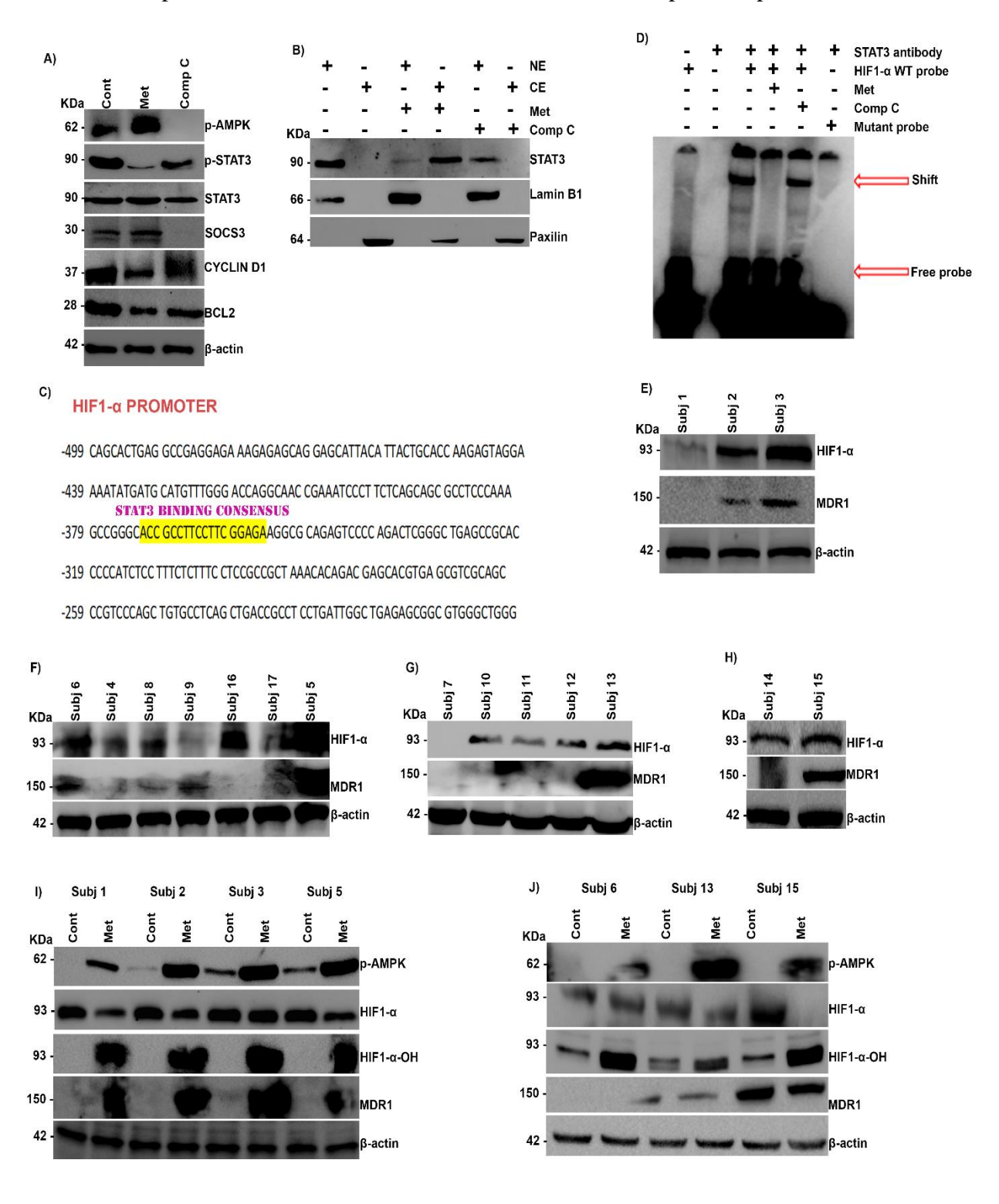


FIGURE 19: Metformin inhibits STAT3 mediated transcription of HIF1-  $\alpha$  in MDS and inhibits HIF1-  $\alpha$  and MDR1 expression in PBMCs. A) MDS-L cells were subjected to metformin (10 mM) or compound C (5 μM) treatment or none and immunoblot analysis was carried out to assess levels of p-STAT3, STAT3, p-AMPK, SOCS3, CYCLIN D1 and BCL2. B) MDS-L cells were treated with metformin (10 mM) or compound C (5 μM) or none and subjected to cell fractionation and immunoblot analysis was carried out to assess levels of STAT3. C) STAT3 binding consensus on HIF1- $\alpha$  promoter at -355 bp. D) MDS-L cells were treated with metformin (10mM) or compound C (5μM) or none and nuclear extracts were taken and subjected to EMSA. E-H) PBMCs were isolated from CML subjects and subjected to immunoblot analysis to assess levels of HIF1- $\alpha$  and MDR1. I) & J) PBMCs were treated with metformin (10mM) or none and subjected to immunoblot analysis to assess levels of HIF1- $\alpha$ , HIF1- $\alpha$ -OH and MDR1. Mean  $\pm$  S.E.M.; N=3.

Cont: control, Met: metformin, Comp C: compound C, CE: cytoplasmic extract, NE: nuclear extract, Subj: subject.

(Fig 19B). Analysis of HIF1- $\alpha$  promoter revealed presence of STAT3 binding element at -355 bp upstream. So, we then analyzed effect of metformin on occupancy of HIF1- $\alpha$  promoter by STAT3. It was seen that STAT3 binding to HIF1- $\alpha$  promoter was lost post to treatment with metformin (Fig 19C &D).

# 1.3.3.5. Metformin promotes HIF1-a hydroxylation and MDR1 suppression in PBMCs of CML subjects

Since, metformin treatment could suppress expression of HIF1- $\alpha$  and its target MDR1, through HIF1- $\alpha$  hydroxylation in MDS-L and K562-WT, IR2 cell lines. We sort to validate if similar effects could be elucidated by metformin on PBMCs isolated from CML subjects. Firstly, PBMCs were isolated from a total of 13 CML subjects along with their age matched controls (n=4). Expression of HIF1- $\alpha$  and MDR1 were analyzed in all CML subjects. It was seen that expression pattern of HIF1- $\alpha$  and MDR1 correlated with clinical manifestation of imatinib resistance in these subjects; wherein imatinib resistant CML subjects 3, 5, 13 and 15 had higher expression of HIF1- $\alpha$  and MDR1 compared to their counter parts (Fig 19E-H). Next, PBMCs from HIF1- $\alpha$  expressing CML subjects were treated with metformin and subjected to immunoblot analysis. It was observed that post to metformin treatment HIF1- $\alpha$  expression was suppressed owing to increased HIF1- $\alpha$  hydroxylation. Concomitantly MDR1 expression was also reduced owing to metformin treatment (Fig 19I & J).

# **DISCUSSION**

### 1.3.4. DISCUSSION

Though rare MDS cases with positive Philadelphia chromosome translocation are difficult to treat and MDS alone itself has limited options for treatment. As of now, the molecular mechanisms involved in onset of MDS and progression of MDS towards leukemia are unknown. However, recent work by Hayashi *et al* has shown key role of normoxic stabilization of HIF1- $\alpha$  in onset of MDS (115). Apart from aiding in onset of MDS, HIF1- $\alpha$  plays a pivotal role in generation of imatinib resistance in CML (119). Thus, HIF1- $\alpha$  targeting

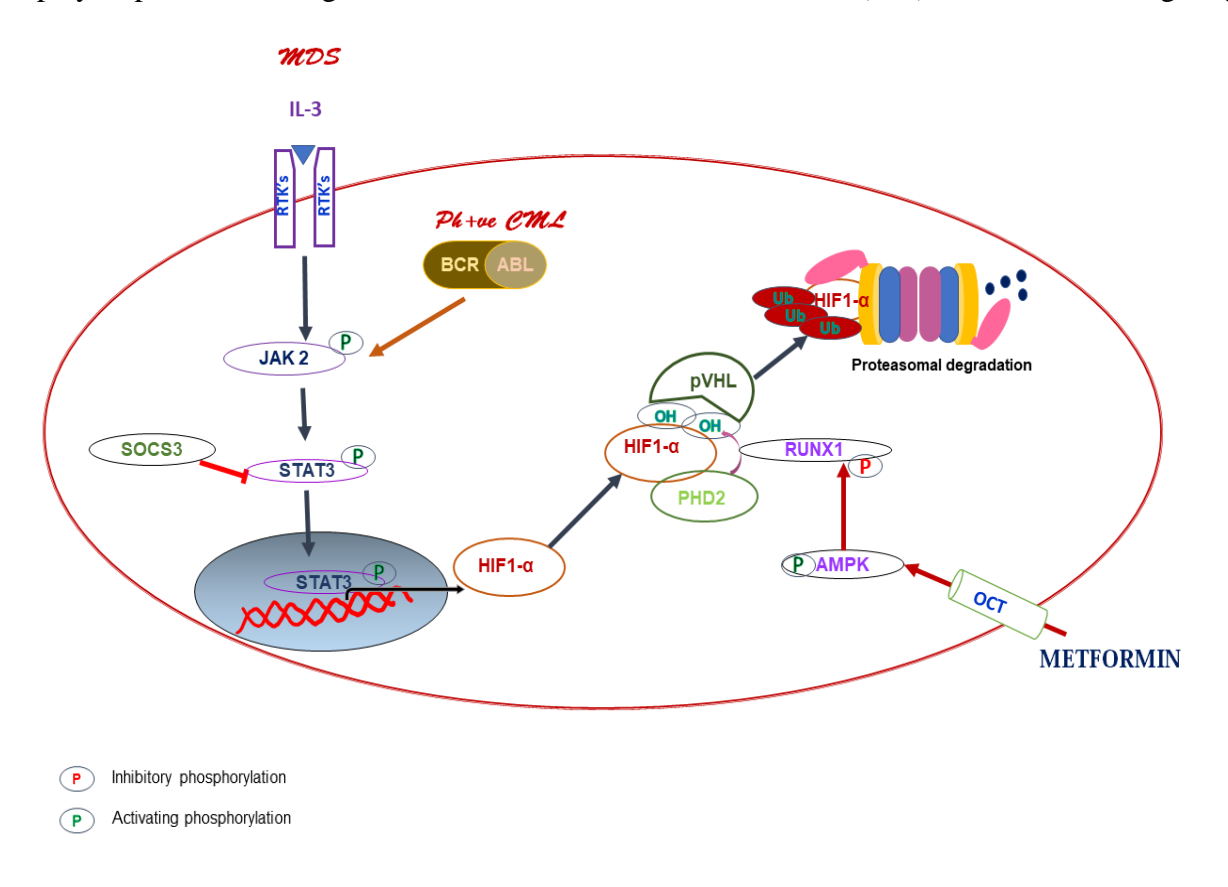


**FIGURE 20:** Schematic representation of metformin promoting HIF1-  $\alpha$  hydroxylation and MDR1 suppression. The current figure integrates the findings from present work with already known facts about MDS and CML. Persistent IL-3 signaling helps in maintenance of MDS-L cell lines. IL-3 mediated activation of STAT3 results in normoxic stabilization of HIF1- $\alpha$ . In case of CML, BCR- ABL takes over need of IL-3 signaling in activating STAT3 and through HIF1- $\alpha$  promotes expression of MDR1, which is involved in imatinib efflux. Intracellularly, imatinib inhibits BCR-ABL kinase activity. Metformin, enters through OCTs and activates AMPK through phosphorylation. RUNX1 is a substrate of AMPK and this phosphorylation results in cytoplasmic retention of RUNX1, which otherwise would inhibit expression of SOCS3, which is a negative regulator of STAT3 phosphorylation. RUNX1 Ser 94 phosphorylation results in increased binding of RUNX1 to PHD2 and altering its affinity towards HIF1- $\alpha$ . PHD2 was bound to HIF1- $\alpha$  results in HIF1- $\alpha$  hydroxylation, which acts as signal for HIF1- $\alpha$  ubiquitination.

would be promising in treatment of both MDS as well as Philadelphia chromosome positive MDS and imatinib resistant CML. The current study has shown the potential of metformin in treatment of both MDS and imatinib resistant CML through suppression of HIF1- $\alpha$  at both transcript and protein level. HIF1- $\alpha$  normoxic stabilization mainly involves inhibition of HIF1- $\alpha$  post translational modifications that can prime HIF1- $\alpha$  for ubiquitination by PHDs. PHDs induce HIF1- $\alpha$  hydroxylation which culminates in ubiquitination of HIF1- $\alpha$ . RUNX1 alters PHD2 substrate affinity to induce enhanced binding to HIF1 $\alpha$ . Compared to unphosphorylated RUNX1, RUNX1 Ser 94 phosphorylation induced by activated AMPK had enhanced binding to PHD2/ HIF1- $\alpha$  complex.

HIF1-α transcription occurs mainly in response to hypoxic cues. However, the normoxic transcriptional regulation of HIF1-α was less explored. Literature review showed that STAT3 activity is needed for hypoxia induced HIF1-α mRNA expression in melanoma cells. MDS-L cell line needs persistent IL-3 signaling for its maintenance and in case of CML, BCR-ABL takes over the job of IL-3 for providing persistent STAT3 activating signals. In both cases HIF1-α expression was high. HIF1-α stability depends on vHL binding to hydroxylated HIF1-α, it was reported that STAT3 could disrupt HIF1-α-vHL association by occupying vHL binding sites on HIF1-α. Thus, we speculated the involvement of STAT3 signaling in normoxic stabilization of HIF1-α in MDS context. In line with our speculation HIF1-α promoter indeed had STAT3 binding elements and this binding was disrupted upon metformin treatment. As, reported in above sections AMPK induced RUNX1 Ser 94 phosphorylation resulted in inhibition of STAT3 nuclear localization and subsequently repression of STAT3 transcriptional activity. This repression was in part mediated by SOCS3 activation in RUNX1 Ser 94 phosphorylation specific manner. Thus, metformin through RUNX1 Ser 94 phosphorylation inhibited HIF1-α expression at both transcript as well as protein level (Fig 20). HIF1-α target MDR1 plays a key role in active efflux of imatinib from cell (120), aiding in generation of imatinib resistance and metformin by virtue of HIF1-α inhibition suppressed MDR1 expression, aiding in improving imatinib sensitivity as reported in earlier.

# **OBJECTIVE 1.4**

Analyzing the effect of RUNX2 and AMPK interactions in bone metastasis of breast cancer

### 1.4.1. LITERATURE REVIEW

Breast cancer is the second leading cancer worldwide and the major cause of death worldwide (121). RUNX2 is highly expressed in breast cancer (122) and more prominently in aggressive tumors (123). RUNX2 has a vast target repertoire which affects several pathways including but not limited to cell cycle progression, DNA damage response etc., which play a key role in cancer transformation (124). Expression of RUNX2 can confer osteoblast like phenotype by upregulation of bone specific proteins like osteopontin (125), osteonectin (126) etc., which helps breast cancer cells to home, colonize and survive in bone causing osteolytic lesions and initiation of secondary tumors (127-129). It was also seen that ectopic expression of RUNX2 confers drug resistance to cancer cells which makes RUNX2 a potent druggable target for cancer treatment (127).

Metformin gained attention as a potent anti-cancer agent owing to its effect on activation of AMP-activated kinase (AMPK), cellular energy sensor which is involved in regulation of energy homeostasis by either inhibiting pathways involved in energy consumption (like cap-dependent protein synthesis (130)) and gluconeogenesis (131). Recent studies using cell culture and animal models have shown that metformin has the ability to inhibit cell proliferation and tumor growth through AMPK/P53 axis (6, 132, 133). However, clinical trials carried out to investigate metformin's anti-cancer ability were not promising in case of solid tumors especially breast cancer and the molecular mechanisms underlying were not clear (134, 135).

Our recent work on regulation of RUNX2 in bone and adipogenic development revealed that RUNX2 is a novel substrate of AMPK, an immediate effector molecule of metformin's action. It was also seen that AMPK mediated phosphorylation of RUNX2 increased the transcriptional activity of RUNX2 (136) .With the knowledge on RUNX2 protective function of metformin in context of osteogenesis, in the current study we aimed to understand dynamics of this relation in breast cancer progression and metastasis.

# **MATERIALS and METHODS**

### 1.4.2. MATERIALS AND METHODS

### 1.4.2.1. *Cell culture*

MDA-MB-231 were grown in L-15 medium (Gibco, USA) along with 15%FBS (Gibco, USA) and 1% Pen-Strep (Gibco, USA) in no CO<sub>2</sub> incubator at 37°C; MCF-7 in RPMI-1640 medium (Gibco, USA) along with 10% FBS (Gibco, USA) and 1% Pen-Strep (Gibco, USA) in 5% CO<sub>2</sub> incubator.

### **1.4.2.2.** *Chemicals*

Metformin, dorsomorphin (compound C), MG-132 and LiCl were procured from Sigma, USA.

### 1.4.2.3. *Sub-cloning*

RUNX2 cDNA (NM\_001024630.3) was procured from Genecopoeia, USA. RUNX2 site directed mutants S118 A, D along with WT were subcloned into pDsRed1-N1 (Clonetech, USA) containing red fluorescent protein. List of the primers used for site directed mutagenesis were:

Target	Forward primer (5'-3')	Reverse primer (5'-3')
RUNX2	CCGCTCGAGACCATGGCATC	GGAAGATCTCGATATGGTCGCCAA
WT	AAACAGCCTCTTCAGC	ACAGATTCATC
RUNX2	CGCACCGACGACCCCAACTTC	GAAGTTGGGGTCGTCGGTGCG
S118 D		
RUNX2	GTCCGCACCGACGCCCCAA	CAGGAAGTTGGGGGCGTCGGTGC
S118 A	CTTCCTG	GGAC

## 1.4.2.4. Nuclear and cytosolic extraction

Cells were treated with indicated drugs for 6 hours and cells were collected in 1X PBS and processed as described earlier (1.1.2.6).

### 1.4.2.5. Electrophoretic mobility shift assay (EMSA)

Cells were treated with indicated drugs and nuclear extracts were prepared as mentioned above. The RUNX2 binding consensus on RICTOR promoter was taken as wild

type probe (5' TTAGGTACCACAGACATG 3') and mutant probe (5' TTAGGTATTACAGACATG 3') was designed with mutations at critical sites. Both wild type and mutant probes were labelled with  $\gamma$ -32P using T4PNK (NEB, USA) enzyme following protocol described earlier.

## 1.4.2.6. Plasmid transfection

MCF-7 cells were seeded in six well plate and were grown to a confluency of 50 %. 2µg of purified plasmid (RUNX2 WT or S 118 A or S 118 D) was transfected using Lipofectamine-3000 (Thermo Fischer, USA) as described in earlier section (1.1.2.8).

# 1.4.2.7. siRNA transfection

The siRNA for rictor (SI05109048), raptor (SI00698677) and RUNX2 (Hs.535845) were purchased from Qiagen (Netherlands) and Thermo fisher scientific (USA) respectively. All the transfections were carried out using RNAifect (Qiagen, Netherlands) following the manufacturer's instructions. In brief,  $1\mu g$  of siRNA and  $3\mu L$  of RNAifect were diluted in  $200\mu L$  of plain DMEM medium (0.5 % FBS) individually and incubated for 5 minutes; later, both were mixed and incubated for 30 minutes before adding the combined solution to cells. Cells were replaced with fresh regular medium after 6 hours of transfection.

### 1.4.2.8. *Immunoblotting*

Cells were lysed in 1X RIPA supplemented with protease and phosphatase inhibitor cocktails (Sigma, USA). Equal number of proteins were subjected for SDS-PAGE followed by blotting using  $\alpha$ -RUNX2,  $\alpha$ -p-AMPK,  $\alpha$ -p-AMPK substrate motif-specific antibody, p-S6K, S6K, rictor, raptor, p-Akt (Ser 473), cofilin, p-cofilin (Ser 3), paxillin (Cell signaling technologies, USA), MMP-9, pan-Akt, VEGF, PKC, ubiquitin, GSK3 $\alpha$ / $\beta$ , CDH11, AMPK and p-PKC $\beta$  (Santa Cruz, USA.) Lamin B1, p-GSK3 $\beta$  (Ser 9) and E-cadherin (Abcam, USA.) antibodies as described in earlier section (1.1.2.9).

## 1.4.2.9. Immunoprecipitation

Cells were lysed in IP lysis buffer (Thermo Scientific, USA) supplemented with protease and phosphatase inhibitor cocktails (Sigma, USA) and equal amounts of protein (500  $\mu$ g) were incubated with 1 ug of  $\alpha$ -RUNX2 or  $\alpha$ -p-AMPK (Cell signaling technologies (CST), USA) at 4°C overnight. Protein A/G Plus- agarose beads (2.5mg/sample) (Santa Cruz, USA) were used to pull down the immunoprecipitated protein complexes and latter were subjected to immunoblotting. For immunoprecipitation TrueBlot secondary antibodies from Rockland

Immunochemicals (USA) were used. The signal was detected by Clarity Western ECL blotting substrates (Bio-Rad, USA) and images were processed using Bio-Rad Chemidoc MP system.

# 1.4.2.10. Confocal analysis

Cells were grown upto confluency (80%) on coverslips followed by treatment for indicated timepoints and were washed with PBS before fixing in 4% formalin for 10 min at room temperature. Cells were stained for primary antibodies  $\alpha$ -RUNX2 (CST, USA), AMPK, GSK3 $\alpha$ / $\beta$  (Santa Cruz, USA) and Rhodamine; followed by respective fluorescence secondary antibodies as described in earlier section (1.1.2.12).

### **1.4.2.11.** *RT-PCR analysis*

Total RNA isolation was carried out by TRIzol (Thermo Fisher Scientific, USA) method following protocol as described previously (1.1.2.11). The quantification of real time data was carried out by  $\Delta$   $\Delta$ CT method. The sequence of primers used were:

Target	Forward primer (5'-3')	Reverse primer (5'-3')
MMP9	ATAGACTACTACAGGCT	TAGCACGGATAGACCA
Rictor	CTGATGGAGTCCGAAATGC	TCATCCGATCCTTCATCCT
POSTN	TGCCCAGCAGTTTTGCCCA	CGTTGCTCTCCAAACCTCT
CTSK	CTTCCAATACGTGCAGCAGA	CTTCAGGGCTTTCTCGTTC
COL1A1	TCTGCGACAACGGCAAGGT	ACGCCGGTGGTTTCTTGGT
VEGF	AGTTAGTCACACTGGAGATTGAC	ATAGGATCGACAGTTGTAACC
RUNX2	CTCTGCACCAAGTCCTTTTAA	AGGAGGGTAAGACTGGTCAT
	TC	AG
CDH11	CAATATCGTTGATGGAGACGG	ACATTGGCGGCCTCTATCTT
E-cadherin	GGTTTTCTACAGCATCACC	CTTCCCCATTTGATGACAC
Actin	GAGAGGGAAATCGTGCGTGAC	CATCTGCTGGAAGGTGGACA

1.4.2.12. Trans-well migration assay

MCF-7 cells were seeded in a six well plate and transfected with RUNX2 WT, S 118A, D and treated with or without metformin (15 mM) for 12 hours post to transfection. Post

transfection cells were trypsinized and approximately 2×10<sup>5</sup> cell per well were diluted in serum free medium and added to upper chamber of transwell plate., The insert was coated with 100μL of type I collagen (Thermo fisher scientific, USA) dissolved in 0.1% acetic acid (Finar, India) and left at 37°C 2 hours for solidification. The insert was then washed twice in 1X PBS after removing excess collagen. 24 hours before, HEK-293 T cells or U2OS cells were seeded in lower chamber of the transwell plate in DMEM medium supplemented with 10% FBS and 1% pen-strep. The set up was then placed in incubator at 37°C for 16 hours. Now, the medium from inserts was aspirated and cells were washed twice in 1X PBS followed by fixation in 3.7% formaldehyde (HiMedia, India) (dissolved in PBS) for 5 minutes. Followed by PBS washes. Cells were then permeabilized by 100% methanol (Sigma, USA) for 20 minutes at room temperature, followed by PBS washes. Cells were then stained by Giemsa (Sigma, USA) for 15 minutes at room temperature in dark. Excess stain was removed and washed twice with PBS. The non -invasive cells were removed by cotton swabs from the upper chamber. The number of invasive cells present on the other side of the insert were counted under bright filed microscope.

## 1.4.2.13. Breast tumor samples

Breast tumor along with adjacent normal tissues were obtained from SRMC, Chennai, India, abiding by the norms of the institutional ethics committee.

### 1.4.2.14. Statistical analysis

All data points are represented as mean  $\pm$  SEM. Statistical analysis was done using one-way ANOVA. P values less than 0.05 were considered statistically significant. A minimum set of three independent experiments was carried out for all the cell line data and for tumor samples experiments were done in duplicates due to tissue availability.

# **RESULTS**

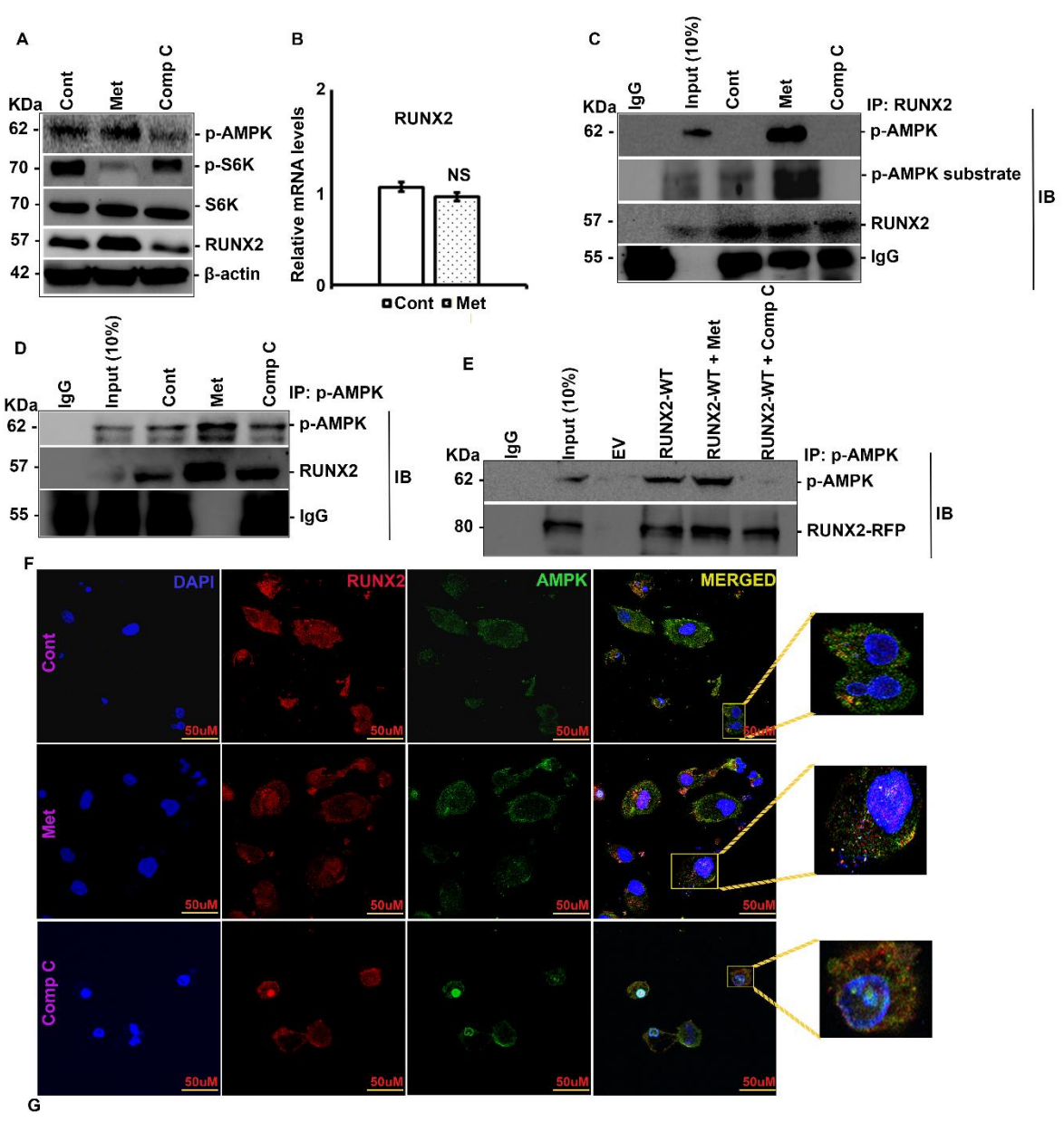
### **1.4.3. RESULTS**

### 1.4.3.1. RUNX2 is a substrate of AMPK in breast cancer cells

MDA-MB-231 cells were treated with metformin and compound C and analyzed the levels of RUNX2 by immunoblotting and RT-PCR. Upon treatment with metformin, there was an increase in RUNX2 levels (Fig 21A), however the mRNA levels were not affected (Fig 21B) and this increase in RUNX2 protein levels was lost upon treatment with compound C (Fig 21A) which is an inhibitor of AMPK kinase activity. Next, we analyzed whether AMPK and RUNX2 interactions were sustained in MDA-MB- 231 cells. For this RUNX2 was subjected to IP in MDA-MB-231 cells and immunoblotted with p-AMPK and p-AMPK substrate specific antibody, post to treatment with metformin, AMPK and RUNX2 interaction was enhanced (Fig21C). Inorder to validate this interaction IP was carried out by pulling down p-AMPK and immunoblotted for RUNX2 where RUNX2 interaction with p-AMPK was enhanced upon metformin treatment and was lost when cells were treated with compound C (Fig 21D). To confirm interactions between RUNX2 and AMPK, RUNX2 was over expressed in MCF-7 and IP was carried out in the presence and/or absence of AMPK activators and inhibitors. Consistent with above results, p-AMPK interaction with RUNX2 was seen when the cells were treated with metformin and was lost upon treatment with compound C (Fig 21E). The interaction of p-AMPK and RUNX2 was confirmed and quantified by immunofluorescence analysis where physical interaction between RUNX2 and p-AMPK was evident upon metformin treatment (Fig 21F &G).

# 1.4.3.2. AMPK mediated phosphorylation of RUNX2 results in increased nuclear localization and transcriptional activity of RUNX2

Since RUNX2 is a transcription factor and AMPK phosphorylates RUNX2 in the DNA binding domain, we next analyzed the effect of AMPK induced RUNX2 phosphorylation on nuclear localization and function of RUNX2. Inorder to study nuclear localization of RUNX2 cytoplasmic and nuclear fractionation was carried out post to metformin and compound C treatment. Metformin treatment enhanced nuclear localization of RUNX2 and the scenario was reversed upon compound C treatment (Fig 22A). Inorder to confirm the role of Ser 118 phosphorylation in enhanced nuclear localization, we performed IP of RUNX2 in nuclear extracts which revealed the presence of high levels phospho-RUNX2 in nuclear fraction upon treatment with metformin (Fig 22B). Analysis of RUNX2 transcriptional targets that aid in breast cancer metastasis revealed, regulation of mTOR promoter by RUNX2 (137).



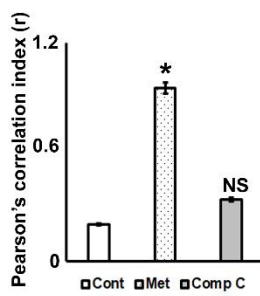


FIGURE 21: RUNX2 is a substrate of AMPK in breast cancer cells. MDA-MB-231 cells were subjected to either metformin (15 mM) or compound C (5 μM) treatment for 12 hours or none and A) immunoblot analysis and B) RT-PCR analysis was done. MDA-MB-231 cells were subjected to metformin (15 mM) or compound C (5 μM) treatment for 12 hours or none and IP by C) RUNX2 pull down and levels of RUNX2, p-AMPK substrate and p-AMPK were analyzed or by D) p-AMPK pull down and levels of RUNX2, p-AMPK were analyzed. E) MCF-7 cells were transfected with either RUNX2 WT or RUNX2 S 94 A or RUNX2 S 94 D or none, along with or without metformin (15 mM) treatment for 12 hours post to 48 hours of transfection and subjected to IP analysis by p-AMPK pull down and levels of p-AMPK and RUNX2-RFP were analyzed. F) MDA-MB-231cells subjected to metformin (15 mM) or compound C (5 μM) treatment for 12 hours and immunofluorescence by anti-RUNX2 (Alexa 594) and anti-AMPK (Alexa 488) antibodies counter stained with DAPI was done. G) Quantification of immunofluorescence data using ImageJ. Mean  $\pm$  S.E.M.; N=3. \*p<0.05 versus control, NSp>0.05 versus control. The immunofluorescence and quantification experiments were carried out on three independent fields.

Cont: control, Met: metformin, Comp C: compound C, IP: immunoprecipitation, IB: immunoblotting, EV: empty vector, WT: wild type, NS: non-significant.

It was also seen that mTORC2 (mammalian target of rapamycin complex 2) is regulated by RUNX2, but the mechanism was unclear (138). Bioinformatic analysis of rictor (a key component in mTORC2) promoter revealed the presence of RUNX2 binding consensus (ACCACA, which is known as Osteoblast Specific cis acting Element 2 (OSE2)) at -1884 kb. The role of RUNX2 Ser 118 phosphorylation on regulation of rictor was further confirmed by transfecting MCF-7 cells with RUNX2 wild type, RUNX2 S 118 A (phosphonull mutant) and RUNX2 S 118 D (phosphomimic mutant) variants and nuclear extracts were subjected to EMSA. It could be seen that RUNX2 WT treated with metformin and phosphomimic mutant had a potent binding to rictor promoter compared to RUNX2 WT or phosphonull mutant (Fig. 22C). Next, we checked the effect of RUNX2 phosphorylation on its transcriptional activity by measuring the mRNA and protein levels of its target genes like rictor, VEGF (139) and MMP-9 (140). MDA-MB-231 cells were treated with metformin and or compound C and protein and mRNA levels of rictor, VEGF and MMP-9 were assessed. Upon treatment with metformin there was upregulation of rictor, MMP-9 and VEGF at both protein and mRNA levels which was lost in case of treatment with compound C (Fig 22D &E). Inorder to confirm the role of RUNX2 in metformin mediated upregulation of rictor, VEGF and MMP-9; We performed knockdown of RUNX2 in MDA-MB-231 cells and analyzed rictor, VEGF and MMP-9 levels. Upon knockdown of RUNX2 even in the presence of metformin there was no upregulation of these genes indicating that RUNX2 is required for metformin mediated

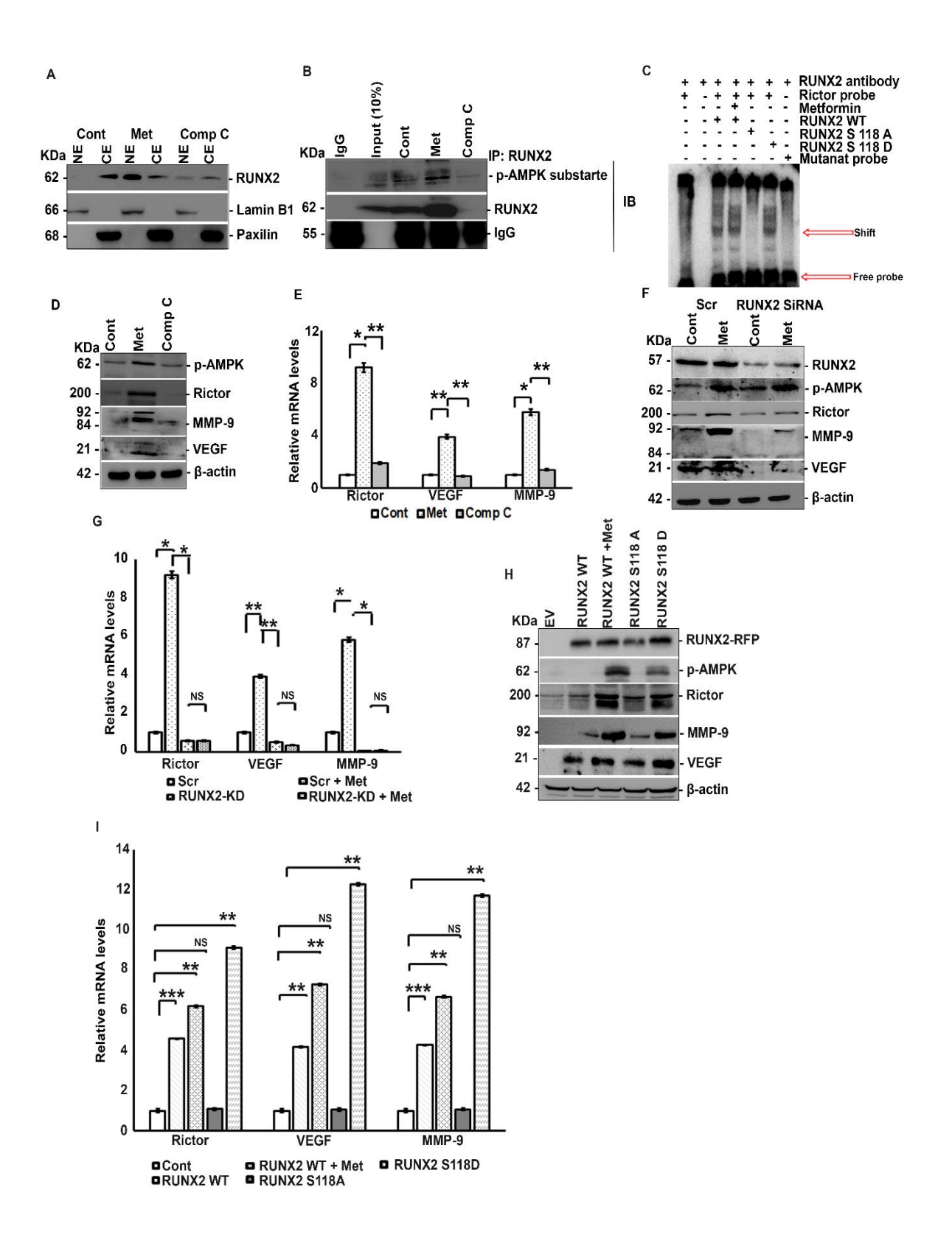


FIGURE 22: AMPK mediated phosphorylation of RUNX2 results in increased nuclear localization and transcriptional activity of RUNX2. MDA-MB-231 cells were exposed to metformin (15 mM) or compound C (5 µM) for 6 hours or none and subjected to nuclear-cytoplasmic extraction followed by A) immunoblot analysis and B) IP analysis of nuclear extracts by RUNX2 pull down and levels of RUNX2, p-AMPK substrate and p-AMPK were analyzed. C) MDA-MB-231 cells were exposed to either metformin (15 mM) or compound C (5 µM) treatments for 6 hours or none and nuclear extracts were subjected to EMSA. MDA-MB-231 cells were exposed to either metformin (15 mM) or compound C (5 μM) for 12 hours and subjected to **D**) immunoblot analysis. MDA-MB-231 cells were exposed to either metformin (15 mM) or compound C (5 µM) for 6 hours and subjected to E) RT-PCR analysis. MDA-MB-231 cells were transfected with RUNX2 siRNA with or without metformin (15 mM) treatment for 12 hours and 6 hours respectively and subjected to F) immunoblot analysis and G) RT-PCR analysis. MCF-7 cells were transfected with either RUNX2 WT or RUNX2 S 94 A or RUNX2 S 94 D or none, along with or without metformin (15 mM) treatment for 12 hours and 6 hours respectively post to 48 hours of transfection and subjected to H) immunoblot analysis and I) RT-PCR analysis. Mean ± S.E.M.; N=3. \*p<0.05 versus control, \*\*p<0.005 versus control, \*\*\*p<0.005 versus control, NSp>0.05 versus control. The immunofluorescence and quantification experiments were carried out on three independent fields.

Cont: control, met: metformin, Comp C: compound C, CE: cytoplasmic extract, NE: nuclear extract, RUNX2-KD: RUNX2 knock down by siRNA, Scr: scrambled, EV: empty vector, WT: wild type, NS: non-significant.

upregulation of rictor, VEGF and MMP-9 (Fig 22F &G). Inorder to validate the role of ser 118 phosphorylation in RUNX2 mediated upregulation of rictor, VEGF and MMP-9, we expressed RUNX2 WT, S118 A & S118 D in MCF-7 cells and checked the target expression levels. In case of metformin treated WT and phosphomimic mutant of RUNX2 there was upregulation of the RUNX2 targets, however this was lost or reduced when transfected with phosphonull mutant or WT in absence of metformin treatment (Fig 22H &I) which clearly indicates the role of RUNX2 Ser 118 phosphorylation in upregulation of rictor, VEGF and MMP-9.

#### 1.4.3.3. mTORC2 is crucial for AMPK/RUNX2 axis

Rictor which was upregulated upon treatment with metformin in a RUNX2 dependent manner, is a key component required for activation of mTORC2 (28). mTORC2 is in turn involved in RUNX2 regulation through inhibition of GSK3 $\beta$  (141), which is one of downstream targets of mTORC2 that is involved in RUNX2 repression. GSK3 $\beta$  also phosphorylates RUNX2 in the runt domain, but this phosphorylation has an inhibitory effect on RUNX2 activity (142). So, we then analyzed the effect of p-AMPK/RUNX2 axis on RUNX2 interaction with GSK3 $\beta$ . Inorder to understand the role of mTORC2 in RUNX2 regulation; rictor and raptor (which are

key components of mTORC2 &C1 respectively) were knocked down by siRNA treatment and RUNX2 levels were analyzed. It was seen that RUNX2 downregulation was specific to rictor knockdown but not raptor (Fig 23A) which indicates that mTORC2 is critical for RUNX2

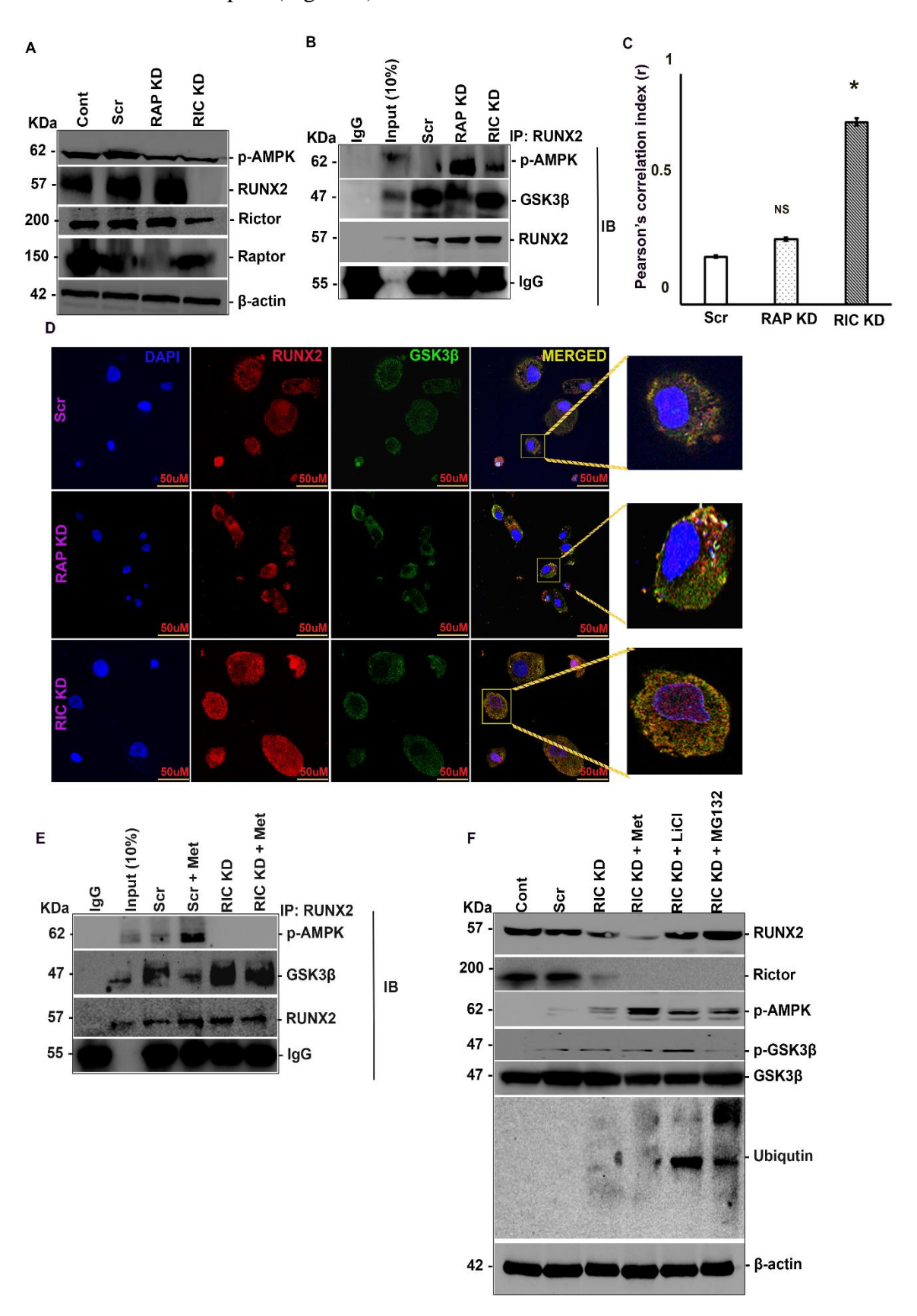


FIGURE 23: mTORC2 is crucial for AMPK/RUNX2 axis. MDA-MB-231 cells were transfected with siRNA's against rictor and raptor or none and 48 hours post transfection subjected to **A**) immunoblot analysis and **B**) IP analysis by RUNX2 pull down and levels of RUNX2, GSK3β and p-AMPK were analyzed. MDA-MB-231 cells were transfected with siRNA's against rictor and raptor or none and 48 hours post transfection subjected to **C**) Quantification of immunofluorescence data using ImageJ. **D**) immunofluorescence by anti-RUNX2 (Alexa 594) and anti-GSK3β (Alexa 488) antibodies counter stained with DAPI. **E**) MDA-MB-231 cells were transfected with rictor siRNA with or without metformin (15 mM) treatment for 12 hours and subjected to IP by RUNX2 pull down and levels of RUNX2, GSK3β and p-AMPK were analyzed. **F**) MDA-MB-231 cells were transfected with rictor siRNA with or without metformin (15 mM) or LiCl (0.5 M) or MG-132 (3 mM) treatment for 12 hours and subjected to immunoblot analysis. Mean ± S.E.M.; N=3. \*p<0.05 versus scrambled, NSp>0.05 versus scrambled. The immunofluorescence and quantification experiments were carried out on three independent fields.

Cont: control, Met: metformin, Comp C: compound C, IP: immunoprecipitation, IB: immunoblotting, Scr: scrambled, Rap: raptor, Ric: rictor, NS: non-significant.

stability and acts possibly upstream of AMPK activation. To further validate role of mTORC2 in RUNX2 regulation; RUNX2 IP was carried out upon raptor and rictor knock down and RUNX2 interaction with p-AMPK and GSK3β were analyzed. RUNX2 and p-AMPK interaction was lost upon rictor knockdown and at the same time RUNX2 interaction with GSK3β was enhanced whereas in case of raptor knock down there is an increased interaction between RUNX2 and p-AMPK along with reduced interaction between RUNX2 and GSK3β (Fig 23B). GSK3β interaction with RUNX2 was further validated by immunofluorescence in presence or absence of rictor (Fig 23C &D). To further understand the effect of mTORC2 on RUNX2 and p-AMPK interaction, cells were subjected to IP by RUNX2 upon rictor knockdown in the presence or absence of metformin. Metformin treatment had no effect on RUNX2 interaction with GSK3β in the absence of rictor and upregulated p-AMPK was also unable to bind to RUNX2 in the absence of rictor; However, the scenario was reversed in the presence of rictor (Fig 23E). To further confirm that mTORC2 action is indeed mediated through GSK3B, cells were treated with LiCl (inhibitor of GSK3 kinase activity), metformin and MG-132 along with downregulation of rictor. RUNX2 levels were downregulated upon rictor knockdown and were rescued when treated with either LiCl or with MG-132 but not upon metformin treatment (Fig 23F) indicating that mTORC2 is upstream of AMPK/RUNX2 axis and is crucial for AMPK/RUNX2 interaction.

#### 1.4.3.4. Metformin promotes EMT and induces osteoblast like phenotype to breast cancer

#### cells thorough p-AMPK/RUNX2/mTORC2 axis

Bone metastasis is the most common anomaly associated with advancement of breast cancer (143). Most of these cells express osteoblast like genes inorder to metastasize and home in bone (144). The bone microenvironment not only provides them with growth factors required to support proliferation but also in helps in development of drug resistance (145). Several studies have shown that metformin is a potent therapeutic candidate for cancer treatment (146). Hitherto, effect of metformin on bone metastasis of breast cancer cells is poorly understood. Recent studies have shown that RUNX2 (147) as well as mTORC2 (148) play a key role in breast cancer metastasis. Thus, we analyzed the effect of metformin treatment on induction of EMT and osteoblast like phenotype in breast cancer cells.

The first event in induction of EMT is transcriptional repression of E- cadherin (Fig 24). Metformin treatment of MDA-MB-231 cells resulted in transcriptional repression of Ecadherin in RUNX2 dependent manner (Fig 25A-D). To confirm the role of Ser 118 phosphorylation in suppression of E-cadherin, MCF-7 cells were transfected with phosphomutants and E-cadherin levels were analyzed with or without metformin treatment. Ecadherin suppression was high in cells transfected with RUNX2 WT along with metformin treatment and in RUNX2 S 118 D mutant (Fig 25E &F). The next important step in EMT is expression of appropriate mesenchymal markers which in this case is CDH11 (149).CDH11 levels were increased in MDA-MB-231 cells post to metformin treatment, which was lost when cells were subjected to RUNX2 knock down (Fig 25A-D). The role of RUNX2 Ser 118 phosphorylation in CDH11 upregulation was established when MCF-7 cells were transfected with RUNX2 variants. RUNX2 transfected cells had CDH11 upregulation, which was lost when transfected with phosphonull mutant (Fig 25E &F), confirming the importance of RUNX2 Ser 118 phosphorylation in CDH11 regulation. Finally, to home in bones the cancer cells should express bone specific surface markers (like CDH11), ECM proteins (like type I collagen (COL1A1), periostin (POSTN), cathepsin K (CTSK) etc.,) and bone remodeling transcription factors (like RUNX2). It was reported that nearly 57 BRG's were expressed in bone metastasizing breast cancer patients (137). So, inorder to check if metformin can induce osteoblast like phenotype in breast cancer cells, we have treated MDA-MB-231 cells with AMPK activator metformin and its inhibitor compound C and analyzed expression of COL1A1, POSTN and CTSK by RT-PCR. It was seen that all the three genes were upregulated in metformin treated samples and this upregulation was lost upon treatment with compound C (Fig 25G). Metformin mediated upregulation of COL1A1, POSTN and CTSK was dependent

on RUNX2 expression which was seen from loss of expression when RUNX2 was knocked down, even in presence of metformin (Fig 25H). Indeed, the upregulation was also dependent on S 118 phosphorylation as seen through MCF-7 cells transfected with RUNX2 variants (Fig 25I).

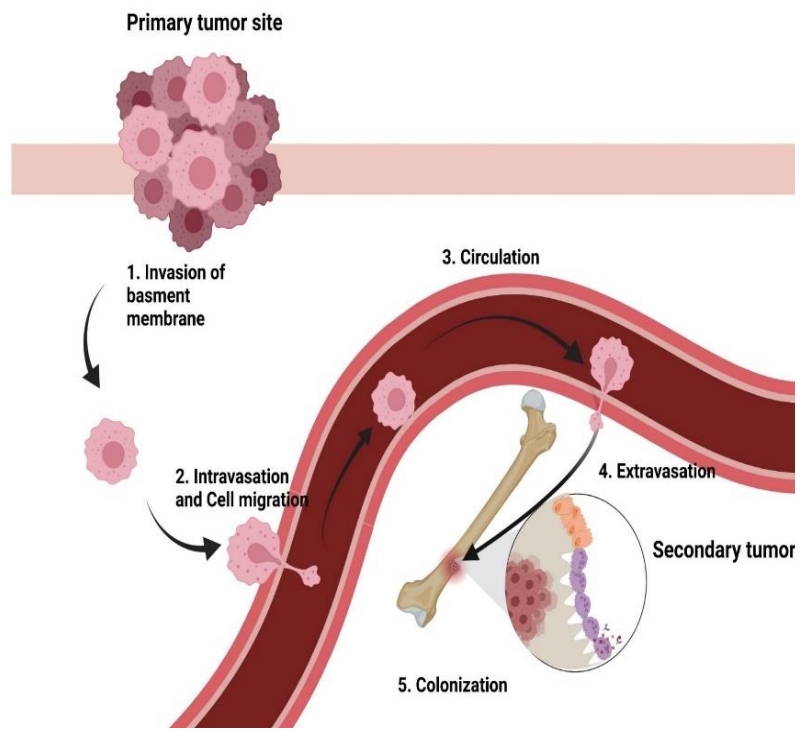


**FIGURE** 24: Schematic representation of steps involved in formation of secondary tumor. 1)The first involved is invasion of basement membrane by expression genes that could repress expression of E-cadherin MMP's. 2) Followed by intravasation and cell migration aided by cytoskeleton reorganization. 3) Then circulation in blood vessels followed by 4) Extravasation at suitable secondary tumor site and finally 5) colonization and homing of tumor cells through expression of genes native to site of invasion.

#### 1.4.3.5. Metformin promotes chemotaxis/ metastasis of transformed breast cancer cells

Next, step involved in cancer progression post to EMT is metastasis/cell motility. Activation of metastasis needs digestion of ECM proteins which can be achieved by upregulation of MMP's, other major event is actin reorganization to aid in cell movement (150). mTORC2 is the major regulator of cytoskeleton organization (30) and it was seen earlier, that metformin treatment resulted in upregulation of mTORC2 through rictor, so the downstream effectors of mTORC2 were analyzed; PKCs and AKT are well known targets of mTORC2 that are involved in activation of Rac1, which finally leads to cofilin phosphorylation and actin severing (148). Metformin treatment activated PKCβ and AKT through phosphorylation which resulted in phosphorylation of cofilin (Fig 26A), in a RUNX2 and mTORC2 dependent manner (Fig 26B). Involvement of RUNX2/AMPK axis in actin reorganization was further established when, MCF-7 cells transfected with RUNX2 Ser 118 phosphorylation variants also exhibited similar result (Fig 26C). The formation of actin stress

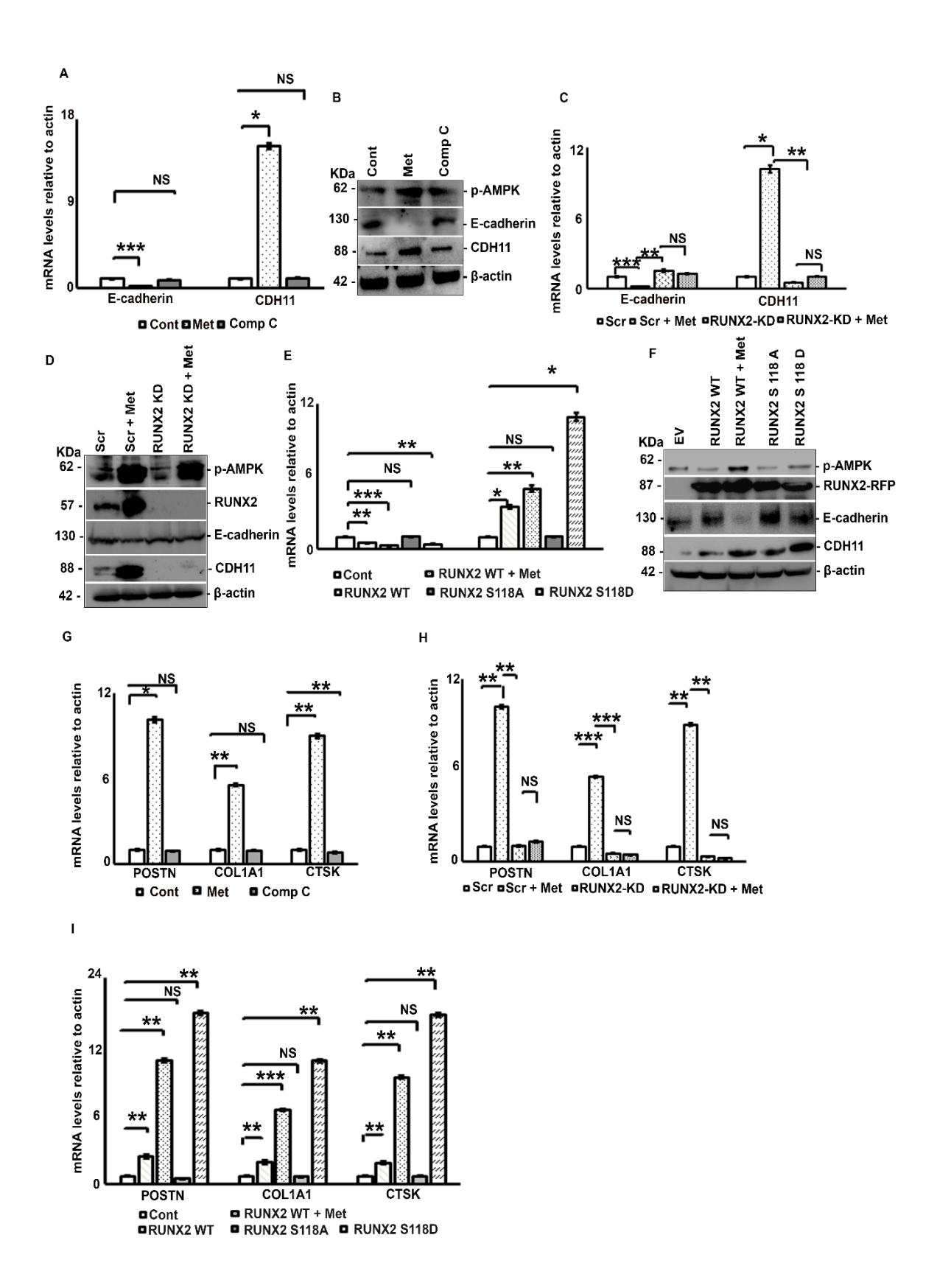


FIGURE 25: Metformin promotes EMT and induces osteoblast like phenotype to breast cancer cells thorough p-AMPK/RUNX2/mTORC2 axis. MDA-MB-231 cells were exposed to either metformin (15 mM) or compound C (5 μM) for 6 and 12 hours respectively and subjected to A) RT-PCR analysis and B) immunoblot analysis. MDA-MB-231 cells were transfected with siRNA against RUNX2 or none and 48 hours post transfection with or without metformin (15 mM) treatment for 6 and 12 hours respectively and subjected to C) RT-PCR analysis and D) immunoblot analysis. MCF-7 cells were transfected with either RUNX2 WT or RUNX2 S 94 A or RUNX2 S 94 D or none, along with or without metformin (15 mM) treatment for 6 and 12 hours respectively post 48 hours of transfection and subjected to E) RT-PCR analysis and F) immunoblot analysis. G) MDA-MB-231 cells were exposed to either metformin (15 mM) or compound C (5 μM) for 6 hours or none and subjected to RT-PCR analysis. H) MDA-MB-231 cells were transfected with siRNA against RUNX2 or none and 48 hours post transfection with o or without metformin (15 mM) treatment for 6 hours and subjected to RT-PCR analysis. I) MCF-7 cells were transfected with either RUNX2 WT or RUNX2 S 94 A or RUNX2 S 94 D or none, along with or without metformin (15 mM) treatment for 6 hours post to 48 hours of transfection and subjected to RT-PCR analysis. Mean ± S.E.M.; N=3. \*p<0.05 versus scrambled or control, \*\*p<0.005 versus scrambled or control, \*\*\*p<0.0005 versus scrambled or control, NSp>0.05 versus scrambled or control. The immunofluorescence and quantification experiments were carried out on three independent fields.

Cont: control, met: metformin, Comp C: compound C, IP: immunoprecipitation, IB: immunoblotting, Scr: scrambled, RUNX2KD: knock down of RUNX2 using siRNA, WT: wild type, NS: non-significant, POSTN: periostin, CTSK: cathepsin K, COL1A1: type I collagen.

fibers is a prerequisite for cell migration (151) and metformin treatment of MDA-MB-231 cells resulted in formation of f-actin stress fibers which were absent in both control and compound C treatment sets (Fig 26D &E). Post to formation of stress fibers is chemotaxis of cells towards favorable secondary niche, which in this case is bone. We next evaluated the role of AMPK induced RUNX2 Ser 118 phosphorylation on bone specific movement of MCF-7 cells transfected with RUNX2 WT or S118 A or S118 D with or without metformin treatment. It was observed that MCF-7 cells transfected with RUNX2 WT along with metformin treatment and phosphomimic mutant had higher number of migrated cells then compared to RUNX2 WT alone or phosphonull mutant (Fig 26F). Migration of MCF-7 cells was lost when the lower chamber was seeded with HEK-293 T cells, indicating AMPK induced RUNX2 Ser 118 phosphorylation mediated chemotaxis to be specific for bone microenvironment (Fig 26G).

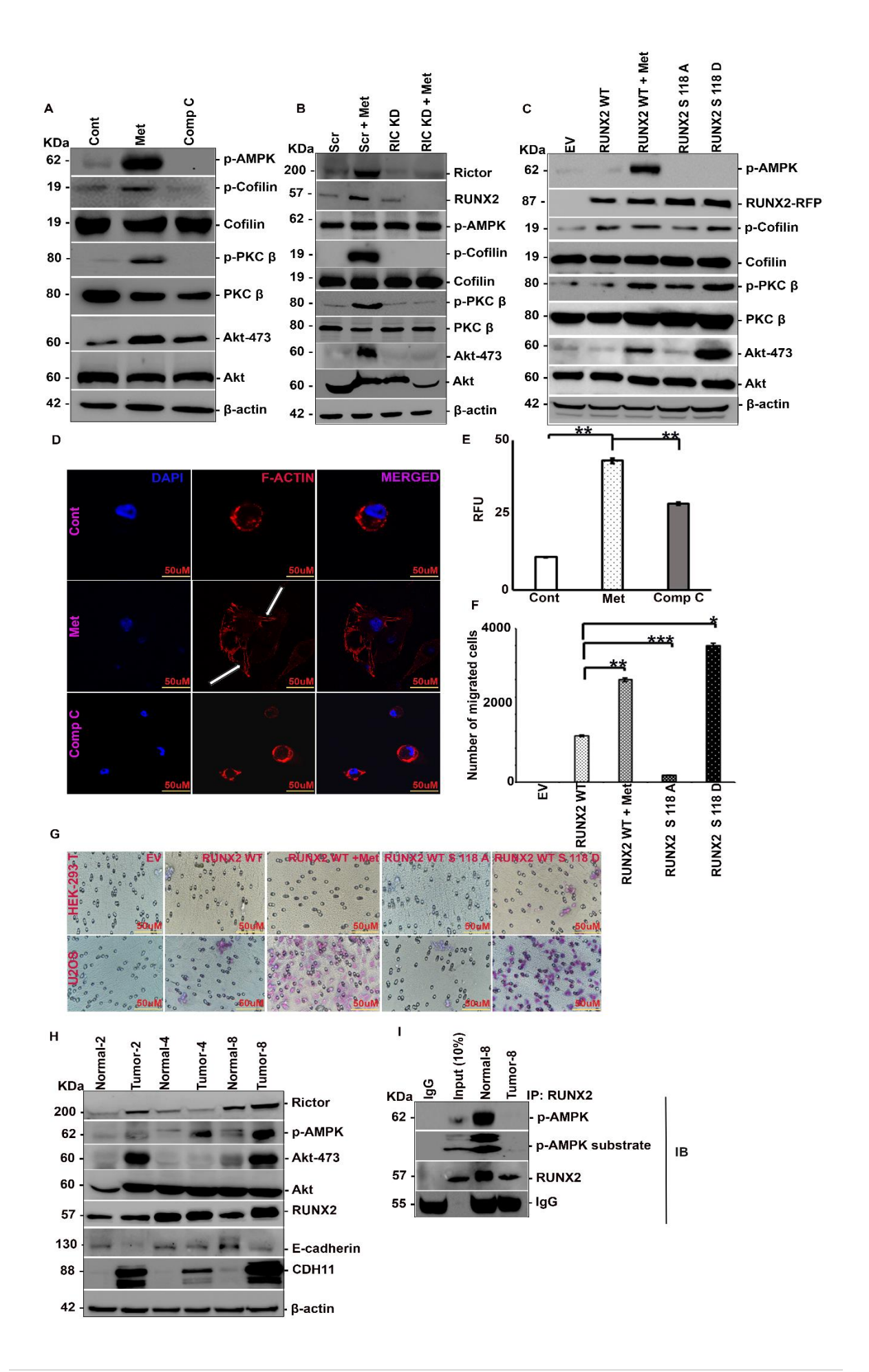


FIGURE 26: Metformin promotes chemotaxis/ metastasis of transformed breast cancer cells. A) MDA-MB-231 cells were exposed to either metformin (15 mM) or compound C (5 µM) for 12 hours or none and subjected to immunoblot analysis. B) MDA-MB-231 cells were transfected with siRNA against rictor or none and 48 hours post transfection with or without metformin (15 mM) treatment for 12 hours and subjected to immunoblot analysis. C) MCF-7 cells were transfected with either RUNX2 WT or RUNX2 S 94 A or RUNX2 S 94 D or none, along with or without metformin (15 mM) treatment for 12 hours post to 48 hours of transfection and subjected to immunoblot analysis. **D)** MDA-MB-231 cells were treated with either metformin (15 mM) or compound C (5 µM) for 12 hours or none and subjected to immunofluorescence stained using Rhodaminephalloidin (540), counter stained by DAPI. E) Quantification of fluorescence signal using ImageJ. F) Quantification of number of migrated cells by electron microscopy. G) MCF-7 cells were transfected with either RUNX2 WT or RUNX2 S 94 A or RUNX2 S 94 D or none, along with or without metformin (15 mM) treatment for 12 hours post to 48 hours of transfection and subjected to migration through collagen coated membrane, with lower chambers coated with either HEK-293 T cells or U2OS cells. Breast tumor tissue along with adjacent normal tissue were subjected protein isolation followed by H) immunoblot analysis and I) IP by RUNX2 pull down and levels of p-AMPK, RUNX2 and p-AMPK substrate specific motif were analyzed. Mean ± S.E.M.; N=3. \*p<0.05 versus control or WT, NSp>0.05 versus control. The immunofluorescence and quantification experiments were carried out on three independent fields.

Cont: control, Met: metformin, Comp C: compound C, IP: immunoprecipitation, IB: immunoblotting, Scr: scrambled, EV: empty vector, WT: wild type.

## 1.4.3.6. AMPK induced RUNX2 Ser 118 phosphorylation is highly expressed in breast tumor tissues

Our *in vitro* data was validated in tumor tissue along with adjacent normal tissues samples. It was seen that p-AMPK and RUNX2 levels were high in tumor samples compared to normal samples. In line with high levels of RUNX2, the downstream targets were also had higher expression like rictor and AKT-473, also tumors had high expression of CDH11and decreased expression of E- cadherin compared to normal samples (Fig 26H &SF 11A). RUNX2 Ser 118 phosphorylation by AMPK was assessed through IP pull down of RUNX2 in both normal and tumor tissues and IB with p-AMPK and p-AMPK substrate specific antibody. It was observed that only in tumor samples RUNX2 and p-AMPK interactions were maintained and RUNX2 was phosphorylated, as seen by p-AMPK substrate specific antibody (Fig 26I; SF 11B &C).

### **DISCUSSION**

#### 1.4.4. DISCUSSION

Survival rates for breast cancer vary from 80% to 40 % depending on the stage of cancer with aggressive stage having lowest survival rate (152). Bone metastasis is the most common occurrence associated with aggressive stage which is one of the reasons for drug resistance (153). Metformin has gained attention as a potent anti-cancer drug (154), owing to its ability to inhibit mTORC1 through p-AMPK, which is a major regulator of cap-dependent protein synthesis and autophagy (155); However, effect of metformin on EMT and bone metastasis remains unclear. Our earlier report on metformin's osteoprotective function has revealed that metformin can stabilize RUNX2 under diabetic conditions through p-AMPK dependent phosphorylation of RUNX2 at S118 position (78). With this background we have investigated whether RUNX2 and p-AMPK interaction was maintained in breast cancer cells expressing RUNX2. It was observed that p-AMPK and RUNX2 interactions were maintained upon metformin treatment in both triple negative and hormone receptor positive breast cell lines (MDA-MB-231 and MCF-7 expressing RUNX2). p-AMPK phosphorylates RUNX2 at runt homology domain, which is responsible for DNA binding ability of RUNX2, resulting in enhanced nuclear localization of RUNX2, post to metformin treatment. It was previously reported that RUNX2 is a major activator of metastasis in cancer cells, owing to its vast transcriptome repertoire (147). Some of the targets that are involved in EMT and metastasis include MMP-9 (156), VEGF (157), rictor and E-cadherin (158) where it either activates or represses them based on interacting partners. So, we examined the effect of metformin on RUNX2 mediated EMT and metastasis and observed that metformin treatment upregulated MMP-9, VEGF and rictor which play a key role in activating EMT by dissolving the ECM, initiating formation of new vascular capillaries and cytoskeletal reorganization to facilitate cell migration respectively.

GSK3β, is another kinase which phosphorylates RUNX2 in runt homology domain (142). But this phosphorylation has a negative effect on RUNX2. mTORC2 which is one of the downstream targets of RUNX2 is a known inhibitor of GSK3β (159). So, we pursued the role of mTORC2 on p-AMPK and RUNX2 interaction. We observed that in the absence of rictor, RUNX2 interaction with GSK3β was enhanced and metformin treatment had no effect on this interaction, indicating that mTORC2 acts upstream of p-AMPK. Rictor knockdown resulted in RUNX2 downregulation which was rescued upon LiCl treatment which is an inhibitor of GSK3β. This shows that mTORC2 and RUNX2 have a feed forward relation and mTORC2 is critical for metformin's action on RUNX2.

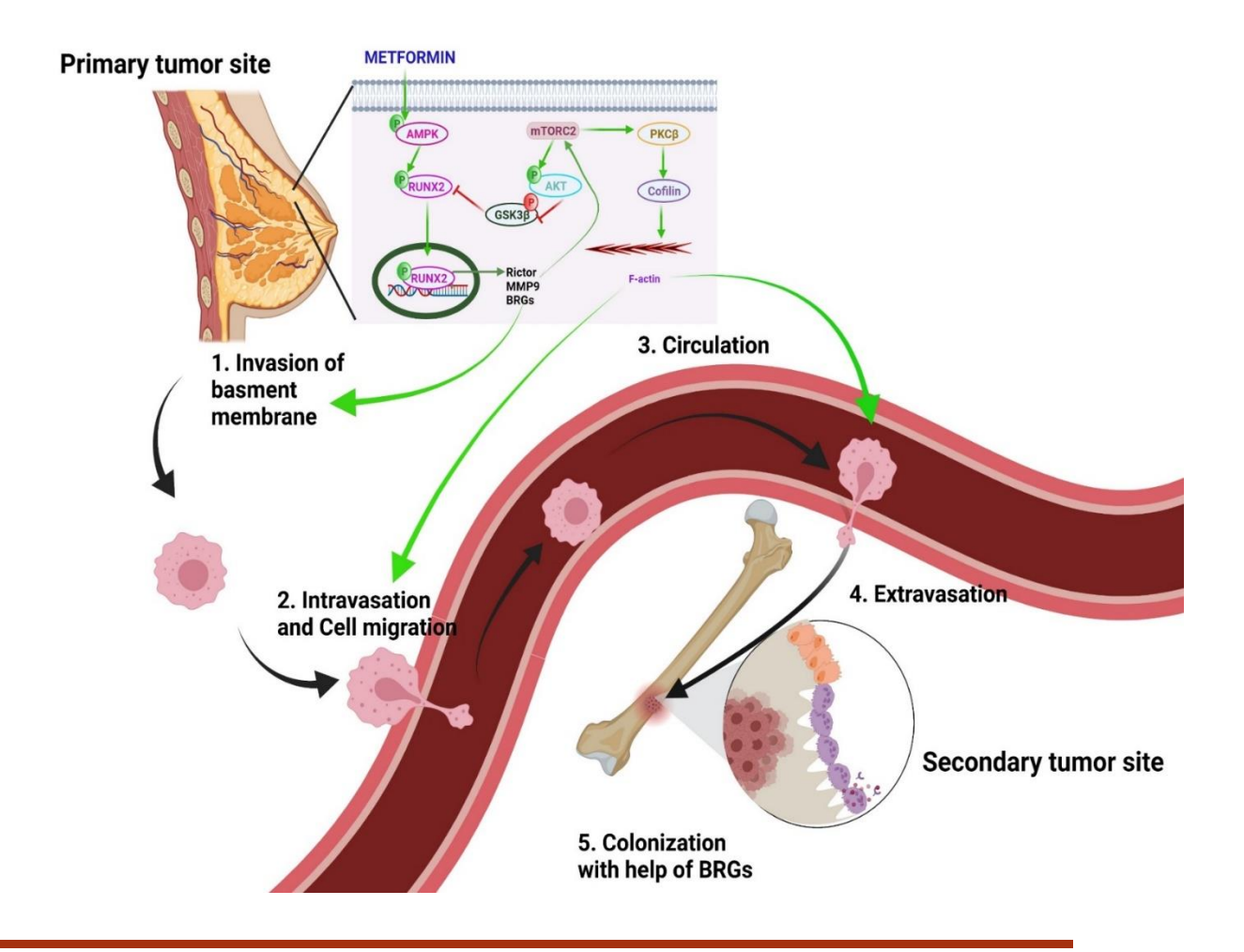


FIGURE 27: Schematic representation of metformin mediated stabilization of mTORC2/RUNX2 axis promotes bone metastasis of breast cancer cells.

1)The first involved in formation of secondary tumor is invasion of basement membrane at the primary tumor site through AMPK / RUNX2 axis mediated repression of E-cadherin and induction expression of MMP's which can digest the cell-to-cell connections. 2) Followed by intravasation and cell migration aided by AMPK/RUNX2/mTORC2 axis mediated cytoskeleton reorganization. 3) Then circulation in blood vessels followed by 4) Extravasation at suitable secondary tumor site and finally 5) colonization and homing of tumor cells through expression of BRGs (bone related genes).

Post to metastasis inorder for cells to establish a successful secondary tumor, the metastatic cells need to express genes that are native to invading tissue. In case of bone metastasis, the invading breast cancer cells need to acquire an osteoblast like phenotype (128, 144). Metformin mediated stabilisation of RUNX2 resulted in generation of osteoblast like phenotype in breast cancer cells, indicating that metformin treatment can promote bone metastasis of these cells.

Taken, together our data demonstrates that metformin treatment results in stabilization of RUNX2 through p-AMPK and these interactions are mTORC2 dependent. RUNX2 and mTORC2 stabilization by metformin results in activation of EMT and bone metastasis of breast cancer cells (Fig 27). The current work depicts as to why there is a different scenario in metformin clinical trials when compared to other cancer types. It also emphasizes that metformin treatment may not be the best clinical strategy, at least in case of breast cancer. However, further studies are warranted in this direction to reach a clear conclusion.

# OBJECTIVE -2

Understanding the effect of AMPK activation on glucose and glutamine metabolism in cancer and diabetes.

#### **OBJECTIVE 2.1**

# Analyzing the effect of metformin in altering glucose metabolism in CML

#### 2.1.1. LITERATURE REVIEW

Metabolic rewiring is a prerequisite for cancer cells to support their high proliferative rates (160). Several nutrient transporters and nutrient responsive pathways were shown to be aberrantly activated in cancers (161). Of these, lactate has recently gained immense importance owing to lactate shuttle theory in cancer (162). Lactate is produced and exported at a higher rate in imatinib resistant cells than that of their wild type counter parts (163). Thus, exported lactate can function either as source of energy or can act as a signaling molecule that can activate G-protein coupled receptors (GPCRs) and induce expression of several angiogenic factors and cytokines that can alter cell signaling and metabolism (164). High lactate producing cells usually have increased dependency on glucose and have enhanced rates of glucose uptake and glycolysis. Cancer cells often overexpress glucose transporters such as GLUT1 and also key enzymes involved in glycolysis such as hexokinase-II (HK-II). High expression of GLUT1 and HK-II correlates with poor survival rate of cancer patients (165-167). Thus, it is important to selectively inhibit glucose metabolism in cancer cells (168). Metformin is a widely used anti-glycemic drug for the treatment of type-2-diabetes. Preliminary studies have shown that metformin exhibits anti-leukemic properties (169). However, the molecular mechanisms by which metformin elicits its anti-leukemic effects remain elusive (170). In the current study, we report a novel mechanism by which metformin inhibits glucose uptake and lactate export and consequent changes in cell signaling in wild type and drug resistant K562 cell lines as well as in PBMCs of CML patients.

### **MATERIALS and METHODS**

#### 2.1.2. MATERIALS AND METHODS

#### **2.1.2.1.** *Cell culture*

Wild-type (WT) and imatinib-resistant (IR2, GR1, IR2-GR1(IGR1) and IR2-GR2(IGR2)) K562 cell lines were cultured in RPMI-1640 (Gibco, USA) medium supplemented with 10% FBS (Gibco, USA) and 1% pen-strep (Gibco, USA) as reported in our earlier study (78). IR2 cells were cultured in 0.25  $\mu$ M imatinib, while GR1, IGR1 and IGR2 cells were cultured in the presence of 0.25  $\mu$ M geldanamycin.

#### **2.1.2.2.** *Chemicals*

Imatinib, metformin and dorsomorphin (compound C) were procured from Sigma (USA). Geldanamycin was procured from TCI chemicals (Japan). Imatinib, geldanamycin and dorsomorphin were dissolved in DMSO (Finar, India), whereas metformin stocks were made in PBS.

#### 2.1.2.3. Isolation of PBMCs from CML patients

Was performed as mentioned in the earlier section (1.2.2.3).

#### 2.1.2.4. Cell viability assay

Was performed as mentioned in the earlier section (1.2.2.7).

#### 2.1.2.5. Lactate assay

A total of 5 X 10<sup>3</sup> cells per well were seeded in a 96-well plate in RPMI-1640 medium and treated with the indicated drugs for 12 hours. After treatment, lactate levels were measured using an L-lactate assay kit (#ab65330, Abcam, USA) following the manufacturer's instructions. Prior to lactate estimation, samples were subjected to deproteinization by the PCA/KOH method, and fluorescence was measured (excitation at 535 nM and emission at 587 nM).

#### 2.1.2.6. Glucose uptake assay

A total of 5 X 10<sup>3</sup> cells per well were seeded in a 96-well plate in RPMI-1640 medium and treated with the indicated drugs for 12 hours. After treatment, glucose levels were measured using a Glucose Uptake-Glo Assay kit (#J1342, Promega, USA) following the manufacturer's instructions. In brief, 24 hours prior to assay, cells were grown in OPTI-MEM (Gibco, USA), and 3 hours before assay, cells were transferred to RPMI-1640 medium without FBS. Cells were washed in PBS, and 50 μL of 1 mM 2-deoxyglucose (2DG) was added and

incubated for 10 minutes. Twenty-five microliters of stop buffer and neutralization buffer were added. Then, 100  $\mu$ L of 2DG6P detection reagent was added and incubated for 1 hour, and luminescence readings were taken.

#### 2.1.2.7. *ATP assay*

A total of 5 X 10<sup>3</sup> cells per well were seeded in a 96-well plate in RPMI-1640 medium and treated with the respective drugs for 12 hours. Following treatment, ATP levels were measured using a CellTiter-Glo luminescent cell viability assay kit (#G7570, Promega, USA) according to the manufacturer's instructions, and luminescence readings were recorded.

#### 2.1.2.8. RNA isolation and real time PCR (RT-PCR)

RNA isolation was carried out as mentioned in earlier sections (1.1.2.11). Real-time PCR was carried out by Bio-Rad SYBR Green QRT- PCR Master mix (Bio-Rad, USA). The quantification of real-time data was carried out by the  $2^{-\Delta\Delta CT}$  method. The sequences of primers used are

Target	Forward primer (5'-3')	Reverse primer (5'-3')
MCT1	TACCTCCAGACTCTCCTGGC	GTCCCCTCCGCAAAGTCTA
MCT4	CGTTCTGGGATGGGACTGAC	ATGTGCCTCTGGACCATGTG
GLUT1	CTGCTCATCAACCGCAAC	CTTCTTCCCGCATCATCT
HK-II	TGATCGCCTGCTTATTCACG	AACCGCCTAGAAATCTCCAGA
Actin	GAGAGGGAAATCGTGCGTGAC	CATCTGCTGGAAGGTGGACA

#### 2.1.2.9. *Immunoblotting*

Following the inhibitor treatments, protein was isolated from cells and subjected to SDS-PAGE followed by immunoblotting as described in earlier section (1.1.2.9). Blots were probed using p-P70S6K (ab2571), P70S6K1/2 (ab32359), GLUT1 (ab115730), GLUT2 (Ab54460), GLUT3 (ab41525), GLUT4 (ab33780) and GLUT5 (ab41533) (Abcam, USA). HK-II (sc-374091), ubiquitin (sc-166553) and HIF1- $\alpha$  (sc-53546) (Santa Cruz Biotechnology Inc., USA) and p-AMPK (mAb#2535) and  $\beta$ -actin (mAb#4967) (Cell Signaling Technologies, USA.) antibodies as described in earlier section.

#### 2.1.2.10. Plasmid transfection

SLC2A1 (NM\_006516) (Cat. No- RC222696) was procured from Origene (USA). 2μg of purified plasmid (SLC2A1 or empty vector) were transfected using Lipofectamine-3000 (Thermo Fischer, USA) as described earlier (1.1.2.8).

#### 2.1.2.11. siRNA transfection

The siRNA for raptor (SI00698677) were purchased from Qiagen (Netherlands). All transfections were carried out using RNAifect (Cat. No- #301005) (Qiagen, Netherlands) following the manufacturer's instructions. In brief, 1  $\mu$ g of siRNA and 3  $\mu$ L of RNAifect were diluted in 200  $\mu$ L of plain DMEM (0.5% FBS) and incubated for 5 minutes; later, both were mixed and incubated for 30 minutes before adding the combined solution to cells. Cells were replaced with fresh regular medium after 6 hours of transfection (171).

#### 2.1.2.12. Statistical analysis

All data points are represented as mean  $\pm$  SEM. Statistical analysis was performed using one-way ANOVA. P values less than 0.05 were considered to be statistically significant. All data points were performed in triplicate, and a minimum of three independent experiments were carried out for all in vitro studies and patient data.

### **RESULTS**

#### **2.1.3. RESULTS**

#### 2.1.3.1. Metformin treatment inhibits lactate export in K562 (WT and resistant) cell lines

To understand the metabolic adaptations in drug resistance, we measured intra- and extracellular levels of lactate in wild-type (WT) K562 and imatinib-resistant cell lines. When compared with the WT cell line, all the imatinib-resistant cell lines showed high extracellular lactate levels with no to slight increase in intracellular lactate levels (Fig 28A & C). Since metformin was proposed to have an antileukemic effect, we then analyzed the effect of metformin on lactate export. Metformin treatment (10 mM for 12 hours) led to increased intracellular (Fig 28B) and reduced extracellular (Fig 28D) lactate levels in both the WT and imatinib-resistant cell lines, which was not seen when these cells were treated with compound C (an AMPK inhibitor) (5 µM for 12 hours) (Fig 28B &D). We then, assessed the effect of metformin treatment on the viability of WT and imatinib-resistant cell lines. As reported earlier (78), imatinib-resistant cell lines displayed higher survival percentage towards imatinib (BCR-ABL inhibitor) (Fig 28E) or geldanamycin (HSP90 inhibitor) (Fig 28F) treatment compared to WT cells. Importantly, metformin treatment inhibited the growth of resistant cell lines to a higher extent than WT (Fig 28G), suggesting the potential of metformin in overcoming imatinib resistance.

## 2.1.3.2. Metformin exerts anti-leukemic effect by inhibiting the expression of MCT1 & MCT4 through p-AMPK

Since lactate export was increased in resistant cells, we next checked the expression levels of lactate transporters. While MCT1 is primarily involved in import, MCT4 is responsible for the export of lactate (172). The expression of both MCT1 and MCT4 was significantly higher in all imatinib-resistant cell lines than in WT cells (Fig 29A); however, the increased expression of MCT4 in imatinib-resistant cell lines was markedly higher than that of MCT1. These results thus indicate the possibility that lactate efflux by MCT4 out-competes with its import by MCT1, leading to reduced lactate accumulation in imatinib-resistant cells. Importantly, metformin treatment led to a reduction in MCT1 and MCT4 expression, which was similar to the respective controls when treated with compound C (Fig 29B &C), suggesting the potential of metformin to interfere with lactate efflux, leading to lactate accumulation and consequent induction of cell death (Fig 28G). Earlier studies suggest that the function of MCT1 is regulated by mTORC1 (173) and that of MCT4 is regulated by hypoxia (174). Notably, all the imatinib-resistant cell lines displayed higher activity of mTORC1, as evident by increased phospho S6K levels (Fig 29D &E) and increased levels of HIF1-α compared to those of the WT cells (Fig

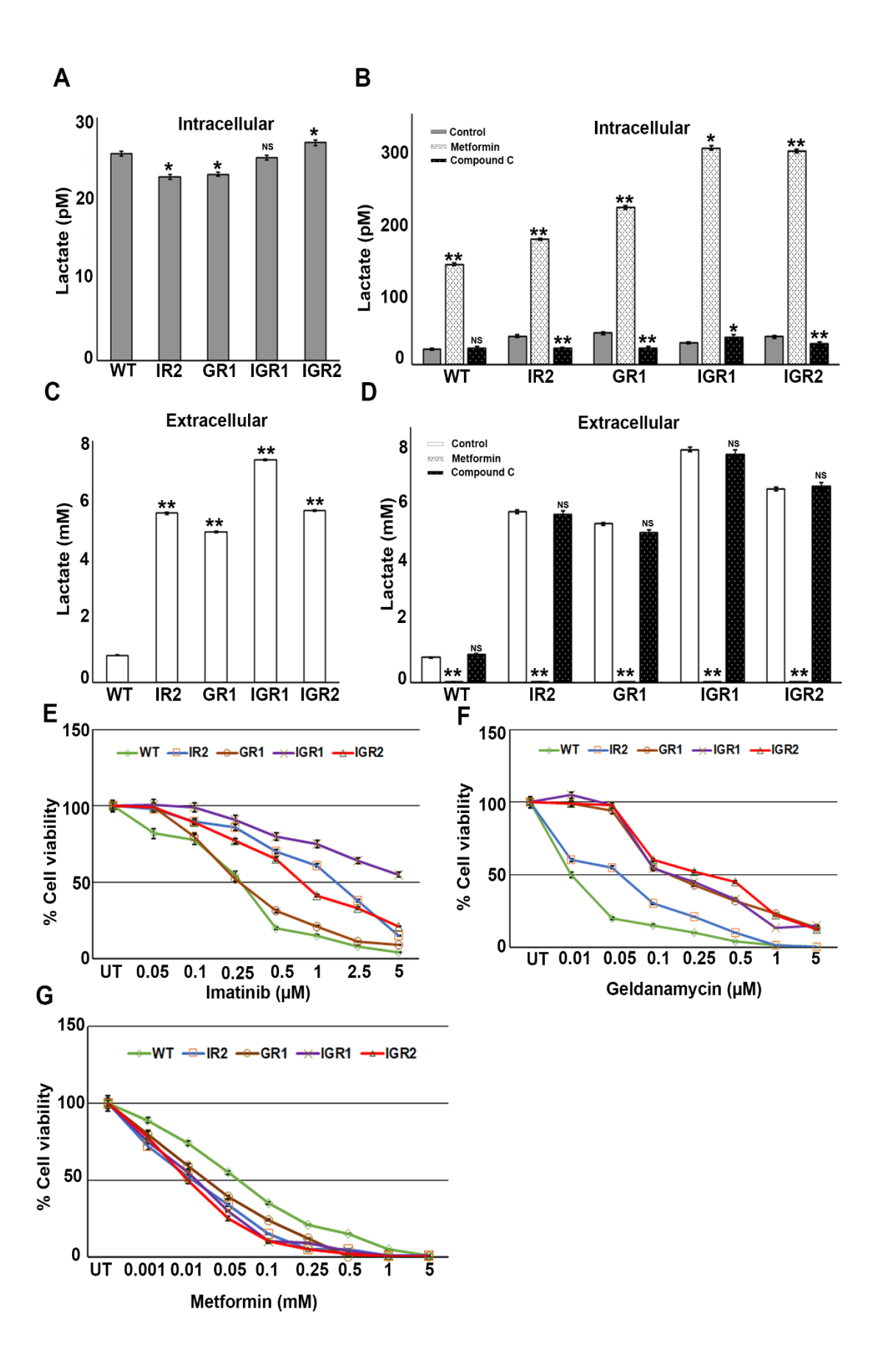


#### FIGURE 28: Metformin treatment inhibits lactate export of K562 (WT and imatinib-resistant) cell lines.

K562 WT, IR2, GR1, IGR1 and IGR2 cells were subjected to either metformin (10 mM) alone or with compound C (5  $\mu$ M) or none for 12 hours and **A**) & **B**) intracellular lactate levels were measured along with **C**) & **D**) extracellular lactate levels. K562 WT, IR2, GR1, IGR1 and IGR2 cell viability was measured when treated with either **E**) imatinib, or **F**) geldanamycin or **G**) metformin. Mean  $\pm$  S.E.M.; N=3, \*p<0.05 versus control or WT, \*\*p<0.05 versus control or WT, NSp>0.05 versus control or WT.

Cont: control, Met: metformin, Comp C: compound C, NS: non-significant, WT: wild type.

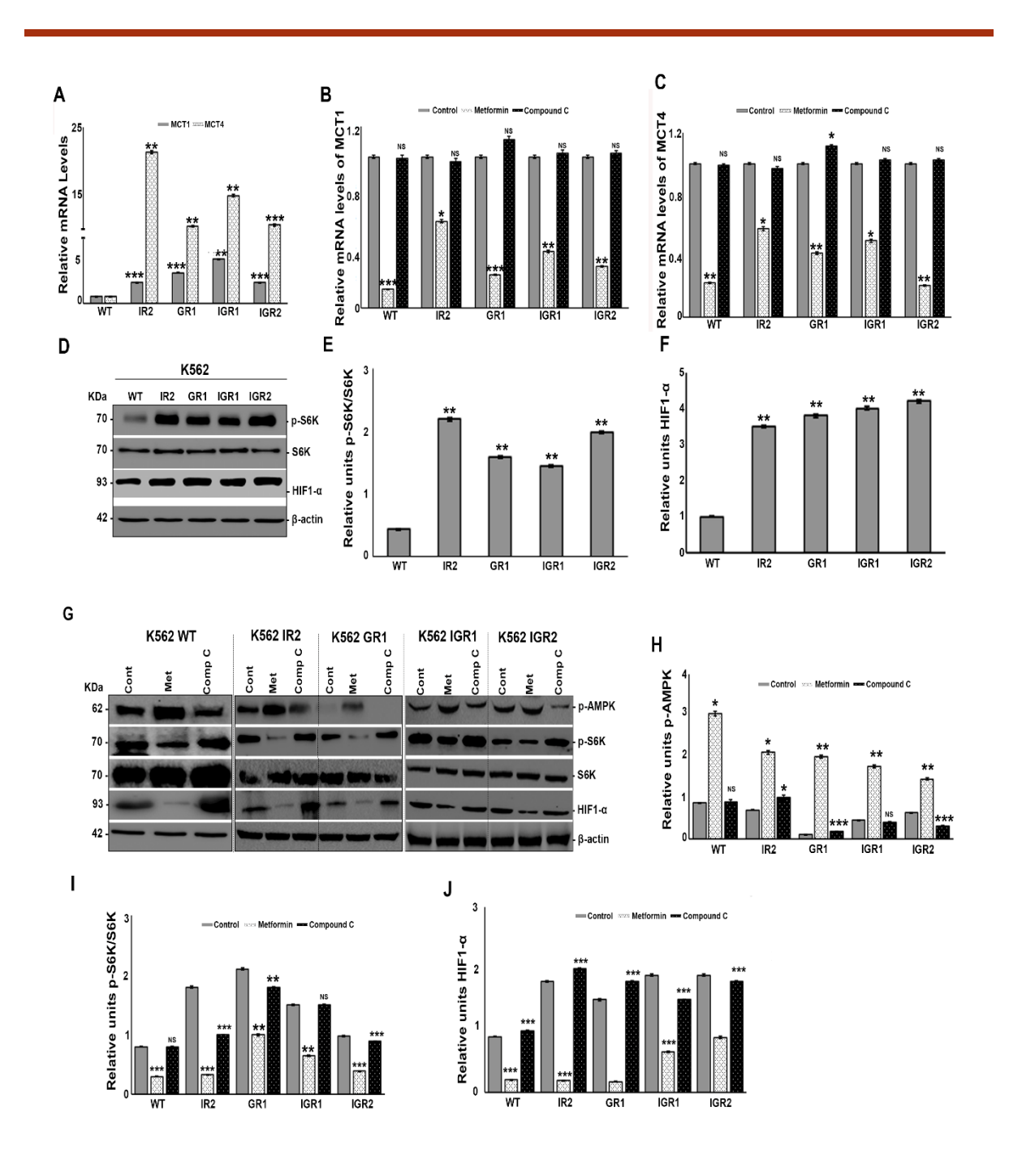


FIGURE 29: Metformin through p-AMPK results in suppression of MCT1 & 4 in K562 (WT and resistant) cell lines. K562 WT, IR2, GR1, IGR1 and IGR2 cells were subjected to **A**) RT-PCR analysis for MCT1 & 4. K562 WT, IR2, GR1, IGR1 and IGR2 cells were treated either with metformin (10 mM) alone or with compound C (5 μM) or none for 6 hours and subjected to RT-PCR analysis for **B**) MCT1 and **C**) MCT4. K562 WT, IR2, GR1, IGR1 and IGR2 cells were subjected to **D**) immunoblot analysis. Quantification of immunoblot data using Image J for **E**) p-S6K and **F**) HIF1-α. K562 cells were subjected to either metformin (10 mM) or compound C (5 μM) or none for 12 hours and immunoblot analysis was performed in **G**) WT, IR2, GR1, IGR1 and IGR2. Quantification of immunoblot data using Image J for **H**) p-AMPK, **I**) p-S6K and **J**) HIF1-α. Mean ± S.E.M.; N=3, \*p<0.05 versus control or WT, \*\*p<0.005 versus control or WT, \*\*\*p<0.0005 versus control or WT, \*\*\*p<0.0005 versus control or WT.

Cont: control, Met: metformin, Comp C: compound C, NS: non-significant, WT: wild type.

29D &F). When treated with metformin (Fig 29G &H), both the activity of mTORC1 (as assessed by phospho S6K levels) (Fig 29I) and the levels of HIF1- $\alpha$  (Fig 29I) were reduced in both WT and resistant cells compared to their respective untreated controls, thus establishing the role of the mTORC1-MCT1 and HIF1- $\alpha$ -MCT4 axes in regulating lactate levels in imatinib-resistant cell lines (Fig 29G-J).

## 2.1.3.3. Metformin attenuates glucose uptake in WT and resistant cells by inhibition of GLUT1

Increased lactate production depends on the uptake of glucose and the extent of its oxidation through glycolysis. Further experimental analysis revealed increased glucose uptake (Fig 30A) and ATP production (Fig 30C) in all imatinib-resistant cell lines compared to the WT-K562 cell line. Moreover, a reduction in glucose uptake and generation of ATP was observed under metformin-treated (10 mM for 12 hours) conditions in both WT-K562 and imatinib-resistant cell lines (Fig 30B &D). Expression analysis revealed a higher expression of GLUT1 in imatinib-resistant cells than in WT cells in comparison with other GLUT isoforms (Fig 30E &G; SF 12A). Additionally, higher expression levels of HK-II (Fig 30E & H; SF 12B), a key enzyme in glycolysis, were observed in imatinib-resistant cells than in WT cells, confirming the enhanced rate of the glycolytic pathway. Interestingly, metformin treatment (Fig 30I) reduced the mRNA expression (SF 12C &D) and protein levels (Fig 30I-L) of both GLUT1 and HK-II, suggesting a role of AMPK activity in regulating enhanced glucose metabolism.

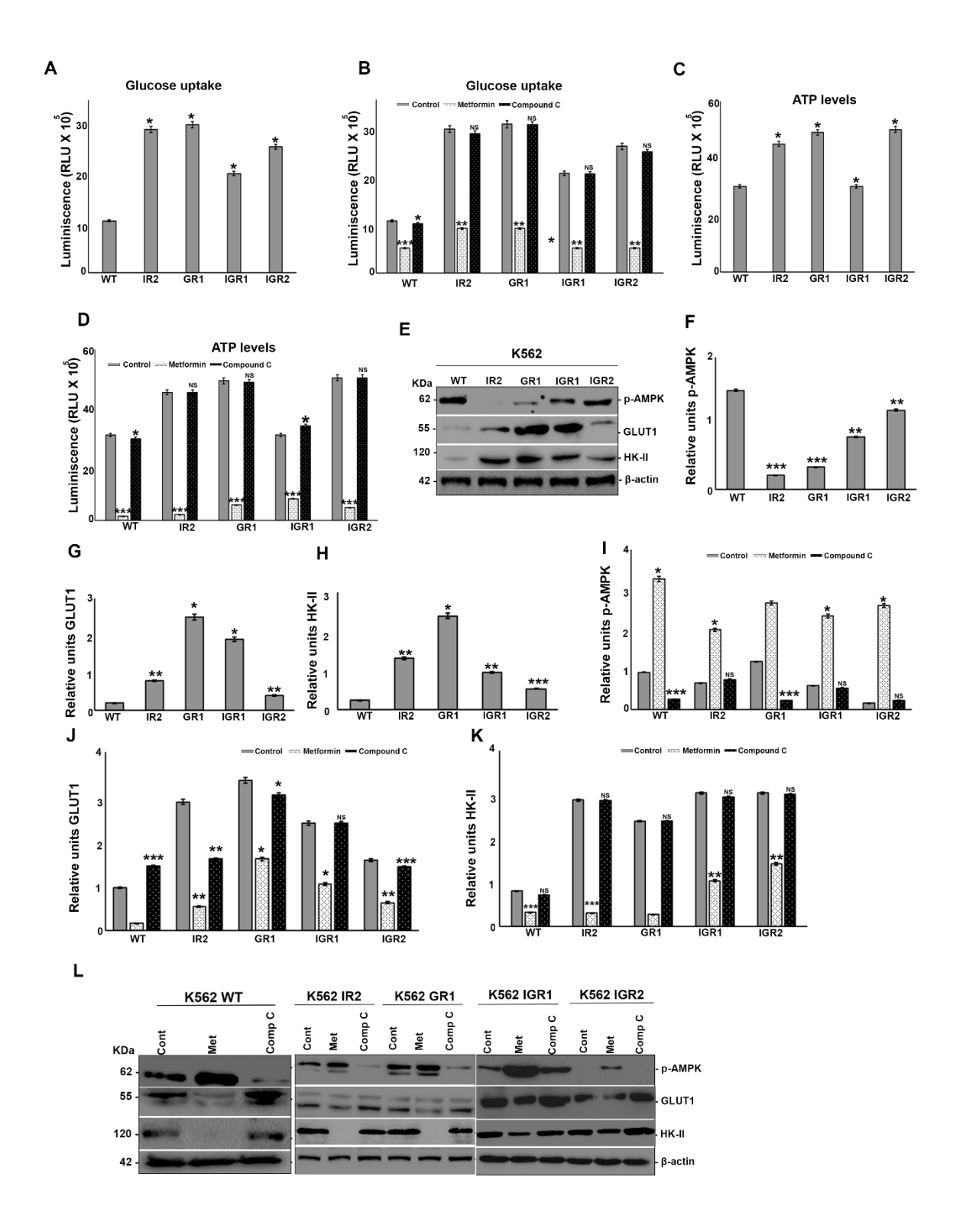


FIGURE 30: Metformin suspends glucose uptake in resistant and WT cells by inhibition of GLUT1. K562 WT, IR2, GR1, IGR1 and IGR2 cells were subjected to metformin (10 mM) or compound C (5  $\mu$ M) or none for 12 hours, and **A**) & **B**) glucose uptake was measured along with **C**) & **D**) ATP levels. K562 WT, IR2, GR1, IGR1 and IGR2 cells were subjected to **E**) immunoblot analysis. Quantification of immunoblot data using Image J for **F**) p-AMPK, **G**) GLUT1 and **H**) HK-II. K562 WT, IR2, GR1, IGR1 and IGR2 cells were subjected to either metformin (10 mM) alone or compound C (5  $\mu$ M) treatment or none for 12 hours and subjected to quantification of immunoblot data using Image J for **I**) p-AMPK, **J**) GLUT1, **K**) HK-II and **L**) immunoblot analysis. Mean  $\pm$  S.E.M.; N=3, \*p<0.05 versus control or WT, \*\*p<0.005 versus control or WT, \*\*\*p<0.0005 versus control or WT, \*\*\*p<0.0005 versus control or WT.

Cont: control, Met: metformin, Comp C: compound C, NS: non-significant, WT: wild type.

#### 2.1.3.4. Activated AMPK results in suppression of HIF1-a

Activation of AMPK is known to inhibit mTORC1 by phosphorylation of raptor, a key component of mTORC1 (175). To understand the regulation of HIF1- $\alpha$  by AMPK, we assessed the mRNA levels of HIF1- $\alpha$ . The mRNA levels of HIF1- $\alpha$  were high in imatinib-resistant cell lines compared to WT cells (Fig 31A). However, post metformin treatment (10 mM for 6 hours), HIF1- $\alpha$  transcript levels were reduced, and HIF1- $\alpha$  was unaffected in compound C treated (5  $\mu$ M for 6 hours) conditions compared with the control (Fig 31B). Concurrent with the transcript levels, HIF1- $\alpha$  protein levels were also reduced in metformin-treated cells (Fig 29G &J). Therefore, we next assessed the involvement of p-AMPK in the regulation of HIF1- $\alpha$  at the posttranslational level. When K562 cells were treated with MG-132 (an inhibitor of proteasomal degradation) along with metformin, HIF1- $\alpha$  levels were rescued in both WT and imatinib-resistant cells (Fig 31C-E), indicating the possibility of AMPK involvement in HIF1- $\alpha$  protein degradation.

### 2.1.3.5. Metformin inhibits lactate export through mTORC1 in WT and imatinib-resistant cells

As discussed above active AMPK could inhibit mTORC1, but to what extent mTORC1 was involved in regulation of lactate export was unclear. So, we have knocked down mTORC1 (by using siRNA directed against rictor, which is a key component of mTORC1 (175)) in K562 WT as well as imatinib-resistant lines and analyzed its effect on lactate export. It was seen that mTORC1 knock down resulted in high intracellular lactate levels in both WT and imatinib-resistant lines and this increase in intracellular lactate levels was similar to when cells were treated with metformin (Fig 32A). Similarly, there was a decrease in the extracellular lactate

levels when cell was subjected to mTORC1 knock down which was in line with observations

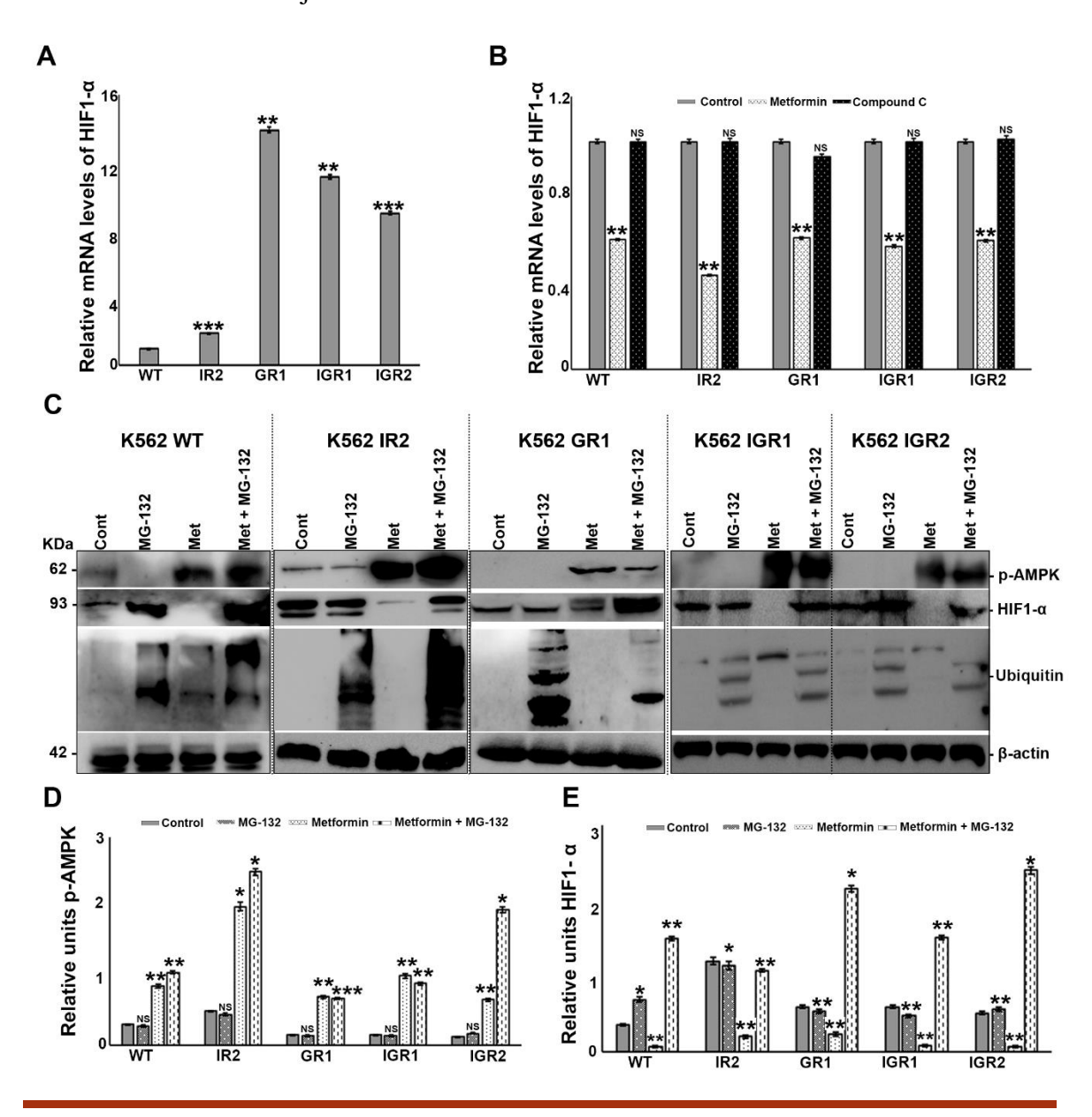


**FIGURE 31:** Activated AMPK results in suppression of HIF1-α. K562 WT, IR2, GR1, IGR1 and IGR2 cells were subjected to **A**) RT-PCR analysis of HIF1-α. K562 WT, IR2, GR1, IGR1 and IGR2 cells were treated either with metformin (10 mM) alone or with compound C (5 μM) or none for 6 hours and subjected to **B**) RT-PCR analysis of HIF1-α. K562 WT, IR2, GR1, IGR1 and IGR2 cells were subjected to either metformin (10 mM) alone or MG-132 alone (10 μM) or both or none for 12 hours and subjected to **C**) immunoblot analysis. Quantification of immunoblot data using Image J for **D**) p-AMPK and **E**) HIF1-α. Mean  $\pm$  S.E.M.; N=3, \*p<0.05 versus control or WT, \*\*\*p<0.005 versus control or WT, \*\*\*p<0.0005 versus control or WT.

Cont: control, Met: metformin, Comp C: compound C, NS: non-significant, WT: wild type.

seen when cells were treated with metformin alone (Fig 32B). When cells were treated with metformin along with mTORC1 knock down there was no further addition to the inhibitory effect observed when cells were subjected to mTORC1 knock down alone, indicating that metformin mainly acts through suppression of mTORC1 to exert an inhibitory effect on lactate export (Fig 32A &B). Since, metformin treatment could inhibit glucose uptake and ATP production of WT and imatinib-resistant cells (Fig 30B &D), we next analyzed the effect of mTORC1 knock down in inhibiting glucose uptake and ATP production. mTORC1 knock down resulted in inhibition of both glucose uptake and ATP production of WT as well as imatinib-resistant cells and this inhibition was similar to when cells were treated with metformin alone or in combination with mTORC1 knock down (Fig 32C &D). As, mTORC1 knock down resulted in inhibition of lactate export as well as glucose uptake and ATP production, we next analyzed the effect of knock down on the molecular players involved. It was evident that mTORC1 knock down resulted in decreased expression of GLUT1 and HK-II along with a reduced expression of HIF1- $\alpha$  (Fig 32E-K), which were key players involved in regulation of glucose and lactate metabolism. Inhibition of mTORC1 also resulted in downregulation of HIF1-α expression as, mTORC1 is required for HIF1-α translation (176), this resulted in reduced expression of both MCT1 (Fig 32L) and MCT4 levels (Fig 32M).

#### 2.1.3.6. GLUT1 overexpression renders metformin resistance to K562 WT and imatinibresistant cells

Metformin could inhibit the lactate export and reduce the viability of K562 WT and imatinib-resistant cells through suppression of mTORC1 and HIF1-α. Thus, we next validated if over expression of any of the downstream targets of mTORC1 and HIF1-α could affect the metformin sensitivity of K562 WT and imatinib-resistant cells. GLUT1 (SLC2A1) which is one of such downstream targets was over expressed in K562 WT, K562- IGR1 and K562-IGR2 lines (Fig 33A & B). It was seen that over expression of SLC2A1 resulted in increased glucose uptake (Fig 33C) by K562 WT, K562- IGR1 and K562- IGR2 lines along with increased ATP production (Fig 33D). In line with increased glucose uptake there was an increase in lactate production which was reflected as increased intra (Fig 33E) and extra cellular lactate levels (Fig 33F). However, the overexpression resulted in reduced metformin sensitivity of K562 WT, K562- IGR1 and K562- IGR2 lines when compared to control and mTORC1 knock down lines (Fig 33G-H).

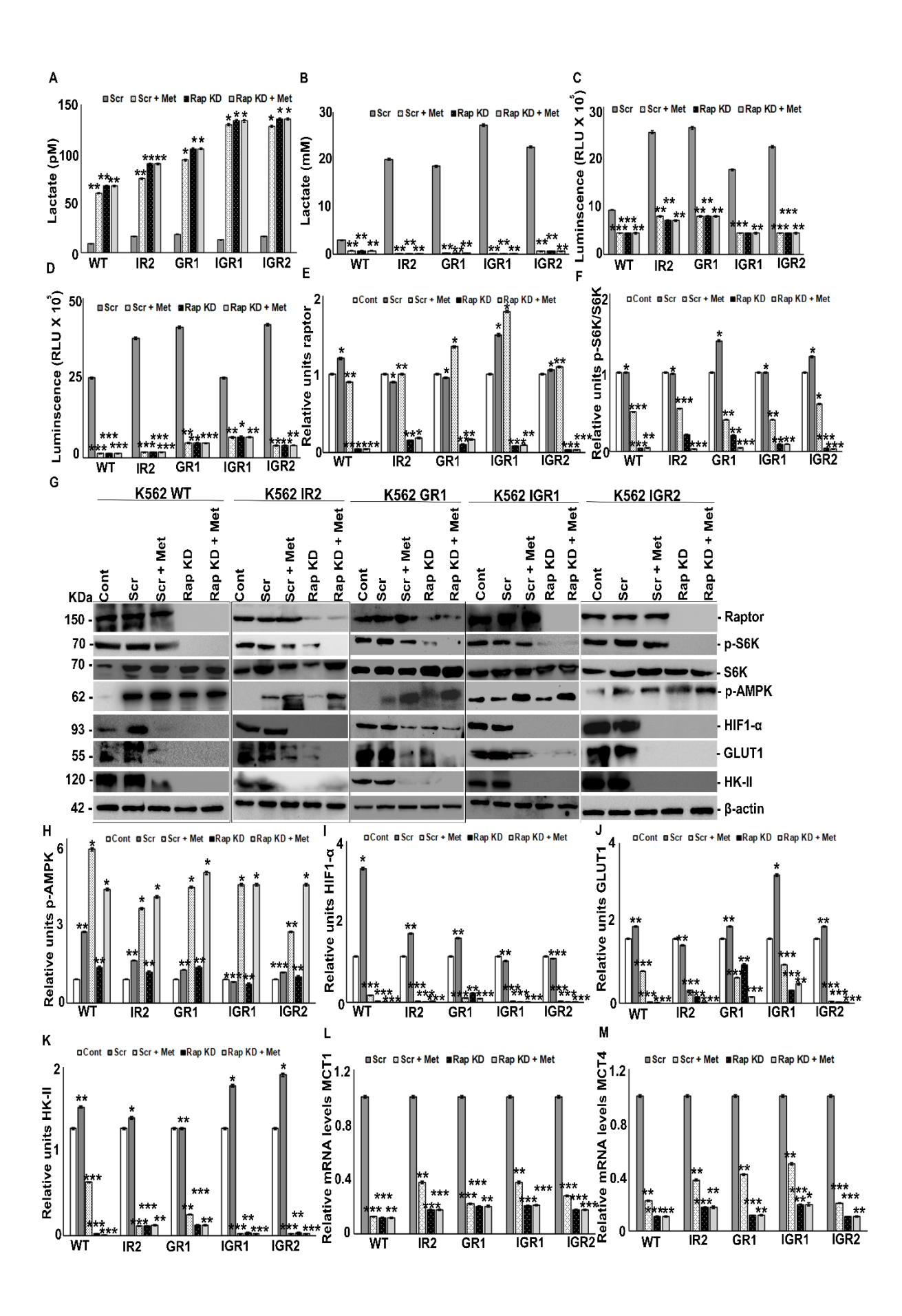
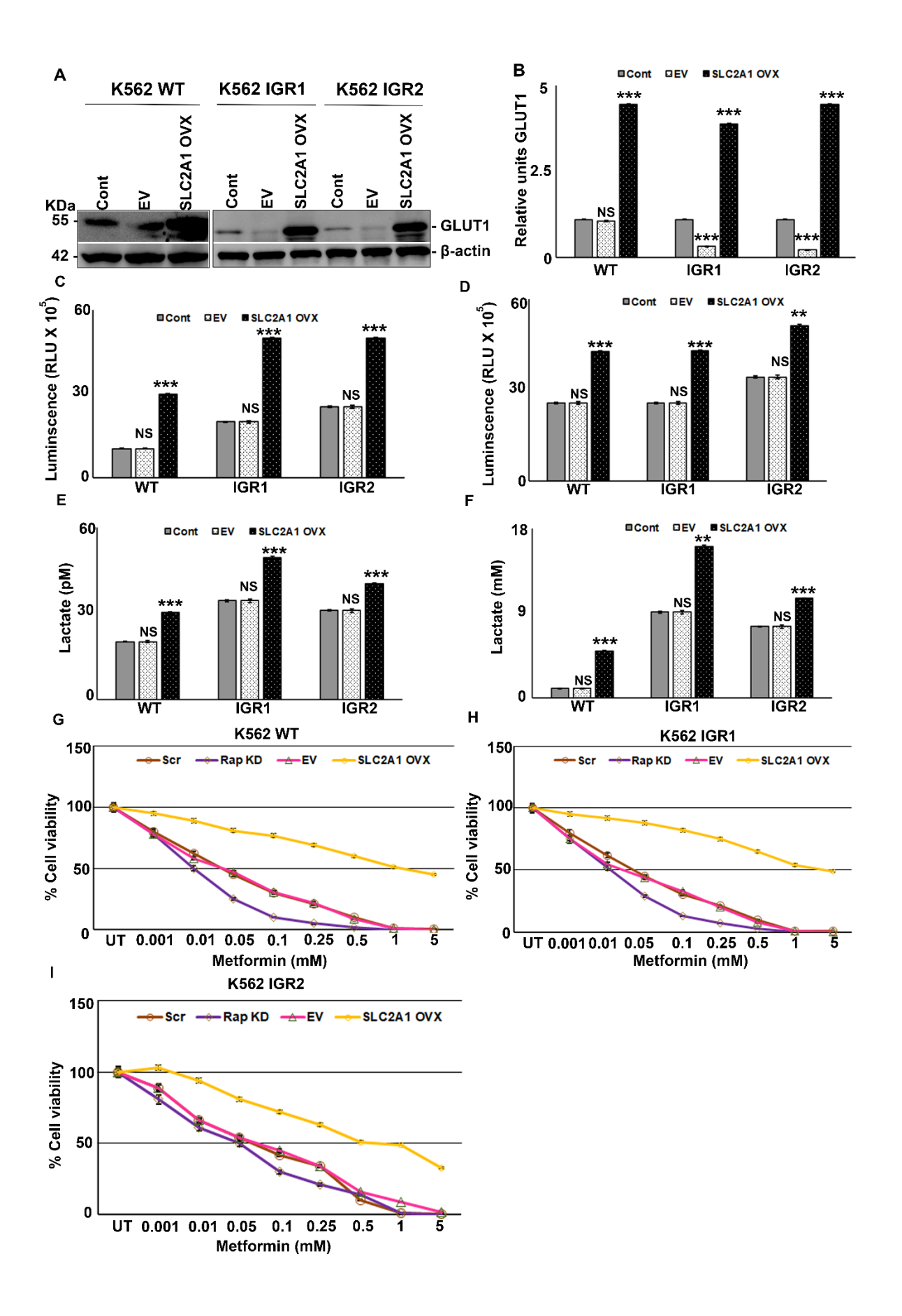


FIGURE 32: Metformin inhibits lactate export through mTORC1 in WT and imatinib-resistant cells. K562 WT and imatinib-resistant cells were transfected with either Scr or raptor siRNA and 48 hours post to transfection were treated with metformin (10mM) alone or none for 12 hours and  $\bf A$ ) intracellular lactate levels,  $\bf B$ ) extracellular lactate levels,  $\bf C$ ) glucose uptake levels and  $\bf D$ ) ATP levels were measured. K562 WT and imatinib-resistant cells were transfected with either Scr or raptor siRNA and 48 hours post to transfection were treated with metformin (10mM) alone or none for 12 hours and subjected to quantification of immunoblot data using Image J for  $\bf E$ ) raptor and  $\bf F$ ) p-S6K.  $\bf G$ ) immunoblot analysis. Quantification of immunoblot data using Image J for  $\bf H$ ) p-AMPK,  $\bf I$ ) HIF1- $\alpha$ ,  $\bf J$ ) GLUT1 and  $\bf K$ ) HK-II. K562 WT and imatinib-resistant cells were transfected with either Scr or raptor siRNA and 48 hours post to transfection were treated with metformin (10mM) alone or none for 6 hours and subjected to RT-PCR analysis of  $\bf L$ ) MCT1 and  $\bf M$ ) MCT4. Mean  $\pm$  S.E.M.; N=3, \*p<0.05 versus control, \*\*p<0.005 versus control, \*\*\*p<0.005 versus control.

Cont: control, met: metformin, Scr: scrambled, RAP KD: raptor knock down through siRNA, RLU: relative luminescence units.

## 2.1.3.7. Metformin attenuates glucose uptake and lactate export in PBMCs derived from CML subjects

We further validated the above findings in clinical samples. PBMCs were isolated from age-matched healthy and confirmed CML human subjects with a sample size of n=17, which included healthy subjects (n=4), imatinib-sensitive subjects (n=9) and imatinib-resistant subjects (n=4). PBMCs subjected to metformin (10 mM) or compound C (5 μM) for 12 hours. In line with the above observations, after metformin treatment, intracellular lactate levels were increased (Fig 34A, SF 13A, 14A &15A), with a concomitant decrease in extracellular lactate levels (Fig 34B, SF 13B, 14B &15B) in PBMCs isolated from healthy imatinib-sensitive and imatinib-resistant subjects, whereas the same was not observed in compound C-treated conditions, implying role of AMPK activation in mediating metformin induced effects on lactate export. Additionally, post metformin treatment (10 mM for 12 hours), there was a decrease in glucose uptake (Fig 34C, SF 13C, 14C &15C) and ATP generation (Fig 34D, SF 13D, 14D &15D), which was not seen in compound C treatment (5 µM for 6 hours). In addition, PBMCs were treated with metformin for 12 hours, and the mTORC1 and HIF1-α pathways were analyzed. Post to metformin treatment, there was reduction in expression of GLUT1 (Fig 34E &F) and HK-II (Fig 34E &G) along with inhibition of HIF1-α (Fig 34E &H) and HIF1-α (Fig 34E &J) in healthy, imatinib-sensitive and imatinib-resistant subjects (Fig 34E-J & SF 13E, 14E &15E). In line with reduced mTORC1 activity and HIF1-α levels, the expression of MCT1 and MCT4 were reduced following metformin treatment (Fig 34K & L; SF 13F &G, 14F &G, 15F &G) in PBMC samples of both imatinib-sensitive and imatinib-



**FIGURE 33: GLUT1 overexpression renders metformin resistance to K562** WT and imatinib-resistant **cells.** K562 WT and imatinib-resistant cells were transfected with either empty vector or with SLC2A1 and subjected to **A**) immunoblotting. Quantification of immunoblot data using Image J for **B**) GLUT1. K562 WT and imatinib-resistant cells were transfected with either empty vector or with SLC2A1 and **C**) glucose uptake levels, **D**) ATP levels, **E**) intracellular lactate levels and **F**) extracellular lactate levels were measured. Cells were transfected with either empty vector or SLC2A1 or siRNA against raptor or with scrambled siRNA and viability was measured post to treatment with metformin for 3 days in **G**) K562-WT, **H**) K562-IGR1 and **I**) K562-IGR2. Mean ± S.E.M.; N=3, \*\*p<0.005 versus control, \*\*\*p<0.0005 versus control, <sup>NS</sup>p>0.05 versus control. EV: empty vector, SLC2A1 OVX: SLC2A1 over expression, Scr: scrambled, RAP KD: raptor knock down through siRNA, RLU: relative luminescence units.

resistant subjects. Increased extracellular lactate levels, glucose uptake and ATP levels (Figure 34A-D; SF 13A-D, 14A-D &15A-D) in PBMCs isolated from imatinib-resistant subjects were observed compared to healthy and imatinib-sensitive subjects, further confirming the mechanistic role of enhanced glycolysis in secondary resistance, as seen in imatinib-resistant cell lines. Furthermore, the viability of PBMCs was assessed following metformin treatment. Similar to our earlier observation seen in cell line models, both imatinib-sensitive and imatinib-resistant clinical subjects exhibited cell death towards metformin treatment (Fig 34M-O; SF 13H-J, 14H-J & 15H-J).

### **DISCUSSION**

#### 2.1.4. DISCUSSION

One of the major adaptations by cancer cells is metabolic rewiring by which they sustain high proliferative rates. Here in we explore the effect of metformin on metabolic adaptations by cancer cells, more specifically in drug resistant cases. It was observed from our work and by others that cancer cells have high glucose consumption rate and glycolysis along with production of high amounts of lactate (177). It is of importance that lactate produced should be exported out of cell, else it can lead to cell death by lowering the pH of the cell. Intracellular acidification results in activation of JNK/c-JUN pathway, which results in upregulation of BAX induced apoptosis(178). The cancer cells overcome this hurdle by increasing the expression of lactate exporters MCTs (179).

It was seen from our current work and also by others that MCT1 & 4 are expressed highly in cancer cells which can aid in rapid clearance of lactate (180). Lactate once sent out can act either as a source of energy or can activate GPCRs depending on the cell type (181). So, it is of primary importance to inhibit lactate export, inorder to hamper cancer cell growth (182). From the above data it can be seen that metformin treatment resulted in inhibition of lactate export by PBMCs and reduced their viability, even in cases where current chemotherapeutic drugs failed to elute cytotoxic effects. In accordance with our work there were earlier reports that metformin can induce cell death when used alone or in combination with current chemotherapy regime (55, 183). But the mechanisms involved were unclear. From current study it could be seen that inhibition of cell growth could be achieved by inhibiting lactate export by cell, which was achieved by inhibiting expression of MCT1 & MCT4, whose expression was reported to correlate with poor survival of cancer patients (180).

The molecular player present behind inhibition of MCT1 & 4 was activation of AMPK which resulted in suppression of mTORC1 activity and HIF1-α expression. Hyperactivity of mTORC1 and induction of hypoxia are common phenomenon noted in aggressive cancers (184, 185), which can aid in metabolic adaptation of cancer cell to sustain their high proliferative rates (186) and metformin by suppressing them could rewire the metabolic adaptation of cancer cells culminating in reduced proliferation index. HIF1-α activation occurs in response to hypoxic conditions (187), but it can also be activated by insulin and insulin like growth factor signaling(188, 189). However, expression of HIF1-α is under tight post-translational control where it depends on the metabolic status of the cell to either activate or inhibit activity of prolyl hydroxylases (PHDs). PHDs once activated hydroxylate HIF1-α, priming it for ubiquitination. Succinate, fumarate and 2-oxoglutarate (2-OG) which are

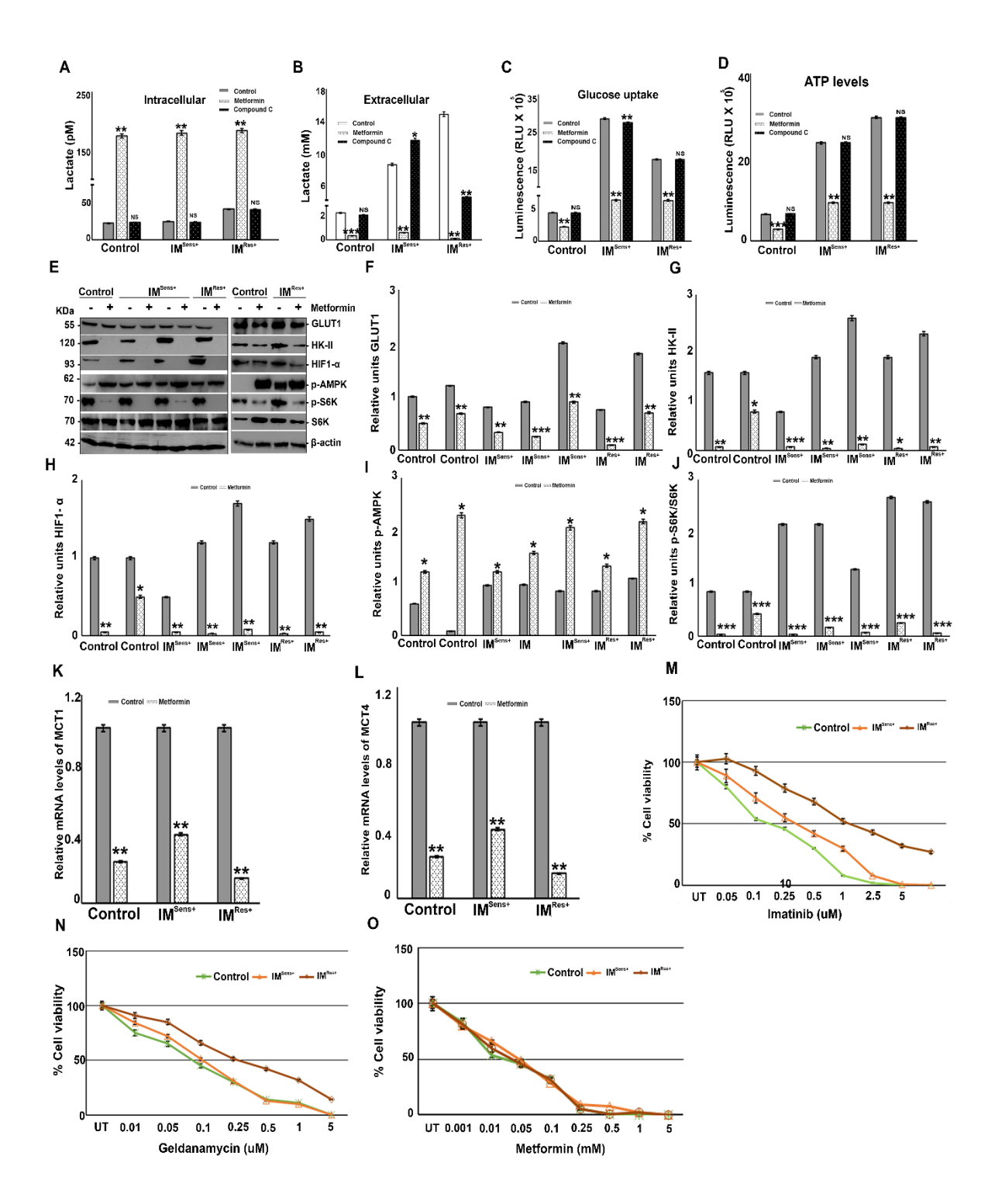


FIGURE 34: Metformin suspends glucose uptake and lactate export in PBMCs derived from CML subjects.

PBMCs were isolated from CML subjects and treated with either metformin (10 mM) alone or with compound C (5  $\mu$ M) or none for 12 hours, and **A**) intracellular lactate levels, **B**) extracellular lactate levels, **C**) glucose uptake levels and **D**) ATP levels were measured. PBMCs were treated with either metformin alone (10 mM) or none for 12 hours and subjected to **E**) immunoblot analysis. Quantification of immunoblot data using Image J for **F**) GLUT1, **G**) HK-II, **H**) HIF1- $\alpha$ , **I**) p-AMPK and **J**) p-S6K. PBMCs were treated with either metformin alone (10 mM) or none for 6 hours and subjected to RT-PCR analysis of **K**) MCT1 and **L**) MCT4. The viability of PBMCs was measured after treatment with either **M**) imatinib, **N**) geldanamycin or **O**) metformin for 3 days. Mean  $\pm$  S.E.M.; N=3, \*p<0.05 versus control, \*\*p<0.005 versus control, \*\*p<0.005 versus control.

Cont: control, Met: metformin, Comp C: compound C, NS: non-significant, Subj: subject IM <sup>Sens+</sup>: imatinib sensitive subjects, IM <sup>Res+</sup>: imatinib resistant subjects.

considered as oncometabolites can inhibit PHDs resulting in aberrant stabilization of HIF1- $\alpha$  (190). Parallelly, P53 was shown to promote HIF1- $\alpha$  degradation (191). It could be seen from our work that metformin could inhibit HIF1- $\alpha$  protein levels by promoting its degradation through proteasomal pathways. As, to how this degradation is achieved is an unanswered question. Whether metformin affects the levels of any of the oncometabolites or activates P53/MDM-2 axis or it is uses a different pathway to promote HIF1- $\alpha$  degradation is unexplored.

However, from our present work it could be seen that apart from promoting HIF1- $\alpha$  degradation, metformin also reduced HIF1- $\alpha$  mRNA levels, so it is highly possible that metformin through activation of AMPK regulates transcription factors involved in HIF1- $\alpha$  expression. Literature review revealed that STAT3 activation plays critical role in inducing HIF1- $\alpha$  expression in retinal endothelial cells (118) and we have seen earlier that metformin inhibited STAT3 expression through RUNX1 Ser 94 phosphorylation. In contrast, to our results SN Jung group has observed that in prostate cancer AMPK is a prerequisite for transcriptional activation of HIF1- $\alpha$  under ROS mediated activation (192). So, may be the dynamics of AMPK/RUNX1 and HIF1- $\alpha$  are tissue specific.

Along with inhibition of lactate export, metformin also reduced glucose uptake and glycolysis rate of cells. Hitherto metformin was known to promote glucose uptake by skeletal muscles through its action on GLUT4, an insulin dependent glucose transporter presents mostly in insulin responsive tissues (193). However, the effect of metformin on other glucose transporter isoforms like GLUT1 was less studied (194). In contrast to GLUT4, GLUT1 is more ubiquitous in its distribution with most of the blood cells expressing GLUT1 and has a

higher affinity to glucose (195). Expression of GLUT1 is hypoxia inducible and is often reported to be overexpressed in cancers (174). GLUT1 expression correlates with overall poor clinical outcome (196). It could be seen that metformin by inhibiting expression of HIF1-α resulted in suppression of GLUT1 levels resulting in lowered glucose uptake by PBMCs. Glucose once entered is subjected to reduction by glycolysis and one of the first reactions in glycolysis is catalyzed by HK-II (197), whose expression is again hypoxia inducible (198). So, inhibition of HIF1-α resulted in low expression levels of HK-II which finally resulted in low ATP levels. Albeit lactic acidosis is commonly observed in diabetic patients on metformin regime, so there was an initial school of thought that metformin induces lactic acidosis in these patients. Hitherto recent studies have proven that there is no direct correlation between lactic acidosis generation and metformin usage (199).

Taken together our data demonstrate that metformin can induce anti-leukemic effects by altering the overall glucose metabolism of cell by inhibiting three out of the four key steps involved in glycolytic flux regulation (197) which are, firstly inhibition of glucose uptake by GLUT1 then downregulation of HK-II resulting in reduced glycolytic flow and finally inhibition of lactate import and export by inhibiting MCT1 & MCT4 (Fig 35). It sheds light on possible mechanisms involved in anti-leukemic effects of metformin.

# Glucose **GLUT1 METFORMIN** Glucose HKII Geldanamycin Glucose-6-HIF1a **AMPK** phosphate Glycolysis HSP90 BCR ABL mTORC1 **Imatinib** Lactate MCT1&

FIGURE 35: Schematic representation of metformin's effect on lactate export and import in CML. Glucose entry is mediated through glucose transporters (GLUT1). Glucose is catabolized through glycolysis, where in conversion of glucose to glucose- 6- phosphate, catalyzed by Hexokinase-II is a rate limiting step. Cancer cells have high consumption of glucose and high rates of glycolysis resulting in increased production of lactate through LDH-A. Lactate export from cell is mediated by MCT4 and uptake of lactate is facilitated by MCT1. BCR-ABL potentiates activity of mTORC1 and HIF1-α, which in turn upregulate expression of GLUT1, HK-II, MCT1 & MCT4. Imatinib inhibits kinase activity of BCR-ABL. HSP-90 stabilizes BCR-ABL, whose activity is inhibited by geldanamycin. Metformin enters into cell through OCTs. Metformin activates AMPK through phosphorylation, which results in inhibition of GLUT1, HK-II, MCT1 & 4 expressions.

# **OBJECTIVE 2.2**

Analyzing the effect of metformin on expression of GLUT1 and GLUT4 in breast cancer.

#### 2.2.1. LITERATURE REVIEW

Metabolic rewiring is one the hallmark characteristics of cancer, especially more prevalent in aggressive tumors. Compared to normal tissue, cancerous cells have a higher demand for glucose owing to their increased proliferations rates, which need continuous pool of ATP and ribose sugars for DNA replication. Often cancer cells meet this demand by over expressing glucose transporters. The glucose transporters mainly belong two major families: the sodium dependent glucose co-transporters (SGLTs) and facilitative glucose transporters (GLUTs). Of the two, the latter is frequently over expressed in breast cancer cells. GLUTs consist of 14 different isoforms, with varying affinity towards glucose. Only GLUT1, 3 and 4 have high affinity for glucose, where they can transport high amounts of glucose into cells irrespective of glucose concentrations in blood. This facilitates cancerous cells to have higher rates of glucose uptake under normal physiological conditions. GLUT1 is highly expressed in breast tissues and the expression correlates with aggressive grade tumor with poor prognostic outcome. GLUT1 expression is regulated by HIF1-α/ mTORC1 axis. GLUT3 is also highly expressed in breast cancer and follows GLUT1 in correlation with poor prognostic outcome of breast cancer patients, it is regulated by MAPK pathway. On the other hand, GLUT4 is responsible for basal glucose uptake in breast cancer cells. GLUT4 is regulated by insulin and insulin-like growth factors. With the view of metformin's inhibitory effect on GLUT1 in CML, metformin's role in modulating glut's expression in breast cancer cells was analyzed.

# **MATERIALS and METHODS**

#### 2.2.2. MATERIALS AND METHODS

#### 2.2.2.1. Cell culture

MDA-MB-231 and MCF-7 cells were grown as described previously. Sub culturing for adherent cells was done using 0.5% trypsin-EDTA (HiMedia, India).

#### **2.2.2.2.** *Chemicals*

Metformin, dorsomorphin (Compound C), 5-aminoimidiazole-4-carboxamide ribonucleotide (AICAR) and Lithium chloride were purchased from sigma, USA.

## 2.2.2.3. siRNA transfection

The siRNA for rictor (SI05109048) and raptor (SI00698677) were purchased from Qiagen (Netherlands). All the transfections were carried out using RNAifect (Qiagen, Netherlands) following the manufacturer's instructions. In brief, 1  $\mu$ g of siRNA and 3  $\mu$ L of RNAifect were diluted in 200  $\mu$ L of plain DMEM medium (0.5 % FBS) individually and incubated for 5 minutes; later, both were mixed and incubated for 30 minutes before adding the combined solution to cells. Cells were replaced with fresh regular medium after 6 hours of transfection.

## 2.2.2.4. Cell viability assay

6,000 cells per well in a 96 well plate was seeded either with or without indicated drugs to RPMI-1640 medium of 250  $\mu$ L final volume and were grown for 3 days. The assay was performed as described in earlier section (1.2.2.7).

## 2.2.2.5. Glucose uptake assay

5,000 cells per well in a 96-well plate were seeded in RPMI-1640 medium and treated with respective drugs for 3 days. Post to treatment glucose levels were measured using Glucose Uptake-Glo Assay kit (#J1342, Promega, USA) following manufacturer's instruction.

### 2.2.2.6. *Immunoblotting*

Cell lysates were subjected to SDS-PAGE followed by immunoblotting as described in earlier section (1.1.2.9) Blots were probed using p-4EBP1, 4EBP1, p-eIF2-α and eIF2-α (Abcam, USA.) AKT, p-AKT-Ser 473, p-P70S6K, P70S6K, rictor, raptor, p-AMPK, p-raptor substrate motif specific, GLUT1 and GLUT4 (Cell Signaling Technologies, USA.) β-actin, p-

AKT-308 (Santa Cruz Biotechnology Inc, USA.) antibodies as described in earlier section (1.1.2.9).

# 2.2.2.7. Statistical analysis

All data points are represented as mean  $\pm$  SEM. All data points were done in duplicates and a minimum of set of three independent experiments were carried out.

# **RESULTS**

#### **2.2.3. RESULTS**

# 2.2.3.1. Insulin and nutrients induce expression of GLUT1, but not GLUT4 in breast cancer

Effect of insulin on induction of GLUT1 and 4 expressions in hormone positive and triple negative breast cancer cells were analyzed. It was seen that in response to insulin GLUT1 expression was upregulated in both hormone positive and triple negative breast cancer cells (Fig 36A &B), whilst this upregulation was lost upon serum starvation. However, GLUT4 expression doesn't correlate with insulin presence, as GLUT4 levels were high under serum starved conditions, but were seen to be down regulated when insulin was added back. Insulin mediated activation of GLUT1 correlates with activation of mTORC1 through AKT-308 axis, whereas AKT-473 phosphorylation was seen correlating with GLUT4 and independent of insulin mediated activation (Fig 36A &B). Apart from insulin nutrients also are reported to activate mTOR complexes. Thus, we next analyzed the role of mTOR complexes in induction of GLUT1 and 4. Upon with drawl of glucose and glutamine GLUT1 expression was reduced in both hormone positive and triple negative breast cancer cells, correlating with loss of mTORC1activation as seen through 4EBP1 phosphorylation, which is a key component of cap-dependent protein synthesis (Fig 36C &D). Hitherto, GLUT4 expression was induced upon with drawl of either glucose or glutamine and was reduced when high levels of either glucose or glutamine was present (Fig 36C &D). Deprivation of glucose or glutamine was known to activate GCN2/ eIF2-α pathway. It was seen that GLUT1 translation depends on mTORC1 activation, whereas GLUT4 expression was correlating with eIF2-α (Fig 36C &D).

# 2.2.3.2. GLUT1 expression was dependent on mTORC1, whereas GLUT4 was dependent on mTORC2

The role of mTOR complexes in regulating GLUT expression was further established, when raptor and rictor were knock down in both hormone positive and triple negative breast cancer cells. Cells were subjected to raptor knock down and then treated with high glutamine levels. It was observed that GLUT1 expression which was increased upon high glutamine conditions was subdued when mTORC1 was inhibited through raptor knock down, whereas GLUT4 expression was unaltered upon raptor knock down and was reduced upon increased

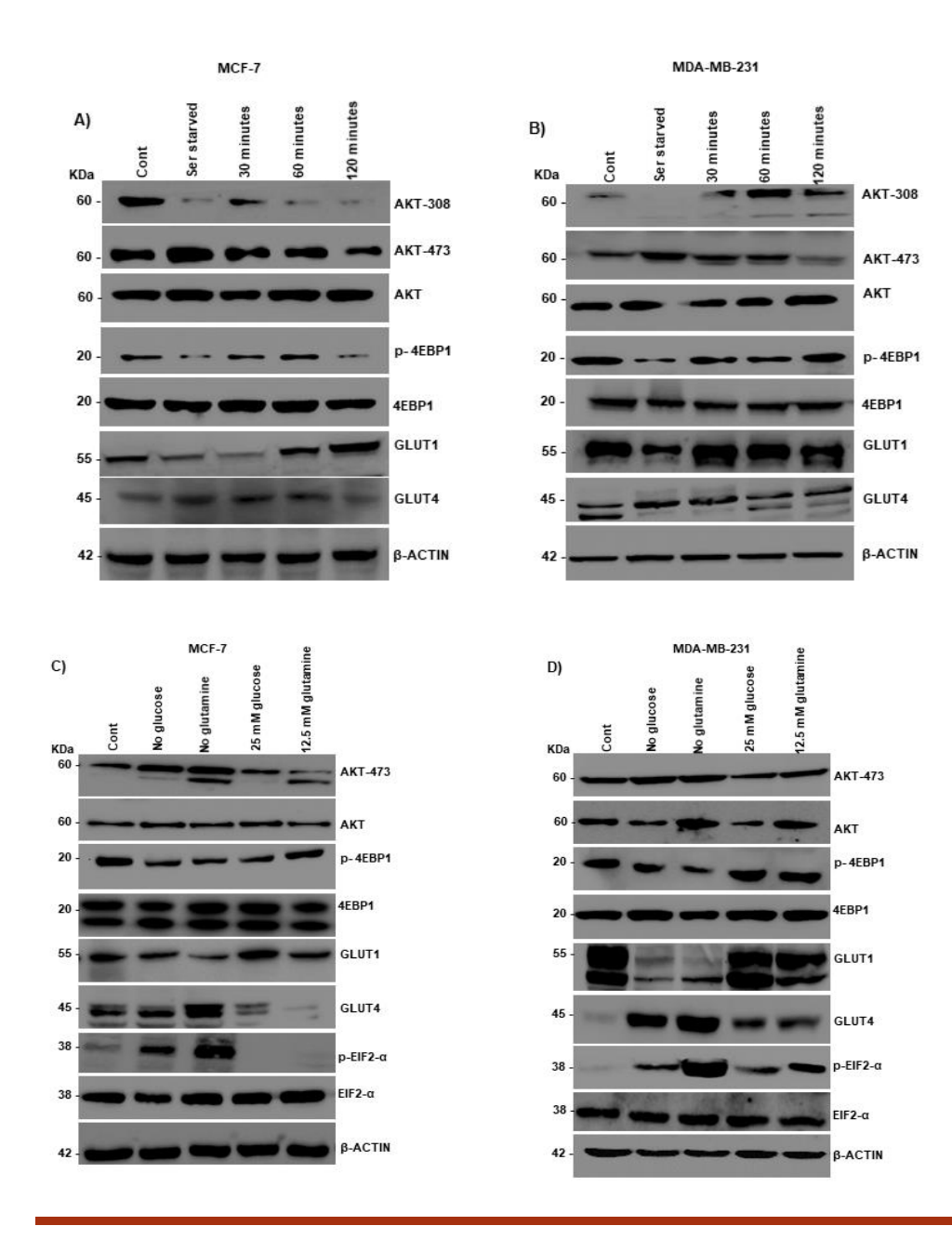


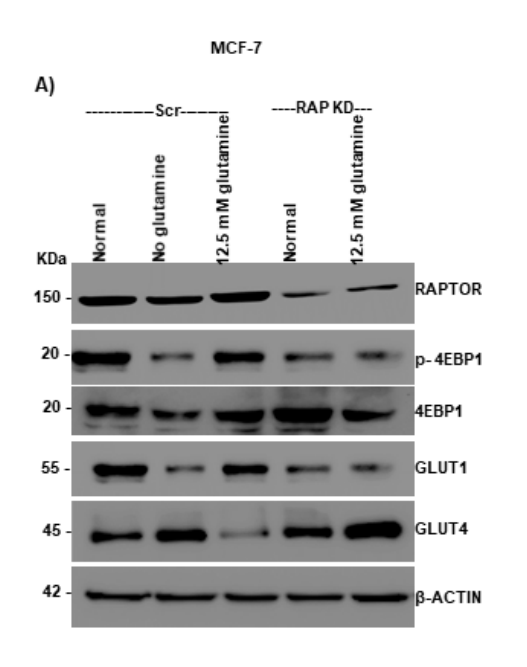
FIGURE 36: Insulin and nutrients induce expression of GLUT1, but not GLUT4 in breast cancer. A) MCF-7 cells were subjected to serum starvation in RPMI-1640 medium with 0.5% FBS for 6 hours and insulin (25ng/mL) was added and incubated for given time points, post to which subjected to immunoblot analysis and mTORC1 and mTORC2 pathways were analyzed. B) MDA-MB-231 cells were subjected to serum starvation in L-15 medium with 0.5% FBS for 12 hours and insulin (25ng/mL) was added and incubated for

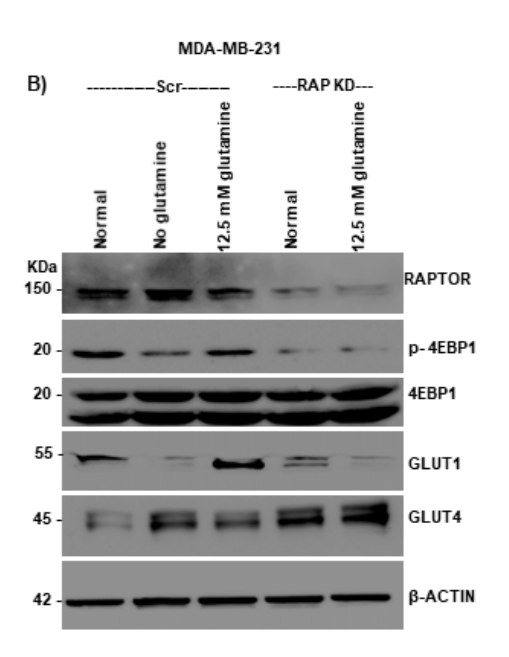
given time points, post to which subjected to immunoblot analysis and mTORC1 and mTORC2 pathways were analyzed. Cells were grown in DMEM medium without glucose and glutamine supplemented with varying concentration of glucose and glutamine and subjected to immunoblot analysis in **C**) MCF-7 and **D**)

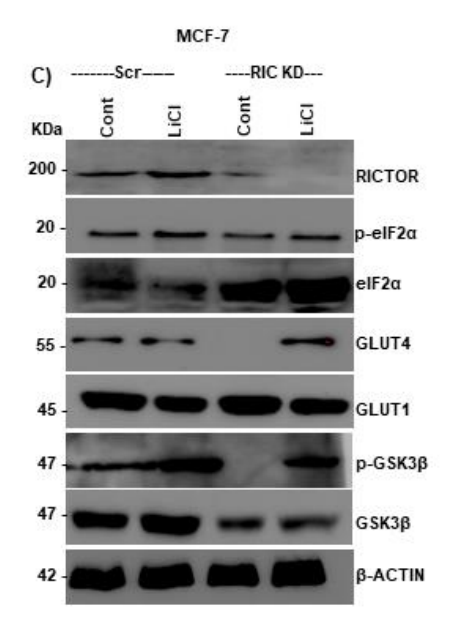
MDA-MB-231. Mean  $\pm$  S.E.M.; N=3.

Cont: control, Ser: serum.

glutamine concentration (Fig 37A &B). Activation of mTORC2 leads to inhibition of GSK3β through AKT-473 phosphorylation. Active GSK3β inhibits GCN2 mediated eIF2α activation. We analyzed role of mTORC2 in induction of GLUT4, for this cell were treated with LiCl along with rictor knock down. Rictor knocks down resulted in inhibition of GLUT4 but not GLUT1. Upon treatment of LiCl, GSK3β was inhibited irrespective of mTORC2 activation.







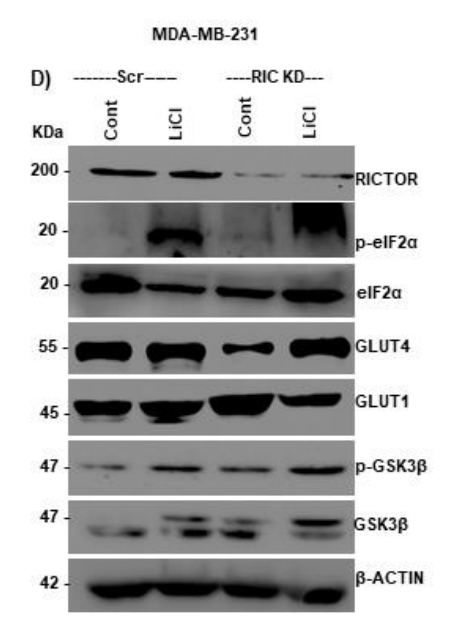


#### FIGURE 37: GLUT1 expression was dependent on mTORC1, whereas GLUT4 was dependent on mTORC2.

Cells were subjected to raptor knock down and were grown under in either normal medium or in high glutamine (12.5mM) or no glutamine conditions for 48 hours post to which cells were subjected to immunoblot analysis in **A**) MCF-7 and **B**) MDA-MB-231 cells. Cells were subjected to rictor knock down and were grown under in either normal medium or in LiCl (0.5 mM) conditions for 48 hours post to which cells were subjected to immunoblot analysis in **C**) MCF-7 and **D**) MDA-MB-231 cells. Mean  $\pm$  S.E.M.; N=3.

Cont: control, Scr: scrambled, RAP KD: raptor knock down.

eIF2 $\alpha$  phosphorylation was observed when treated with LiCl and GLUT4 induction was seen to follow a similar trend (Fig 37C &D) establishing role of mTORC2/ GSK3 $\beta$  axis in GLUT4 regulation.

## 2.2.3.3. Metformin treatment inhibits GLUT1 expression, but promotes GLUT4 induction

As metformin was seen to have anti- cancer effects, at the same time involved in increase of glucose uptake in muscles. We then analyzed effect of metformin on expression of GLUT1 and GLUT4 in breast cancer cells. Post to treatment with AMPK activators mTORC1 activity was inhibited through phosphorylation of raptor by AMPK which resulted in inhibition of GLUT1 expression in both hormone positive and triple negative breast cancer cells. However, GLUT4 levels were increased post to treatment with AMPK activators along with increased mTORC2 activity (Fig 38A &B). Treatment with rapamycin for longer times inhibits both mTORC1 and C2 resulting in suppression of expression of both GLUT1 and 4 (Fig 38A &B). Glucose uptake was increased in both hormone positive and triple negative breast cancer cells post to metformin treatment (Fig 38C) despite suppression of GLUT1 expression, possibly mediated through GLUT4.

# **DISCUSSION**

#### 2.2.4. DISCUSSION

Metabolic rewiring is a key phenomenon needed for breast cancer progression and development of drug resistance. Metformin has a dual functionality where it inhibits cell proliferation in certain cancers and at the same time aids in glucose uptake in muscles. One of the common observations in cancer cells is, they have a high uptake of glucose inorder to meet the need of continuous supply of ribose back bone for DNA replication. So, how metformin can elicit the proclaimed anti-cancerous effects were unclear. The metformin clinical trials in breast cancer scenario also yielded mixed results.

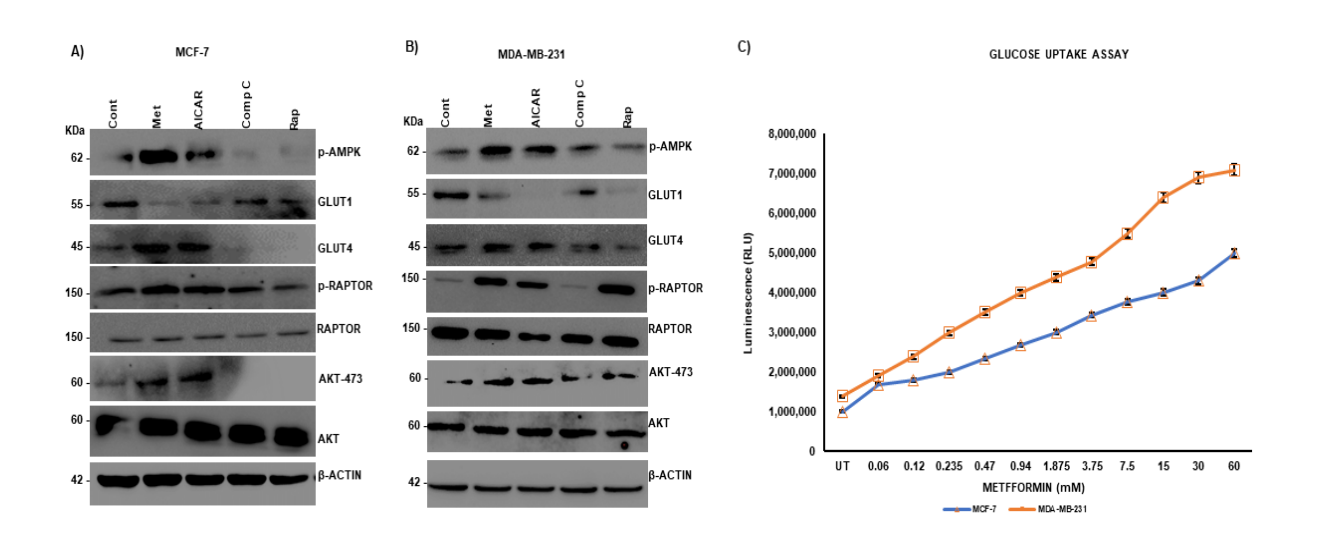
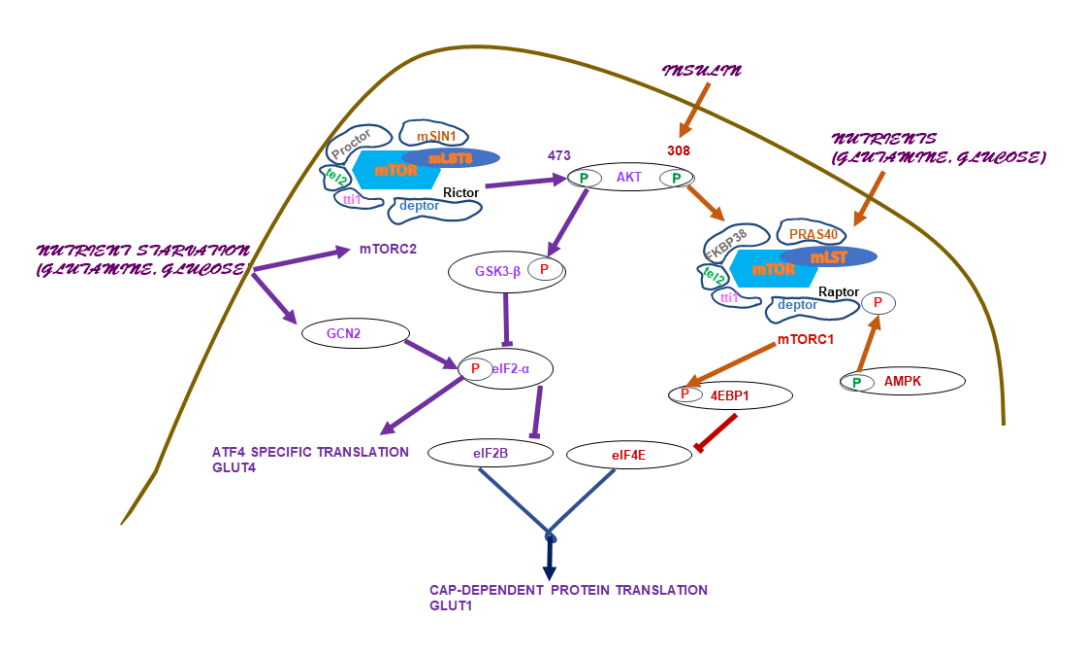


FIGURE 38: GLUT1 expression was dependent on mTORC1, whereas GLUT4 was dependent on mTORC2. Cells were treated with either AICAR (0.5mM) or metformin (20 mM) or compound C (5  $\mu$ M) or rapamycin (20  $\mu$ M) for 12 hours post to which cells were subjected to immunoblot analysis in A) MCF-7 and B) MDA-MB-231 cells. C) MCF-7 and MDA-MB-231 cells were treated with metformin for 72 hours at given concentrations and viability was assessed by MTT assay. Mean  $\pm$  S.E.M.; N=3.

Cont: control, Met: metformin, Comp C: compound C, Rap: rapamycin.

In the above objectives we have seen that metformin functions to promote bone metastasis of breast cancer cells through RUNX2 stabilization. Here in, it was seen that though metformin could inhibit GLUT1 expression through inhibition of mTORC1; metformin also resulted in activation of mTORC2 through inhibition of mTORC1 by raptor phosphorylation. Activation of mTORC2 results in AKT 473 phosphorylation, which in turn inhibited GSK3 $\beta$ . Active GSK3 $\beta$  results in inhibition of eIF2- $\alpha$  Ser 51 phosphorylation and activation of capdependent protein synthesis. mTORC1 once activated either through insulin signaling or by

nutrients results in inhibition of 4EBP1, which otherwise inhibits global cap-dependent protein translation by sequestering eIF4E. Metformin treatment results in inhibition of mTORC1, thus indirectly activating 4EBP1 and activation of mTORC2 facilitates eIF2-  $\alpha$  Ser 51 phosphorylation, which finally culminates in inhibition of global cap-dependent protein translation and activation of ATF4 specific protein translation. Close analysis of GLUT1 and 4 mRNA reveals presence of large 5' UTR on GLUT1 which was absent in the latter. Work done by Tai *et al* has shed light on converse control of insulin on translation of GLUT1 and 4. Together with our results it could be seen that GLUT1 translation occurs mainly through mTORC1 mediated cap-dependent protein translation whereas GLUT4 translation is independent of cap-dependent protein synthesis and follows trend similar to ATF4 mediated translation. Metformin though inhibits GLUT1 expression, but due its activation effect on mTORC2 results in upregulation of GLUT4 and finally results in increase in net glucose uptake by breast cancer cells (Fig 39).



- P Inhibitory phosphorylation
- P Activating phosphorylation

**FIGURE 39:** Metformin promotes glucose uptake in breast cancer cells through induction of GLUT4 expression. GLUT1 expression is mediated through mTORC1 mediated activation of cap-dependent protein synthesis by 4EBP1. Both insulin (by AKT-308 phosphorylation) and nutrients result in activation of mTORC1, which results in inhibition of 4EBP1 through phosphorylation. Active 4EBP1 sequesters eIF4E and inhibits cap-dependent protein translation. Serum starvation or nutrients deprivation can activate mTORC2, which inhibits GSK3β through AKT-473 phosphorylation. Active GSK3β inhibits eIF2- $\alpha$  Ser 51 phosphorylation. Active eIF2- $\alpha$  along with eIF2B and eIF4E helps in cap-dependent protein translation. Deprivation of nutrients can activate GCN2 which results in eIF2- $\alpha$  Ser 51 phosphorylation and inhibition of cap-dependent protein synthesis. Metformin through raptor phosphorylation inhibits mTORC1 activity and through activation of mTORC2 results in eIF2- $\alpha$  Ser 51 phosphorylation, thus increasing GLUT4 expression and inhibiting GLUT1 expression.

# **OBJECTIVE 2.3**

Analyzing the effect of metformin treatment on diabetes induced bone adipogenicity.

#### 2.3.1. LITERATURE REVIEW

High glucose-induced bone fragility (5) and adipogenesis (200) are the leading secondary complications associated with diabetes, characterized by the loss of bone mineralization (201) and increase in the adipogenic commitment of precursor mesenchymal stromal cells (MSCs) (200). Nutrients, especially glucose and glutamine, influence the insulin secretion of pancreatic-β cells and their imbalance is associated with diabetes and diabetesrelated complications (202, 203). Despite being a major disorder, the molecular mechanisms underlying the biochemistry of nutrient metabolism in diabetes remain elusive and recent studies are directed towards new dimensions of physiology. It was hypothesized that nutrient regulation can improve diabetes management, but there are many niches to be explored in order to understand the nutrient control of cell fate and role of nutrients in diabetes management (204). mTOR complexes (mTORC1 and mTORC2) are key players in integrating external cues, such as metabolic and nutrient signals, to downstream pathways. mTOR is present as two different multi-protein subunit complexes namely, mTORC1 (characterized by RAPTOR, PRAS40, deptor, mLST8, and mTOR) and mTORC2 (characterized by rictor, mSIN1, and protor). Growth factor signaling and nutrients activate mTORC1, though little is known about mTORC2 activation (205).

Several studies have revealed that mTORC1 is critical in glucose metabolism, insulin secretion, and energy homeostasis. Hyperactivation of mTORC1 due to chronic conditions, such as chronic high glucose exposure or diabetes, or over-expression of any one of the components of the mTORC1 complex lead to the destruction of β-islet cells, insulin resistance, loss of glucose homeostasis, and obesity (206). Under similar conditions, mTORC1 hyperactivation is also linked to decreased mTORC2 function and impaired AKT signaling, leading to a loss of mitogenic signaling (207, 208).

Glutamine is a potent activator of mTORC1, and its function in promoting adipogenesis was thought to be carried out through hyperactivation of mTORC1 (209). There are conflicting reports on the involvement of glucose or glutamine in mTORC1 activation since the levels of both seems to be high in diabetes; however, studies by Moloughney *et al.* and others demonstrated that under glucose-depleted conditions, the presence of glutamine rescues mTORC1 activation, whereas other amino acids did not show much significance. Further, these studies also revealed that mTORC2 was activated when glutamine levels were decreased (210, 211).

The plasma glutamine levels of diabetic patients, though ambiguous, tend to be higher than in matched controls (212, 213). High levels of glucose were shown to inhibit osteogenesis mainly through the suppression of RUNX2 levels (214). Our earlier studies demonstrated that p-AMPK drives MSCs to become osteocytes, whereas under diabetes conditions, the loss of AMPK activity correlates with ubiquitination of RUNX2 and favors adipogenesis. We also demonstrated that metformin attenuates diabetes-induced bone adipogenesis and bone loss in a mouse model, which correlates with the epidemiological data that indicate that diabetes patients who are on metformin have healthier bones than those on non-metformin drugs. Recent reports have also shown that mTORC1 is indispensable for insulin-mediated adipogenesis (215-218), whereas mTORC2 seems to be crucial for osteogenesis (219, 220) and high levels of glucose increased the adipogenic commitment of MSCs, but it is unclear which critical molecular players are involved in this cross-talk (221). Taking all these into consideration, the current study aims to unravel the molecular mechanisms involved in the differential regulation of MSC fate by glucose and glutamine and their roles in the regulation of mTORC1 and mTORC2 signaling and their cross-talk under diabetes conditions.



#### 2.3.2. MATERIALS AND METHODS

#### 2.3.2.1. *Cell culture*

C3H10T1/2 (Cat. No-CCL-226), hereafter called murine MSCs, C2C12 (Cat. No-CRL-1772) (murine skeletal muscle cells), and U2OS (Cat. No-HTB-96) (human bone osteosarcoma epithelial cells) were procured from ATCC (USA). All the cell lines, including BM-MSCs, were maintained in IMDM (Cat. No-12200069) (Gibco, USA) supplemented with 10% FBS (Cat. No-10082147) (Gibco, USA) and 1% pen-strep (Cat. No-1514022) (Gibco, USA) in 5% CO<sub>2</sub> incubator at 37°C. For the glucose and glutamine treatments, media without glucose or glutamine (Cat. No-A1443001) (Gibco, USA), respectively was used. BM-MSCs from BALB/c male mice, 6-8 weeks of age, were isolated and characterized by florescence assisted cell sorting using CD44<sup>+</sup>, CD90<sup>+</sup> and CD45<sup>-</sup> as markers. A more detailed information about BM-MSCs isolation and characterization was previously described in our earlier paper (136). The cells were maintained in IMDM supplemented with 1% minimum essential amino acids (Cat. No-11140050) (Gibco, USA) acids for 5 days. The medium was changed every alternative day and subcultured using 0.25% trypsin-EDTA (Cat. No-25200056) (Gibco, USA).

#### **2.3.2.2.** *Chemicals*

MG-132 (Cat. No-M8699), L-ascorbic acid (Cat. No-A92902), dexamethasone (Cat. No-D4902), 3-isobutyl-1- methylxanthine (IBMX) (Cat. No-I5879), rosiglitazone (Cat. No-R2408), metformin (Cat. No-1396309), glucose (Cat. No-1181302), oil-red-o (Cat. No-O0625), alizarin-red-s (Cat. No-A5533), β-glycerophosphate (Cat. No-G9422), and LiCl (Cat. No-L9650) were purchased from Sigma (USA). Insulin (Cat. No-12585014), L-glutamine (Cat. No-25030081) and Human BMP-2 (Cat. No-#PHC7141) were purchased from Gibco (USA).

# 2.3.2.3. Ethics statement

All experiments involving animals were conducted according to the ethical policies and procedures approved by the ethics committee of the Institutional Animal Ethics Committee (IAEC)-University of Hyderabad, India (Approval no. IAEC/UH/151/2016/11/BMR/P3).

### 2.3.2.4. Streptozotocin-induced diabetic model

Male BALB/c mice, 6-7 weeks of age, were used for the study as previously described by adhering to norms instituted by the Institutional Animal Ethics Committee-University of

Hyderabad, governed by the CPCSEA-Govt of India. Diabetes was induced by low doses of streptozotocin (Cat. No-S0130) (Sigma, USA) in citrate buffer pH 4.5 given for 5 days and the control group were administered with citrate buffer alone. At the fifth day the blood glucose of mice was estimated using glucometer and mice having blood glucose greater than 300 mg/dL were considered diabetic (136). Mice were sacrificed at 10 weeks of age after confirmation of diabetes. Metformin control and treated mice were given 60 mg/kg body weight metformin daily (intraperitoneal) for 10 weeks.

## 2.3.2.5. Differentiation and transdifferentiation protocols

Murine-MSCs and BM-MSCs were differentiated into adipocytes by treating them with 0.5 mM IBMX, 20 nM insulin, and 0.1  $\mu$ M dexamethasone, along with IMDM medium and 10% FBS, for 48 hours. After 48 hours, the cells were maintained for an additional 8 to 21 or 16 days in growth medium supplemented with 20 nM insulin. The medium was changed on alternate days. Murine-MSCs were differentiated into osteocytes using 0.5 mM IBMX, 0.1  $\mu$ M dexamethasone, and 1 mM L-ascorbic acid, along with IMDM medium and 10% FBS, for 7 days or until they reached 80% confluence. On the 7<sup>th</sup> day, 1 mM  $\beta$ -glycerophosphate was added and maintained for 21 days; the medium was changed on alternate days. C2C12 transdifferentiation to the osteogenic lineage was performed using BMP-2 at a concentration of 200 ng/mL in growth medium, along with 10% FBS, and maintained for 14 days with a change in medium every 48 hours. U2OS cells were transdifferentiated into adipocytes using 1  $\mu$ M rosiglitazone in growth medium, along with charcoal-stripped FBS (Cat. No-#12676029) (Gibco, USA), for 14 days.

#### 2.3.2.6. Oil- red-o staining

Oil-red-o stock of 0.5% was prepared in isopropanol (Finar, India). Working solution was prepared in distilled water at 6:4 ratio. After differentiation, the medium was aspirated and cells were washed twice with 1X PBS and fixed in 10% formalin (Finar, India) for 1 hour at room temperature, followed by another 1X PBS wash. After the wash, the cells were incubated in 60% isopropanol for five minutes, followed by staining with the oil-red-o working solution for five minutes. The excess stain was removed by washing with water 3-4 times and visualized under a microscope. Quantification was done by eluting oil-red-o in isopropanol and the absorbance was measured at 500 nM.

#### 2.3.2.7. Alizarin-red-s staining

Alizarin-red-s stain (2%) was prepared in water by adjusting the pH to 4.1 with an ammonium hydroxide solution and then the stain solution was filtered. After differentiation, cells were washed twice with 1X PBS and fixed in 10% formalin (Finar, India) for 1 hour at room temperature, followed by another 1X PBS wash. Afterward, cells were stained with alizarin-red-s for 45 minutes, and then washed with water 3-4 times and visualized under a microscope. Quantification was done by adding 10% acetic acid (Finar, India) to each well and incubating the cells for 30 minutes. Cells were then scraped and vortexed for 30 seconds followed by brief heating at 85°C. Afterward, they were incubated on ice for 5 minutes, followed by centrifugation at 14,000 rpm for 20 minutes. For the absorbance measurement,  $200 \,\mu\text{L}$  of 10% ammonium hydroxide was added to  $500\mu\text{L}$  of supernatant and the absorbance was measured at  $405 \,\text{nM}$ .

# 2.3.2.8. siRNA transfection

Was performed as mentioned in the earlier section (1.4.2.7).

# 2.3.2.9. RNA isolation and real-time PCR (RT-PCR)

For the RT-PCR analysis, total RNA isolation cDNA synthesis and RT-PCR were carried out as described previously (1.1.2.9). The sequences of the primer sets used were:

Target	Forward primer (5'-3')	Reverse primer (5'-3')
OCN	GGAAAGTGGTCCACATCGAG	TTCACTCTCCCGCAGGATGG
PPAR-γ	AGCTAAAGGCCCGTCTATCG	AACACCCCACACAGGAGTA
Adipo Q	AGTTAGTCACACTGGAGATT	ATAGGATCGACAGTTGTA
Actin	GAGAGGGAAATCGTGCGTGAC	CATCTGCTGGAAGGTGGACA

#### 2.3.2.10. Immunoblotting

Protein isolation and SDS-PAGE was done as described in 1.1.2.9 methods section. The blots were probed for antibodies p-P70S6K (Cat. No- #9205), P70S6K1/2 (Cat. No- #9202),  $\alpha$ -RUNX2 (Cat. No- #8486),  $\alpha$ -p-AMPK (Cat. No- #2523), raptor (Cat. No- #2280), rictor (Cat. No- #2114), p-AKT (473) (Cat. No- #9217) and AKT (Cat. No- #6703) (Cell Signaling Technologies (USA)); GSK3 $\alpha$ / $\beta$  (Cat. No- sc-7291) and  $\beta$ -actin (Cat. No- sc-47778)

(Santa Cruz Biotechnology Inc. (USA)); p-GSK3 $\beta$  (Ser 9) (Cat. No- ab107166) and PPAR- $\gamma$  (Cat. No- ab272718) (Abcam (USA)) as described in earlier section (1.1.2.9).

## 2.3.2.11. *Immunoprecipitation (IP)*

Cells were processed as described earlier (1.1.2.10).

# 2.3.2.12. Confocal microscopy

Cells were grown to confluence (80%) on coverslips, treated for the indicated time points, and processed as mentioned in earlier sections (1.1.2.12).

# 2.3.2.13. Statistical analysis

All data points are represented as mean  $\pm$  SEM. Statistical analysis was performed with Student's t-test by comparing the differences between mean values of controls with the experimental sets individually. P values less than 0.1 were considered statistically significant. A minimum set of two to three independent experiments was carried out for all the *in vitro* studies using cell lines except freshly isolated BM-MSCs and immunoprecipitation experiments due to limitations in the use of animals, whereas each mouse was considered one subject for the *in vivo* experiments.

# **RESULTS**

#### **2.3.3. RESULTS**

## 2.3.3.1. mTORC1, but not mTORC2, is indispensable for adipogenesis and vice versa

MSCs have the capacity to give rise to a repertoire of lineages, including osteocytes and adipocytes. Several molecular players, like RUNX2 (for osteogenesis) and PPAR-7 (adipogenesis), were known to play a critical role in lineage commitment (136, 222). However, little is known whether mTOR complexes are involved in regulating the fate of MSCs. Here, we first analyzed the activation of mTORC1 and mTORC2 during osteogenic and adipogenic differentiation and transdifferentiation. Our data shows that mTORC2/AKT-473 pathway was activated during C3H10T1/2 (MSCs) osteogenic differentiation along with increase in levels of RUNX2, whereas mTORC1 activity (as measured through p-70S6K levels) was at basal level (Fig 40A) during osteogenic commitment. The osteogenic differentiation was further confirmed by analysis of key regulators like RUNX2 and OCN at mRNA level (Fig 40B). Similar results were established in C2C12 (myoblasts) transdifferentiation model (Fig 40C &D). Whereas, the mTORC1/p-70S6K pathway was activated under C3H10T1/2 adipogenic differentiation along with increase in PPAR-y levels and reduced mTORC2 activity (as measured through p-AKT473 levels) (Fig 40E). To further confirm the adipogenic differentiation PPAR-y, Adipo Q levels at mRNA were measured (Fig 40F). Similar results were established in U2OS transdifferentiation (Fig 40G &H).

# 2.3.3.2. mTORC1 promotes the adipogenic lineage through inhibition of the mTORC2/AKT-473/RUNX2 axis

The lineage commitment of MSCs is a mutually exclusive process where suppression of one lineage promotes the activation of another lineage specific commitment. It was shown that commitment to adipocytes is accompanied by suppression of osteogenic differentiation and they have quite distinct diversification processes (223). Since RUNX2 is the master regulator of osteogenesis, we first analyzed the effects of knockdown of raptor (for mTORC1 KD) and rictor (for mTORC2 KD) on RUNX2 expression levels in undifferentiated MSCs. Raptor, but not rictor, knockdown resulted in increased RUNX2 expression, whereas rictor knockdown resulted in a reduction in RUNX2 levels (SF 16A), indicating that mTORC1 negatively regulates RUNX2, whereas mTORC2 seems to positively regulate RUNX2. Next, we checked the importance of raptor and rictor knockdown of mTOR complexes in MSC differentiation. These results suggested that knockdown of raptor resulted in loss of adipogenesis, whereas the

loss of rictor enhanced adipogenesis, as shown by immunoblot (Fig 41A), RT-PCR (SF 16B-F), Alizarin red S staining (Fig 41B &C) and oil red O (Fig 41D &E) analyses. Our results

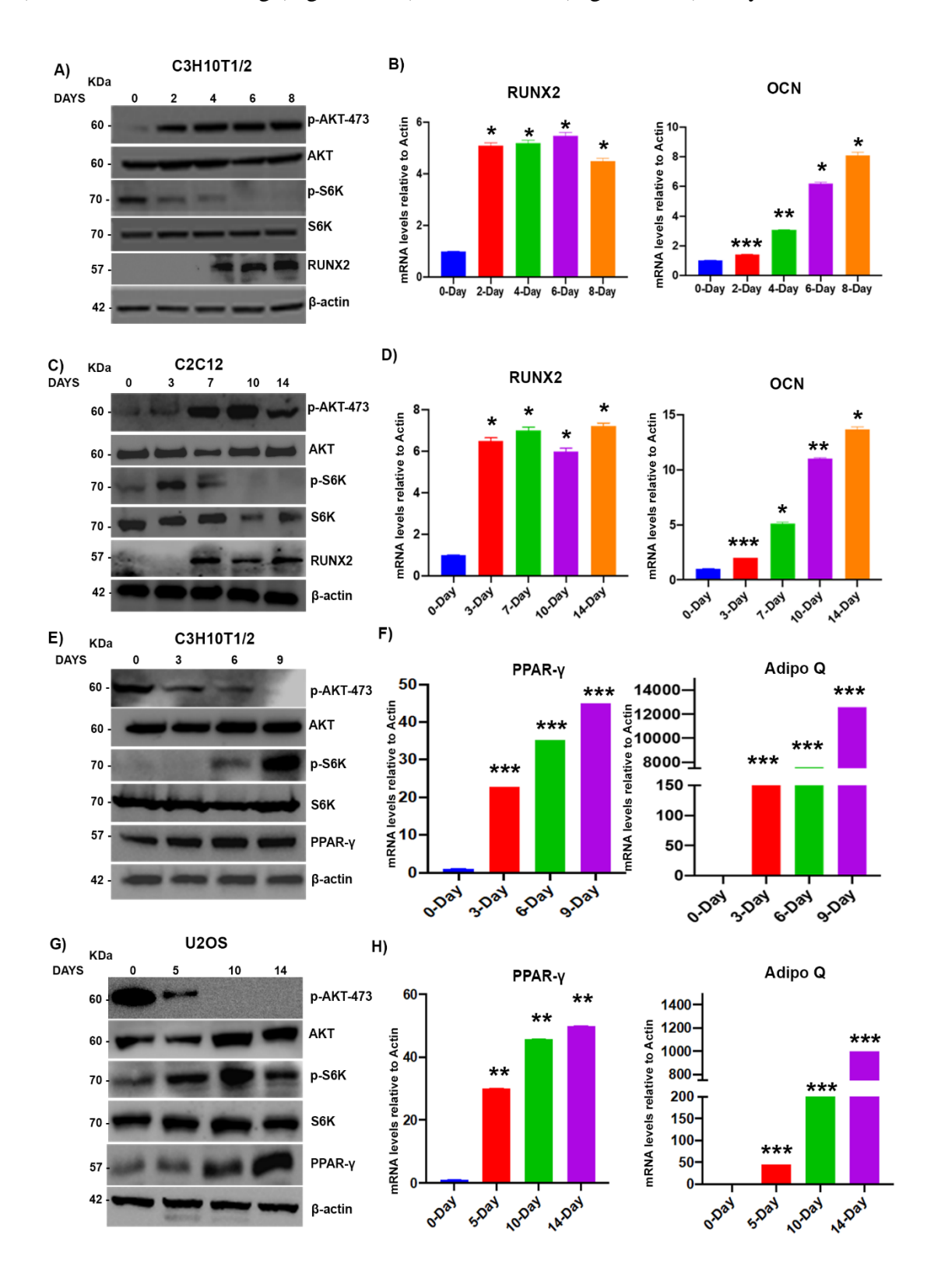


FIGURE 40: mTORC1, but not mTORC2, is indispensable for adipogenesis and vice versa. Murine MSCs (C3H10T1/2) were subjected to osteogenic differentiation and lysates were collected at indicated time points and proceeded for A) immunoblot analysis using the indicated antibodies and B) RT-PCR. C) C2C12 (skeletal myocytes) were subjected to osteogenic transdifferentiation and cell lysates were subjected to immunoblot and D) RT-PCR. Murine MSCs were subjected to adipogenic differentiation and cell lysates were collected at indicated time points and E) subjected to immunoblotting and F) RT-PCR as indicated. U2OS cells were subjected to adipogenic transdifferentiation and cell lysates were collected and G) subjected to immunoblot analysis and H) RT-PCR analysis as indicated. Mean ± S.E.M.; N=3, \*p<0.1 versus control, \*\*p<0.01 versus control; \*\*\*p<0.001 versus control.

RUNX2: runt-related transcription factor 2, OCN: Osteocalcin, Adipo Q: adiponectin Q, PPAR-γ: peroxisome proliferator-activated receptor gamma.

demonstrated that mTORC1 knockdown (through anti-raptor siRNA) not only resulted in the suppression of adipogenic differentiation (Fig 41D) but also increased the levels of RUNX2 (Fig 41A &SF 16A) protein and RUNX2 downstream signaling targets, such as OCN and ALP (SF 146 &C) (224); However, there was no effect on RUNX2 transcript levels (SF 16F), indicating posttranslational control of RUNX2 by mTORC1. These effects were accompanied by a gain of osteocyte-like features by MSCs, as shown by RT-PCR (SF 16B &C) and Alizarin red staining of differentiated MSCs (Fig 41B &C), and a reduction in adipogenesis (Fig 41D &E). Hitherto, mTORC2 knockdown (through siRNA against rictor) resulted in increased adipogenesis, as shown by oil red O staining (Fig 41D &E), along with loss of RUNX2 (Fig 41A &SF 16A) and osteocyte-like features by MSCs (SF 16B &C) with no effect on RUNX2 mRNA levels (SF 16F), indicating possible posttranslational control of RUNX2 by mTORC2. Based on these results, we hypothesized that mTORC1 was involved in the suppression of osteogenesis of MSCs through RUNX2 suppression. Since GSK3β is a well-known regulator of the ubiquitination of several key proteins involved in osteogenesis and acts downstream of the mTORC2/AKT-473 axis and involved in adipogenesis (159), we checked the involvement of GSK3β in the posttranslational regulation of RUNX2 in the differentiation of MSCs. Our studies on the interaction between RUNX2 and GSK3β, by immunoprecipitation of RUNX2 in MSCs followed by mTORC1 and C2 knockdown, demonstrated that the interaction between RUNX2 and GSK3β was reduced upon knockdown of mTORC1, whereas the same was

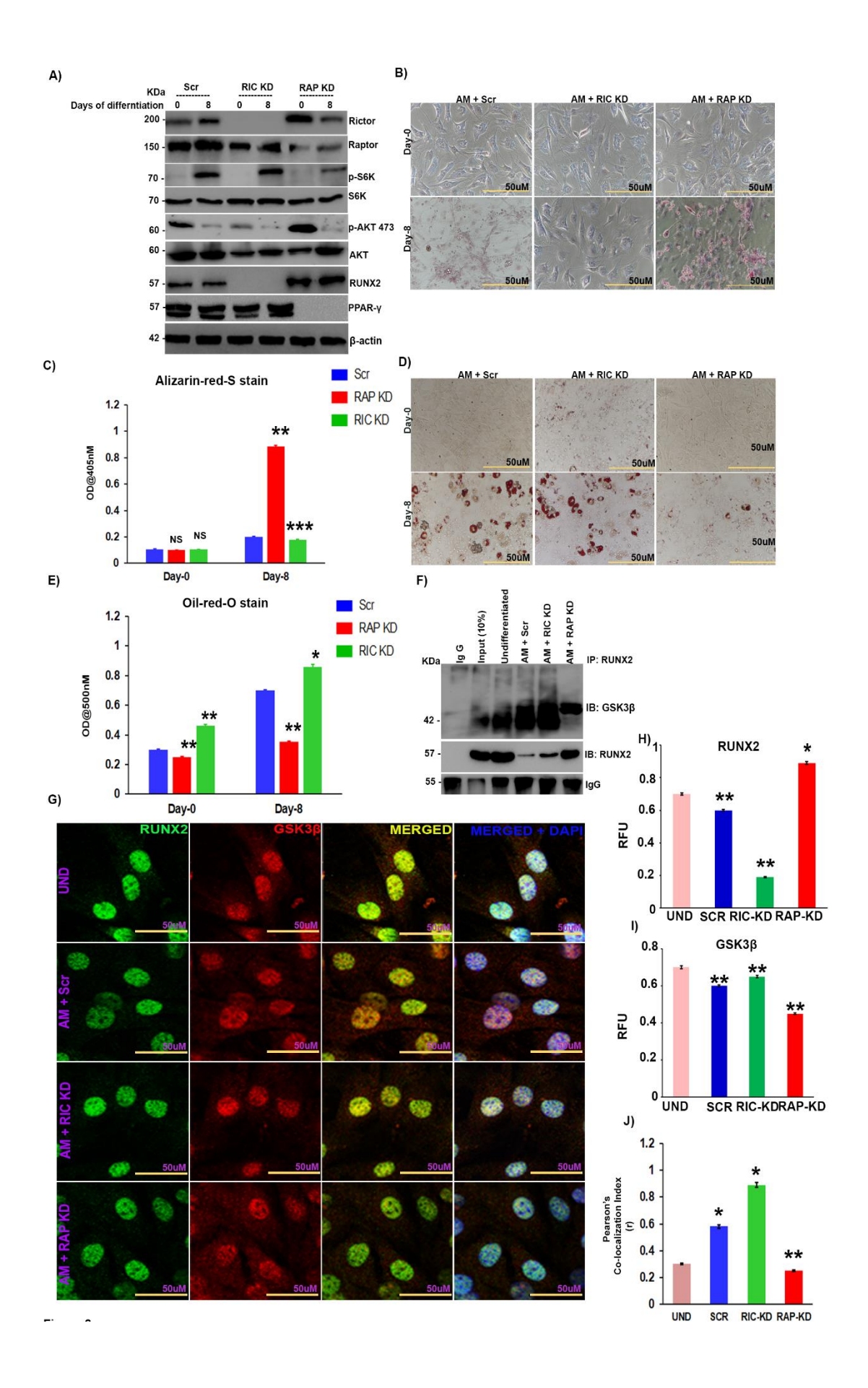


FIGURE 41: mTORC1 promotes adipogenic lineage through inhibition of the mTORC2/AKT-473/RUNX2 axis. MSCs were transfected with siRNAs against rictor and raptor after which they were induced to adipogenic differentiation and subjected to A) immunoblot analysis. B) Alizarin-red-s-stained calcium deposition of ECM in murine MSCs induced to adipogenic differentiation post-transfection at indicated time points and C) quantification of the same. D) Oil-red-o-stained murine MSCs that were induced to adipogenic differentiation post-transfection at indicated time points and E) quantification of the same. F) Immunoprecipitation analysis of transfected murine MSCs with or without induction to adipogenic differentiation. Complexes with anti-RUNX2 were pulled down and immunoblotted with anti-GSK3β and anti-RUNX2. G) Confocal images of transfected murine MSCs induced to adipogenic differentiation for 8 days, co-stained with anti-RUNX2 (Alexa 488) and anti-GSK3β (Alexa 594) and counter-stained with DAPI (400). Quantification of confocal staining by ImageJ analysis for H) RUNX2, I) GSK3β and J) Pearson's correlation index. Mean  $\pm$  S.E.M.; N=3, \*p<0.1 versus control, \*\*p<0.01 versus control. AM: adipogenic medium, Scr: scrambled siRNA, RAP KD: raptor knockdown with siRNA, RIC KD: rictor knockdown with siRNA, UND: undifferentiated, ALP: alkaline phosphatase.

enhanced upon mTORC2 knockdown (Fig 41F). Similar results were confirmed by confocal analysis (Fig 41G-J).

### 2.3.3.3. mTORC2 stabilizes RUNX2 through the AKT-473/GSK3\beta axis

As mTOR complexes appears to regulate RUNX2 stabilization and the osteogenic commitment of MSCs through GSK3  $\beta$ , we investigated the role of GSK3 $\beta$  in the RUNX2 interaction and its regulation during adipogenic differentiation. MSCs were subjected to mTORC2 knockdown in the presence or absence of LiCl and instigated for adipogenesis. LiCl treatment rescued the mTORC2 knockdown-mediated loss of RUNX2 expression (Fig 42A) without altering RUNX2 mRNA levels (Fig 42B). Since it was seen earlier that mTORC2 knockdown resulted in increased adipogenesis, we analyzed if this increase in adipogenesis was indeed mediated through GSK3\(\beta\). Our differentiation model in MSCs confirmed that, upon treatment with LiCl, there was a decrease in adipogenesis due to the suppression of GSK3β (Fig 42C &D). Since post-translational regulation of RUNX2 was obvious and it is known that GSK3β regulates several keys signaling molecules by ubiquitination, we analyzed the role of GSK3ß in the proteasomal degradation of RUNX2. Our experiments in MSCs with or without MG-132 treatment (an inhibitor of proteasomal degradation) and with or without mTORC2 knockdown demonstrated that the loss of RUNX2 protein levels upon mTORC2 knockdown was redeemed upon exposure to MG-132. These results, along with the interaction of RUNX2 and GSK3β, indicate that GSK3β is involved in RUNX2 ubiquitination (Fig 42E).

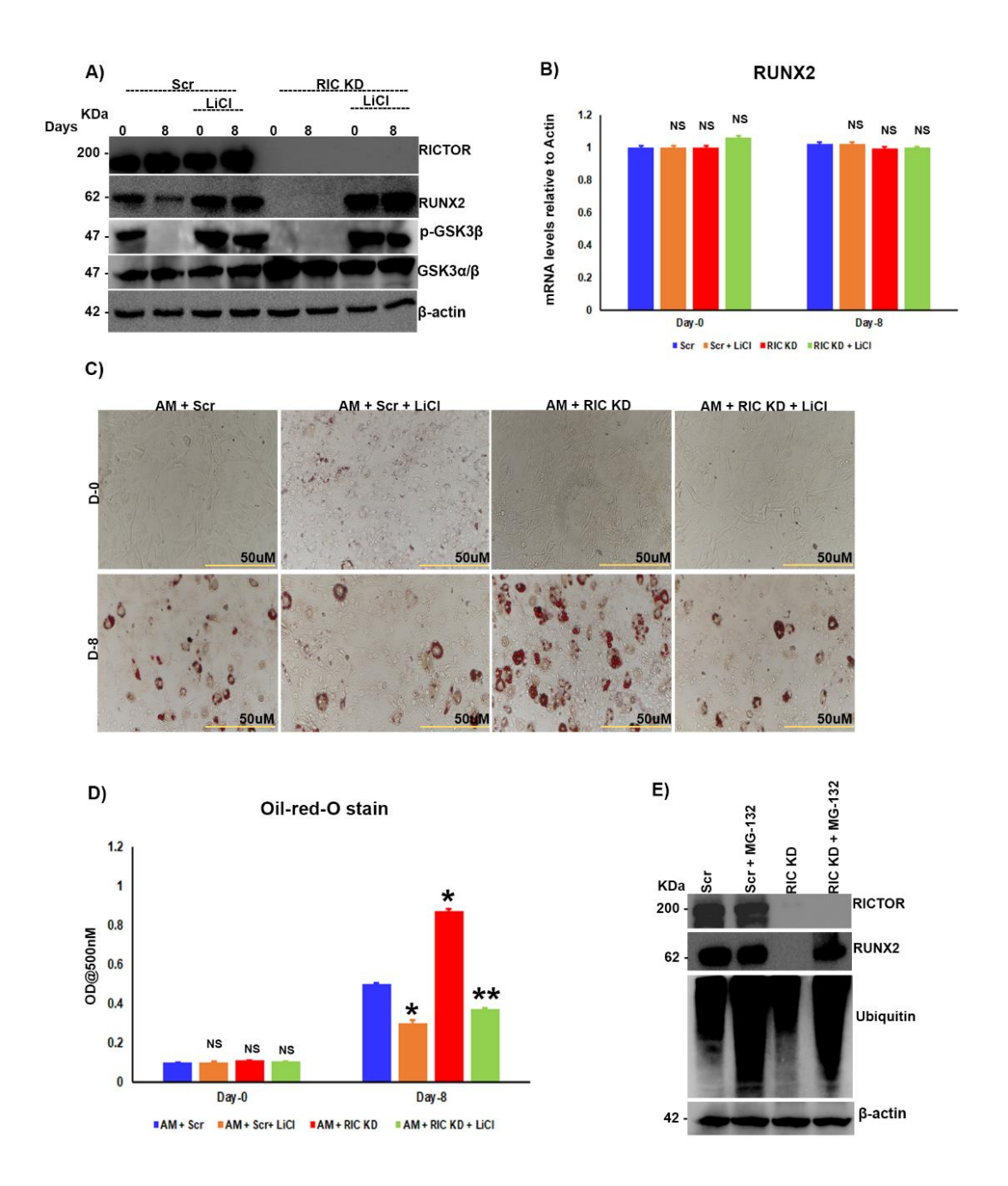


FIGURE 42: mTORC2 stabilizes RUNX2 through the AKT-473/ GSK3β axis. Murine MSCs were treated with LiCl (0.5 mM), with or without siRNA against rictor, along with adipogenic induction and A) subjected to immunoblot analysis and B) RT-PCR as indicated. C) Oil-red-o-stained images of murine MSCs treated with LiCl (0.5 mM), with or without siRNA against rictor, along with adipogenic induction as indicated and D) quantification of oil-red-o stain by spectrophotometry. Murine MSCs were transfected with siRNA against rictor in the presence or absence of MG-132 for 48 hours after transfection and E) immunoblot analysis was performed after 48 hours for the indicated antibodies. Mean  $\pm$  S.E.M.; N=3, \*p<0.1 versus control, \*\*p<0.01 versus control, NSp>0.1 versus control.

AM: adipogenic medium, Scr: scrambled siRNA, RIC KD: rictor knock down with siRNA, NS: not significant.

# 2.3.3.4. Diabetes-induced RUNX2 loss is mediated through the mTORC1/p-70S6K/GSK3\$\beta\$ axis

We and others have shown that diabetes-induced high glucose levels resulted in a loss of RUNX2; however, the molecular mechanisms involved in high glucose-mediated RUNX2 ubiquitination remained elusive (136). As our data suggests mTORC1 and C2 regulate RUNX2 ubiquitination through GSK3β, we asked whether RUNX2 is ubiquitinated by mTOR -GSK3β axis in diabetes condition. To test this, C3H10T1/2 cells were grown in high- and low-glucose conditions and analyzed the activity of mTORC1 (measured through S6K phosphorylation status) and mTORC2 (measured through AKT-473 phosphorylation). Under low-glucose conditions (which mimics starved physiological conditions) mTORC1 activity is reduced, owing to activation of p-AMPK. Whilst mTORC2 activity increased resulting in inhibition of GSK3\beta through Ser 9 phosphorylation, thus stabilizing RUNX2 levels (Fig 43A). However, under high-glucose conditions (which correlates with physiological diabetic conditions), inhibition of mTORC2 activity was observed, owing to hyperactivation of mTORC1. Low levels of AKT-473 lead to GSK3β activation, resulting in low levels of RUNX2 (Fig 43B). Similar to RUNX2 protein levels under high-glucose conditions, there was decrease in the ECM calcification of MSCs, which was increased under low-glucose and GSK3β-inhibited conditions (Fig 43C &D). Owing to the high mTORC1 activity under high-glucose conditions, there was increase in the adipogenesis of MSCs, whereas under low-glucose conditions, mTORC1 activity was reduced resulting in inhibition of GSK3β and stabilization of RUNX2, which resulted in decreased adipogenesis (Fig 43E &F). Similar results were recapitulated in experiments with primary bone marrow-MSCs (BM-MSCs) (Fig 43G). In order to delineate the role of GSK3β in high-glucose-triggered RUNX2 loss, we next inhibited GSK3β in MSCs with LiCl and subjected MSCs to adipogenic differentiation in normal and high-glucose conditions. The results showed that the loss of RUNX2 protein levels observed in high-glucose conditions was attenuated when the MSCs were exposed to LiCl (Fig 43H). Similarly, there was increase in ECM calcification (Fig 43C &D) and decrease in adipogenesis (Fig 43E &F) in the presence of LiCl.

# 2.3.3.5. High glucose induced glutamine sparring triggers RUNX2 loss under diabetic conditions

Under high-glucose conditions, mTORC1 is hyperactivated, which results in feedback inhibition of mTORC2 through p-70S6k and finally a loss of RUNX2 protein levels; However, the mechanism behind hyperactivation of mTORC1 with increasing glucose concentrations is

unclear. Recent studies have shown that under high-glucose conditions, glutamine sparing from mitochondria increases mTORC1 activity (225-227). Therefore, we hypothesized that a similar phenomenon could occur in the context of diabetes. To test our hypothesis, we subjected MSCs

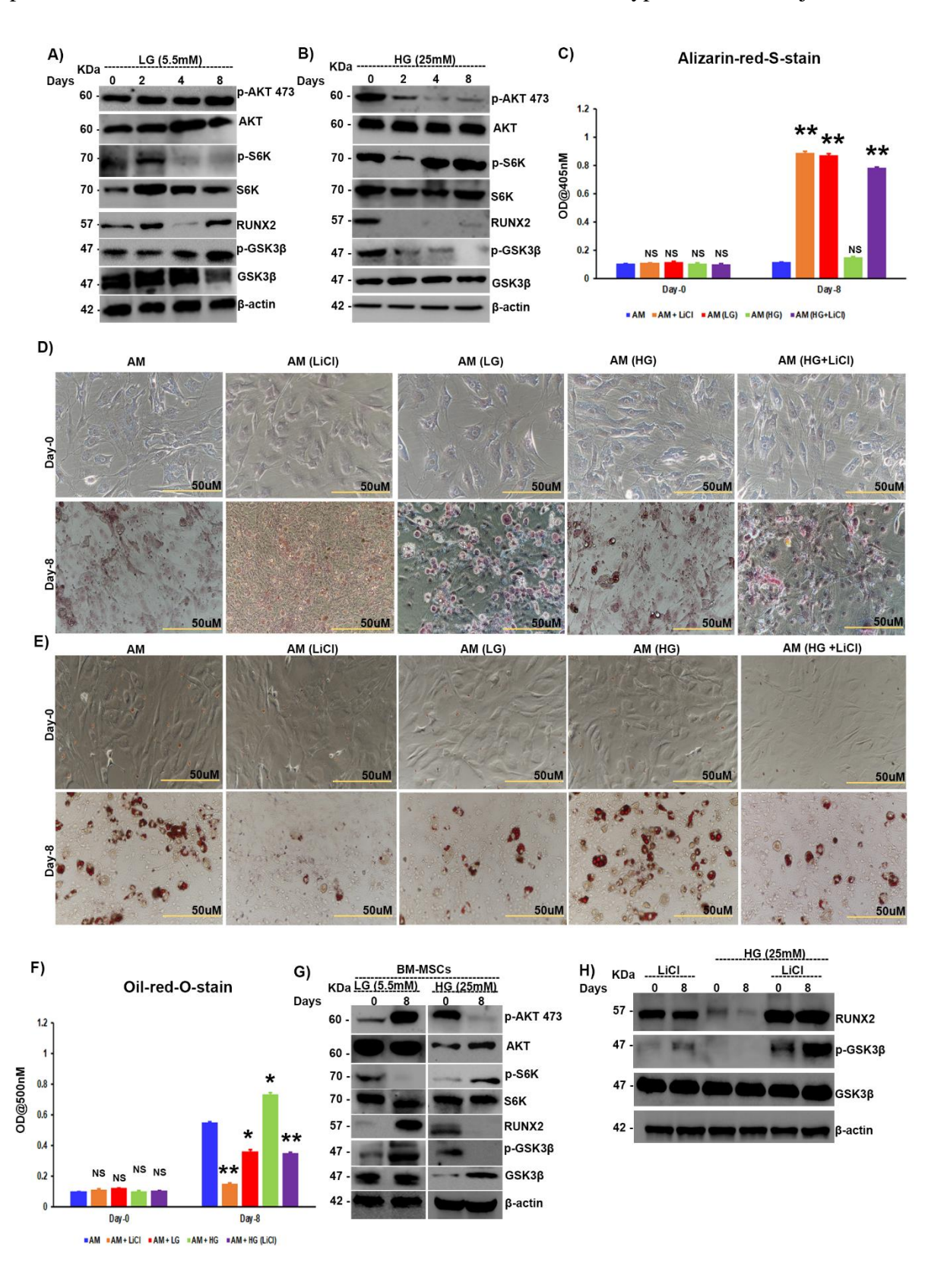
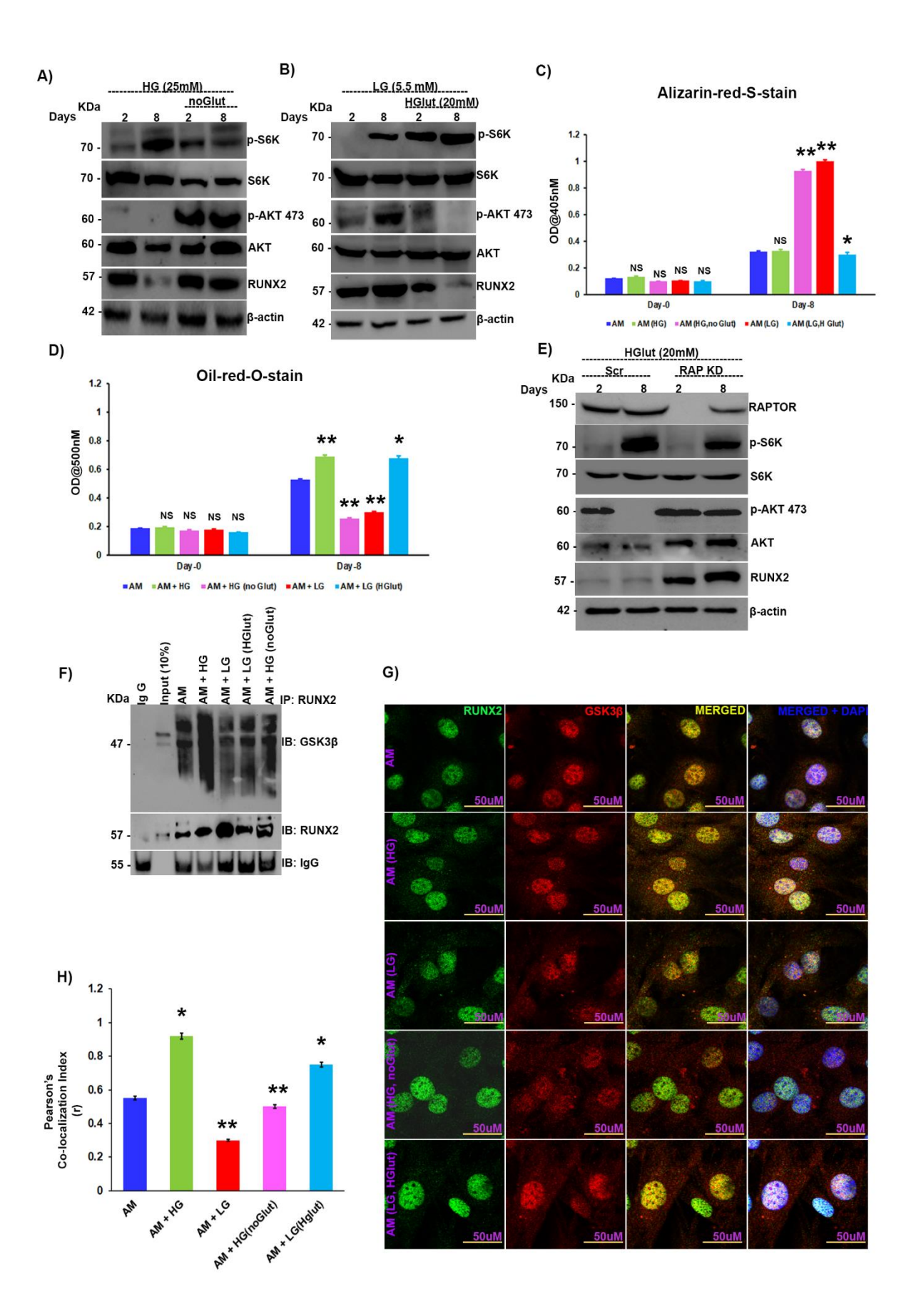


FIGURE 43: Diabetes-induced RUNX2 loss is mediated through the mTORC1/p-7086K/GSK3β axis. Murine MSCs were subjected to adipogenic differentiation in the presence of either low (5.5 mM) or high (25 mM) levels of glucose in the medium and subjected to A) & B) immunoblot analysis as indicated. C) quantification of alizarin-red-s stain by spectrophotometry and D) Alizarin-red-s-stained images of murine MSCs, which were induced to adipogenic differentiation with either low (5.5 mM) or high (25 mM) levels of glucose and with or without LiCl (0.5 mM) treatment, as indicated. E) Oil-red-o-stained murine MSCs, which were subjected to adipogenic differentiation in the presence of either low (5.5 mM) or high (25 mM) levels of glucose and with or without LiCl (0.5 mM) treatment, as indicated, and F) quantification of oil-red-o stain by spectrophotometry. G) Bone marrow-derived MSCs (BM-MSCs) were subjected to adipogenic differentiation in the presence of either low (5.5 mM) or high (25 mM) levels of glucose and cell lysates were collected and subjected to immunoblot analysis as indicated. Murine MSCs treated with LiCl (0.5 mM) with or without treatment by high glucose (25 mM) and H) immunoblot analysis, as indicated. Mean ± S.E.M.; N=3, \*p<0.1 versus control, \*\*p<0.01 versus control, NSp>0.1 versus control.

AM: adipogenic medium, LG: low glucose, HG: high glucose, NS: not significant.

to adipogenic differentiation under high-glucose conditions with or without glutamine. We found that upon withdrawal of glutamine, even in presence of high glucose mTORC1 hyperactivation was lost and so was inhibition of the mTORC2/AKT-473 axis, resulting in a resurrection of RUNX2 levels that otherwise were repressed (Fig 44A) hinting upon glutamine sparing by high glucose. The role of glutamine in RUNX2 regulation was further established by treating MSCs with low levels of glucose along with high or normal levels of glutamine in adipogenic differentiation medium. The levels of glutamine were determined by a dose responsive treatment of MSCs with varying levels of glutamine and mTORC1 activity was measured (SF 17A). mTORC2 activity was aborted upon addition of high glutamine levels due to the hyperactivation of mTORC1 by glutamine sparing and culminated in a loss of RUNX2 expression (Fig 44B), along with a reduction in ECM calcification (Fig 44C &SF 17B) and increase in adipogenesis (Fig 44D &SF 17C). The high-glucose-instigated increase in adipogenesis was also subdued upon withdrawal of glutamine (Fig 44D &SF 17C) and the reverse was seen in the case of ECM calcification (Fig 44C &SF 17B). In order to confirm that glutamine's action indeed mediated through mTORC1, MSCs were subjected to mTORC1 knockdown and then exposed to high glutamine concentrations, which resulted in activation of the mTORC2/AKT-473 axis and subsequently stabilized RUNX2 levels (Fig 44E), indicating that glutamine indeed acts through mTORC1. In our earlier section, we have observed that



### FIGURE 44: High glucose induced glutamine sparring triggers RUNX2 loss under diabetic conditions.

Murine MSCs were subjected to adipogenic differentiation  $\bf A$ ) in the presence of high glucose (25 mM) with or without glutamine (4 mM) and  $\bf B$ ) in the presence of low glucose (5.5 mM) with or without high glutamine (20 mM) followed by immunoblot analysis at indicated intervals.  $\bf C$ ) Quantification of alizarin-red-s stain by spectrophotometry.  $\bf D$ ) Quantification of oil-red-o stain by spectrophotometry. Murine MSCs were subjected to adipogenic differentiation in the presence of high glutamine (20 mM), with or without RAPTOR siRNA, and cell lysates were subjected to  $\bf E$ ) immunoblot analysis as indicated.  $\bf F$ ) Immunoprecipitation analysis of murine MSCs induced to adipogenic differentiation under varying glucose and glutamine concentrations and anti-RUNX2 complexes were pulled and immunoblotted with anti-GSK3 $\beta$  and anti-RUNX2.  $\bf G$ ) Confocal images of murine MSCs induced to adipogenic differentiation under varying glucose and glutamine concentrations for 8 days and stained with anti-RUNX2 (Alexa 488) and anti-GSK3 $\beta$  (Alexa 594) and counter-stained with DAPI (400).  $\bf H$ ) Quantification of confocal images by ImageJ software. Mean  $\pm$  S.E.M.; N=3, \*p<0.1 versus control, \*\*p<0.01 versus control; \*\*\*p<0.001 versus control, \*\*Sp>0.1 versus control.

Glut: glutamine, HGlut: high glutamine, AM: adipogenic medium, LG: low glucose, HG: high glucose, IP: immunoprecipitation, IB: immunoblotting, NS: not significant.

RUNX2 loss was due to increased physical interaction between GSK3 $\beta$  and RUNX2, so the same was examined under varying glutamine and glucose concentrations. Immunoprecipitation by RUNX2 and immunoblotting with GSK3 $\beta$  in MSCs revealed elevated levels of interaction between RUNX2 and GSK3 $\beta$  in high-glutamate conditions (Fig 44F). The same results were confirmed by immunofluorescence with confocal microscopy (Fig 44G &H).

# 2.3.3.6. Metformin rescues the mTORC2/RUNX2 axis by inhibition of the mTORC1/p-70S6K pathway

Metformin is the most widely used anti-glycemic drug and is known to activate p-AMPK and regulate glucose uptake by cells. Metformin is also known to have osteoprotective functions through the p-AMPK/RUNX2 axis (136). Here, we examined the effects of metformin under high-glutamine conditions in MSCs. It was observed that metformin treatment resulted in the abrogation of glutamine-triggered mTORC1 activation, resulting in increased mTORC2 activity, thus stabilizing the AKT-473/RUNX2 axis (Fig 45A). The inhibition of glutamine-induced mTORC1 activation by metformin was further validated in BM-MSCs, whose results were the same as those seen in MSCs (Fig 45B). The role of the mTORC2/GSK3β/RUNX2 axis was further analyzed in streptozotocin-induced diabetic mice with or without metformin treatment. It could be seen that mTORC2 activity was down-regulated under diabetic conditions and was rescued when treated with metformin. Under

diabetic conditions, GSK3 $\beta$  was active due to mTORC2 inhibition, which resulted in the down-regulation of RUNX2 and the situation was reversed upon metformin treatment (Fig 45C). The interaction between RUNX2 and GSK3 $\beta$  was further confirmed in protein lysates of diabetic muscle tissues, where the interaction was greater in diabetic samples than in controls and metformin-treated diabetic mouse tissues. These results can be taken to mean that under diabetic conditions, the interaction between RUNX2 and GSK3 $\beta$  was enhanced due to a loss of mTORC2 regulation on GSK3 $\beta$ , which was reversed upon metformin treatment (Fig 45D).

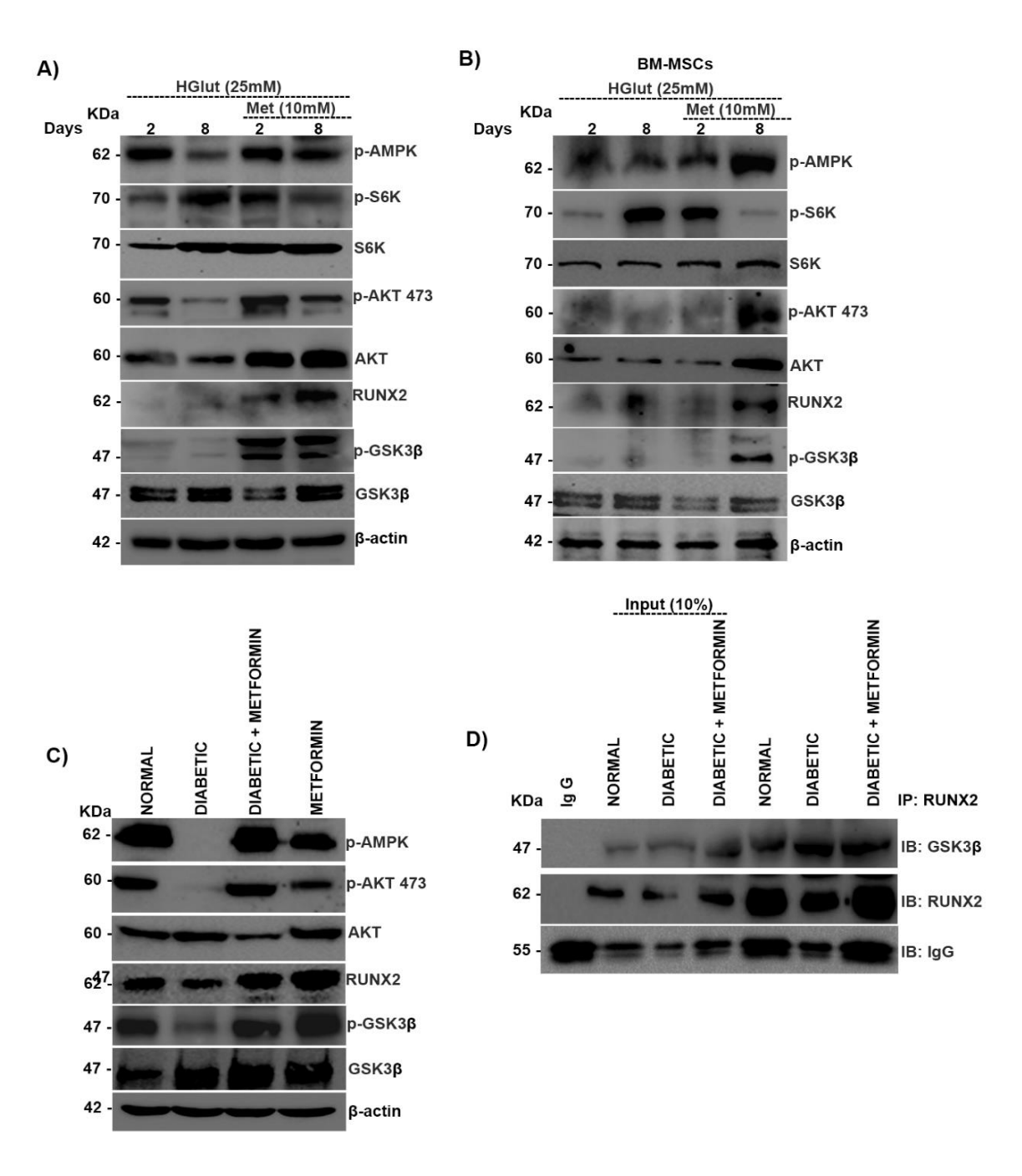


FIGURE 45: Metformin rescues the mTORC2/RUNX2 axis by inhibition of the mTORC1/p-70S6K pathway. A) Murine MSCs and B) BM-MSCs were subjected to adipogenic differentiation in the presence of high glutamine (20 mM), with or without metformin (10 mM), and proceeded for immunoblot analysis as indicated. Normal and diabetic BALB/c male mice, with and without metformin treatment, were sacrificed and muscle tissue was excised from the hind limbs and subjected to C) immunoblot analysis with anti-GSK3-β and anti-RUNX2 and D) immunoprecipitation by anti-RUNX2. Mean  $\pm$  S.E.M.; N=3.

IP: immunoprecipitation, IB: immunoblotting, HGlut: high glutamine, Met: metformin.

## **DISCUSSION**

#### DISCUSSION

The lineage commitment of MSCs is a dynamic process carried out under the tight regulation of growth factors, hormones, and available nutrients (228). In recent times, the role of nutrients like glucose and glutamine in MSC regulation has gained significance since activation of the nutrient sensors mTORC1 and mTORC2 was shown to direct MSC commitment towards specific lineages. (220). Activation of specific mTOR complexes to maintain the homeostasis of lineage commitment under normal physiological and metabolic conditions was a known phenomenon, but its significance in selective commitment is still elusive. The preference for adipogenesis over osteogenesis under deregulated metabolic conditions and the influence of excess nutrients, such as glucose, glutamine, and their metabolites/catabolites, leading to differential commitment of MSCs are critical in the management of secondary diabetic complications and aging. The current study discloses the role of nutrients in activating mTORC1/p-70S6K-induced adipogenesis while inhibiting osteogenesis and role of mTORC2/AKT-473 in maintaining osteogenesis, and impact of negative regulation of mTORC1 on mTORC2 levels and increased adipogenesis of MSCs. Both the mTOR complexes exerted their effects in part through RUNX2 regulation, where mTORC2 stabilizes RUNX2 by inhibiting GSK3β, which would otherwise induce RUNX2 ubiquitination. It is well known that active mTORC2 inhibits GSK3\beta by inhibitory phosphorylation at serine 9 GSK3β. On the other hand, mTORC1 hyperactivation by insulin or glutamine resulted in activation of GSK3β (due to the loss of inhibitory phosphorylation) by inhibiting mTORC2 through p-70S6K, which culminated in the repression of RUNX2 and osteogenic commitment of MSCs.

Diabetes-induced high glucose levels were known to down-regulate RUNX2, but the similarly differential regulation of mTOR complexes in the regulation of RUNX2 under high-glucose conditions, thus resulting in a loss of osteogenesis, was not clear. From our studies, it was observed that mTORC2 was inhibited under diabetic conditions due to hyperactivation of mTORC1, and as a result RUNX2 was suppressed. However, glucose as such has no direct role in activating mTORC1. From this study, it was observed that increased intracellular glutamine levels were the cause of mTORC1 activation under high-glucose conditions and the absence of glutamine resulted in an abrogation of mTORC1 hyperactivation. Our studies show that irrespective of glucose levels, an increased glutamine concentration in the medium was sufficient to trigger adipogenesis over osteogenesis. How increasing glucose levels could result in increased intracellular levels of glutamine is not clear. It could be possible

that at higher concentrations, glucose would spare glutamine entry into the tri-carboxylic-acid (TCA) cycle, which resulted in high glutamine levels intracellularly (226). The crucial step for glutamine entry into the mitochondrial TCA cycle is the conversion of glutamine to glutamate, catalyzed by glutamine synthetase (GLS) (229). Active GSK3β can inhibit GLS by inhibiting c-MYC, which otherwise would activate glutamine oxidation by upregulating GLS expression (230). Inhibition of GLS by GSK3β results in increased intracellular glutamine levels and can potentiate the hyperactivation of mTORC1, which would result in adipogenesis. Parallel to this, GSK3β also ubiquitinates rictor, thus resulting in a loss of mTORC2 and inhibition of osteogenesis (231).

Active mTORC2 favors osteogenesis by inhibiting GSK3β through AKT-473, which results in the stabilization of RUNX2, the master regulator of osteogenesis. Inhibition of GSK3ß activates GLS, and thus glutamine oxidation, in cells, which could result in low intracellular glutamine levels, thereby downregulating mTORC1 hyperactivation and adipogenesis. GSK3β, once active, can induce RUNX2 ubiquitination and thus downregulate osteogenesis. Any aberrations in glucose and glutamine levels were shown to influence mTORC2; Similarly, our data showed that low levels or the absence of glucose and glutamine, respectively, could activate mTORC2, which then paved a path for the osteocyte-like signature of MSCs, even in the absence of osteogenic-inducing medium (OM). Despite the absence of OM, MSCs have shown osteocyte-like signatures when the mTORC2 pathway was activated, either by altering glucose or glutamine levels or by downregulating the mTORC1 axis. This sheds light on the importance of cross-talk between the mTOR complexes in MSC fate regulation. The mTORC1 activation was clearly mediated either by amino acids, like glutamine, or by growth factor and insulin signaling, whereas the mTORC2 activation process was not clear until now. Here we have shown that nutrient limitation, either glucose or glutamine, could activate mTORC2. The major difference between adipogenic- and osteogenic-inducing media is the presence of insulin in the earlier case, which could drive MSC fate towards adipogenesis by hyperactivating mTORC1, leading to inhibition of mTORC2 (232). Thus, this signals to us that activation of mTORC2 occurs prior to insulin signaling cascade activation. Insulin signaling activates mTORC1 by inhibition of TSC2 through AKT-308 phosphorylation and at the same time it inhibits the rise of cAMP levels (233), whereas components like IBMX, dexamethasone, and ascorbic acid, which are among the components of OM, were shown to increase cAMP levels (234-236). cAMP was known to trigger insulin secretion upon sensing high glucose levels and is involved in energy homeostasis through PKA

and other important signaling mediators (237). Therefore, it will be interesting to see the role of such an important secondary messenger, cAMP, in interconnecting mTORC1 and mTORC2 homeostasis in the normal physiological setup.

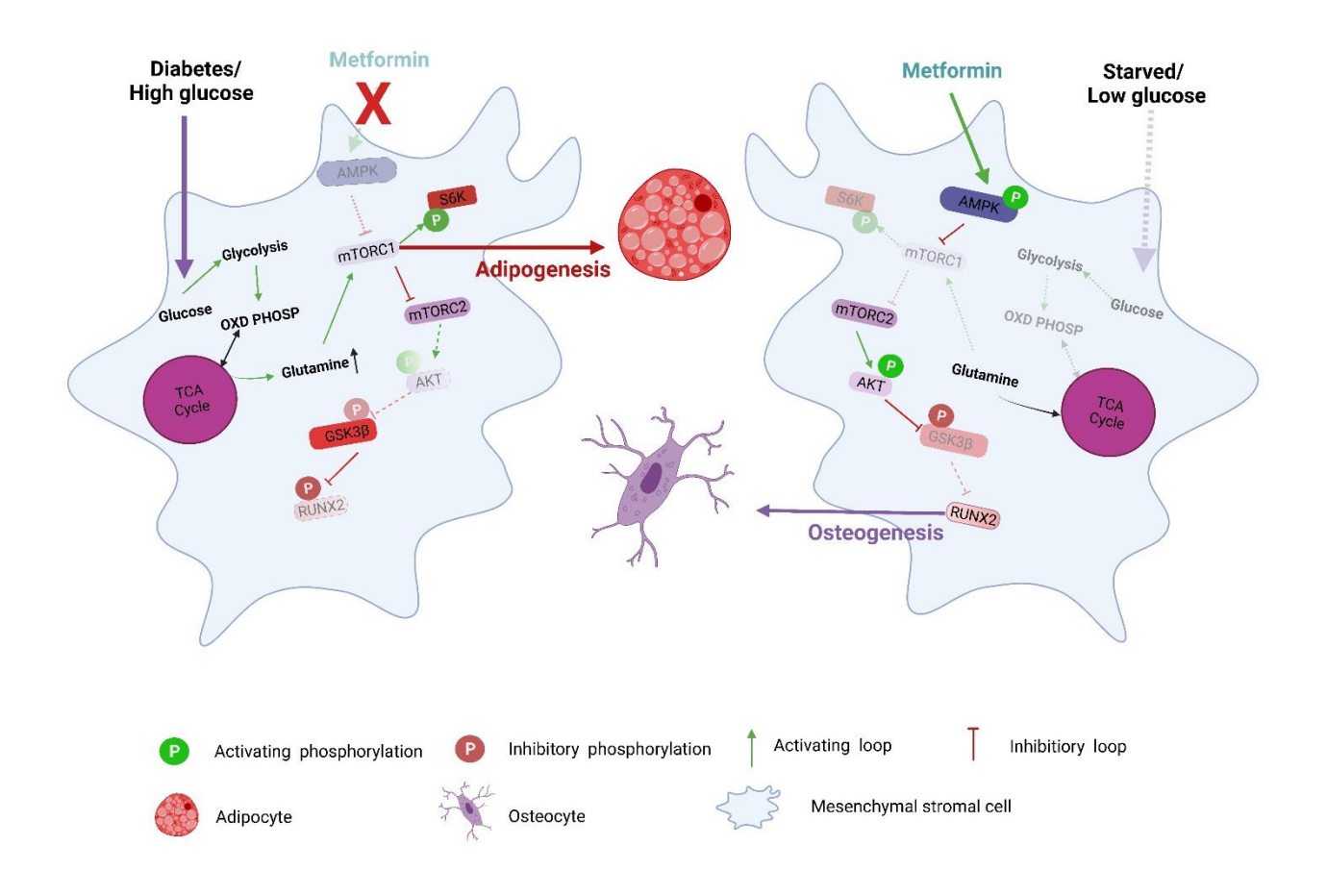


FIGURE 46: Schematic representation of mTOR cross-talk in RUNX2 regulation. This figure summarizes, along with the findings from the current study, where, at physiological levels, activation of mTORC2 by PIP2 resulted in activation of AKT by phosphorylation at Ser473. pSer473AKT inhibits GSK3β by phosphorylation at Ser9. Inhibitory/in-active Ser-9GSK3β fails to interact with RUNX2, and thus RUNX2 is stabilized from its degradation. Active RUNX2 can enhance ECM calcification and promote osteogenesis of MSCs. Increasing levels of glucose and glutamine or insulin can hyperactivate mTORC1, through which p-70S6k inhibits mTORC2. Inhibition of mTORC2 results in destabilization of RUNX2 through the loss of pSer473AKT, which leads to activation of GSK3β. Active GSK3β interacts with RUNX2 and primes it for ubiquitination. mTORC1 also activates lipogenesis and helps to increase adipogenesis. Metformin activates AMPK by phosphorylation at Thr172, which inhibits mTORC1 and rescues mTORC2 under high-glucose and/or high-glutamine conditions.

Metformin is a common anti-glycemic drug which was shown to have osteoprotective effects (238). It could be seen in the present study that, metformin, through activation of p-

AMPK, repressed mTORC1 hyperactivation under high-glutamine conditions and thus activated the mTORC2/AKT-473/RUNX2 axis. p-AMPK inhibits mTORC1 activation by phosphorylating RAPTOR, which interferes with mTORC1 complex assembly (239). Activated AMPK can also alter glutamine oxidation through mitochondria (240), thus affecting intracellular glutamine levels and mTORC1 activation. Diabetic patients were shown to have reduced glutamine oxidation and low levels of GLS activity (241), which can induce high intracellular glutamine levels and result in hyperactivation of mTORC1 and inhibition of mTORC2, resulting in bone adipogenesis. From our work, it could be seen that when treated with metformin, glutamine-induced mTORC1 hyperactivation was subdued, resulting in rescue of the mTORC2/AKT-473 axis. Activation of mTORC2 by metformin through AMPK resulted in the activation of AKT by phosphorylation at the Ser 473 position, which inhibits GSK3β, due to which RUNX2 was rescued from ubiquitination. Metformin, by activating AMPK and inhibiting GSK3β, could modulate the intracellular levels of glutamine through GLS.

Taken together, our data indicate that RUNX2 is stabilized directly by the mTORC2/AKT-473 axis by inhibiting GSK3β. Under an excess of nutrients like glutamine and/or glucose, mTORC1 is hyperactivated, resulting in activation of GSK3β, which destabilizes RUNX2 and suppresses the osteogenic fate of MSCs, leading to bone loss and adipogenesis. The current work emphasizes the important cross-talk between the mTOR complexes in directing MSC fate under normal and diabetic conditions (Fig 46).

### CONCLUSIONS

#### CONCLUSIONS

- Along with RUNX2, RUNX1 also serves as a novel substrate of AMPK under physiological conditions.
- Metformin aids in treatment of CML through AMPK mediated RUNX1 Ser 94 phosphorylation.
- RUNX1 Ser 94 phosphorylation results in inhibition of STAT3 activation, which is a major driver of imatinib resistance in CML.
- Metformin treatment results in inhibition of HSF1 activation, through AMPK mediated phosphorylation; HSF1 activation results in generation of geldanamycin resistance.
- AMPK induced RUNX1 Ser 94 phosphorylation induces HIF1-α ubiquitination through PHD2 mediated ubiquitination and down regulation of MDR1, thus improving drug sensitivity of CML subjects.
- AMPK induced RUNX2 Ser 118 phosphorylation results in upregulation of rictor and drives bone metastasis of breast cancer cells.
- AMPK through inhibition of MCT1 and MCT4 inhibits lactate fluxes in CML, along with inhibition of glycolysis.
- AMPK also inhibits GLUT1 driven glucose uptake in breast cancer cells.
- AMPK induced stabilization of mTORC2 results in stabilization of RUNX2 under diabetic conditions by inhibiting GSK3β.

### **SIGNIFICANCE**

### **SIGNIFICANCE**

Imatinib resistance is one of the growing phenomena among CML patients and current work highlights the potential of metformin to be used in the treatment regime of CML patients either alone or in combination with imatinib. MDS or pre-leukemia stage lack proper treatment regimen and from our current work it could be seen that metformin has a potential in treatment of MDS, through inhibition of HIF1-α facilitated by AMPK mediated RUNX1 phosphorylation. The current study also sheds light on the possible mechanism of why metformin breast cancer clinical trials were not encouraging, owing to AMPK mediated RUNX2 stabilization in breast cancer. Low bone mineral density and bone adiposity are common occurrences seen among diabetic subjects. The current works highlights the osteo-protective phenomenon of metformin under diabetic condition (Fig 47).

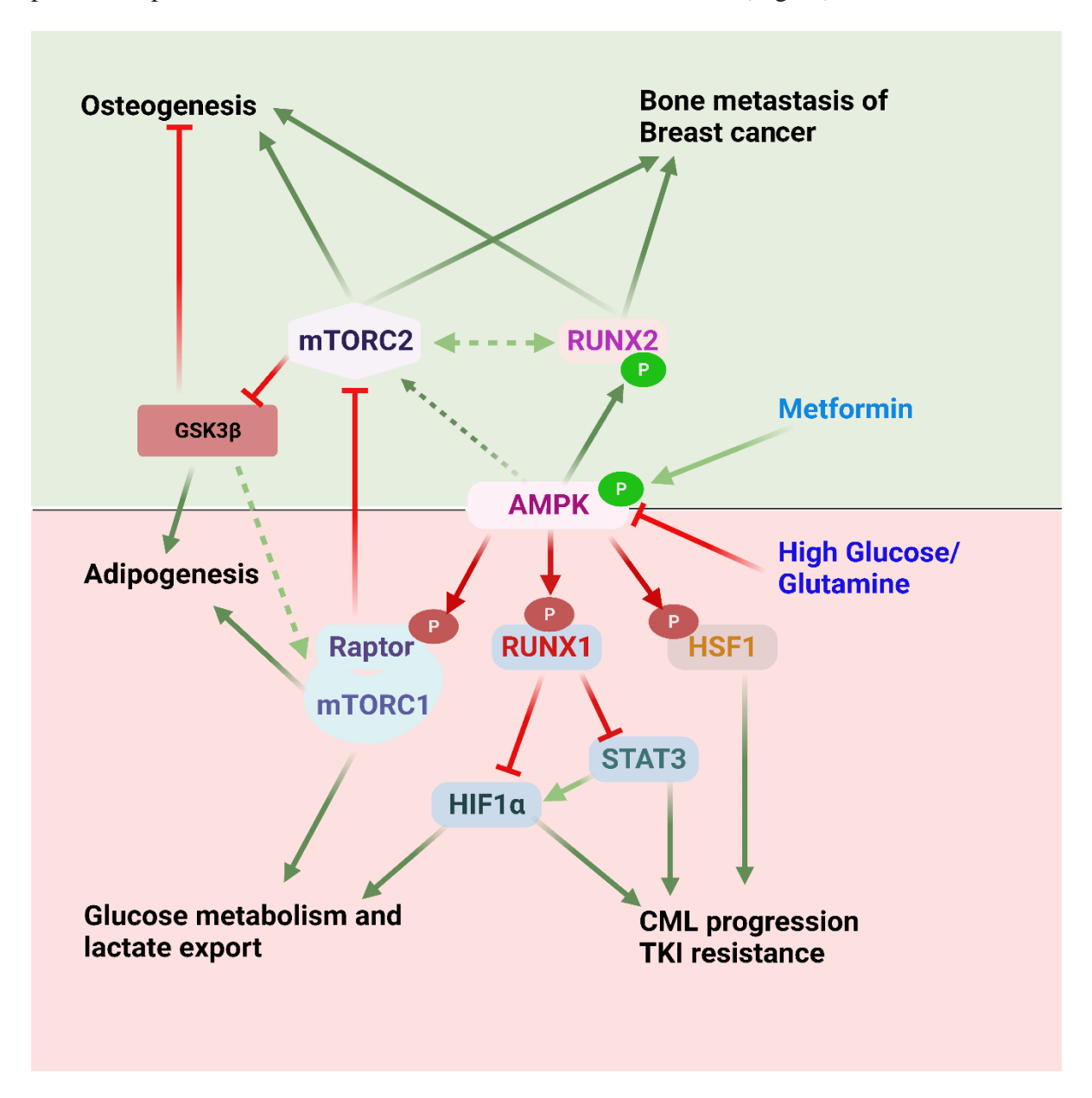


FIGURE 47: Schematic representation of AMPK substrates affecting progression of CML, bone metastasis of breast cancer cells and commitment of MSCs. This figure summarizes the findings from the current study, where metformin treatment results in activation of AMPK through phosphorylation at Thr 172 resulting in phosphorylation of AMPK substrates, RUNX1, HSF1, RUNX2 and raptor. Phosphorylation of RUNX1 by AMPK results in increased interaction and cytoplasmic retention of STAT3 and inhibits activation of STAT3. AMPK mediated RUNX1 phosphorylation also results in inhibition of HIF1-α on one hand by promoting the latter's ubiquitination and on the other through STAT3 inhibition. AMPK induced phosphorylation of HSF1 promotes destabilization and inhibition of HSF1 activity. HSF1, STAT3 and HIF1-α together promote CML progression and aid in generation of TKI resistance. AMPK mediated inhibition of mTORC1 and HIF1-α results in down regulation of glucose metabolism and lactate export, which in turn aid in generation of TKI resistance and CML progression. AMPK mediated phosphorylation of RUNX2 results in stabilization of RUNX2, which facilitates bone metastasis of breast cancer cells through activation of mTORC2 in a phospho-RUNX2 dependent manner. mTORC2 in turn stabilizes RUNX2 through inhibition of GSK3β, which is involved in RUNX2 ubiquitination. RUNX2/ mTORC2 axis also plays a key role in promoting osteogenic commitment of MSCs whereas mTORC1/ GSK3β axis is involved mainly in adipogenic commitment of MSCs. High glucose/ glutamine levels regulate the switch in MSCs through altering the activation of AMPK.

### **FUTURE ASPECTS**

#### **FUTURE ASPECTS**

The AMPK motif present in the runt domain of RUNX proteins is conserved across all the fusion proteins generated from RUNX1 translocations. So it would be of great potential use, validate if RUNX1 fusion proteins would also serve as AMPK substrates and if so, what would be the effect of AMPK induced phosphorylations on their transcriptional activation. Analyzing along these lines could aid in a better understanding of the potential role metformin as an anti-leukemic drug.

In the current work we have observed that AMPK induced RUNX phosphorylation had diverse effects when it came to modulating the nuclear localization and transcriptional activation of RUNX proteins, where on one hand in case of RUNX1 it resulted in reduced nuclear localization and activation, whereas in case of RUNX2 it resulted in increased nuclear localization and stabilization of RUNX2. Looking closely into structural differences present between RUNX1 and RUNX2, the major contributing factor for such differences is presence of QA domain. Understanding the reason behind the observed opposing effects seen in case of RUNX1 and RUNX2 could help in our better understanding of protein structure to function relationship.

We have also observed the opposing effects of AMPK activation on mTOR complex activation and also on GLUT1 and GLUT4 expression. Further analysis of the AMPK/mTOR/GLUT axis will help us to understand the dynamics of GLUT regulation in cells which can help in better treatment of diabetes.

### **PUBLICATIONS**

### **PUBLICATIONS**

Chava S, Chennakesavulu S, **Gayatri BM**, Reddy ABM. A novel phosphorylation by AMP-activated kinase regulates RUNX2 from ubiquitination in osteogenesis over adipogenesis. Cell Death & Disease. 2018;9(7):754.

Chava, S, **Gayatri MB**, Reddy AB. Chapter 3 - EMT Contributes to Chemoresistance in Pancreatic Cancer in Breaking Tolerance to Pancreatic Cancer Unresponsiveness to Chemotherapy, p. 25-43. Edited by Nagaraju GP 2019, Academic Press.

Vadlakonda L, Indracanti M, Kalangi SK, **Gayatri BM**, Naidu NG, Reddy ABM. The Role of Pi, Glutamine and the Essential Amino Acids in Modulating the Metabolism in Diabetes and Cancer. Journal of Diabetes & Metabolic Disorders. 2020;19(2):1731-1775.

Arolla RG, Malladi S, Bhaduri U, **Gayatri MB**, Pattamshetty P, Mohan V, et al. Analysis of cellular models of clonal evolution reveals co-evolution of imatinib and HSP90 inhibitor resistances. Biochemical and Biophysical Research Communications. 2021; 534:461-7.

**Gayatri, M.B.,** Gajula, N.N., Chava, S. et al. High glutamine suppresses osteogenesis through mTORC1-mediated inhibition of the mTORC2/AKT-473/RUNX2 axis. Cell Death Discov. 8, 277 (2022).

### IN COMMUNICATION

**Gayatri** *et al.* Novel phosphorylation site on RUNX1 by AMP- activated kinase promotes Imatinib sensitivity of resistant CML subjects.

**Gayatri** *et al.* Metformin as a therapeutic alternative for treatment of clonally evolved imatinib-geldanamycin resistant CML cases.

**Gayatri** *et al.* Metformin exerts anti-leukemic effects through lactate metabolism and overcomes imatinib resistance in CML.

**Gayatri** *et al.* Metformin destabilizes HIF1-α expression in pre-leukemic and CML through AMPK induced RUNX1 Ser 94 phosphorylation.

**Gayatri** *et al.* Metformin promotes bone metastasis of breast cancer cells through p-AMPK/mTORC2/AKT-473/RUNX2 axis.

### REFERENCES

#### REFERENCES

- 1. Sung H, Ferlay J, Siegel RL, Laversanne M, Soerjomataram I, Jemal A, et al. Global Cancer Statistics 2020: GLOBOCAN Estimates of Incidence and Mortality Worldwide for 36 Cancers in 185 Countries. CA: A Cancer Journal for Clinicians. 2021;71(3):209-49.
- 2. Khan MAB, Hashim MJ, King JK, Govender RD, Mustafa H, Al Kaabi J. Epidemiology of Type 2 Diabetes Global Burden of Disease and Forecasted Trends. J Epidemiol Glob Health. 2020;10(1):107-11.
- 3. Otálora-Otálora BA, Henríquez B, López-Kleine L, Rojas A. RUNX family: Oncogenes or tumor suppressors (Review). Oncol Rep. 2019;42(1):3-19.
- 4. Ito Y, Bae S-C, Chuang LSH. The RUNX family: developmental regulators in cancer. Nature Reviews Cancer. 2015;15(2):81-95.
- 5. Jiao H, Xiao E, Graves DT. Diabetes and Its Effect on Bone and Fracture Healing. Curr Osteoporos Rep. 2015;13(5):327-35.
- 6. Cerezo M, Tichet M, Abbe P, Ohanna M, Lehraiki A, Rouaud F, et al. Metformin blocks melanoma invasion and metastasis development in AMPK/p53-dependent manner. Mol Cancer Ther. 2013;12(8):1605-15.
- 7. Kaizuka T, Hara T, Oshiro N, Kikkawa U, Yonezawa K, Takehana K, et al. Tti1 and Tel2 are critical factors in mammalian target of rapamycin complex assembly. J Biol Chem. 2010;285(26):20109-16.
- 8. Wang L, Harris TE, Roth RA, Lawrence JC, Jr. PRAS40 regulates mTORC1 kinase activity by functioning as a direct inhibitor of substrate binding. J Biol Chem. 2007;282(27):20036-44.
- 9. Kim DH, Sarbassov DD, Ali SM, King JE, Latek RR, Erdjument-Bromage H, et al. mTOR interacts with raptor to form a nutrient-sensitive complex that signals to the cell growth machinery. Cell. 2002;110(2):163-75.
- 10. Ganley IG, Lam du H, Wang J, Ding X, Chen S, Jiang X. ULK1.ATG13.FIP200 complex mediates mTOR signaling and is essential for autophagy. J Biol Chem. 2009;284(18):12297-305.

- 11. Shang L, Chen S, Du F, Li S, Zhao L, Wang X. Nutrient starvation elicits an acute autophagic response mediated by Ulk1 dephosphorylation and its subsequent dissociation from AMPK. Proc Natl Acad Sci U S A. 2011;108(12):4788-93.
- 12. Porstmann T, Santos CR, Griffiths B, Cully M, Wu M, Leevers S, et al. SREBP activity is regulated by mTORC1 and contributes to Akt-dependent cell growth. Cell Metab. 2008;8(3):224-36.
- 13. de la Cruz López KG, Toledo Guzmán ME, Sánchez EO, García Carrancá A. mTORC1 as a Regulator of Mitochondrial Functions and a Therapeutic Target in Cancer. Front Oncol. 2019;9:1373-.
- 14. Inoki K, Li Y, Zhu T, Wu J, Guan KL. TSC2 is phosphorylated and inhibited by Akt and suppresses mTOR signalling. Nat Cell Biol. 2002;4(9):648-57.
- 15. Tee AR, Manning BD, Roux PP, Cantley LC, Blenis J. Tuberous sclerosis complex gene products, Tuberin and Hamartin, control mTOR signaling by acting as a GTPase-activating protein complex toward Rheb. Curr Biol. 2003;13(15):1259-68.
- 16. Saito K, Araki Y, Kontani K, Nishina H, Katada T. Novel role of the small GTPase Rheb: its implication in endocytic pathway independent of the activation of mammalian target of rapamycin. J Biochem. 2005;137(3):423-30.
- 17. Kim E, Goraksha-Hicks P, Li L, Neufeld TP, Guan KL. Regulation of TORC1 by Rag GTPases in nutrient response. Nat Cell Biol. 2008;10(8):935-45.
- 18. Sancak Y, Peterson TR, Shaul YD, Lindquist RA, Thoreen CC, Bar-Peled L, et al. The Rag GTPases bind raptor and mediate amino acid signaling to mTORC1. Science. 2008;320(5882):1496-501.
- 19. Hara K, Yonezawa K, Weng QP, Kozlowski MT, Belham C, Avruch J. Amino acid sufficiency and mTOR regulate p70 S6 kinase and eIF-4E BP1 through a common effector mechanism. J Biol Chem. 1998;273(23):14484-94.
- 20. Long X, Ortiz-Vega S, Lin Y, Avruch J. Rheb binding to mammalian target of rapamycin (mTOR) is regulated by amino acid sufficiency. J Biol Chem. 2005;280(25):23433-6.
- 21. Guertin DA, Stevens DM, Thoreen CC, Burds AA, Kalaany NY, Moffat J, et al. Ablation in mice of the mTORC components raptor, rictor, or mLST8 reveals that mTORC2

- is required for signaling to Akt-FOXO and PKCalpha, but not S6K1. Dev Cell. 2006;11(6):859-71.
- 22. Frias MA, Thoreen CC, Jaffe JD, Schroder W, Sculley T, Carr SA, et al. mSin1 is necessary for Akt/PKB phosphorylation, and its isoforms define three distinct mTORC2s. Curr Biol. 2006;16(18):1865-70.
- 23. Peterson TR, Laplante M, Thoreen CC, Sancak Y, Kang SA, Kuehl WM, et al. DEPTOR is an mTOR inhibitor frequently overexpressed in multiple myeloma cells and required for their survival. Cell. 2009;137(5):873-86.
- 24. Pearce LR, Huang X, Boudeau J, Pawłowski R, Wullschleger S, Deak M, et al. Identification of Protor as a novel Rictor-binding component of mTOR complex-2. Biochem J. 2007;405(3):513-22.
- 25. Thedieck K, Polak P, Kim ML, Molle KD, Cohen A, Jenö P, et al. PRAS40 and PRR5-like protein are new mTOR interactors that regulate apoptosis. PLoS One. 2007;2(11):e1217.
- 26. Oh WJ, Jacinto E. mTOR complex 2 signaling and functions. Cell Cycle. 2011;10(14):2305-16.
- 27. Sarbassov DD, Guertin DA, Ali SM, Sabatini DM. Phosphorylation and regulation of Akt/PKB by the rictor-mTOR complex. Science. 2005;307(5712):1098-101.
- 28. Hresko RC, Mueckler M. mTOR.RICTOR is the Ser473 kinase for Akt/protein kinase B in 3T3-L1 adipocytes. J Biol Chem. 2005;280(49):40406-16.
- 29. García-Martínez JM, Alessi DR. mTOR complex 2 (mTORC2) controls hydrophobic motif phosphorylation and activation of serum- and glucocorticoid-induced protein kinase 1 (SGK1). Biochem J. 2008;416(3):375-85.
- 30. Sarbassov DD, Ali SM, Kim DH, Guertin DA, Latek RR, Erdjument-Bromage H, et al. Rictor, a novel binding partner of mTOR, defines a rapamycin-insensitive and raptor-independent pathway that regulates the cytoskeleton. Curr Biol. 2004;14(14):1296-302.
- 31. Ikenoue T, Inoki K, Yang Q, Zhou X, Guan KL. Essential function of TORC2 in PKC and Akt turn motif phosphorylation, maturation and signalling. Embo j. 2008;27(14):1919-31.
- 32. Gulhati P, Bowen KA, Liu J, Stevens PD, Rychahou PG, Chen M, et al. mTORC1 and mTORC2 regulate EMT, motility, and metastasis of colorectal cancer via RhoA and Rac1 signaling pathways. Cancer Res. 2011;71(9):3246-56.

- 33. Jacinto E, Loewith R, Schmidt A, Lin S, Rüegg MA, Hall A, et al. Mammalian TOR complex 2 controls the actin cytoskeleton and is rapamycin insensitive. Nat Cell Biol. 2004;6(11):1122-8.
- 34. Gan X, Wang J, Su B, Wu D. Evidence for direct activation of mTORC2 kinase activity by phosphatidylinositol 3,4,5-trisphosphate. J Biol Chem. 2011;286(13):10998-1002.
- 35. Yuan H-X, Guan K-L. The SIN1-PH Domain Connects mTORC2 to PI3K. Cancer Discov. 2015;5(11):1127-9.
- 36. Hawley SA, Pan DA, Mustard KJ, Ross L, Bain J, Edelman AM, et al. Calmodulin-dependent protein kinase kinase-beta is an alternative upstream kinase for AMP-activated protein kinase. Cell Metab. 2005;2(1):9-19.
- 37. Thirunavukkarasu K, Mahajan M, McLarren KW, Stifani S, Karsenty G. Two domains unique to osteoblast-specific transcription factor Osf2/Cbfa1 contribute to its transactivation function and its inability to heterodimerize with Cbfbeta. Mol Cell Biol. 1998;18(7):4197-208.
- 38. Lin M-E, Chen T, Leaf EM, Speer MY, Giachelli CM. Runx2 Expression in Smooth Muscle Cells Is Required for Arterial Medial Calcification in Mice. Am J Pathol. 2015;185(7):1958-69.
- 39. Lam JD, Oh DJ, Wong LL, Amarnani D, Park-Windhol C, Sanchez AV, et al. Identification of RUNX1 as a Mediator of Aberrant Retinal Angiogenesis. Diabetes. 2017;66(7):1950-6.
- 40. Meng S, Cao J, Zhang X, Fan Y, Fang L, Wang C, et al. Downregulation of MicroRNA-130a Contributes to Endothelial Progenitor Cell Dysfunction in Diabetic Patients via Its Target Runx3. PLOS ONE. 2013;8(7):e68611.
- 41. Yzaguirre AD, de Bruijn MF, Speck NA. The Role of Runx1 in Embryonic Blood Cell Formation. Adv Exp Med Biol. 2017;962:47-64.
- 42. Adnan Awad S, Dufva O, Ianevski A, Ghimire B, Koski J, Maliniemi P, et al. RUNX1 mutations in blast-phase chronic myeloid leukemia associate with distinct phenotypes, transcriptional profiles, and drug responses. Leukemia. 2021;35(4):1087-99.
- 43. Sood R, Kamikubo Y, Liu P. Role of RUNX1 in hematological malignancies. Blood. 2017;129(15):2070-82.

- 44. Awad S, Kankainen M, Dufva O, Heckman CA, Porkka K, Mustjoki S. RUNX1 Mutations Identify an Entity of Blast Phase Chronic Myeloid Leukemia (BP-CML) Patients with Distinct Phenotype, Transcriptional Profile and Drug Vulnerabilities. Blood. 2018;132(Supplement 1):4257-.
- 45. Solari L, Bauer T, Dicker F, Haferlach C, Grießhammer M, Schnittger S, et al. A novel recurrent AML1–ETO fusion: tight in vivo association with BCR–ABL1. Leukemia. 2013;27(6):1397-400.
- 46. Shen L, Zhu J, Chen F, Lin W, Cai J, Zhong J, et al. RUNX1-Evi-1 fusion gene inhibited differentiation and apoptosis in myelopoiesis: an in vivo study. BMC Cancer. 2015;15:970-.
- 47. Yamamoto K, Tsuzuki S, Minami Y, Yamamoto Y, Abe A, Ohshima K, et al. Functionally Deregulated AML1/RUNX1 Cooperates with BCR-ABL to Induce a Blastic Phase-Like Phenotype of Chronic Myelogenous Leukemia in Mice. PLOS ONE. 2013;8(9):e74864.
- 48. Mikhail FM, Sinha KK, Saunthararajah Y, Nucifora G. Normal and transforming functions of RUNX1: a perspective. J Cell Physiol. 2006;207(3):582-93.
- 49. Scheitz CJ, Lee TS, McDermitt DJ, Tumbar T. Defining a tissue stem cell-driven Runx1/Stat3 signalling axis in epithelial cancer. Embo j. 2012;31(21):4124-39.
- 50. Sarper SE, Kurosaka H, Inubushi T, Ono Minagi H, Kuremoto K-i, Sakai T, et al. Runx1-Stat3-Tgfb3 signaling network regulating the anterior palatal development. Scientific Reports. 2018;8(1):11208.
- 51. Bluyssen HAR, Rastmanesh MM, Tilburgs C, Jie K, Wesseling S, Goumans M-J, et al. IFNγ-dependent SOCS3 expression inhibits IL-6-induced STAT3 phosphorylation and differentially affects IL-6 mediated transcriptional responses in endothelial cells. American Journal of Physiology-Cell Physiology. 2010;299(2):C354-C62.
- 52. Bar-Natan M, Nelson EA, Xiang M, Frank DA. STAT signaling in the pathogenesis and treatment of myeloid malignancies. JAKSTAT. 2012;1(2):55-64.
- 53. Bewry NN, Nair RR, Emmons MF, Boulware D, Pinilla-Ibarz J, Hazlehurst LA. Stat3 contributes to resistance toward BCR-ABL inhibitors in a bone marrow microenvironment model of drug resistance. Mol Cancer Ther. 2008;7(10):3169-75.

- 54. Kuepper MK, Bütow M, Herrmann O, Ziemons J, Chatain N, Maurer A, et al. Stem cell persistence in CML is mediated by extrinsically activated JAK1-STAT3 signaling. Leukemia. 2019;33(8):1964-77.
- 55. Vakana E, Altman JK, Glaser H, Donato NJ, Platanias LC. Antileukemic effects of AMPK activators on BCR-ABL–expressing cells. Blood. 2011;118(24):6399-402.
- 56. Bernardin-Fried F, Kummalue T, Leijen S, Collector MI, Ravid K, Friedman AD. AML1/RUNX1 increases during G1 to S cell cycle progression independent of cytokine-dependent phosphorylation and induces cyclin D3 gene expression. J Biol Chem. 2004;279(15):15678-87.
- 57. Leslie K, Lang C, Devgan G, Azare J, Berishaj M, Gerald W, et al. Cyclin D1 is transcriptionally regulated by and required for transformation by activated signal transducer and activator of transcription 3. Cancer Res. 2006;66(5):2544-52.
- 58. Bhattacharya S, Ray RM, Johnson LR. STAT3-mediated transcription of Bcl-2, Mcl-1 and c-IAP2 prevents apoptosis in polyamine-depleted cells. Biochem J. 2005;392(Pt 2):335-44.
- 59. Redell MS, Ruiz MJ, Alonzo TA, Gerbing RB, Tweardy DJ. Stat3 signaling in acute myeloid leukemia: ligand-dependent and -independent activation and induction of apoptosis by a novel small-molecule Stat3 inhibitor. Blood. 2011;117(21):5701-9.
- 60. Al-Jamal HA, Jusoh SA, Yong AC, Asan JM, Hassan R, Johan MF. Silencing of suppressor of cytokine signaling-3 due to methylation results in phosphorylation of STAT3 in imatinib resistant BCR-ABL positive chronic myeloid leukemia cells. Asian Pac J Cancer Prev. 2014;15(11):4555-61.
- 61. Sawyers CL, Hochhaus A, Feldman E, Goldman JM, Miller CB, Ottmann OG, et al. Imatinib induces hematologic and cytogenetic responses in patients with chronic myelogenous leukemia in myeloid blast crisis: results of a phase II study. Blood. 2002;99(10):3530-9.
- 62. Deininger M, Buchdunger E, Druker BJ. The development of imatinib as a therapeutic agent for chronic myeloid leukemia. Blood. 2005;105(7):2640-53.
- 63. Sacha T, Hochhaus A, Hanfstein B, Muller MC, Rudzki Z, Czopek J, et al. ABL-kinase domain point mutation as a cause of imatinib (STI571) resistance in CML patient who progress to myeloid blast crisis. Leuk Res. 2003;27(12):1163-6.

- 64. Swords R, Quinn J, Fay M, O'Donnell R, Goldman J, Murphy PT. CML clonal evolution with resistance to single agent imatinib therapy. Clin Lab Haematol. 2005;27(5):347-9.
- 65. Mohamed AN, Pemberton P, Zonder J, Schiffer CA. The effect of imatinib mesylate on patients with Philadelphia chromosome-positive chronic myeloid leukemia with secondary chromosomal aberrations. Clin Cancer Res. 2003;9(4):1333-7.
- 66. Bavaro L, Martelli M, Cavo M, Soverini S. Mechanisms of Disease Progression and Resistance to Tyrosine Kinase Inhibitor Therapy in Chronic Myeloid Leukemia: An Update. Int J Mol Sci. 2019;20(24):6141.
- 67. Coppo P, Flamant S, De Mas V, Jarrier P, Guillier M, Bonnet ML, et al. BCR-ABL activates STAT3 via JAK and MEK pathways in human cells. Br J Haematol. 2006;134(2):171-9.
- 68. Samanta AK, Lin H, Sun T, Kantarjian H, Arlinghaus RB. Janus kinase 2: a critical target in chronic myelogenous leukemia. Cancer Res. 2006;66(13):6468-72.
- 69. Awidi A, Ababneh N, Magablah A, Bsoul N, Mefleh R, Marei L, et al. ABL kinase domain mutations in patients with chronic myeloid leukemia in Jordan. Genet Test Mol Biomarkers. 2012;16(11):1317-21.
- 70. Kamal A, Thao L, Sensintaffar J, Zhang L, Boehm MF, Fritz LC, et al. A high-affinity conformation of Hsp90 confers tumour selectivity on Hsp90 inhibitors. Nature. 2003;425(6956):407-10.
- 71. An WG, Schulte TW, Neckers LM. The heat shock protein 90 antagonist geldanamycin alters chaperone association with p210bcr-abl and v-src proteins before their degradation by the proteasome. Cell Growth Differ. 2000;11(7):355-60.
- 72. Peng C, Brain J, Hu Y, Goodrich A, Kong L, Grayzel D, et al. Inhibition of heat shock protein 90 prolongs survival of mice with BCR-ABL-T315I–induced leukemia and suppresses leukemic stem cells. Blood. 2007;110(2):678-85.
- 73. Jhaveri K, Modi S. Ganetespib: research and clinical development. Onco Targets Ther. 2015;8:1849-58.
- 74. Banerji U, O'Donnell A, Scurr M, Pacey S, Stapleton S, Asad Y, et al. Phase I pharmacokinetic and pharmacodynamic study of 17-allylamino, 17-demethoxygeldanamycin in patients with advanced malignancies. J Clin Oncol. 2005;23(18):4152-61.

- 75. Samarasinghe B, Wales CT, Taylor FR, Jacobs AT. Heat shock factor 1 confers resistance to Hsp90 inhibitors through p62/SQSTM1 expression and promotion of autophagic flux. Biochem Pharmacol. 2014;87(3):445-55.
- 76. Kijima T, Prince TL, Tigue ML, Yim KH, Schwartz H, Beebe K, et al. HSP90 inhibitors disrupt a transient HSP90-HSF1 interaction and identify a noncanonical model of HSP90-mediated HSF1 regulation. Scientific Reports. 2018;8(1):6976.
- 77. Mendillo ML, Santagata S, Koeva M, Bell GW, Hu R, Tamimi RM, et al. HSF1 drives a transcriptional program distinct from heat shock to support highly malignant human cancers. Cell. 2012;150(3):549-62.
- 78. Arolla RG, Malladi S, Bhaduri U, Gayatri MB, Pattamshetty P, Mohan V, et al. Analysis of cellular models of clonal evolution reveals co-evolution of imatinib and HSP90 inhibitor resistances. Biochemical and Biophysical Research Communications. 2021;534:461-7.
- 79. Shi R, Lin J, Gong Y, Yan T, Shi F, Yang X, et al. The antileukemia effect of metformin in the Philadelphia chromosome-positive leukemia cell line and patient primary leukemia cell. Anticancer Drugs. 2015;26(9):913-22.
- 80. Biondani G, Peyron J-F. Metformin, an Anti-diabetic Drug to Target Leukemia. Frontiers in Endocrinology. 2018;9(446).
- 81. Liu S, Yang J, Sun G, Zhang Y, Cheng C, Xu J, et al. RUNX1 Upregulates CENPE to Promote Leukemic Cell Proliferation. Frontiers in Molecular Biosciences. 2021;8(767).
- 82. Krakowiak J, Zheng X, Patel N, Feder ZA, Anandhakumar J, Valerius K, et al. Hsf1 and Hsp70 constitute a two-component feedback loop that regulates the yeast heat shock response. Elife. 2018;7:e31668.
- 83. Dai S, Tang Z, Cao J, Zhou W, Li H, Sampson S, et al. Suppression of the HSF1-mediated proteotoxic stress response by the metabolic stress sensor AMPK. The EMBO Journal. 2015;34(3):275-93.
- 84. Blagosklonny MV, Fojo T, Bhalla KN, Kim JS, Trepel JB, Figg WD, et al. The Hsp90 inhibitor geldanamycin selectively sensitizes Bcr-Abl-expressing leukemia cells to cytotoxic chemotherapy. Leukemia. 2001;15(10):1537-43.
- 85. Khajapeer KV, Baskaran R. Hsp90 Inhibitors for the Treatment of Chronic Myeloid Leukemia. Leuk Res Treatment. 2015;2015:757694-.

- 86. Mahon FX, Belloc F, Lagarde V, Chollet C, Moreau-Gaudry F, Reiffers J, et al. MDR1 gene overexpression confers resistance to imatinib mesylate in leukemia cell line models. Blood. 2003;101(6):2368-73.
- 87. O'Callaghan-Sunol C, Gabai VL, Sherman MY. Hsp27 modulates p53 signaling and suppresses cellular senescence. Cancer Res. 2007;67(24):11779-88.
- 88. Khaleque MA, Bharti A, Sawyer D, Gong J, Benjamin IJ, Stevenson MA, et al. Induction of heat shock proteins by heregulin beta1 leads to protection from apoptosis and anchorage-independent growth. Oncogene. 2005;24(43):6564-73.
- 89. Mambula SS, Calderwood SK. Heat shock protein 70 is secreted from tumor cells by a nonclassical pathway involving lysosomal endosomes. J Immunol. 2006;177(11):7849-57.
- 90. Ciocca DR, Arrigo AP, Calderwood SK. Heat shock proteins and heat shock factor 1 in carcinogenesis and tumor development: an update. Arch Toxicol. 2013;87(1):19-48.
- 91. Nimmanapalli R, O'Bryan E, Bhalla K. Geldanamycin and Its Analogue 17-Allylamino-17-demethoxygeldanamycin Lowers Bcr-Abl Levels and Induces Apoptosis and Differentiation of Bcr-Abl-positive Human Leukemic Blasts. Cancer Research. 2001;61(5):1799-804.
- 92. McCollum AK, TenEyck CJ, Stensgard B, Morlan BW, Ballman KV, Jenkins RB, et al. P-Glycoprotein-mediated resistance to Hsp90-directed therapy is eclipsed by the heat shock response. Cancer Res. 2008;68(18):7419-27.
- 93. Thomas J, Wang L, Clark RE, Pirmohamed M. Active transport of imatinib into and out of cells: implications for drug resistance. Blood. 2004;104(12):3739-45.
- 94. Harrach S, Schmidt-Lauber C, Pap T, Pavenstadt H, Schlatter E, Schmidt E, et al. MATE1 regulates cellular uptake and sensitivity to imatinib in CML patients. Blood Cancer J. 2016;6:e470.
- 95. Kimura N, Okuda M, Inui K. Metformin transport by renal basolateral organic cation transporter hOCT2. Pharm Res. 2005;22(2):255-9.
- 96. Umehara KI, Iwatsubo T, Noguchi K, Kamimura H. Functional involvement of organic cation transporter1 (OCT1/Oct1) in the hepatic uptake of organic cations in humans and rats. Xenobiotica. 2007;37(8):818-31.

- 97. Li J, Yang Z, Tuo B. Role of OCT1 in hepatocellular carcinoma. Onco Targets Ther. 2019;12:6013-22.
- 98. Christensen MM, Pedersen RS, Stage TB, Brasch-Andersen C, Nielsen F, Damkier P, et al. A gene-gene interaction between polymorphisms in the OCT2 and MATE1 genes influences the renal clearance of metformin. Pharmacogenet Genomics. 2013;23(10):526-34.
- 99. Nair RR, Tolentino JH, Hazlehurst LA. Role of STAT3 in Transformation and Drug Resistance in CML. Front Oncol. 2012;2:30.
- 100. Adnan Awad S, Dufva O, Ianevski A, Ghimire B, Koski J, Maliniemi P, et al. RUNX1 mutations in blast-phase chronic myeloid leukemia associate with distinct phenotypes, transcriptional profiles, and drug responses. Leukemia. 2020.
- 101. Zhao LJ, Wang YY, Li G, Ma LY, Xiong SM, Weng XQ, et al. Functional features of RUNX1 mutants in acute transformation of chronic myeloid leukemia and their contribution to inducing murine full-blown leukemia. Blood. 2012;119(12):2873-82.
- 102. Corey SJ, Minden MD, Barber DL, Kantarjian H, Wang JC, Schimmer AD. Myelodysplastic syndromes: the complexity of stem-cell diseases. Nat Rev Cancer. 2007;7(2):118-29.
- 103. Tefferi A, Vardiman JW. Myelodysplastic syndromes. N Engl J Med. 2009;361(19):1872-85.
- 104. Vundinti BR, Kerketta L, Jijina F, Ghosh K. Cytogenetic study of myelodysplastic syndrome from India. Indian J Med Res. 2009;130(2):155-9.
- 105. Chen J, Kao YR, Sun D, Todorova TI, Reynolds D, Narayanagari SR, et al. Myelodysplastic syndrome progression to acute myeloid leukemia at the stem cell level. Nat Med. 2019;25(1):103-10.
- 106. Haase D, Germing U, Schanz J, Pfeilstöcker M, Nösslinger T, Hildebrandt B, et al. New insights into the prognostic impact of the karyotype in MDS and correlation with subtypes: evidence from a core dataset of 2124 patients. Blood. 2007;110(13):4385-95.
- 107. Gupta R, Soupir CP, Johari V, Hasserjian RP. Myelodysplastic syndrome with isolated deletion of chromosome 20q: an indolent disease with minimal morphological dysplasia and frequent thrombocytopenic presentation. Br J Haematol. 2007;139(2):265-8.

- 108. Keung YK, Beaty M, Powell BL, Molnar I, Buss D, Pettenati M. Philadelphia chromosome positive myelodysplastic syndrome and acute myeloid leukemia-retrospective study and review of literature. Leuk Res. 2004;28(6):579-86.
- 109. Katalinic D. De Novo Philadelphia Chromosome (BCR/ABL1) Positive Myelodysplastic Syndrome: Is it a Distinct Molecular and Clinical Entity? Indian J Hematol Blood Transfus. 2018;34(2):365-7.
- 110. Chelapareddy LR, Sen S. Philadelphia Translocation in MDS: A Case Report and a Brief Review of the Literature Looking at Its Prevalence, Disease Progression, and Treatment Options. Case Rep Hematol. 2018;2018:5865321-.
- 111. Park SJ, Lee HW, Jeong SH, Park JS, Kim HC, Seok JY, et al. Acquisition of a BCR-ABL1 transcript in a patient with disease progression from MDS with fibrosis to AML with myelodysplasia-related changes. Ann Clin Lab Sci. 2011;41(4):379-84.
- 112. Gill H, Leung AYH, Kwong Y-L. Molecular and Cellular Mechanisms of Myelodysplastic Syndrome: Implications on Targeted Therapy. Int J Mol Sci. 2016;17(4):440-
- 113. Zöchbauer S, Gsur A, Götzl M, Wallner J, Lechner K, Pirker R. MDR1 gene expression in myelodysplastic syndrome and in acute myeloid leukemia evolving from myelodysplastic syndrome. Anticancer Res. 1994;14(3b):1293-5.
- 114. Wood EM, McQuilten ZK. Outpatient transfusions for myelodysplastic syndromes. Hematology. 2020;2020(1):167-74.
- 115. Hayashi Y, Zhang Y, Yokota A, Yan X, Liu J, Choi K, et al. Pathobiological Pseudohypoxia as a Putative Mechanism Underlying Myelodysplastic Syndromes. Cancer Discovery. 2018;8(11):1438-57.
- 116. Zhao S, Guo J, Zhao Y, Fei C, Zheng Q, Li X, et al. Chidamide, a novel histone deacetylase inhibitor, inhibits the viability of MDS and AML cells by suppressing JAK2/STAT3 signaling. Am J Transl Res. 2016;8(7):3169-78.
- 117. Lee SH, Bae SC, Kim KW, Lee YM. RUNX3 inhibits hypoxia-inducible factor- $1\alpha$  protein stability by interacting with prolyl hydroxylases in gastric cancer cells. Oncogene. 2014;33(11):1458-67.

- 118. Labazi M, Lamoke F, Marcus DM, Caldwell RB, Bartoli M. Stat3-dependent Hif-1alpha Activation in Hypoxic Retinal Endothelial Cells. Investigative Ophthalmology & Visual Science. 2009;50(13):2942-.
- 119. Zhao F, Mancuso A, Bui TV, Tong X, Gruber JJ, Swider CR, et al. Imatinib resistance associated with BCR-ABL upregulation is dependent on HIF-1alpha-induced metabolic reprograming. Oncogene. 2010;29(20):2962-72.
- 120. Chen J, Ding Z, Peng Y, Pan F, Li J, Zou L, et al. HIF-1α inhibition reverses multidrug resistance in colon cancer cells via downregulation of MDR1/P-glycoprotein. PLoS One. 2014;9(6):e98882.
- 121. Siegel RL, Miller KD, Jemal A. Cancer statistics, 2020. CA: A Cancer Journal for Clinicians. 2020;70(1):7-30.
- 122. Barnes GL, Javed A, Waller SM, Kamal MH, Hebert KE, Hassan MQ, et al. Osteoblast-related Transcription Factors Runx2 (Cbfa1/AML3) and MSX2 Mediate the Expression of Bone Sialoprotein in Human Metastatic Breast Cancer Cells. Cancer Research. 2003;63(10):2631-7.
- 123. Nagaraja GM, Othman M, Fox BP, Alsaber R, Pellegrino CM, Zeng Y, et al. Gene expression signatures and biomarkers of noninvasive and invasive breast cancer cells: comprehensive profiles by representational difference analysis, microarrays and proteomics. Oncogene. 2006;25(16):2328-38.
- 124. Wysokinski D, Blasiak J, Pawlowska E. Role of RUNX2 in Breast Carcinogenesis. Int J Mol Sci. 2015;16(9):20969-93.
- 125. Reufsteck C, Lifshitz-Shovali R, Zepp M, Bauerle T, Kubler D, Golomb G, et al. Silencing of skeletal metastasis-associated genes impairs migration of breast cancer cells and reduces osteolytic bone lesions. Clin Exp Metastasis. 2012;29(5):441-56.
- 126. Ribeiro N, Sousa SR, Brekken RA, Monteiro FJ. Role of SPARC in bone remodeling and cancer-related bone metastasis. J Cell Biochem. 2014;115(1):17-26.
- 127. Sugimoto H, Nakamura M, Yoda H, Hiraoka K, Shinohara K, Sang M, et al. Silencing of RUNX2 enhances gemcitabine sensitivity of p53-deficient human pancreatic cancer AsPC-1 cells through the stimulation of TAp63-mediated cell death. Cell Death Discov. 2015;1:15010.

- 128. Bellahcène A, Bachelier R, Detry C, Lidereau R, Clézardin P, Castronovo V. Transcriptome analysis reveals an osteoblast-like phenotype for human osteotropic breast cancer cells. Breast Cancer Res Treat. 2007;101(2):135-48.
- 129. Kozlow W, Guise TA. Breast cancer metastasis to bone: mechanisms of osteolysis and implications for therapy. J Mammary Gland Biol Neoplasia. 2005;10(2):169-80.
- 130. Green AS, Chapuis N, Maciel TT, Willems L, Lambert M, Arnoult C, et al. The LKB1/AMPK signaling pathway has tumor suppressor activity in acute myeloid leukemia through the repression of mTOR-dependent oncogenic mRNA translation. Blood. 2010;116(20):4262-73.
- 131. Grzybowska M, Bober J, Olszewska M. [Metformin mechanisms of action and use for the treatment of type 2 diabetes mellitus]. Postepy Hig Med Dosw (Online). 2011;65:277-85.
- 132. Ben Sahra I, Laurent K, Giuliano S, Larbret F, Ponzio G, Gounon P, et al. Targeting cancer cell metabolism: the combination of metformin and 2-deoxyglucose induces p53-dependent apoptosis in prostate cancer cells. Cancer Res. 2010;70(6):2465-75.
- 133. Gu JJ, Zhang Q, Mavis C, Czuczman MS, Hernandez-Ilizaliturri FJ. Metformin Induces p53-Dependent Mitochondrial Stress in Therapy-Sensitive and -Resistant Lymphoma Pre-Clinical Model and Primary Patients Sample with B-Cell Non-Hodgkin Lymphoma (NHL). Blood. 2015;126(23):4008-.
- 134. Cazzaniga M, DeCensi A, Pruneri G, Puntoni M, Bottiglieri L, Varricchio C, et al. The effect of metformin on apoptosis in a breast cancer presurgical trial. Br J Cancer. 2013;109(11):2792-7.
- 135. Nanni O, Amadori D, De Censi A, Rocca A, Freschi A, Bologna A, et al. Metformin plus chemotherapy versus chemotherapy alone in the first-line treatment of HER2-negative metastatic breast cancer. The MYME randomized, phase 2 clinical trial. Breast Cancer Res Treat. 2019;174(2):433-42.
- 136. Chava S, Chennakesavulu S, Gayatri BM, Reddy ABM. A novel phosphorylation by AMP-activated kinase regulates RUNX2 from ubiquitination in osteogenesis over adipogenesis. Cell Death & Disease. 2018;9(7):754.

- 137. Tan C-C, Li G-X, Tan L-D, Du X, Li X-Q, He R, et al. Breast cancer cells obtain an osteomimetic feature via epithelial-mesenchymal transition that have undergone BMP2/RUNX2 signaling pathway induction. Oncotarget. 2016;7(48):79688-705.
- 138. Tandon M, Chen Z, Pratap J. Runx2 activates PI3K/Akt signaling via mTORC2 regulation in invasive breast cancer cells. Breast Cancer Res. 2014;16(1):R16-R.
- 139. Kwon TG, Zhao X, Yang Q, Li Y, Ge C, Zhao G, et al. Physical and functional interactions between Runx2 and HIF-1α induce vascular endothelial growth factor gene expression. J Cell Biochem. 2011;112(12):3582-93.
- 140. Pratap J, Javed A, Languino LR, van Wijnen AJ, Stein JL, Stein GS, et al. The Runx2 osteogenic transcription factor regulates matrix metalloproteinase 9 in bone metastatic cancer cells and controls cell invasion. Mol Cell Biol. 2005;25(19):8581-91.
- 141. Tandon M, Chen Z, Pratap J. Runx2 activates PI3K/Akt signaling via mTORC2 regulation in invasive breast cancer cells. Breast Cancer Res. 2014;16(1):R16.
- 142. Kugimiya F, Kawaguchi H, Ohba S, Kawamura N, Hirata M, Chikuda H, et al. GSK-3beta controls osteogenesis through regulating Runx2 activity. PLoS One. 2007;2(9):e837.
- 143. Kennecke H, Yerushalmi R, Woods R, Cheang MC, Voduc D, Speers CH, et al. Metastatic behavior of breast cancer subtypes. J Clin Oncol. 2010;28(20):3271-7.
- 144. Scimeca M, Urbano N, Bonfiglio R, Schillaci O, Bonanno E. Breast osteoblast-like cells: a new biomarker for the management of breast cancer. British Journal of Cancer. 2018;119(9):1129-32.
- 145. Meads MB, Hazlehurst LA, Dalton WS. The Bone Marrow Microenvironment as a Tumor Sanctuary and Contributor to Drug Resistance. 2008;14(9):2519-26.
- 146. Chae YK, Arya A, Malecek MK, Shin DS, Carneiro B, Chandra S, et al. Repurposing metformin for cancer treatment: current clinical studies. Oncotarget. 2016;7(26):40767-80.
- 147. Chimge N-O, Baniwal SK, Little GH, Chen Y-b, Kahn M, Tripathy D, et al. Regulation of breast cancer metastasis by Runx2 and estrogen signaling: the role of SNAI2. Breast Cancer Research. 2011;13(6):R127.
- 148. Morrison Joly M, Williams MM, Hicks DJ, Jones B, Sanchez V, Young CD, et al. Two distinct mTORC2-dependent pathways converge on Rac1 to drive breast cancer metastasis. Breast Cancer Research. 2017;19(1):74.

- 149. Tamura D, Hiraga T, Myoui A, Yoshikawa H, Yoneda T. Cadherin-11-mediated interactions with bone marrow stromal/osteoblastic cells support selective colonization of breast cancer cells in bone. Int J Oncol. 2008;33(1):17-24.
- 150. Tse JC, Kalluri R. Mechanisms of metastasis: epithelial-to-mesenchymal transition and contribution of tumor microenvironment. J Cell Biochem. 2007;101(4):816-29.
- 151. Burridge K, Guilluy C. Focal adhesions, stress fibers and mechanical tension. Exp Cell Res. 2016;343(1):14-20.
- 152. Alkabban FM, Ferguson T. Breast Cancer. StatPearls. Treasure Island (FL)2021.
- 153. Tahara RK, Brewer TM, Theriault RL, Ueno NT. Bone Metastasis of Breast Cancer. Adv Exp Med Biol. 2019;1152:105-29.
- 154. De A, Kuppusamy G. Metformin in breast cancer: preclinical and clinical evidence. Curr Probl Cancer. 2020;44(1):100488.
- 155. Howell JJ, Hellberg K, Turner M, Talbott G, Kolar MJ, Ross DS, et al. Metformin Inhibits Hepatic mTORC1 Signaling via Dose-Dependent Mechanisms Involving AMPK and the TSC Complex. Cell Metab. 2017;25(2):463-71.
- 156. Wang Q, Yu W, Huang T, Zhu Y, Huang C. RUNX2 promotes hepatocellular carcinoma cell migration and invasion by upregulating MMP9 expression. Oncol Rep. 2016;36(5):2777-84.
- 157. Kwon T-G, Zhao X, Yang Q, Li Y, Ge C, Zhao G, et al. Physical and functional interactions between Runx2 and HIF-1α induce vascular endothelial growth factor gene expression. J Cell Biochem. 2011;112(12):3582-93.
- 158. Li Q, Zhao H, Xia S, Wei H, Chen F, Jin P. RUNX2 promotes epithelial differentiation of ADSCs and burn wound healing via targeting E-cadherin. Oncotarget. 2017;9(2):2646-59.
- 159. Ciaraldi TP, Oh DK, Christiansen L, Nikoulina SE, Kong AP, Baxi S, et al. Tissue-specific expression and regulation of GSK-3 in human skeletal muscle and adipose tissue. Am J Physiol Endocrinol Metab. 2006;291(5):E891-8.
- 160. Samanta D, Semenza GL. Metabolic adaptation of cancer and immune cells mediated by hypoxia-inducible factors. Biochim Biophys Acta Rev Cancer. 2018;1870(1):15-22.
- 161. Ganapathy V, Thangaraju M, Prasad PD. Nutrient transporters in cancer: relevance to Warburg hypothesis and beyond. Pharmacol Ther. 2009;121(1):29-40.

- 162. Gladden LB. Lactate as a key metabolic intermediate in cancer. Ann Transl Med. 2019;7(10):210.
- 163. Klawitter J, Kominsky DJ, Brown JL, Klawitter J, Christians U, Leibfritz D, et al. Metabolic characteristics of imatinib resistance in chronic myeloid leukaemia cells. Br J Pharmacol. 2009;158(2):588-600.
- 164. Morland C, Lauritzen KH, Puchades M, Holm-Hansen S, Andersson K, Gjedde A, et al. The lactate receptor, G-protein-coupled receptor 81/hydroxycarboxylic acid receptor 1: Expression and action in brain. J Neurosci Res. 2015;93(7):1045-55.
- 165. Yu M, Yongzhi H, Chen S, Luo X, Lin Y, Zhou Y, et al. The prognostic value of GLUT1 in cancers: a systematic review and meta-analysis. Oncotarget. 2017;8(26):43356-67.
- 166. Wu J, Hu L, Wu F, Zou L, He T. Poor prognosis of hexokinase 2 overexpression in solid tumors of digestive system: a meta-analysis. Oncotarget. 2017;8(19):32332-44.
- 167. Mathupala SP, Ko YH, Pedersen PL. Hexokinase II: cancer's double-edged sword acting as both facilitator and gatekeeper of malignancy when bound to mitochondria. Oncogene. 2006;25(34):4777-86.
- 168. Annibaldi A, Widmann C. Glucose metabolism in cancer cells. Curr Opin Clin Nutr Metab Care. 2010;13(4):466-70.
- 169. Yuan F, Cheng C, Xiao F, Liu H, Cao S, Zhou G. Inhibition of mTORC1/P70S6K pathway by Metformin synergistically sensitizes Acute Myeloid Leukemia to Ara-C. Life Sciences. 2020;243:117276.
- 170. Biondani G, Peyron JF. Metformin, an Anti-diabetic Drug to Target Leukemia. Front Endocrinol (Lausanne). 2018;9:446.
- 171. Gayatri MB, Gajula NN, Chava S, Reddy ABM. High glutamine suppresses osteogenesis through mTORC1-mediated inhibition of the mTORC2/AKT-473/RUNX2 axis. Cell Death Discovery. 2022;8(1):277.
- 172. Petersen C, Nielsen MD, Andersen ES, Basse AL, Isidor MS, Markussen LK, et al. MCT1 and MCT4 Expression and Lactate Flux Activity Increase During White and Brown Adipogenesis and Impact Adipocyte Metabolism. Scientific Reports. 2017;7(1):13101.

- 173. Lopes-Coelho F, Nunes C, Gouveia-Fernandes S, Rosas R, Silva F, Gameiro P, et al. Monocarboxylate transporter 1 (MCT1), a tool to stratify acute myeloid leukemia (AML) patients and a vehicle to kill cancer cells. Oncotarget. 2017;8(47):82803-23.
- 174. Allen E, Mieville P, Warren CM, Saghafinia S, Li L, Peng MW, et al. Metabolic Symbiosis Enables Adaptive Resistance to Anti-angiogenic Therapy that Is Dependent on mTOR Signaling. Cell Rep. 2016;15(6):1144-60.
- 175. Gwinn DM, Shackelford DB, Egan DF, Mihaylova MM, Mery A, Vasquez DS, et al. AMPK phosphorylation of raptor mediates a metabolic checkpoint. Mol Cell. 2008;30(2):214-26.
- 176. Dodd KM, Yang J, Shen MH, Sampson JR, Tee AR. mTORC1 drives HIF-1α and VEGF-A signalling via multiple mechanisms involving 4E-BP1, S6K1 and STAT3. Oncogene. 2015;34(17):2239-50.
- 177. Kominsky DJ, Klawitter J, Brown JL, Boros LG, Melo JV, Eckhardt SG, et al. Abnormalities in Glucose Uptake and Metabolism in Imatinib-Resistant Human BCR-ABL-Positive Cells. Clinical Cancer Research. 2009;15(10):3442-50.
- 178. Zanke BW, Lee C, Arab S, Tannock IF. Death of tumor cells after intracellular acidification is dependent on stress-activated protein kinases (SAPK/JNK) pathway activation and cannot be inhibited by Bcl-2 expression or interleukin 1beta-converting enzyme inhibition. Cancer Res. 1998;58(13):2801-8.
- 179. Pérez-Escuredo J, Van Hée VF, Sboarina M, Falces J, Payen VL, Pellerin L, et al. Monocarboxylate transporters in the brain and in cancer. Biochim Biophys Acta. 2016;1863(10):2481-97.
- 180. Payen VL, Mina E, Van Hée VF, Porporato PE, Sonveaux P. Monocarboxylate transporters in cancer. Molecular Metabolism. 2020;33:48-66.
- 181. Sun Z, Han Y, Song S, Chen T, Han Y, Liu Y. Activation of GPR81 by lactate inhibits oscillatory shear stress-induced endothelial inflammation by activating the expression of KLF2. IUBMB Life. 2019;71(12):2010-9.
- 182. Brooks GA. The Science and Translation of Lactate Shuttle Theory. Cell Metabolism. 2018;27(4):757-85.
- 183. Lee J, Park D, Lee Y. Metformin Synergistically Potentiates the Antitumor Effects of Imatinib in Colorectal Cancer Cells. Dev Reprod. 2017;21(2):139-50.

- 184. Populo H, Lopes JM, Soares P. The mTOR signalling pathway in human cancer. Int J Mol Sci. 2012;13(2):1886-918.
- 185. Nalwoga H, Ahmed L, Arnes JB, Wabinga H, Akslen LA. Strong Expression of Hypoxia-Inducible Factor-1alpha (HIF-1alpha) Is Associated with Axl Expression and Features of Aggressive Tumors in African Breast Cancer. PLoS One. 2016;11(1):e0146823.
- 186. Song K, Xu X-J, Xuan L, Huang G-N, Song X-L, Liu Q-F. HIF-1α and GLUT1 Gene Expression is Associated with Chemoresistance of Acute Myeloid Leukemia. Asian Pacific journal of cancer prevention : APJCP. 2014;15:1823-9.
- 187. Semenza G. Signal transduction to hypoxia-inducible factor 1. Biochem Pharmacol. 2002;64(5-6):993-8.
- 188. Doronzo G, Russo I, Mattiello L, Riganti C, Anfossi G, Trovati M. Insulin activates hypoxia-inducible factor-1alpha in human and rat vascular smooth muscle cells via phosphatidylinositol-3 kinase and mitogen-activated protein kinase pathways: impairment in insulin resistance owing to defects in insulin signalling. Diabetologia. 2006;49(5):1049-63.
- 189. Fukuda R, Hirota K, Fan F, Jung YD, Ellis LM, Semenza GL. Insulin-like growth factor 1 induces hypoxia-inducible factor 1-mediated vascular endothelial growth factor expression, which is dependent on MAP kinase and phosphatidylinositol 3-kinase signaling in colon cancer cells. J Biol Chem. 2002;277(41):38205-11.
- 190. Kaelin WG, Ratcliffe PJ. Oxygen Sensing by Metazoans: The Central Role of the HIF Hydroxylase Pathway. Molecular Cell. 2008;30(4):393-402.
- 191. Choy MK, Movassagh M, Bennett MR, Foo RS. PKB/Akt activation inhibits p53-mediated HIF1A degradation that is independent of MDM2. J Cell Physiol. 2010;222(3):635-9.
- 192. Jung SN, Yang WK, Kim J, Kim HS, Kim EJ, Yun H, et al. Reactive oxygen species stabilize hypoxia-inducible factor-1 alpha protein and stimulate transcriptional activity via AMP-activated protein kinase in DU145 human prostate cancer cells. Carcinogenesis. 2008;29(4):713-21.
- 193. Lee JO, Lee SK, Kim JH, Kim N, You GY, Moon JW, et al. Metformin regulates glucose transporter 4 (GLUT4) translocation through AMP-activated protein kinase (AMPK)-mediated Cbl/CAP signaling in 3T3-L1 preadipocyte cells. J Biol Chem. 2012;287(53):44121-9.

- 194. Ciaraldi TP, Kong APS, Chu NV, Kim DD, Baxi S, Loviscach M, et al. Regulation of Glucose Transport and Insulin Signaling by Troglitazone or Metformin in Adipose Tissue of Type 2 Diabetic Subjects. Diabetes. 2002;51(1):30-6.
- 195. Mueckler M, Thorens B. The SLC2 (GLUT) family of membrane transporters. Mol Aspects Med. 2013;34(2-3):121-38.
- 196. Wang J, Ye C, Chen C, Xiong H, Xie B, Zhou J, et al. Glucose transporter GLUT1 expression and clinical outcome in solid tumors: a systematic review and meta-analysis. Oncotarget. 2017;8(10):16875-86.
- 197. Tanner LB, Goglia AG, Wei MH, Sehgal T, Parsons LR, Park JO, et al. Four Key Steps Control Glycolytic Flux in Mammalian Cells. Cell Syst. 2018;7(1):49-62 e8.
- 198. Koczula KM, Ludwig C, Hayden R, Cronin L, Pratt G, Parry H, et al. Metabolic plasticity in CLL: adaptation to the hypoxic niche. Leukemia. 2016;30(1):65-73.
- 199. Misbin RI. The Phantom of Lactic Acidosis due to Metformin in Patients With Diabetes. Diabetes Care. 2004;27(7):1791-3.
- 200. Aguiari P, Leo S, Zavan B, Vindigni V, Rimessi A, Bianchi K, et al. High glucose induces adipogenic differentiation of muscle-derived stem cells. Proc Natl Acad Sci U S A. 2008;105(4):1226-31.
- 201. Akin O, Gol K, Akturk M, Erkaya S. Evaluation of bone turnover in postmenopausal patients with type 2 diabetes mellitus using biochemical markers and bone mineral density measurements. Gynecol Endocrinol. 2003;17(1):19-29.
- 202. Rebelato E, Santos LR, Carpinelli AR, Rorsman P, Abdulkader F. Short-term high glucose culture potentiates pancreatic beta cell function. Scientific Reports. 2018;8(1):13061.
- 203. Mary C, Aoife K, Neville HM, Peter RF, Philip N. Glutamine regulates expression of key transcription factor, signal transduction, metabolic gene, and protein expression in a clonal pancreatic β-cell line. Journal of Endocrinology.190(3):719-27.
- 204. Mazur A. Why were "starvation diets" promoted for diabetes in the pre-insulin period? Nutr J. 2011;10:23.
- 205. Howell JJ, Manning BD. mTOR couples cellular nutrient sensing to organismal metabolic homeostasis. Trends Endocrinol Metab. 2011;22(3):94-102.

- 206. Ardestani A, Maedler K. mTORC1 and IRS1: Another Deadly Kiss. Trends in Endocrinology & Metabolism. 2018;29.
- 207. A Negative Feedback Mechanism Regulates mTORC2 Activity. Cancer Discovery. 2014;4(1):16-.
- 208. Liu P, Gan W, Inuzuka H, Lazorchak AS, Gao D, Arojo O, et al. Sin1 phosphorylation impairs mTORC2 complex integrity and inhibits downstream Akt signalling to suppress tumorigenesis. Nature Cell Biology. 2013;15(11):1340-50.
- 209. Wang Y, Huang Y-F, Watford M. Glutamine is required for 3T3 L1 adipocyte differentiation and lipid accumulation. The FASEB Journal. 2007;21(5):A703-A.
- 210. Moloughney JG, Kim PK, Vega-Cotto NM, Wu C-C, Zhang S, Adlam M, et al. mTORC2 Responds to Glutamine Catabolite Levels to Modulate the Hexosamine Biosynthesis Enzyme GFAT1. Molecular Cell. 2016;63(5):811-26.
- 211. Wellen K, Lu C, Mancuso A, Lemons J, Ryczko M, Dennis J, et al. The hexosamine biosynthetic pathway couples growth factor-induced glutamine uptake to glucose metabolism. Genes & development. 2010;24:2784-99.
- 212. Rhee SY, Jung ES, Park HM, Jeong SJ, Kim K, Chon S, et al. Plasma glutamine and glutamic acid are potential biomarkers for predicting diabetic retinopathy. Metabolomics. 2018;14(7):89.
- 213. Menge BA, Schrader H, Ritter PR, Ellrichmann M, Uhl W, Schmidt WE, et al. Selective amino acid deficiency in patients with impaired glucose tolerance and type 2 diabetes. Regul Pept. 2010;160(1-3):75-80.
- 214. Wu X, Zhang Y, Xing Y, Zhao B, Zhou C, Wen Y, et al. High-fat and high-glucose microenvironment decreases Runx2 and TAZ expression and inhibits bone regeneration in the mouse. J Orthop Surg Res. 2019;14(1):55.
- 215. Vila-Bedmar R, Lorenzo M, Fernandez-Veledo S. Adenosine 5'-monophosphate-activated protein kinase-mammalian target of rapamycin cross talk regulates brown adipocyte differentiation. Endocrinology. 2010;151(3):980-92.
- 216. Carnevalli LS, Masuda K, Frigerio F, Le Bacquer O, Um SH, Gandin V, et al. S6K1 plays a critical role in early adipocyte differentiation. Dev Cell. 2010;18(5):763-74.

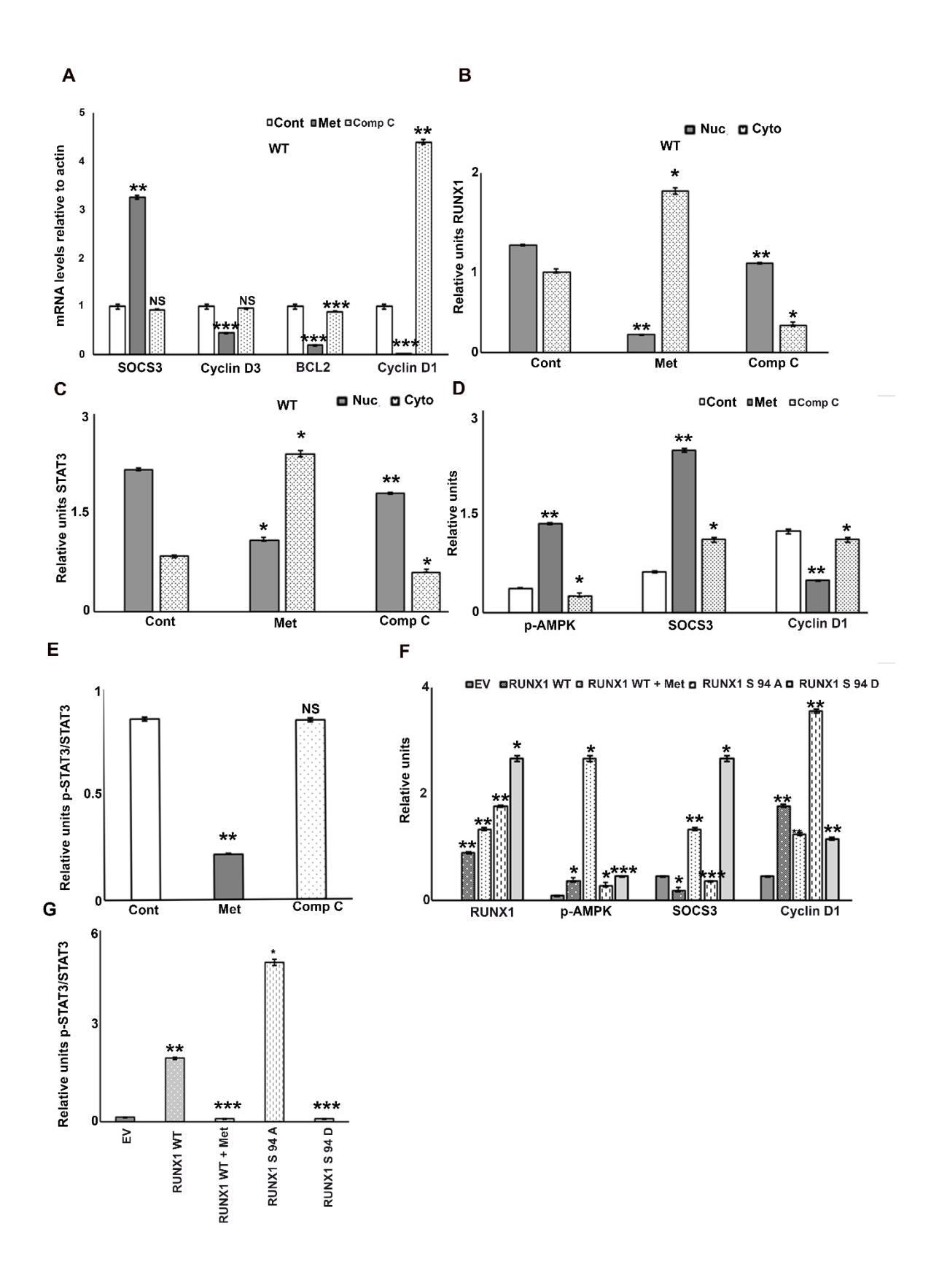
- 217. El-Chaar D, Gagnon A, Sorisky A. Inhibition of insulin signaling and adipogenesis by rapamycin: effect on phosphorylation of p70 S6 kinase vs eIF4E-BP1. Int J Obes Relat Metab Disord. 2004;28(2):191-8.
- 218. Gagnon A, Lau S, Sorisky A. Rapamycin-sensitive phase of 3T3-L1 preadipocyte differentiation after clonal expansion. J Cell Physiol. 2001;189(1):14-22.
- 219. Sen B, Xie Z, Case N, Thompson WR, Uzer G, Styner M, et al. mTORC2 regulates mechanically induced cytoskeletal reorganization and lineage selection in marrow-derived mesenchymal stem cells. J Bone Miner Res. 2014;29(1):78-89.
- 220. Martin SK, Fitter S, Dutta AK, Matthews MP, Walkley CR, Hall MN, et al. Brief Report: The Differential Roles of mTORC1 and mTORC2 in Mesenchymal Stem Cell Differentiation. STEM CELLS. 2015;33(4):1359-65.
- 221. Jackson RM, Griesel BA, Gurley JM, Szweda LI, Olson AL. Glucose availability controls adipogenesis in mouse 3T3-L1 adipocytes via up-regulation of nicotinamide metabolism. Journal of Biological Chemistry. 2017;292(45):18556-64.
- 222. Rosen ED, Sarraf P, Troy AE, Bradwin G, Moore K, Milstone DS, et al. PPARγ Is Required for the Differentiation of Adipose Tissue In Vivo and In Vitro. Molecular Cell. 1999;4(4):611-7.
- 223. James AW. Review of Signaling Pathways Governing MSC Osteogenic and Adipogenic Differentiation. Scientifica (Cairo). 2013;2013:684736.
- 224. Komori T. Regulation of bone development and maintenance by Runx2. Front Biosci. 2008;13:898-903.
- 225. Bernfeld E, Menon D, Vaghela V, Zerin I, Faruque P, Frias MA, et al. Phospholipase D-Dependent mTORC1 Activation by Glutamine. Journal of Biological Chemistry. 2018.
- 226. Shaw E, Talwadekar M, Mohan N, Acharya A, Kolthur-Seetharam U. Anabolic SIRT4 exerts retrograde control over TORC1 signalling by glutamine sparing in the mitochondria. bioRxiv. 2019:635565.
- 227. Li C, Buettger C, Kwagh J, Matter A, Daikhin Y, Nissim IB, et al. A signaling role of glutamine in insulin secretion. J Biol Chem. 2004;279(14):13393-401.

- 228. Chen Q, Shou P, Zheng C, Jiang M, Cao G, Yang Q, et al. Fate decision of mesenchymal stem cells: adipocytes or osteoblasts? Cell Death & Differentiation. 2016;23(7):1128-39.
- 229. Owen OE, Kalhan SC, Hanson RW. The Key Role of Anaplerosis and Cataplerosis for Citric Acid Cycle Function. Journal of Biological Chemistry. 2002;277(34):30409-12.
- 230. Momcilovic M, Lee JT, Braas D, Graeber T, Parlati F, Demo S, et al. B02 The GSK3 Signaling Axis Regulates Adaptive Glutamine Metabolism in Lung Squamous Cell Carcinoma. Journal of Thoracic Oncology. 2020;15:S27.
- 231. Koo J, Wu X, Mao Z, Khuri FR, Sun S-Y. Rictor undergoes GSK3-dependent, FBXW7-mediated ubiquitination and proteasomal degradation. Journal of Biological Chemistry. 2015.
- 232. Guillén C, Benito M. mTORC1 Overactivation as a Key Aging Factor in the Progression to Type 2 Diabetes Mellitus. Frontiers in Endocrinology. 2018;9(621).
- 233. Marchmont RJ, Houslay MD. Insulin triggers cyclic AMP-dependent activation and phosphorylation of a plasma membrane cyclic AMP phosphodiesterase. Nature. 1980;286(5776):904-6.
- 234. Perchellet J-P, Boutwell RK. Effects of 3-Isobutyl-1-methylxanthine and Cyclic Nucleotides on 12-O-Tetradecanoylphorbol-13-acetate-induced Ornithine Decarboxylase Activity in Mouse Epidermis <em>in Vivo</em>. Cancer Research. 1981;41(10):3918-26.
- 235. Baus E, Van Laethem F, Andris F, Rolin S, Urbain J, Leo O. Dexamethasone increases intracellular cyclic AMP concentration in murine T lymphocyte cell lines. Steroids. 2001;66:39-47.
- 236. Kaya F, Belin S, Diamantidis G, Fontes M. Ascorbic acid is a regulator of the intracellular cAMP concentration: Old molecule, new functions? FEBS letters. 2008;582:3614-8.
- 237. Haihua Y, Linghai Y. Targeting cAMP/PKA pathway for glycemic control and type 2 diabetes therapy. Journal of Molecular Endocrinology. 2016;57(2):R93-R108.
- 238. Jiang GJ, Han X, Tao YL, Deng YP, Yu JW, Cai J, et al. Metformin ameliorates insulitis in STZ-induced diabetic mice. PeerJ. 2017;2017.

- 239. Gwinn D, Shackelford D, Egan D, Mihaylova M, Mery A, Vasquez D, et al. AMPK Phosphorylation of Raptor Mediates a Metabolic Checkpoint. Molecular cell. 2008;30:214-26.
- 240. Voss CM, Pajęcka K, Stridh MH, Nissen JD, Schousboe A, Waagepetersen HS. AMPK Activation Affects Glutamate Metabolism in Astrocytes. Neurochemical Research. 2015;40(12):2431-42.
- 241. Lieth E, LaNoue KF, Antonetti DA, Ratz M, The Penn State Retina Research G. Diabetes Reduces Glutamate Oxidation and Glutamine Synthesis in the Retina. Experimental Eye Research. 2000;70(6):723-30.

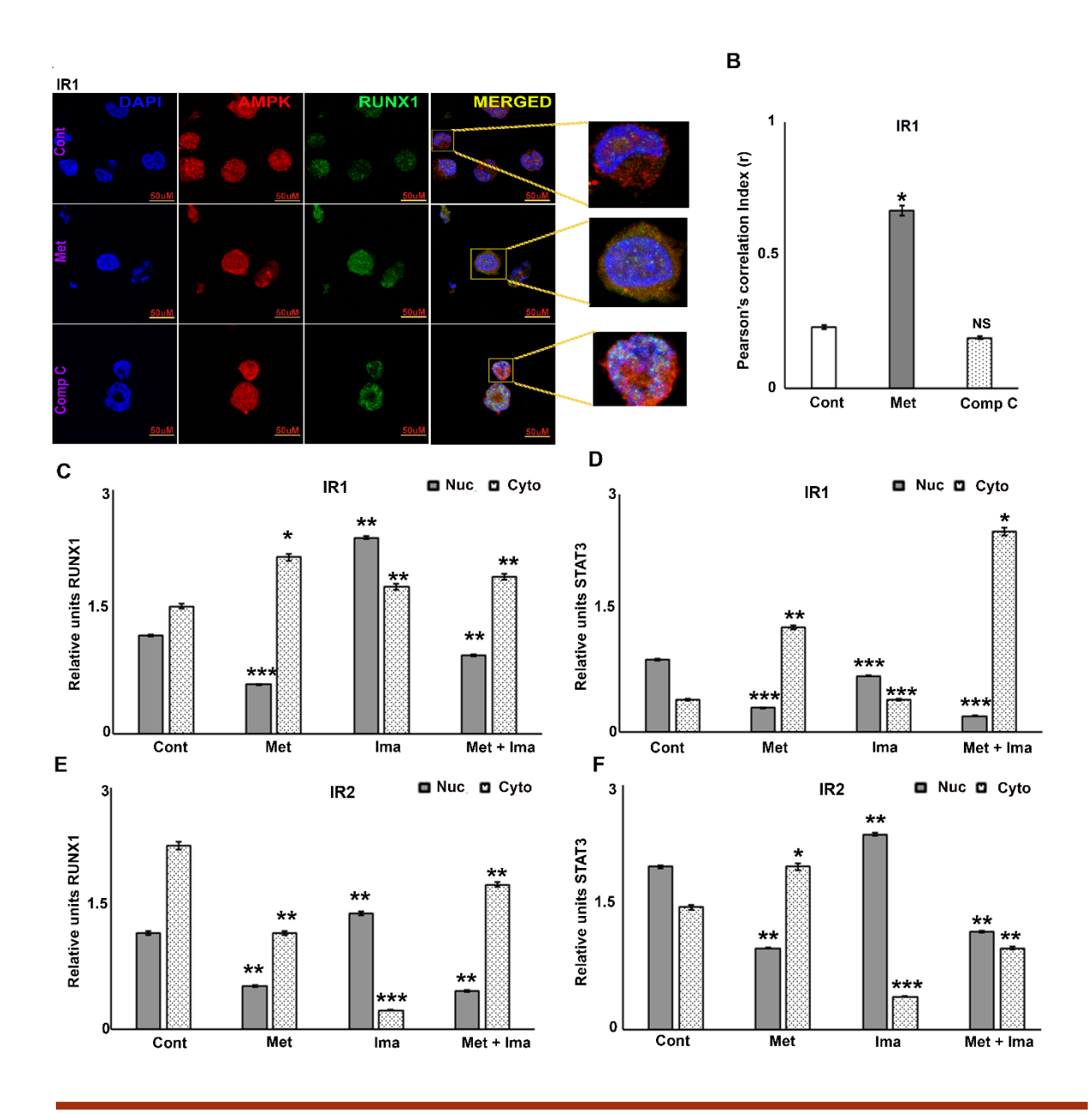
# SUPPLEMENTARY FIGURES

## **SUPPLEMENTARY FIGURES:**



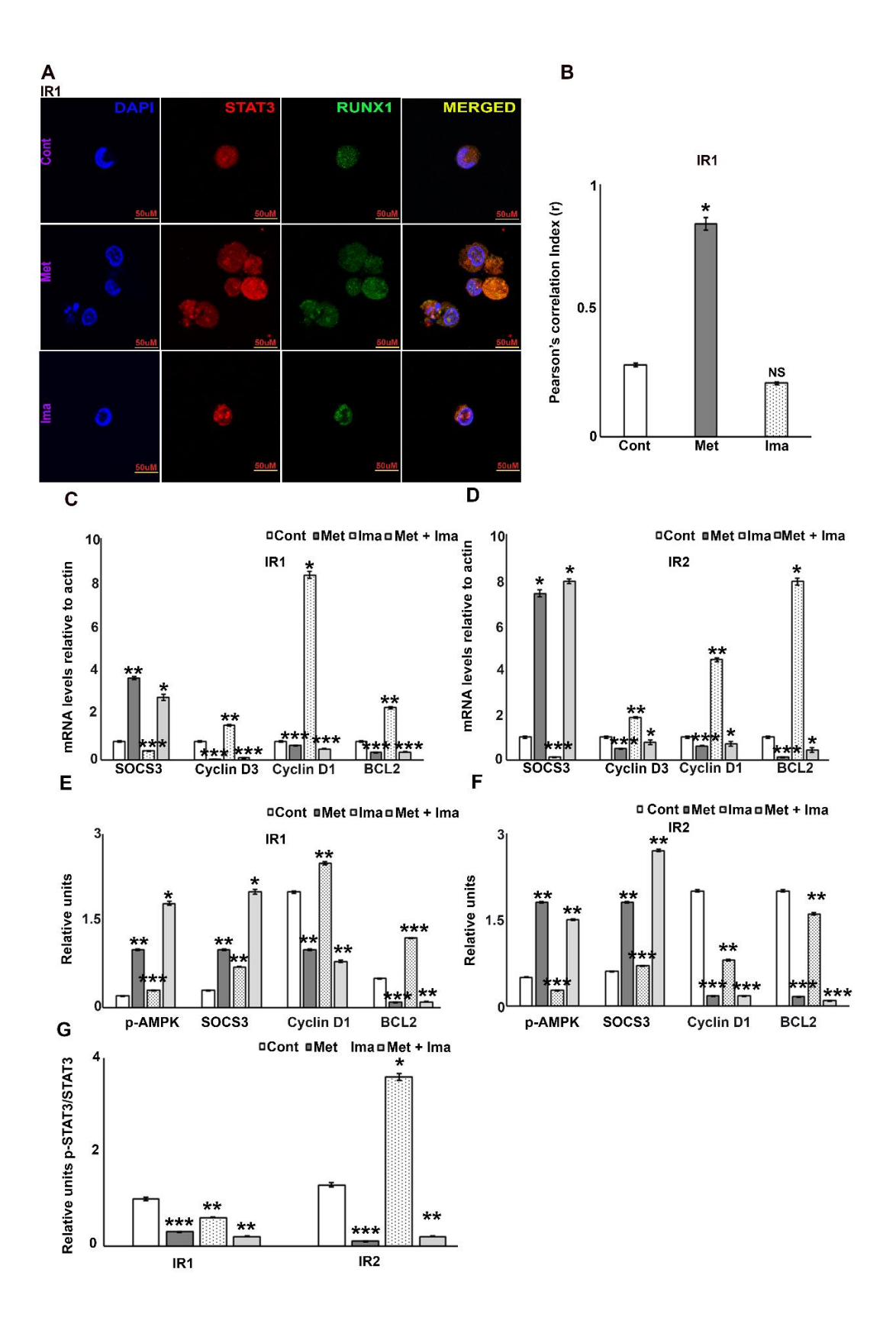
SUPPLEMENTARY FIGURE 1: A) RT-PCR analysis of K562 WT cells showing levels of SOCS3, BCL2, Cyclin D1 and D3 in response to metformin (10mM) treatment alone or with compound C (5μM) for 6 hours. B) Quantification of RUNX1 immunoblot data of WT cells post metformin and compound C treatment where nuclear values are normalized against Lamin B1 and cytoplasmic values against paxillin. C) Quantification of STAT3 immunoblot data of WT cells post metformin and compound C treatment. D) Quantification of immunoblot data of WT cells post metformin and compound C treatment for 12 hours showing levels of p-AMPK, RUNX1, SOCS3 and Cyclin D1 normalized to actin. E) Quantification of p-STAT3 immunoblot data of WT cells post metformin and compound C treatment for 12 hours normalized to STAT3. F) Quantification of immunoblot data of HEK-293T cells transfected with either RUNX1 WT or RUNX1 S 94 A or RUNX1 S 94 D with or without metformin (10mM) treatment following transfection (after 48 hours) for 12 hours showing levels of p-AMPK, RUNX1, SOCS3 and Cyclin D1 normalized to actin G) and p-STAT3 levels normalized to STAT3. N=3, Mean ± SEM \*p<0.05 versus control, \*\*p<0.005 versus control.

Cont: Control, Met: Metformin, Comp C: Compound C, EV: empty vector, WT: wild type, Nuc: nuclear extract, Cyto: Cytoplasmic extract, NS: non-significant.



**SUPPLEMENTARY FIGURE 2: A)** Co-localization analysis showing increased physical interaction between endogenous RUNX1 (Alexa 488) and AMPK (Alexa 546) up on metformin (10mM for 6 hours) treatment than compound C (5 $\mu$ M for 6 hours) in K562 IR1 cells. **B)** Quantification of immunofluorescence data in K562 IR1 cells, using Image J software on three independent fields and experiments. K562 IR1 cells treated with metformin (10mM) alone or with imatinib (1 $\mu$ M) or none or both (imatinib 1 $\mu$ M; metformin 10mM) for 6 hours and subjected to quantification of immunoblot data for **C)** RUNX1 and **D)** STAT3. K562 IR2 cells treated with metformin (10mM) alone or with imatinib (1 $\mu$ M) or none or both (imatinib 1 $\mu$ M; metformin 10mM) for 6 hours and subjected to quantification of immunoblot data for **E)** RUNX1 and **F)** STAT3. N=3, Mean  $\pm$  SEM \*p<0.05 versus control, \*\*p<0.005 versus control, \*\*p<0.005 versus control.

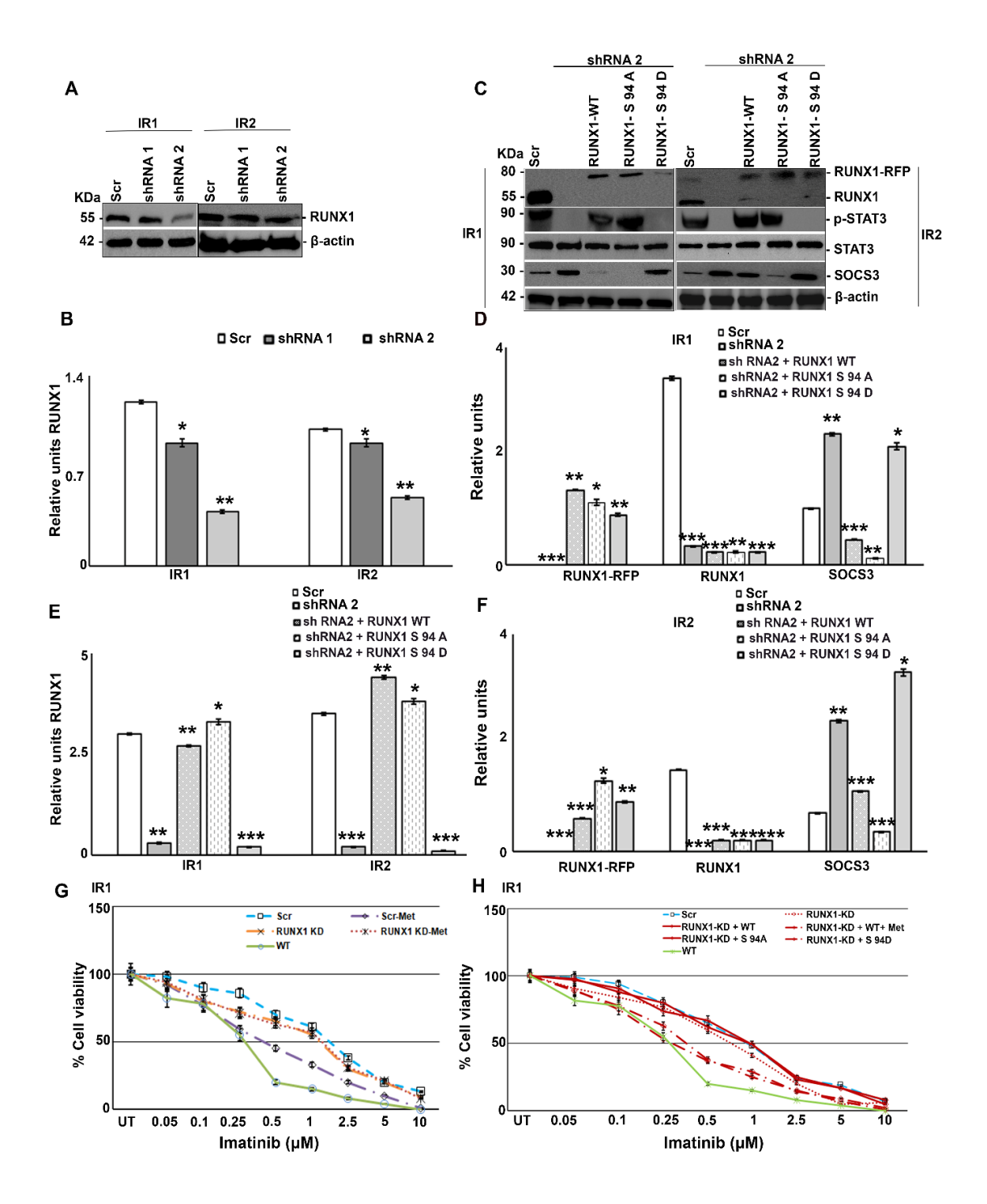
Cont: Control, Met: Metformin, Comp C: Compound C, Ima: imatinib, Nuc: nuclear extract, Cyto: Cytoplasmic extract, NS: non-significant.



SUPPLEMENTARY FIGURE 3: A) Co-localization analysis showing increased physical interaction between endogenous RUNX1 (Alexa 488) and STAT3 (Alexa 546) up on metformin (10mM for 6 hours) treatment than compound C (5μM for 6 hours) in K562 IR1 cells. B) Quantification of immunofluorescence data in K562 IR1 cells, using Image J software on three independent fields and experiments. RT-PCR analysis of C) K562 IR1 and D) K562 IR2cells showing levels of SOCS3, BCL-2, Cyclin D1 and D3 in response to metformin (10mM) and or imatinib (1μM) alone or both or none for 6 hours. E) K562 IR1 cells treated with metformin (10mM) alone or with imatinib (1μM) or none or both (imatinib 1μM; metformin 10mM) for 12 hours and subjected to quantification of immunoblot data for SOCS3, BCL-2, Cyclin D1 and p-AMPK. F) K562 IR2 cells treated with metformin (10mM) alone or with imatinib (1μM) or none or both (imatinib 1μM; metformin 10mM) for 12 hours and subjected to quantification of immunoblot data for SOCS3, BCL-2, Cyclin D1 and p-AMPK. G) K562 IR1 and IR2 cells treated with metformin (10mM) alone or with imatinib (1μM) or none or both (imatinib 1μM; metformin 10mM) for 12 hours and subjected to quantification of immunoblot data for p-STAT3.

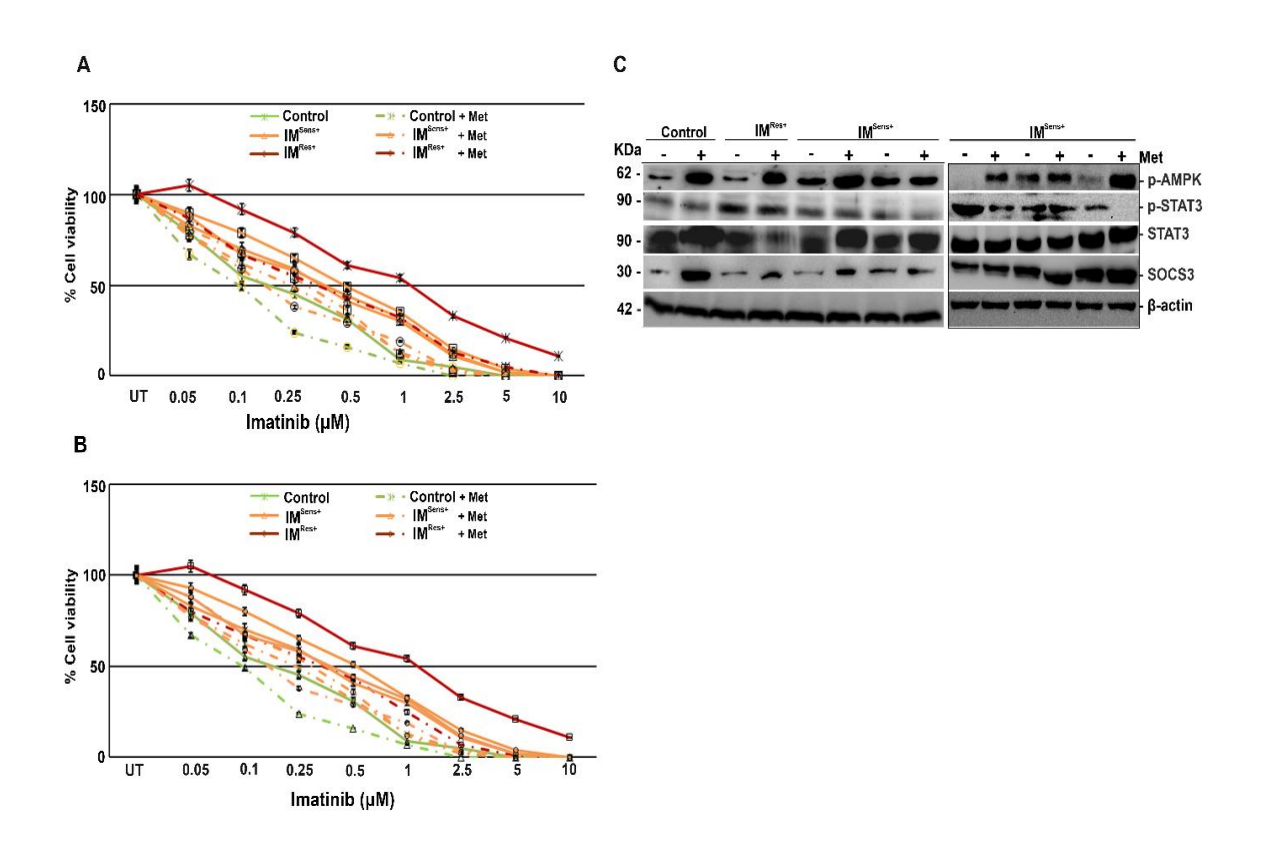
Mean ± SEM \*p<0.05 versus control, \*\*p<0.005 versus control, \*\*\*p<0.0005 versus control, <sup>NS</sup>p>0.05 versus control.

Cont: Control, Met: Metformin, Ima: imatinib, NS: non-significant.



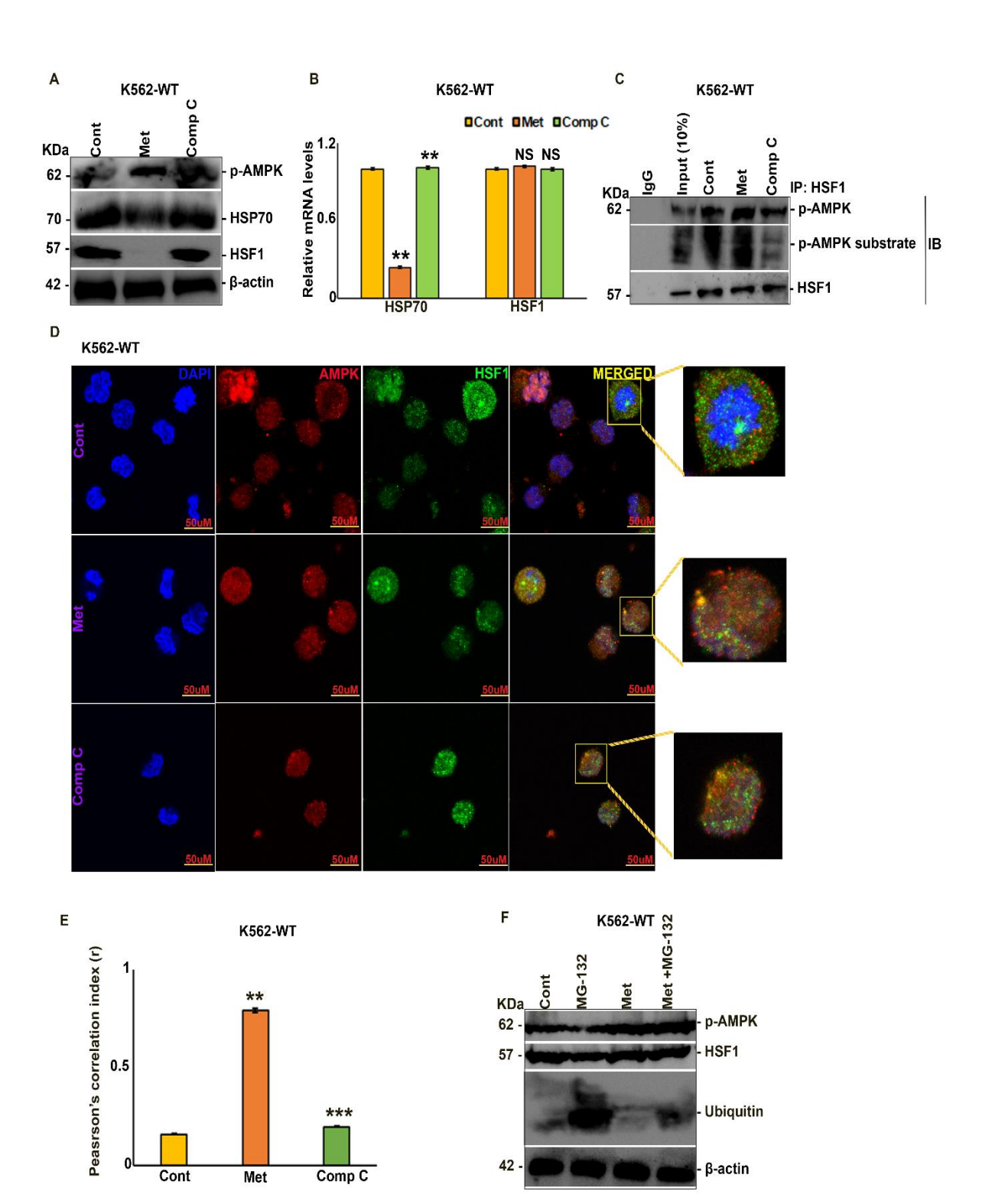
**SUPPLEMENTARY FIGURE 4: A)** Immunoblot analysis of K562 IR1and IR2 cells, showing efficiency of knock down of RUNX1 by shRNAs. **B)** Quantification of immunoblot data. **C)** Immunoblot analysis of K562 IR1 or IR2-RUNX1 KD (with shRNA 2), RUNX1 WT, RUNX1 S 94 A and RUNX1 S 94 D transduced cells showing levels of p-STAT3, STAT3, SOCS3, RUNX1 and RUNX1-RFP. **D-F)** Quantification of immunoblot data. **G)** Cell viability analysis of K562 IR1 cells transduced with either Scr or RUNX1 KD with or without metformin along with imatinib treatment, using WT as control. **H)** Cell viability analysis of K562 IR1-RUNX1 KD, RUNX1 WT, RUNX1 S 94 A and RUNX1 S 94 D transduced cells in response to imatinib treatment alone or along with metformin (0.25mM) for 72 hours with K562 WT as control, showing decreased cell viability in presence of metformin and in RUNX1 S 94 D cells which was reversed upon RUNX1 KD and in RUNX1 WT and RUNX1 S 94 A. N=3, Mean ± S.E.M. \*p<0.05 versus control, \*\*p<0.005 versus control, \*\*\*p<0.005 versus control, \*\*\*p<0.005

Cont: control, met: metformin, Ima: imatinib, WT: wild type, UT: untreated, Scr: scrambled, KD: knock down, NS: non-significant.

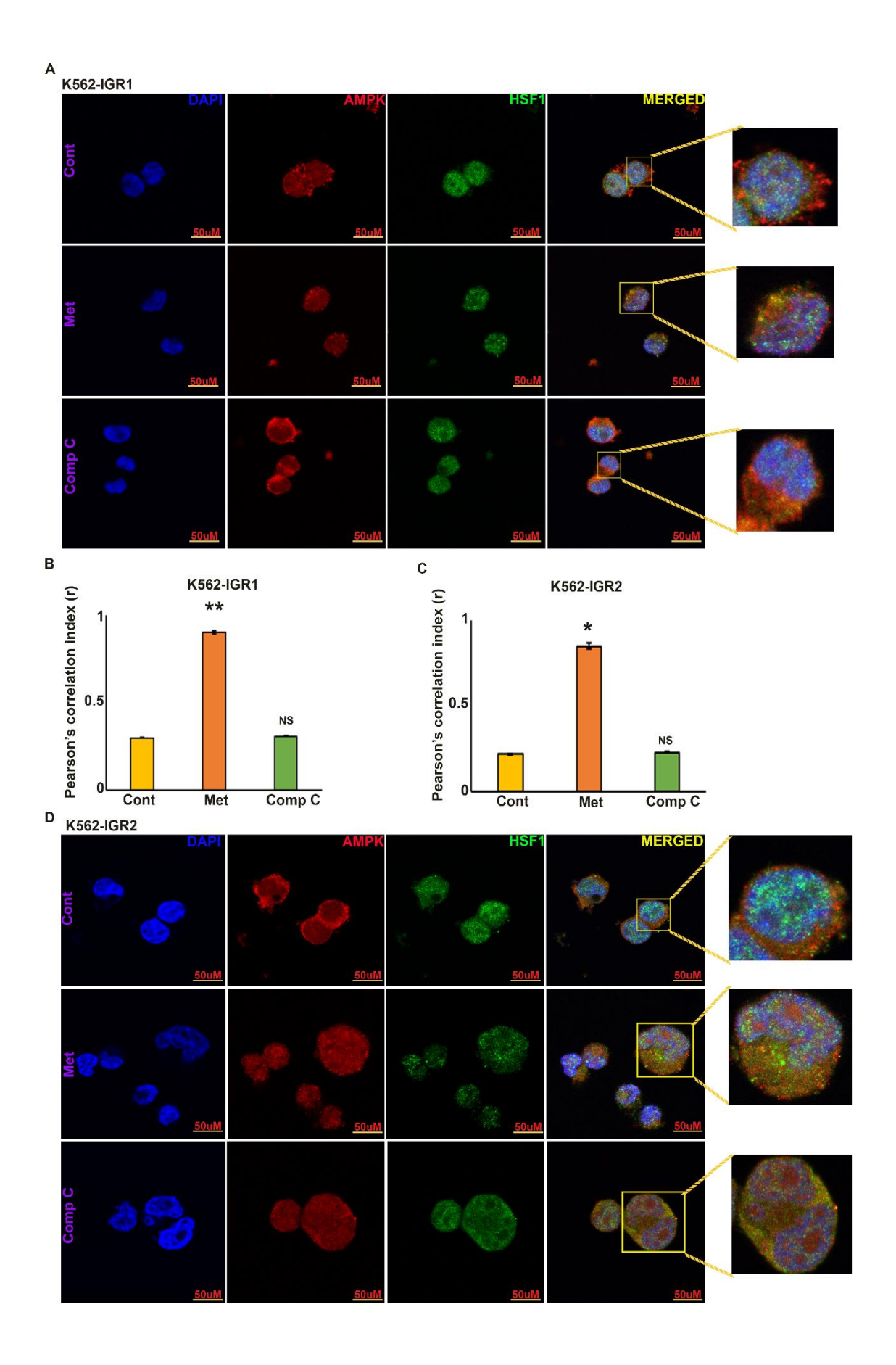


**SUPPLEMENTARY FIGURE 5: A &B)** Cell viability analysis of PBMCs post to treatment with imatinib alone or in combination with metformin (0.25mM) for 72 hours showing increased imatinib sensitivity. **C)** Immunoblot analysis of healthy and CML subject's PBMCs showing levels of p-STAT3, STAT3 and SOCS3 in response to metformin (10mM) treatment for 12 hours. N=3, Mean ± S.E.M.

Control: healthy subjects, IM<sup>Sens+</sup>: Imatinib Sensitive CML subjects, IM <sup>Res+</sup>: Imatinib resistant subjects, Met: metformin.

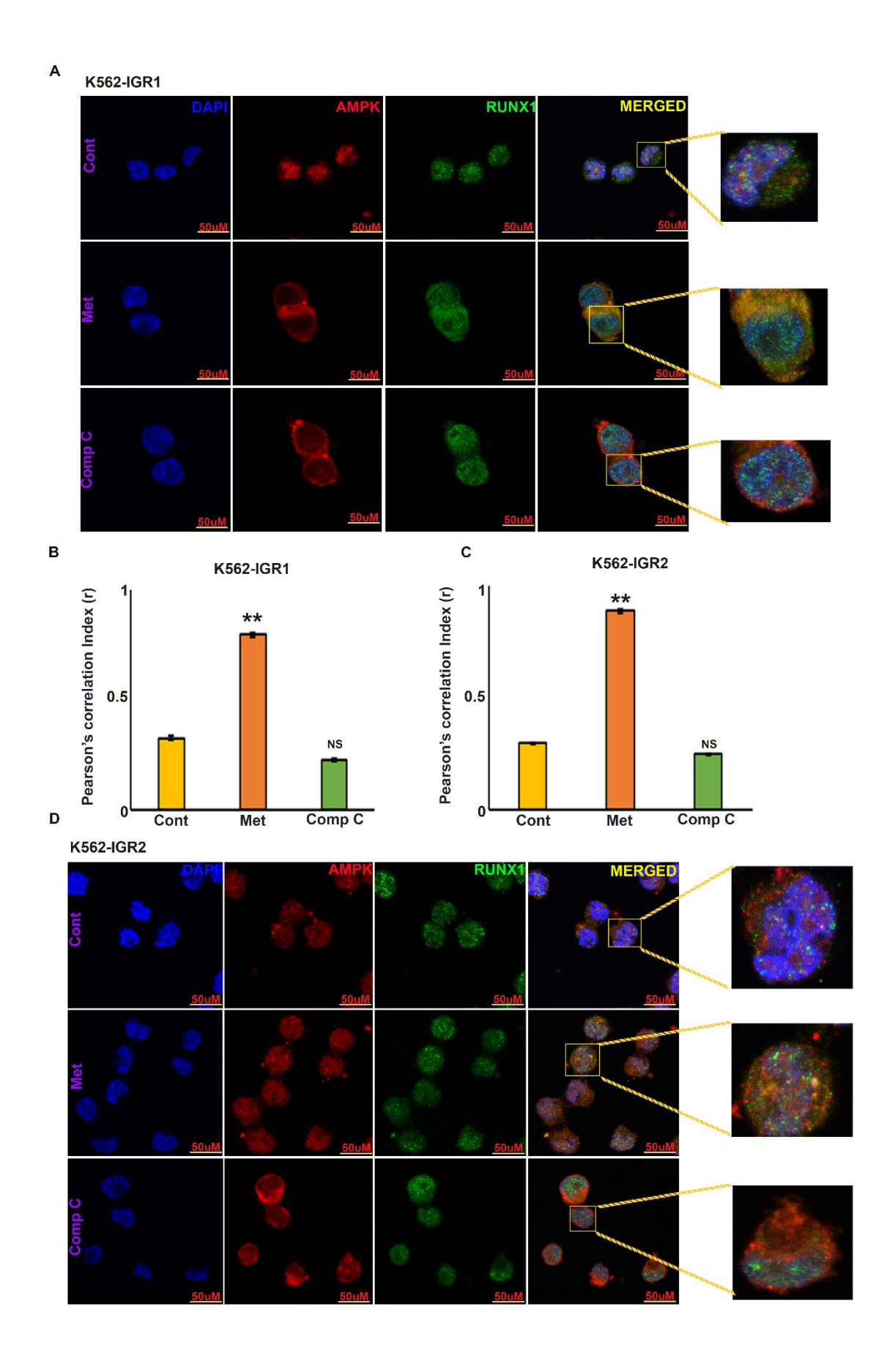


**SUPPLEMENTARY FIGURE 6: A)** K562-WT cells were subjected to metformin (10 mM for 12 hours) or compound C (5  $\mu$ M for 12 hours) treatment or none for 12 hours and immunoblot analysis was carried out to assess levels of HSF1 and HSP70. **B)** K562-WT cells were treated with either metformin (10 mM) or with compound C (5  $\mu$ M) or none for 6 hours and subjected to RT-PCR analysis to assess levels of HSF1 and HSP70. **C)** K562-WT cells were treated with either metformin (10 mM) or with compound C (5  $\mu$ M) or none for 12 hours and subjected to IP by HSF1 to assess HSF1 interaction with p-AMPK. **D)** K562-WT cells were treated with either metformin (10 mM) or with compound C (5  $\mu$ M) or none for 12 hours and subjected to immunofluorescence by anti-HSF1 (Alexa 488) and anti-AMPK (Alexa 594) antibodies counter stained with DAPI. **E)** Quantification of immunofluorescence data using ImageJ. **F)** K562-WT cells were treated with either metformin (10 mM) or with MG-132 (3 mM) or both or none for 12 hours and subjected to immunoblot to assess HSF1 levels. The immunofluorescence and quantification experiments were carried out on three independent fields. N=3, Mean  $\pm$  S.E.M.; \*\*p<0.005 versus control, \*\*\*p<0.0005 versus control, RSp>0.05 versus control. Cont: control, Met: metformin, Comp C: compound C, IP: immunoprecipitation, IB: immunoblotting, NS: non-significant, WT: wild type.



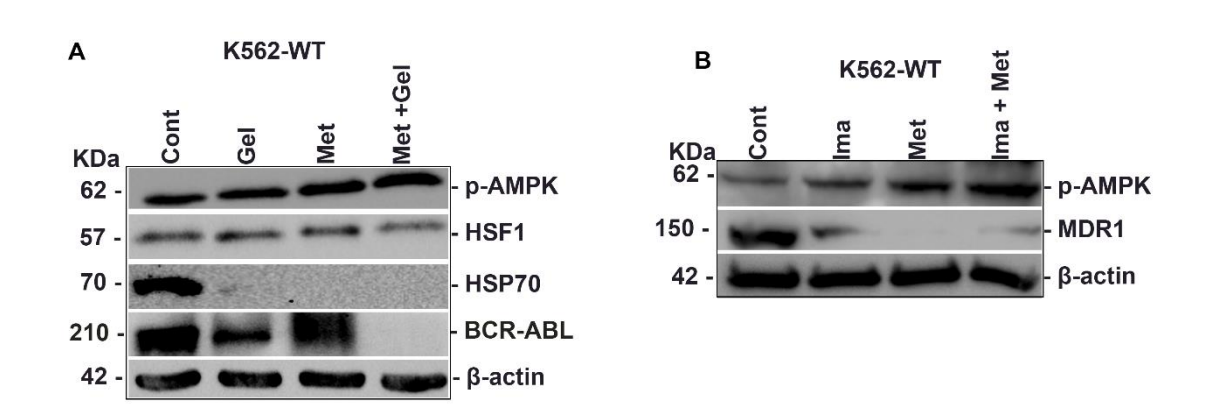
**SUPPLEMENTARY FIGURE 7: A)** K562- IGR1 cells were subjected to metformin (10 mM) or compound C (5  $\mu$ M) treatment or none for 12 hours and immunofluorescence by anti-HSF1 (Alexa 488) and anti-AMPK (Alexa 594) antibodies was carried out, counter stained with DAPI. **B)** Quantification of immunofluorescence data using ImageJ. **C)** Quantification of immunofluorescence data using ImageJ. **D)** K562- IGR2 cells were subjected to either metformin (10 mM) or compound C (5  $\mu$ M) or none for 12 hours and subjected to immunofluorescence by anti-HSF1 (Alexa 488) and anti-AMPK (Alexa 594) antibodies counter stained with DAPI. The immunofluorescence and quantification experiments were carried out on three independent fields. N=3, Mean  $\pm$  S.E.M.; \*p<0.05 versus control, \*\*p<0.005 versus control, \*\*p<0.005 versus control.

Cont: control, Met: metformin, Comp C: compound C, NS: non-significant.



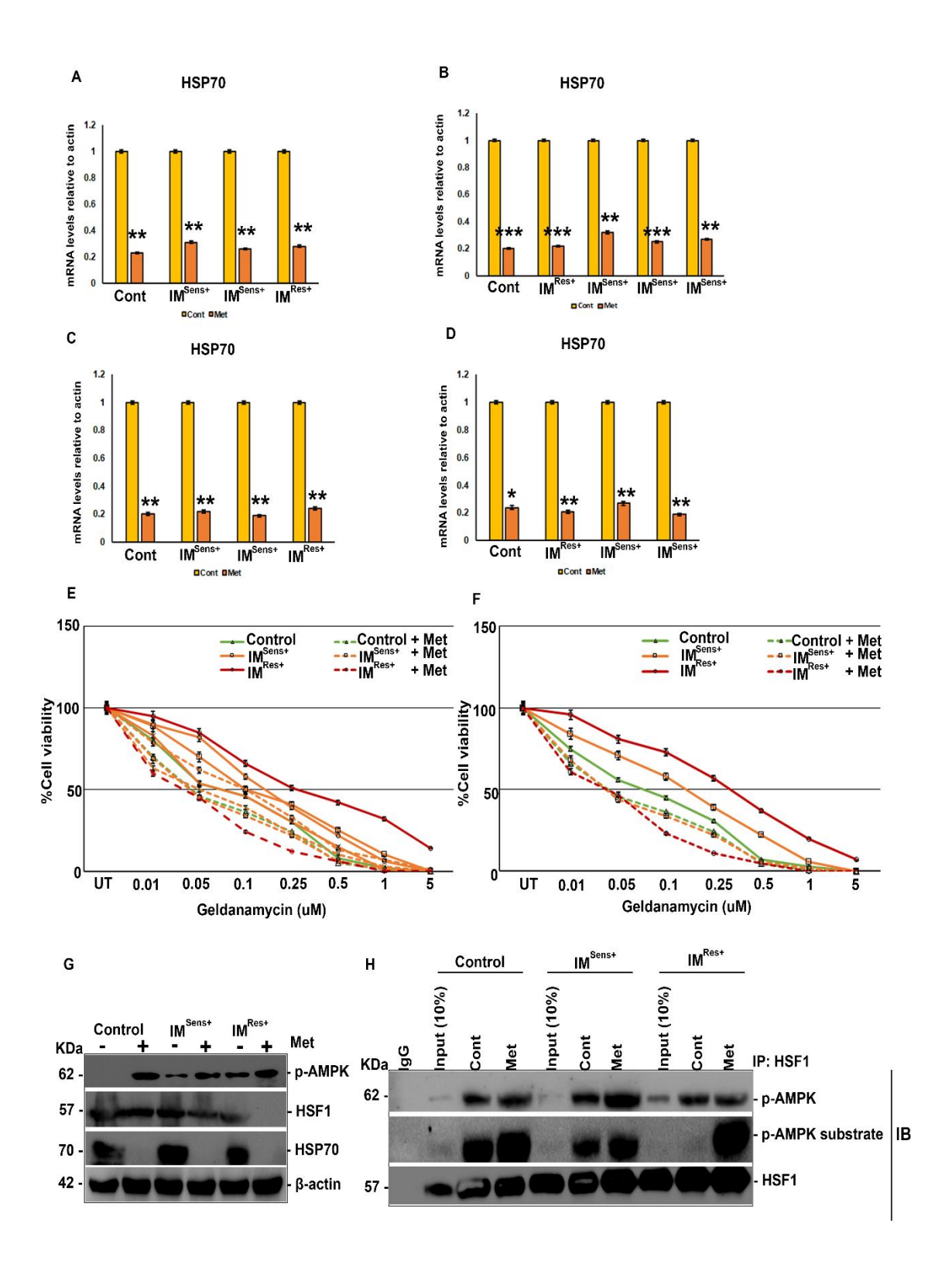
**SUPPLEMENTARY FIGURE 8: A)** K562- IGR1 cells were subjected to metformin (10 mM) or with compound C (5  $\mu$ M) or none for 12 hours and subjected to immunofluorescence by anti-RUNX1 (Alexa 488) and anti-AMPK (Alexa 594) antibodies counter stained with DAPI. **B)** Quantification of immunofluorescence data using ImageJ. **C)** Quantification of immunofluorescence data using ImageJ. **D)** K562- IGR2 cells were exposed to either metformin (10 mM) or with compound C (5  $\mu$ M) or none for 12 hours and subjected to immunofluorescence by anti-RUNX1 (Alexa 488) and anti-AMPK (Alexa 594) antibodies counter stained with DAPI. The immunofluorescence and quantification experiments were carried out on three independent fields. N=3, Mean  $\pm$  S.E.M.; \*\*p<0.005 versus control, <sup>NS</sup>p>0.05 versus control.

Cont: control, Met: metformin, Comp C: compound C, NS: non-significant.



**SUPPLEMENTARY FIGURE 9: A)** K562- WT cells were treated with either geldanamycin (0.5  $\mu$ M) or metformin (10 mM) or both or none for 12 hours and subjected to immunoblot analysis to assess levels of HSF1, HSP70 and BCR- ABL. **B)** K562- WT cells were treated with either metformin (10 mM) alone or with imatinib alone (1  $\mu$ M), or both (metformin- 10mM; imatinib- 1  $\mu$ M) or none and subjected to immunoblot analysis to assess MDR1 levels. N=3, Mean  $\pm$  S.E.M.;

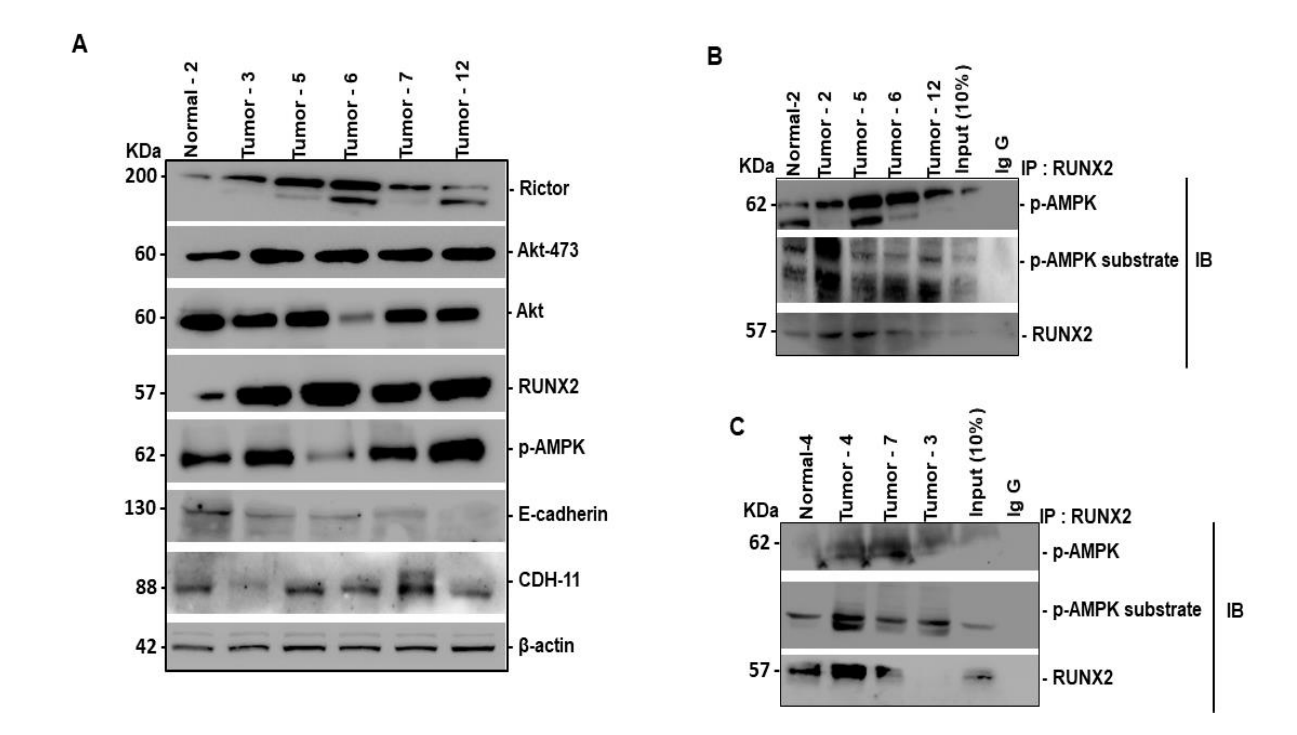
Cont: control, Met: metformin, Ima: imatinib, Gel: geldanamycin.



**SUPPLEMENTARY FIGURE 10: A-D)** PBMCs isolated from CML subjects were treated with metformin (10 mM) for 6 hours and HSP70 mRNA levels were assessed by RT-PCR analysis. **E & F)** Cell viability of PBMCs isolated from CML subjects was assessed by alamar blue, post to treatment with geldanamycin alone or along with metformin (0.25 mM) at indicated concentrations for 72 hours. **G)** PBMCs isolated from CML subjects were treated with either metformin (10 mM) or none for 12 hours and subjected to immunoblot analysis to assess HSF1 and HSP70 levels. **H)** PBMCs isolated from CML subjects were treated with either metformin (10 mM) or none for 12 hours and subjected to immunoprecipitation by HSF1 to validate HSF1 interaction with p-AMPK. N=3, Mean ± S.E.M.;

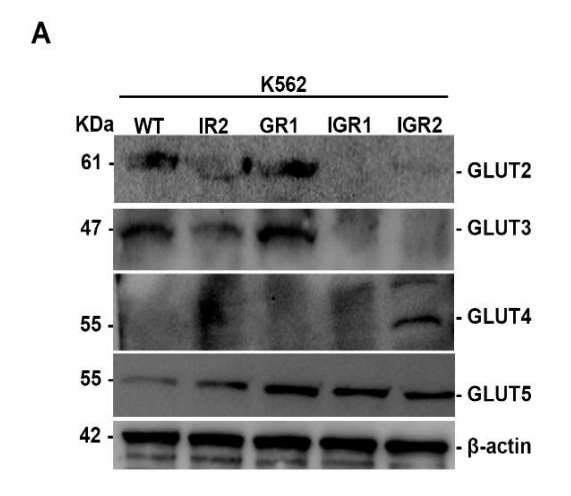
Cont: control, Met: metformin, IP: immunoprecipitation, IB: immunoblotting, Control: healthy subjects, IM <sup>Sens+</sup>: imatinib sensitive subjects, IM <sup>Res+</sup>: imatinib resistant subjects.

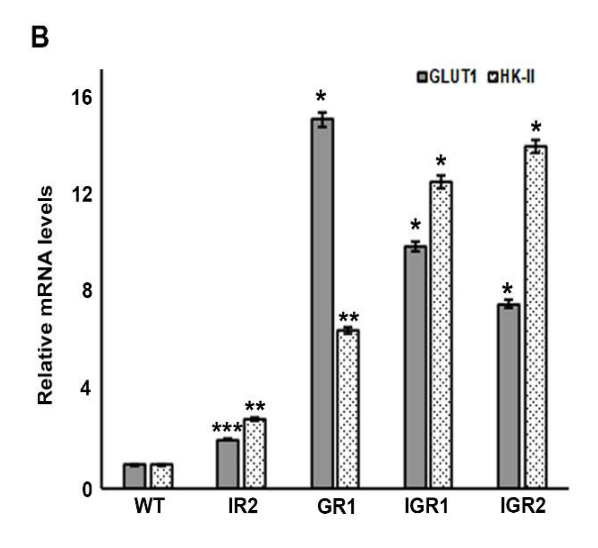
<sup>\*\*</sup>p<0.005 versus control, \*\*\*p<0.0005 versus control.

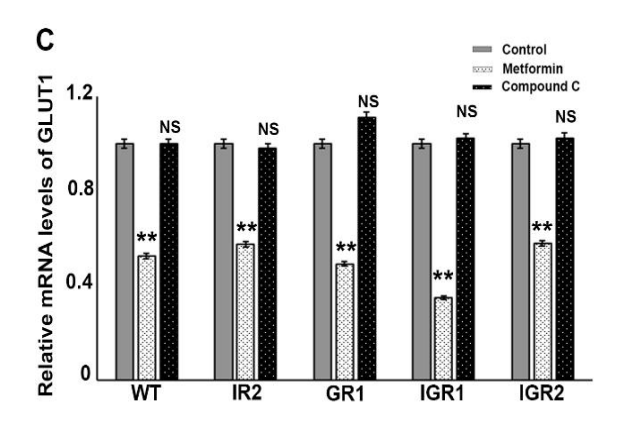


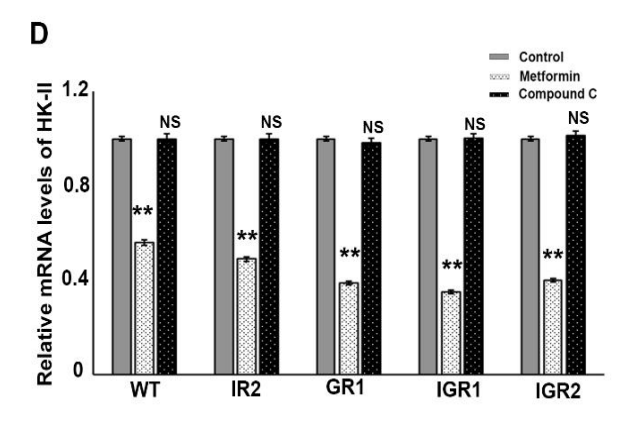
**SUPPLEMENTARY FIGURE 11:** Breast tumor tissue along with adjacent normal tissue were subjected protein isolation followed by **A**) immunoblot analysis and **B &C**) IP by RUNX2 pull down and levels of p-AMPK, RUNX2 and p-AMPK substrate specific motif were analyzed. N=3.

IP: immunoprecipitation, IB: immunoblotting.



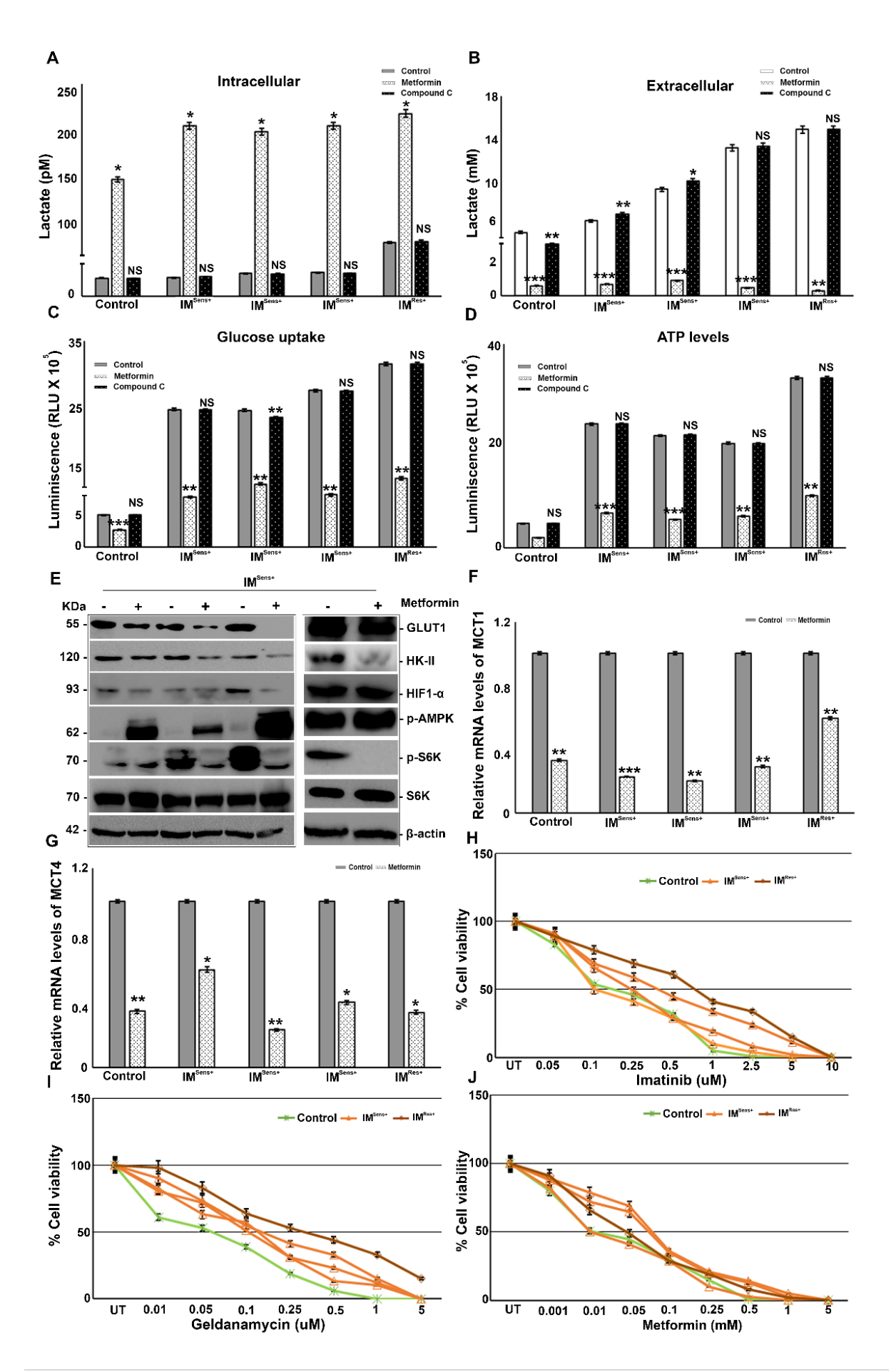






**SUPPLEMENTARY FIGURE 12:** K562 WT, IR2, GR1, IGR1 and IGR2 cells were subjected to **A**) immunoblot analysis. K562 WT, IR2, GR1, IGR1 and IGR2 cells were subjected to **B**) RT-PCR analysis of GLUT1 and HK-II. K562 WT, IR2, GR1, IGR1 and IGR2 cells were treated either with metformin (10 mM) alone or with compound C (5  $\mu$ M) or none for 6 hours and subjected to RT-PCR analysis of **C**) GLUT1 and **D**) HK-II. Mean  $\pm$  S.E.M.; N=3, \*p<0.05 versus control or WT, \*\*p<0.005 versus control or WT.

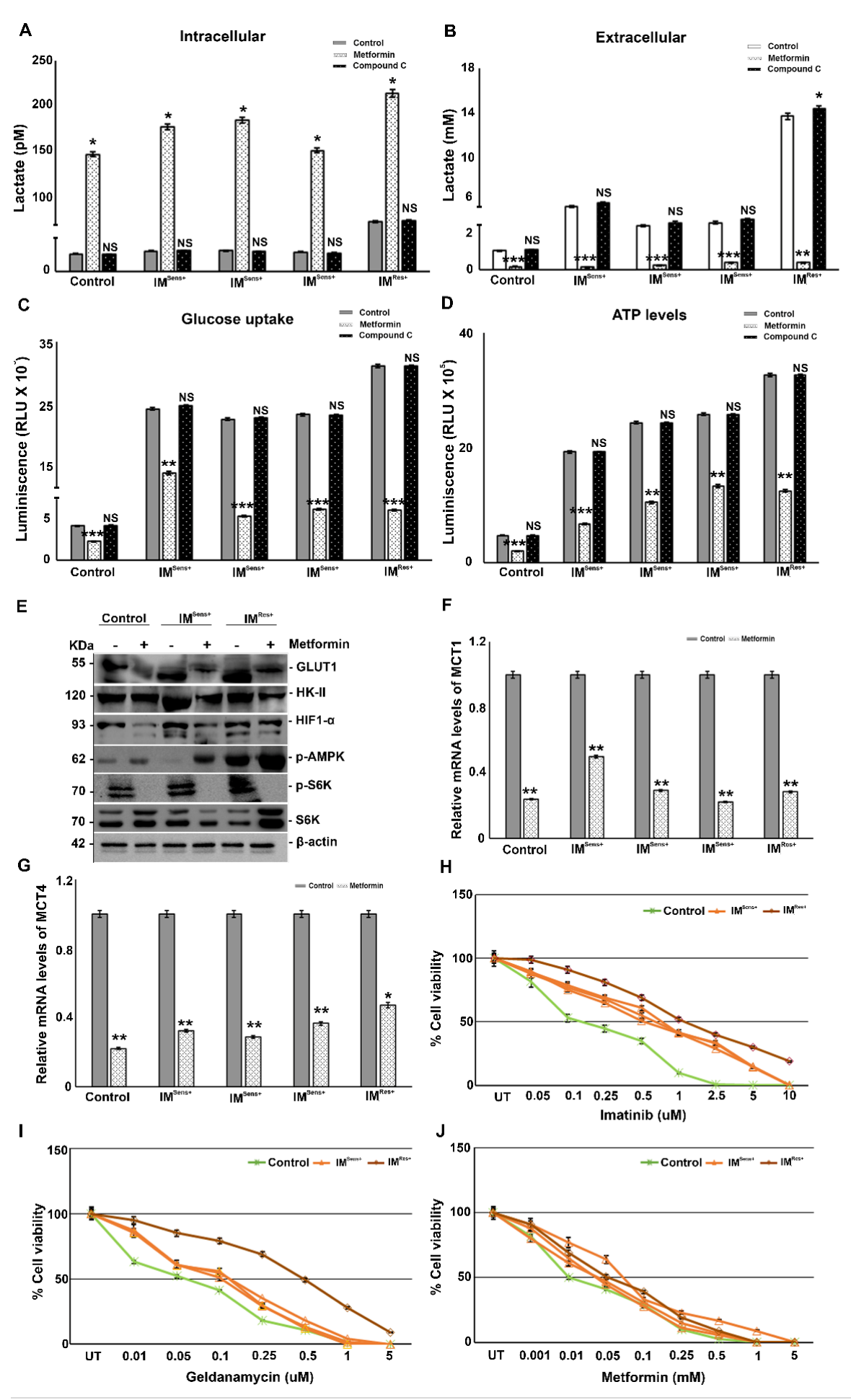
Cont: control, Met: metformin, Comp C: compound C, NS: non-significant, WT: wild type.



**SUPPLEMENTARY FIGURE 13:** PBMCs were isolated from CML subjects and exposed to either metformin (10 mM) alone or with compound C (5  $\mu$ M) or none for 12 hours, and **A**) intracellular lactate levels, **B**) extracellular lactate levels, **C**) glucose uptake levels and **D**) ATP levels were measured. PBMCs were treated with either metformin alone (10 mM) or none for 12 hours and subjected to **E**) immunoblot analysis. PBMCs were treated with either metformin alone (10 mM) or none for 6 hours and subjected to RT-PCR analysis of **F**) MCT1 and **G**) MCT4. The viability of PBMCs was measured after treatment with either **H**) imatinib, **I**) geldanamycin or **J**) metformin for 3 days. Mean  $\pm$  S.E.M.; N=3, \*p<0.05 versus control, \*\*p<0.0005 versus control, \*\*p<0.0005 versus control.

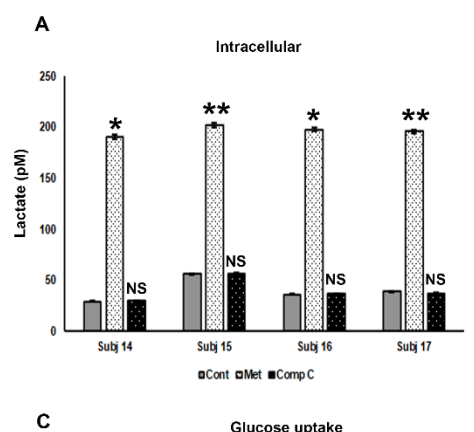
Cont: control, Met: metformin, Comp C: compound C, NS: nonsignificant, RLU: relative luminescence units.

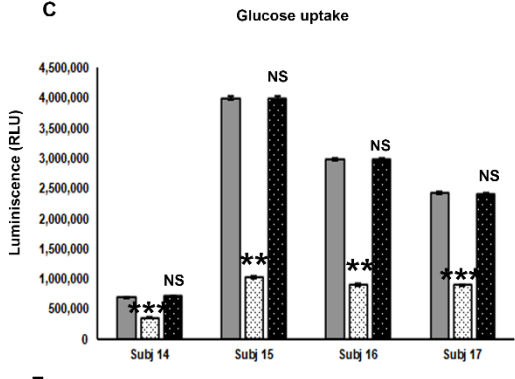
Control: Healthy, IM Sens+: Imatinib sensitive, IM Res+: Imatinib resistant subjects.

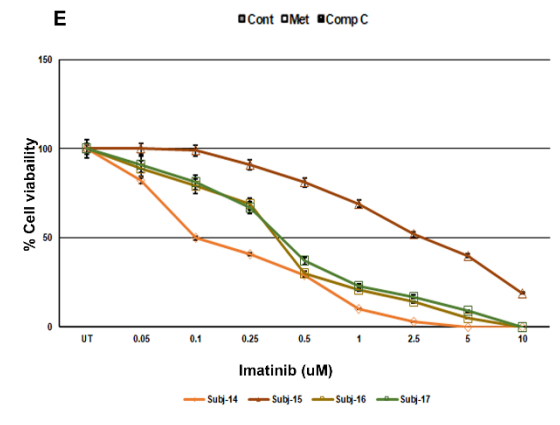


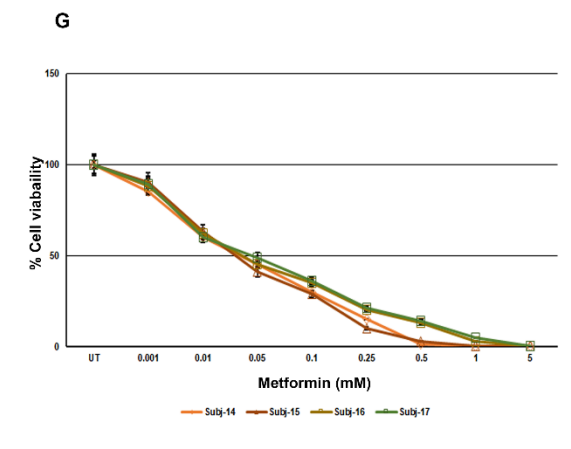
**SUPPLEMENTARY FIGURE 14:** PBMCs were isolated from CML subjects and exposed to metformin (10 mM) alone or with compound C (5  $\mu$ M) or none for 12 hours, and **A**) intracellular lactate levels, **B**) extracellular lactate levels, **C**) glucose uptake levels and **D**) ATP levels were measured. PBMCs were treated with either metformin alone (10 mM) or none for 12 hours and subjected to **E**) immunoblot analysis. PBMCs were treated with either metformin alone (10 mM) or none for 6 hours and subjected to RT-PCR analysis of **F**) MCT1 and **G**) MCT4. The viability of PBMCs was measured after treatment with either **H**) imatinib, **I**) geldanamycin or **J**) metformin for 3 days. Mean  $\pm$  S.E.M.; N=3, \*p<0.05 versus control, \*\*p<0.005 versus control, \*\*\*p<0.005 versus control, \*\*\*p<0.0005 versus control.

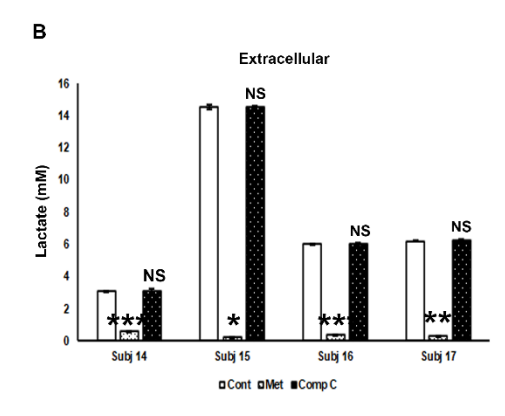
Cont: control, Met: metformin, Comp C: compound C, NS: nonsignificant, RLU: relative luminescence units. Control: Healthy, IM Sens+: Imatinib sensitive, IM Res+: Imatinib resistant subjects.

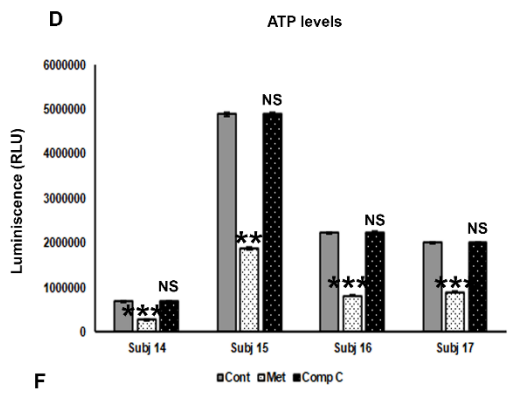


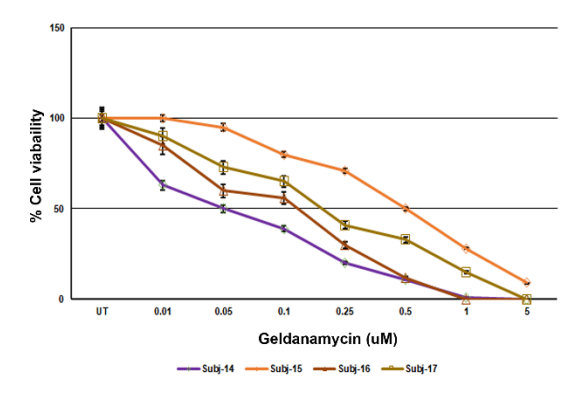


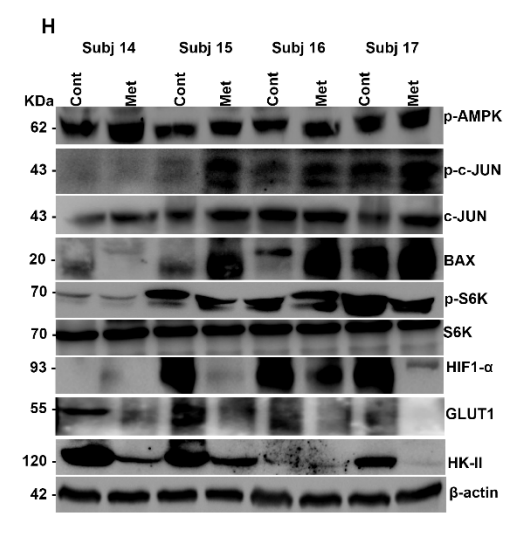








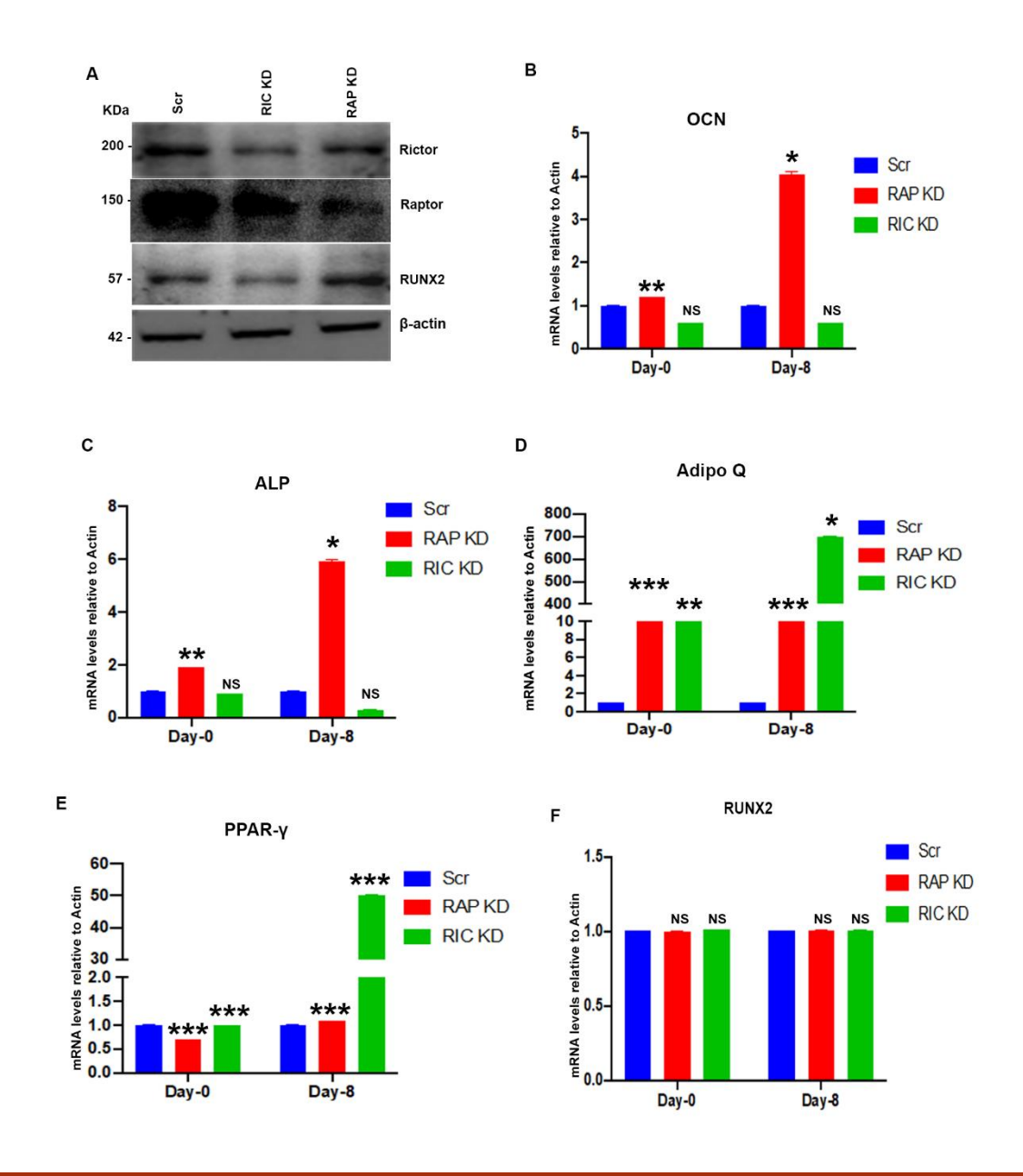




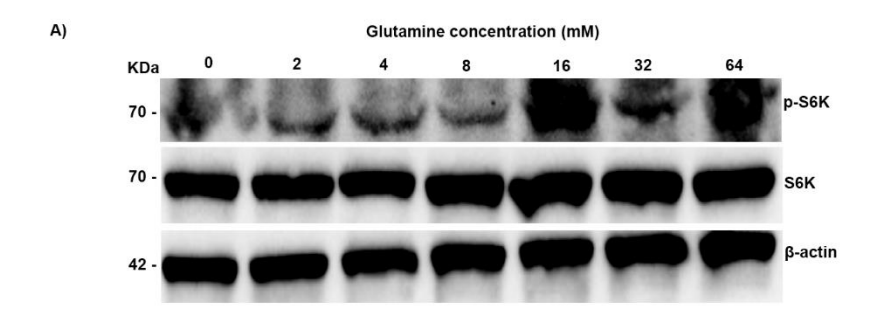
**SUPPLEMENTARY FIGURE 15:** PBMCs were isolated from CML subjects and subjected to metformin (10 mM for 12 hours) treatment or with compound C (5  $\mu$ M) or none for 12 hours, and **A**) intracellular lactate levels, **B**) extracellular lactate levels, **C**) glucose uptake levels and **D**) ATP levels were measured. PBMCs were treated with either metformin alone (10 mM) or none for 12 hours and subjected to **E**) immunoblot analysis. PBMCs were treated with either metformin alone (10 mM) or none for 6 hours and subjected to RT-PCR analysis of **F**) MCT1 and **G**) MCT4. The viability of PBMCs was measured after treatment with either **H**) imatinib, **I**) geldanamycin or **J**) metformin for 3 days. Mean  $\pm$  S.E.M.; N=3, \*p<0.05 versus control, \*\*p<0.005 versus control, \*\*p<0.005 versus control.

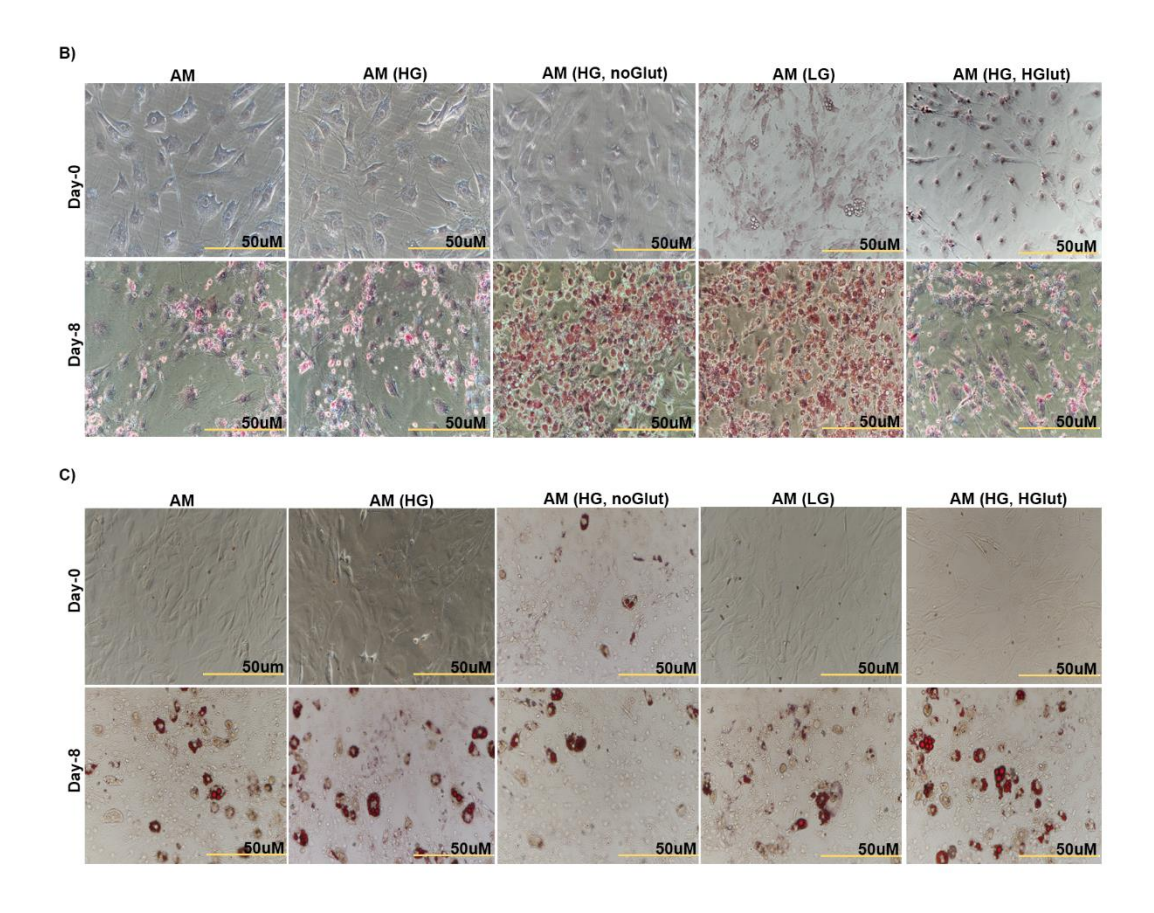
Cont: control, Met: metformin, Comp C: compound C, NS: nonsignificant, RLU: relative luminescence units.

Control: Healthy, IM Sens+: Imatinib sensitive, IM Res+: Imatinib resistant subjects.



**SUPPLEMENTARY FIGURE 16:** MSCs were transfected with siRNAs against RICTOR and RAPTOR and subjected to **A**) immunoblotting. MSCs were transfected with siRNAs against RICTOR and RAPTOR, after which they were induced to adipogenic differentiation and subjected to total RNA isolation. The mRNA levels of **B**) OCN, **C**) ALP, **D**) Adipo Q, **E**) PPAR- $\gamma$  and **F**) RUNX2 were analyzed. Mean  $\pm$  S.E.M.; n=3, \*p<0.1 versus control, \*\*p<0.01 versus control; \*\*\*p<0.001 versus control.





**SUPPLEMENTARY FIGURE 17:** Murine MSCs were subjected to adipogenic differentiation in the presence of high glucose (25mM) with or without glutamine (4mM) and in the presence of low glucose (5.5mM) with or without high glutamine (20mM) followed by **A**) Alizarin- red-s-staining and **B**) Oil-red-o-staining. N=3, Mean  $\pm$  S.E.M.

AM: adipogenic medium, HG: high glucose, LG: low glucose, Glut: glutamine, HGlut: high glutamine.

## ANTI-PLAGIARISM CERTIFICATE

## Effect of AMPK mediated RUNX phosphorylation on progression of cancer and diabetic bone health

by Meher Gayatri Bolisetti

Submission date: 02-Nov-2022 11:16AM (UTC+0530)

**Submission ID:** 1942191967

File name: Meher\_Gayatri\_Bolisetti.pdf (26.88M)

Word count: 27378

Character count: 148695

## Effect of AMPK mediated RUNX phosphorylation on progression of cancer and diabetic bone health

**ORIGINALITY REPORT** 

22%

21%

20%

2%

SIMILARITY INDEX

**INTERNET SOURCES** 

**PUBLICATIONS** 

STUDENT PAPERS

**PRIMARY SOURCES** 



### www.nature.com

Internet Source

16%

Meher Bolisetti Gayatri, Navya Naidu Gajula, Suresh Chava, Aramati B. M. Reddy. "High glutamine suppresses osteogenesis through mTORC1-mediated inhibition of the mTORC2/AKT-473/RUNX2 axis", Cell Death Discovery, 2022

Publication



Publication



www.biorxiv.org

Internet Source

Indicated Similarity Sources
1,2 & 3 are students < 1 %

Papers, are part of Hs. Gayatri's



www.mdpi.com

Internet Source

theris. I, as a Superisor

A. Bindu Madnava Red Assistant Professor Dept. of Animal Biology School of Life Sciences University of Hyderabad Hyderabad-500 046.